

LEBANESE AMERICAN UNIVERSITY

An Evaluation of Short-Term Effects of Different Soil Management Systems on Soil Physical, Structural and Hydraulic Properties and an Estimation and Optimization of Water Infiltration for Layered Domains Using a Restructured Green-Ampt Model in an Agricultural Terrain, Lebanon

By

Caroline Merheb

A thesis

Submitted in partial fulfillment of the requirements
for the degree of Master of Science in Engineering

School of Engineering

July 2022

THESIS APPROVAL FORM

Student Name: Caroline Merheb I.D. #: 202004734

Thesis Title : An Evaluation of Short-Term Effects of Different Soil Management Systems on Soil Physical, Structural and Hydraulic Properties and an Estimation and Optimization of Water Infiltration for Layered Domains Using a Restructured Green-Ampt Model in an Agricultural Terrain


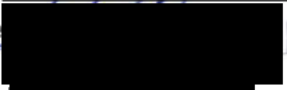
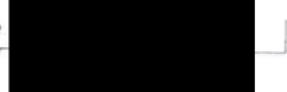
Program: Master of Science

Department: Civil and Environmental Engineering

School: Engineering

The undersigned certify that they have examined the final electronic copy of this thesis and approved it in **Partial** Fulfillment of the requirements for the degree of:

Master of Science in the major of Civil and Environmental Engineering

Thesis Advisor's Name	Dr. Jean Chatila	Signature		DATE: <u>15 / 07 / 2022</u> Day Month Year
Committee Member's Name	Dr. Mahmoud Wazne	Signature		DATE: <u>15 / 07 / 2022</u> Day Month Year
Committee Member's Name	Dr. Moustapha Harb	Signature		DATE: <u>15 / 07 / 2022</u> Day Month Year

THESIS COPYRIGHT RELEASE FORM

LEBANESE AMERICAN UNIVERSITY NON-EXCLUSIVE DISTRIBUTION LICENSE

By signing and submitting this license, you (the author(s) or copyright owner) grants the Lebanese American University (LAU) the non-exclusive right to reproduce, translate (as defined below), and/or distribute your submission (including the abstract) worldwide in print and electronic formats and in any medium, including but not limited to audio or video. You agree that LAU may, without changing the content, translate the submission to any medium or format for the purpose of preservation. You also agree that LAU may keep more than one copy of this submission for purposes of security, backup and preservation. You represent that the submission is your original work, and that you have the right to grant the rights contained in this license. You also represent that your submission does not, to the best of your knowledge, infringe upon anyone's copyright. If the submission contains material for which you do not hold copyright, you represent that you have obtained the unrestricted permission of the copyright owner to grant LAU the rights required by this license, and that such third-party owned material is clearly identified and acknowledged within the text or content of the submission. IF THE SUBMISSION IS BASED UPON WORK THAT HAS BEEN SPONSORED OR SUPPORTED BY AN AGENCY OR ORGANIZATION OTHER THAN LAU, YOU REPRESENT THAT YOU HAVE FULFILLED ANY RIGHT OF REVIEW OR OTHER OBLIGATIONS REQUIRED BY SUCH CONTRACT OR AGREEMENT. LAU will clearly identify your name(s) as the author(s) or owner(s) of the submission, and will not make any alteration, other than as allowed by this license, to your submission.

Name: Caroline Merheb

Signature: _____  Digitally signed by Caroline Merheb
Date: 2022.07.01 10:49:06 +03'00'

Date: July 15, 2022


PLAGIARISM POLICY COMPLIANCE STATEMENT

I certify that:

1. I have read and understood LAU's Plagiarism Policy.
2. I understand that failure to comply with this Policy can lead to academic and disciplinary actions against me.
3. This work is substantially my own, and to the extent that any part of this work is not my own I have indicated that by acknowledging its sources.

Name: Caroline Merheb

Signature: _____

 Digitally signed by Caroline Merheb
Date: 2022.07.07 09:48:52 +03'00'

Date: July 15, 2022

To my loving parents Edmond and Samira

I hope that this achievement will complete the dream you had for me
when you chose to give me the best education you could.

Acknowledgement

First of all, I would like to express my sincere gratitude to the Graduate Program Scholarship awarded by the Lebanese American University, for giving me the opportunity to be a part of this institution and allowing me to contribute to this institution's continuous growth. In addition, I would like to thank the university for funding the necessary equipment that were crucial for this work. The process of approval and order was light and excluded from difficulties due to the hard work, effort and time that the faculty and staff have maintained. In this regard, I would like to acknowledge Mrs. Salwa Najjar and Mrs Reine El Khoury for their determination, effort, and time to order the equipment and receive them on time.

I am thankful to my thesis advisor Dr. Jean Chatila for his incessant and persistent guidance. Dr. Chatila was supportive and insistent about doing the work precociously and on a strict time basis. I am grateful for his tenacious effort to ask for the equipment that were needed to perform the experimental part of this work. Yet, I am thankful for his mentoring including the flexibility, self-dependence, and time-management skills that he relied on me to acquire. I would like also to concede everyone who played a role in my academic accomplishments. In particular, my committee researchers, each of whom has provided me direct and indirect guidance through courses and advises throughout these couple years in particular Dr. Mustapha Harb, Dr. Mahmoud Wazne, Dr. Volcan Cakir, and Dr. Nadim Zgheib.

My appreciation also extends to the lab supervisor, Mr. George Shakkour who guided me in my work in the lab and managed to ease on me the use of all required equipment on and off the campus. Furthermore, my gratitude is to the team of the Medical imaging & Cath lab in the Medical Center of the Lebanese American Univerity-St. John Hospital, especially Dr. Selim Hani the hospital director for his approval to use the lab, Ms. Nancy Abi Younes the supervisor who gave me the approval to access the lab and easen the process of imaging, Mr. Omar El Helou, Mr. Mike Atallah, Mr. Chaker Al Kaii, Ms. Justina Harb and Mr. Peter Soueid who assisted me with the imaging and carrying the samples.

Further, to all who donated financially by providing services and products, I am forever indebted. To all who contributed by providing the land and to all who helped

in the field work especially my father, my husband, my uncle and my sisters, I am forever grateful. I cannot forget to recognize the continuous support of my family: my husband Mario, my parents Edmond and Samira, my sisters Tania and Cynthia, my mother-in-law Foutine, my sister-in-law Josephine, and my brother-in-law Antonio. My continuous motivation is to make you all proud. Thank you for always carrying my burdens, my negativity, and my weaknesses. Finally, my ultimate gratefulness is to God in whom my faith will always be solid and who is continuously my source of strength, motivation, confidence, and perception.

An Evaluation of Short-Term Effects of Different Soil Management Systems on Soil Physical, Structural and Hydraulic Properties and an Estimation and Optimization of Water Infiltration for Layered Domains Using a Restructured Green-Ampt Model in an Agricultural Terrain, Lebanon

Caroline Merheb

Abstract

Soil management systems are widely used in agricultural systems due to their diverse functionality in enhancing water infiltration, soil aggregate stability, and ultimately crop yield. In this regard, each system provokes alteration to the soil physique. Such changes are sometimes reported as contradicting. Consequently, choosing a system to enhance water infiltration in an agricultural terrain seems site-specific. Nevertheless, implementing all management systems to determine water infiltration capacities for a specific site can be costly and time-consuming. Hence, the need for a mathematical model that computes infiltration into agricultural soils is necessary. As this stands, this study attempt to solve three questions: (1) what are the changes and their significance that the soil management systems impose on soil properties? (2) which mathematical model is best used to compute infiltration in layered agricultural soils under different irrigation rates while taking into consideration ponding effects? (3) what is the best soil management system to be implemented in loamy sand agricultural land that is cultivated by apple trees and legumes and vegetables in-between rows to carry water to depths of 40cm faster with less water consumption while maintaining the subsurface moisture for longer periods? The first part includes the determination of soil properties. Two sites are chosen: loamy sand and clay loam soils. Five management systems were implemented: NT (no-tillage), CC+NT (cover crop), MC+NT (chicken manure cover), RT+NT (tilled soil by rotation using a tractor), MTA+NT (tilled soil mixed with chicken manure), and MT+NT (tilled soil mixed with crop residues). The organic matter content, the aggregate size distribution, the densities (in addition to porosities and residual moisture content), and the saturated hydraulic conductivities were measured in the laboratory using the loss on ignition, sieve analysis, coring, and constant head permeability methods, respectively while the pore structure was

analyzed from CT-scan images of undisturbed samples. In both soils, tillage application decreased the densities, the aggregate mean weight diameter, the residual moisture content, and the fine pore volumes while increased the organic matter content, the porosity, the saturated hydraulic conductivity, and the amount of large pores of undisturbed soil. Likewise, the addition of organic matter supplemented the behavior of RT. In loamy sand soils, NT layer proved to be more adequate for maximum crop production, to have good air capacity for soil aeration while maintaining a better storage for subsequent use of water, and to maintain a good aggregate stability. Albeit the rotary tilled layer had a similar good structure and environment for soil aeration to NT, it lacked the qualities to maintain water and to structurally hold water for plant growth. However, the addition of organic matter enhanced such qualities with some limitations. The advantage of tilled layers over undisturbed soils is the better conductivity of water due to larger and better sorted pores. However, in clay loam soils, NT lacked all criteria for good physical quality indications in opposition to RT. Even the addition of organic matter was not shown to be advantageous as the large pores found in RT were further decreased by the deposition of the organics. Notwithstanding, the role of organics was consistent in improving the water conductivity. Yet, the crop residues proved to be highly adsorptive to water and tend to activate preferential flow while chicken manure is more conductive. The second part included the derivation of the mathematical model which resulted in good Nash-Sutcliffe Efficiency. For irrigation rate smaller than 0.05cm/min, NT was faster since all the other systems had larger pore structure for which more time is needed to saturate. For higher irrigation rates, systems have only tilled layer are more efficient especially those amalgamated with chicken manure. Hence, it is recommended to use crop residues as soil covers in case of ponding irrigation. Finally, the third part resulted in having MTA+NT as the optimal system in loamy sand soil in which the addition of artificial macropores filled with straw residues would enhance water storage and drainage.

Keywords: Soil Management System, Tillage Systems, Soil Physical Properties, Pore Structure, Soil Physical Quality, Agricultural Soils, Infiltration, Green-Ampt Model, Layered Soil Profile, Artificial Macropore, CT-Scanning.

Table of Contents

Acknowledgement	vi
Abstract.....	viii
Table of Contents	x
List of Figures.....	xii
List of Tables	xv
List of Appendices	xvi

Chapter	Page
I-Introduction	1
II-Literature Review	9
2.1 Infiltration.....	9
2.2 Soil Pore Size Identification.....	11
2.3 Soil Management Systems	12
2.4 Effect of Soil Management Systems	13
2.4.1 Effect on Infiltration.....	13
2.4.2 Spatial Variation on Soil Physical Properties and Structure.....	15
2.4.3 Effect on Preferential Flow	17
2.4.4 Macropore Significance	18
2.5 Infiltration Models.....	20
2.5.1 Green-Ampt Model	21
2.5.2 Infiltration in Dual-Permeability Soil	25
III-Methodology	27
3.1 Physical, Structural and Hydraulic Properties.....	27
3.1.1 Testing Sites	27
3.1.2 Experimental Design and Land Preparation	28
3.1.3 Sample Collection and Preparation.....	31
3.1.4 Soil Pore Structure	32
3.1.5 Soil Properties	32
3.1.6 Preferential flow.....	39
3.1.7 Statistical Analysis	42
3.2 Mathematical Model.....	42

3.2.1 Infiltration in one-layer micropore domain.....	43
3.2.2 Infiltration in multi-layered micropore domain	48
3.2.3 Model Validation	54
3.3 Optimal Soil Management System.....	55
3.3.1 Model Simulation.....	55
3.3.2 Soil Treatment Optimization.....	56
IV-Results and Discussion	59
4.1 Soil Properties	59
4.1.1 Organic Matter Additives.....	59
4.1.2 Site 1 – Loamy Sand	67
4.1.3 Site 2 – Clay Loam.....	91
4.1.4 Spatial Variation Analysis	104
4.2 GARALS Model.....	108
4.3 Model Simulation	110
4.4 Soil Management System Optimization in Site 1	117
V-Conclusion	122
Bibliography	123
Appendices	Page
A-Soil Properties	153
Site 1: Loamy Sand	153
Site 2: Clay Loam	158
Crop Residues & Chicken Manure	162
B-Soil-Pore Structure.....	165
C-Experimental Data – Preferential Flow for Site 1.....	166
D-MATLAB Code for GARALS	169
2-Layers Soil Profile	169
3-Layers Soil Profile	171
E-Wetting Front at Field Irrigation Rate	175
F-Field Data for Optimization	177

List of Figures

Figure 1: (a) Geographical position, (b) Topography map, (c) Land-use map and (d) Soil description map of Hasroun village 28

Figure 2: Soil profiles variation with respect to the soil management systems (not to scale) 30

Figure 3: Scheme of the device for wetting front location and surface runoff with volume reading in calibrating cylinder (not to scale)..... 41

Figure 4: Water Infiltration in layered soil media..... 45

Figure 5: Infiltration profile in an unsaturated micropore domain (not to scale) 47

Figure 6: Field experimental setup to optimize the optimal management system with the creation of artificial macropores 58

Figure 7: Physical properties of straw residues and chicken manure 60

Figure 8: CT scanning images for (a) straw residues and (b) chicken manure. On the left, the picture is the result of the CT-scan which is cropped to a diameter of 4cm, after which brightness and contrast are adjusted while filters are applied to convert the picture into 8-bit image with a threshold of two colors 0 (matter) and 255 (pore space) 64

Figure 9: Porosity Distribution for straw residues and chicken manure from the analysis of volumetric contents of pore sizes in ImageJ 65

Figure 10: Soil water retention curve for straw residues and chicken manure (a) and (b) are the simulated SWRC using RETC software vs the calculated values using CT-scans for straw residues and chicken manure, respectively and (c) predicted characteristics moisture of straw residues and chicken manure. Units of α : 1/mm... 66

Figure 11: Bulk, dry, and saturated densities of individual homogeneous layers of different soil management systems in Site 1 – Loamy Sand 68

Figure 12: Moisture volumetric contents for NT, RT, MTA, MT, CC, and MC in Site 1 – Loamy Sand, (a) porosity or saturated volumetric moisture content θ_s , (b) residual volumetric moisture content θ_r 70

Figure 13: OMC Statistical Analysis for NT, RT, MTA, MT in Site 1 (a) Interval plot with 95% CI for the mean, (b) Tukey 95%CI, (c) Fisher LSD pairwise comparison with 95%CI, (d) Dunnett 95%CI with a control treatment NT..... 72

Figure 14: Mean weight diameter (MWD) from the frequency density function of the aggregate distribution (f) in Site 1 for NT, RT, MTA, MT	74
Figure 15: Saturated Hydraulic Conductivity, K_s for individual layer in Site 1 for NT, RT, MTA, MT.....	76
Figure 16: CT scanning images for (a) NT, (b) RT, (c) MTA, and (d) MT in Site 1	77
Figure 17: Porosity Distribution for NT, RT, MTA, and MT from the analysis of volumetric contents of pore sizes in ImageJ in Site 1	78
Figure 18: Fitted van Genuchten parameters for NT, RT, MTA, MT, CC, and MC in Site 1 (α in [1/mm]).....	80
Figure 19: Fitted soil water retention curves for NT, RT, MTA, MT, CC, and MC in Site 1	82
Figure 20: Pore volume distribution PVD functions for NT, RT, MTA, MT, CC, and MC in Site 1	83
Figure 21: Vertical and lateral preferential flow variation along a 40cm soil profile of different soil management systems and under an irrigation rate of 5.18mm/min.....	90
Figure 22: Bulk, dry, and saturated densities of individual homogeneous layers of different soil management systems in Site 2 – Clay Loam.....	92
Figure 23: Porosity and residual moisture content of individual homogeneous layers of different soil management systems in Site 2 – Clay Loam.....	93
Figure 24: OMC Statistical Analysis for NT, RT, MTA, MT in Site 2 (a) Interval plot with 95% CI for the mean, (b) Tukey 95%CI.....	94
Figure 25: Mean weight diameter (MWD) from the frequency density function of the aggregate distribution (f) in Site 2 for NT, RT, MTA, MT	95
Figure 26: Mean weight diameter (MWD) from the frequency density function of the aggregate distribution (f) in Site 2 for NT, RT, MTA, MT	96
Figure 27: CT scanning images for (a) NT, (b) RT, (c) MTA, and (d) MT in Site 2	97
Figure 28: Porosity Distribution for NT, RT, MTA, and MT from the analysis of volumetric contents of pore sizes in ImageJ in Site 2.....	99
Figure 29: Fitted van Genuchten parameters for NT, RT, MTA, MT, CC, and MC in Site 2 (α in [1/mm]).....	100
Figure 30: Fitted soil water retention curves for NT, RT, MTA, MT, CC, and MC in Site 2	101

Figure 31: Pore volume distribution PVD functions for NT, RT, MTA, and MT in Site 2.....	101
Figure 32: Physical, structural and hydraulic properties for NT, RT, MTA, and MT in Sites 1 and 2	105
Figure 33: Soil water retention curves for contrasting individual layers in Sites 1 and 2.....	107
Figure 34: GARALS validation of wetting front depth z_m with experimental observed data	109
Figure 35: GARALS validation of infiltration rate v_m with experimental data computed from observed surface runoff data.....	110
Figure 36: GARALS simulation for different soil profiles exhibiting different combinations of soil management systems under different irrigation rates (0.01, 0.05, 0.1, 0.5, 1, 2, 5, 10, 20, 40cm/min)	117
Figure 37: GARALS simulation for different soil profiles exhibiting different combinations of soil management systems under Site 1 field irrigation rate (0.04cm/min).....	117
Figure 38: Moisture content variation at depth between 20 and 40cm for MTA+NT soil management system (a) MTA+NT replicated in plots 1a and 1b, (b) MTA+NT with empty AM replicated in plots 2a and 2b, (c) MTA+NT with filled AM + crop residues replicated in plots 3a and 3b (the dashed red line is the boundary that indicates the end of the irrigation event)	119
Figure 39: Moisture content variation at depth between 20 and 40cm for MTA+NT soil management system after the end of irrigation experiment	120

List of Tables

Table 1: Soil treatment combinations used in this research work.....	29
Table 2: Physical, hydraulic and structural properties of cover layer materials	30
Table 3: Summary of parameters and properties tested for each tillage system in each site	31
Table 4: Soil particle size definitions.....	33
Table 5: Optimal ranges or critical limits for soil physical quality indicators (Reynolds et al., 2009).....	37
Table 6 [Eq. (25)]: Wetting front depth, L for preferential flow experimental study	41
Table 7: Infiltration into layered agricultural soil with and without ponding.....	44
Table 8: Initial, boundary and physical properties of the experiments for model validation.....	55
Table 9: Initial properties of the different soil management systems for water infiltration simulation.....	56
Table 10: Soil physical quality indicators for straw residues and chicken manure ..	67
Table 11: Location and shape parameters of the PVD functions for NT, RT, MTA, MT, CC, and MC in Site 1	85
Table 12: Soil physical quality indicators for NT, RT, MTA, MT, CC, and MC in Site 1.....	87
Table 13: Location and shape parameters of the PVD functions for NT, RT, MTA, MT, CC, and MC in Site 2	102
Table 14: Soil physical quality indicators for NT, RT, MTA, MT, CC, and MC in Site 2.....	103
Table 15: Cumulative infiltration (Zp) prior to ponding and time of arrivals of wetting fronts to 10, 20, 30, 40cm and z_p measured from the initial surface soil for treatments having wetting front depths larger than 40cm prior to ponding in Site 1 using the field irrigation rate (0.04cm/min)	118

List of Appendices

Appendix 1: Soil Size Distribution - Site 1	153
Appendix 2: Soil Classification - Site 1.....	153
Appendix 3: BD and DD – Site 1	154
Appendix 4: SD – Site 1	154
Appendix 5: Porosity – Site 1	154
Appendix 6: Residual Moisture Content – Site 1	155
Appendix 7: Organic Matter Content – Site 1	155
Appendix 8: Saturated Hydraulic Conductivity – Site 1	156
Appendix 9: Frequency density function (f) of the aggregate distribution – Site 1	157
Appendix 10: Soil Size Distribution - Site 2	158
Appendix 11: Soil Classification - Site 2.....	158
Appendix 12: BD and DD – Site 2	158
Appendix 13: SD – Site 2	159
Appendix 14: Porosity – Site 2	159
Appendix 15: Residual Moisture Content – Site 2	160
Appendix 16: Organic Matter Content – Site 2	160
Appendix 17: Saturated Hydraulic Conductivity – Site 2	161
Appendix 18: Frequency density function (f) of the aggregate distribution – Site 2	162
Appendix 19: BD and DD – CC & MC.....	162
Appendix 20: SD – CC & MC.....	163
Appendix 21: Porosity – CC & MC.....	163
Appendix 22: Residual Moisture Content – CC & MC.....	163
Appendix 23: Organic Matter Content – CC & MC.....	163
Appendix 24: Saturated Hydraulic Conductivity – CC & MC.....	164
Appendix 25: Frequency density function (f) of the aggregate distribution – CC & MC	164
Appendix 26: Volumetric content of pores as calculated in ImageJ.....	165
Appendix 27: Experimental vs Theoretical Wetting Front with respect to time	166
Appendix 28: Time variation of wetting front arrivals at 1cm depth increment	175

Appendix 29: Field moisture content variation with respect to time during and after the irrigation test application..... 177

Chapter One

Introduction

Soils are the basic means that tolerate gaseous, hydrological and nutrient fluxes to pass from the earth's surface to subsoil layers. These systems also structure the habitat for micro-organisms, animals, and plant root growth. Such phenomenon exists in the pore structure of the soil domain which is either filled with water, air or both. Soil pore structure cogitates connectivity, tortuosity, lateral and vertical size distribution of pores. Thus, these parameters are dependent on hydraulic and physical properties, soil type, soil particle size distribution, and surrounding climatic factors (**Kutilek, 2004**). For instance, shrinking and swelling soils, also-called expansive soils, induce porosity changes when subjected to a decrease and increase in soil moisture content, respectively. Affected by the contiguous climatic factors, as moisture content drops, air-filled void spaces are subjected to capillary stresses applied from the surrounding surface of soil particles. This increase in surface tension shrinks soil volume by pulling adjacent soil particles together resulting in smaller pores between inter-aggregates while causing the formation of cracks in which bigger pores are formed. Notwithstanding, the opposite occurs in swelling soils in which minerals in aggregates attract and absorb water favoring pore water pressure over tension surface. Indices such as the Atterberg limits are used to qualify expansive soils: soils have very high, high, medium and low expansion degree for a plasticity index of more than 35, 25-41, 15-28, less than 18, respectively, and a shrinkage limit of less than 11, 7-12, 10-16, greater than 15, respectively (**Holtz, 1959, U.S. Bureau of Reclamation, 1974**). On the other hand, three types of soils are defined: poorly graded soil (PG) that has a uniform grain size, well-graded soil (WG) in which particle sizes are distributed over a wide range, and a gap graded soil (GG) which has a combination of two or more particle fraction sizes (**Das and Sohban, 2014, p. 57**). Pores in PG are uniform between inter-aggregates, have a mixed structure in WG and tortuous paths along the bigger soil particle sizes in GG. Nonetheless, density which is a measure to compare the extent of compaction of soil media affects the porosity in addition to hydraulic parameters such as the field moisture content, soil matric potential, and saturated hydraulic conductivity.

In agricultural systems, good quality soil exists through the optimization of pore structure that contains long, large, and well-connected pores to allow a rapid and satisfying cumulative of water infiltration and nutrients transport to the root zone while minimizing surface runoff. Meanwhile, these fluxes are stimulated not to flow into deeper zones so that nutrients are not wasted and lost into the vadose zones. During non-irrigated periods, the soil domain must have high water holding capacity to maintain water and dissolved nutrients. The water capture and saving condition is essential in agricultural systems that are exposed to the effects of climate change causing more intense and frequent rainfall events and droughts (**Pryor et al., 2014**).

Accordingly, soil management systems are incorporated in the cultivation process to modify the soil media profile. The most ancient system is conventional tillage which consists of altering completely the soil structure to a certain depth. Applications such as moldboard/disk/chisel plowing, rotary harrowing, rotary tiller are extensively used around the world in agricultural systems. Conventional tillage consisted of using human, animal and later on mechanical power at a certain depth to destroy soil clogs (**Alvaro-Fuentes et al., 2008**), aerate soil pores (**Alvarez et al., 2001**), transport nutrients, and increase hydraulic conductivity (**Lindstorm and Onstad, 1984**). Soil disturbance causes small pores to widen by allowing more air to fill in the voids during the movement and rotation of soil layer, thus increasing the total porosity through the intensification of the number of pores of sizes ranging from $0.5\mu m$ to $500\mu m$ (**Osborne et al., 1979; North and Brown, 1982**). Yet, these systems induced problems due to soil disturbance such as soil roughness imposed by post-application of heavy rainfall drops or abrasive winds causing soil erosion (**Govers et al., 1999; Saber and Mrabet, 2002; López et al., 2003**). Hence, erosion causes nutrients losses needed for plant growth (**Yan et al., 2005, 2013; Su et al., 2017; Lal, 2018; Zou et al., 2018; Wang et al., 2020b**). **Hacisalihoglu et al. (2010)** states that erosion detaches soil sediments thus threatening plant growth and soil stability because it transports the part of the soil containing most of the organic matter. It was also shown that higher losses of organic nitrogen, potassium, phosphates and organic matter existed in these systems (**Gómez et al., 2009b**). Replenishing such alterations increases off-site and on-site production costs by about 25% each year (**Pimentel et al., 1995**). Further, high production costs were also observed in conventional tillage systems (**Castellini and Ventrella, 2012**). In addition, some studies found that when whirling the soil in the

tilled layer, embedded moist soil reaches the surface along which it gets exposed more rapidly to evaporation and slower infiltration rates (**Hatfield et al., 2001**). Moreover, prolonged periods of tillage decreased soil degradation (**Yang and Wander, 1998; Mrabet et al., 2001**) pertaining to a decline in soil quality. The exacerbated problems motivated researchers to investigate new methods. It was found that adding organic matter to the soil enhances soil stability by enriching the soil with nutrients and the pore structure allowing for better hydraulic fluxes and water holding capacities (**Findeling et al., 2003**). Hence, new ways to solve the roughness of tillage applications in conventional system are established by incorporating organic matter with soil with potential limited and reduced tillage operation. Exemplars are mulch tillage, reduced tillage, manure tillage, and cover crop. **Gómez et al. (2009b)** noted a reduction in the runoff for crop cover in olive tree cropping plots of 59 mm. year⁻¹ compared to the conventional tillage treatment. Crop covers inhibit soil losses two orders of magnitude smaller than those measured in the conventional tilled plots. In the aforementioned systems, soil disturbance caused by tillage is minimized and organic matter including either crop residues or animal manures are added to the soil surface and sometimes mixed with the soil (mulch tillage and manure tillage) experiencing better enhanced fluxes in soil (**Findeling et al., 2003**) while causing higher crop productivity (**Gómez et al., 2004, 2009a; Triplett and Dick, 2008; Bechara et al., 2018; Bogunovic et al., 2018; Rodrigo-Comino, 2019; Bogunovic et al. 2020**). As such, organic matter coherently aids in fluxes movement by enhancing aggregate hydrophobicity (**Chenu et al., 2000**) and improves soil structure since it works as a binding agent for aggregate formation (**Tisdall and Oades, 1982; Amézketa, 1999; Bronick and Lal, 2005**), thus promoting aggregate stability (**Mamedov et al., 2000; Six et al., 2000; Baumhardt et al., 2004; Pinheiro et al., 2004**) and preventing soil surface crusting or sealing (**Blevins and Frye, 1993; Lascano and Baumhardt, 1996**) which is caused by splash effects of potential energy in heavy rainfall events.

Despite the decline of production costs of conservative tillage in comparison with conventional tillage, a further cheap system (No-tillage) was familiarized by eliminating any tillage application. It is economically beneficial to agriculture (**Blanco-Canqui et al., 2017**) as it constitutes a growing sector for many developing and developed countries (**Kefi et al., 2009**). This method configured higher capacities

to hold water (**Unger, 1994; Drury et al., 1999**) and maintain soil biopores (**Francis and Knight, 1993**) due to the lack of disturbance. Consequently, it creates an environment that facilitates roots to grow deeper and wider (**Martino and Shaykewich, 1994**).

The incongruent systems invigorated researchers to go in depth with their effects on soil physical properties. Yet, the literature proves to have opposing evaluations for systems because the implementation of tillage systems incorporates nuisance factors including site conditions, equipment specifications, climatic factors, and testing errors due to human inaccuracies. Though, temporal and spatial variation of systems majorly influences the assessment of their effects (**Messing and Jarvis, 1993; Prieksat et al., 1994; Coutadeur et al., 2002**). In other words, factors combine the historical management systems applied on the site, the number of years of which the system is applied, the time (which affects climatic and soil conditions) at which sampling and testing are implemented after tillage application (**Alletto and Coquet, 2009**), and the location depending on the soil type, structure, and properties (**van ES, 1993**). For instance, an increase in the hydraulic conductivity occurs after short-term tillage period followed by a decrease during the growing season (**Angulo-Jaramillo et al., 1997; Azevedo et al., 1998; Bormann and Klaassen, 2008**) which is caused by the instability of the porosity created by tillage operations (**Alletto and Coquet, 2009**).

Nevertheless, the disputing evaluation of effects of the tillage system is wide, diligent, and in continuous search for choosing a soil management system that generates soil media of excellent soil quality and copious crop productivity. In general, a perfect system is not applicable, yet a system might be advantageous for a certain agricultural field while not efficient in other fields. For example, **Sauer et al. (1996)** found that conservation tillage systems incorporating residues and mulches surface covers are able to reduce surface water evaporation by 34 to 50% while evaporation rates are increased by 7% on bare stripped soils as found in the no-tillage systems. Additionally, conservation tillage with residue covers had lower soil temperatures than those found in conventional systems (**Allmaras et al., 1964; Anderson and Russell, 1964; Greb, 1966; Wilhelm et al., 1989**). This is beneficial in hot climate periods in which moisture is maintained in the soil media (**Lascano and Baumhardt, 1996**) and unfavorable in cooler seasons in which lower crop growth can assimilate since warmth is needed for microbial activity. Prior to evaporation events, tillage operations increase

in silty clay loam (**Blanco-Canqui et al., 2017**), in loam sand soils (**Lindstorm and Onstad, 1984**), in clay soils (**Negi et al., 1981**) and in sandy clay soils (**Ciollaro and Lamaddalena, 1998**), decrease in sandy loam soils under unsaturated conditions (**Datiri and Lowery, 1991**) and in clay/silty loam soils (**Wu et al., 1992**) or have no effect on hydraulic conductivities in sandy loam soil near saturation (**Datiri and Lowery, 1991**). Similar patterns of increase (**Tanaka and Anderson, 1997; Lyon et al., 1998; Stone and Schlegel, 2010**), decrease (**Unger, 1992; Baumhardt et al., 1993; Blanco-Canqui et al., 2004; McVay et al., 2006**) and no variation (**Unger, 1992; Pikul and Aase, 1995**) are found in no-tillage systems on soil water retention. Such discrepancies are reflected in the assessments of pore structure in different soil management systems. Macropores of sizes greater than 3cm were reduced in no-tillage systems in sandy and silty loam soils when compared with tilled systems (**Schjønning and Rasmussen, 2000**). However, converting from tilled to no-tilled soils, fractions of macropores of sizes between 10 and 50 cm are increased following by a decrease of fractions of macropores of sizes between 3 and 10 cm (**Kay and VandenBygaart, 2002**) due to the effects of swelling and shrinking soils. Although their fractions are considerable small, hydraulic fluxes are enhanced by preferential flows due to the presence of macropores (**Sauer et al., 1990; Reynolds et al., 1995; Moret and Arrue, 2007b; Mubarak et al., 2009b**) while diffusing at a slower rate into the bulk soil matrix (**Gerke and van Genuchten, 1993; Köhne and Mohanty, 2005**). According to **Moret and Arrue (2007a)**, water fluxes are largely maintained by macropores regardless of the tillage system. Macropores are thus naturally formed either through the presence of soil fauna, the action of roots penetration, or the fallouts of shrinking soils (**Tebrugge and During, 1999; Stewart, 2018**). Aside, the concept of artificial macropores (AM) was introduced in experimental studies (**Castiglione et al., 2003; Mori and Hirai, 2014; Guertault and Fox, 2020**) and can be applied to mimic natural structures lacking these pores such as short-termed tilled soil layers. As such, AM were applied in agricultural degraded soils of poor drainage in the objective of ameliorating infiltration rates and enhance crop growth followed by an increase in organic matter (**Mori et al., 2014**).

Nonetheless, the assessment of tillage applications in the literature review is generally applied to an agricultural land (large-scale experimental sites) during the whole period of cultivation of a certain crop either over a one-time life cycle or over a numerous

number of years (**Blanco-Canqui et al., 2017**). The successive and consistent manipulation of lands can exhaust soil media and deteriorate its structure (**Karlen et al., 1994; Pagliai et al., 2004; McVay et al., 2006; D'Haene et al., 2008**). Such practices must be used in the right place and at the right time (**Wall, Nielsen, & Six, 2015**). Hence, prediction of hydraulic fluxes in these systems using a mathematical model is suggested. In the literature, models approximating infiltration rates are alienated between empirical and physical-based models. Their varieties and dissimilarities aggravate a challenge of choosing one that complies to a soil media subjected to different soil management systems. The latter is evidently shown to be affecting infiltration by altering physical properties (**Khurshid et al., 2006**), profile layout (**Sarauskis et al., 2012**), and organic contents (**Alam et al., 2014**) of the soil. Accordingly, the Green-Ampt model (GA) was chosen in this research work because it is proven to be the most flexible physical model which can be modified and adjusted to fit in the abrupt conditions (**Fok, 1970; Hsu and Hilpert 2011; Stewart, 2018**). Different GA were modified by incorporating various modifications on the porous media. Some are interested for the sake of this research work as they resemble the settings presented with the application of the different soil management systems such as presence of cracks, properties of porosity, wettability, interfacial tension, water density, soil grain size, preferential flow, and layering of the soil profile. The development of the mathematical model inquires a restructuring of the GA models.

The outcome model incorporates the effects of different soil management systems on infiltration such as physical, and chemical characteristics of the soil, preferential flow, and layered profile, except for the effects of water/nutrient root uptake. Additionally, it accounts only for short-term effects of the application of soil management systems, while the results and conclusions are only applicable to flat lands subjected to a soil management system under different rainfall rates. On the other hand, the validation is accomplished through experimental testing. The data collection includes soil physical properties for each soil management system. Hence, the systems which are commonly applied by local farmers in the area of testing include no-tillage (NT), rotary tillage (RT), cover crop (CC), manure cover (MC) and manure tillage application (MTA). Yet, the design of experiments is performed in spring 2022. Winter measurements are not possible since the chosen lands are at elevations higher than 1450 meters above sea level, thus they will be covered by snow mainly from January till early March.

The aim of the research combines four fragments: (1) evaluate the effects of tillage systems on soil physical properties, soil structure and soil quality, (2) propose a new methodology to measure preferential flow, (3) propose a mathematical model that simulates water infiltration into layered agricultural soil profile taking into consideration prior and post ponding conditions, and (4) optimize the best soil management system simulated using the restructured Green-Ampt model in loamy sand soils in agricultural fields. Accordingly, the objectives are:

- Prepare design experiments in field and apply six different soil management systems (NT, CC, MC, RT, MT, MTA).
- Test for soil physical properties and structure parameters.
- Prepare an experimental setup to perform rainfall simulation of slow rate on soil profile while taking records of the real wetting front depths which will be compared with the theoretical wetting front.
- Assess the soil profiles having difference between the theoretical and experimental wetting fronts to determine preferential flow depths.
- Model the effects of different soil management systems on the soil, water, and profile properties for different soil types.
- Restructure the Green-Ampt model for layered soil profile.
- Validate the mathematical with experimental measurements results.
- Simulate the infiltration for different soil management systems under different irrigation rates.
- Determine the soil treatment profile using field irrigation rate that infiltrate water more rapidly into higher depths without having surface runoff.
- Optimize the system by introducing the concept of artificial macropores and using crop residues as soil cover to assess the protection of water for longer periods.

The first fragment of the results is important because it adds to the wide body of research patterns that tillage systems can cause to the soil media. Additionally, the assessment can help farmers cultivating in similar soils to choose the optimal system. On the other hand, the developed mathematical model can be used for predicting infiltration rates and solute transport properties for soils subjected to different soil management systems. The prediction allows for a water and soil quantity/quality

assessment prior to the implementation of the soil management system. Additionally, it allocates strategies for implementing integrated management plans for water, soil, and erosion in agricultural systems. A sensitivity analysis can be performed for any soil type in response with applying the best fitting soil management while avoiding waste of water and nutrients in fertilizers percolating into soils. The third part is a model design that farmers can adopt to increase water infiltration to reach the roots of apple trees while watering the vegetables cultivated in between rows.

Chapter Two

Literature Review

2.1 Infiltration

Infiltration is a significant process in the hydrological cycle in which mass and energy exchange take place between surface and subsurface hydrosphere (**Emerson et al., 1978**). It attributes to the overland flow thereby affecting runoff time and flow rates. Modelling infiltration configure a substantial role in mitigation flood risk, controlling groundwater contamination, and managing water supplies in agricultural areas when dealing with root water uptake (**Chen et al., 2019**). Soil constitutes the media that supports this exchange -driven by gravity and driving forces- by comprising inter-connected pores spaces through which channels exist and allow the movement of water and solute transport into vadose zones and later groundwater storages. The process is mainly affected by porosities, hydraulic conductivity, and initial soil moisture content. The porous media is consisted of two domains: solid particles and void spaces (are filled with water and/or air). The pore space is classified into micropores and macropores (**Kutilek and Nielsen, 1964, p. 20**). The micropores, also known as capillary pores, are the domains that contributes to the redistribution and upward flow of water, while the second domain, macropores, subsidizes downward pathways for water. Such flows are similar to water flows in thin films. The phenomenon depends on the porosity content and the pore size, continuity and distribution along a porous media profile. For instance, infiltration is directly related to macro-porosities (**Wang et al., 1986; Horton et al., 1987**) which is influenced by soil densities. **Nassif and Wilson (1975)** found that increasing the soil density allows for a declination in infiltration rates. This hypothesize was also supported by **Pikul and Aase (1995)**, **Bharati et al. (2002)**, **Gregory et al. (2006)**, **Patle et al. (2018)**, and **Harisuseno et al. (2019)**. Moreover, **Fitzmaurice (1997)** identified a positive correlation between porosity and saturated/unsaturated hydraulic conductivity of the soil media. **Voorhees et al. (1986)** tested that as bulk density increased from 1.05 to 1.25 Mg.m³, saturated hydraulic conductivity of a clay loam soil decreased by 50%. The relationship granted the identification of another positive link between infiltration and hydraulic

conductivity. Yet for soil moisture contents, infiltration rates decline with an increasing degree of saturation (**Yen and Akan, 1983**). It was experimentally observed that an increasing soil moisture content affects positively the time of concentration for the precipitated water particle to reach an equilibrium runoff rate, ultimately initiated by a decrease in infiltration (**Harisuseno et al., 2019**). However, this was not evident when infiltration rates were tested in sand columns. It seems that the infiltration rate was higher in pre-wetted sand columns than that in dry columns because the former is affected by a strong dynamic pressure of capillary pressure (**Hsu et al., 2017**).

Other parameters were shown to be associated with infiltration such as soil surface conditions, soil size distribution and texture, presence of stratified soil layers (double layers or more), and distance from water source to the wetting front. Soil surface conditions including surface residues, roughness and soil crusting can alter the infiltration rate thereby affecting the time to runoff. Soil crust for example causes a seal layer on the upper surface of soil. The sealing's hydraulic conductivity is lower than that of the underlying layer thereby causing a decrease in infiltration (**McIntyre, 1958**). On the other hand, **Mwendera and Feyen (1993)** found that delayed surface runoff occurs with an increased surface roughness which is enhanced due to tillage practices. Thus, it was argued in other studies that soil roughness is not as significant as soil residues to impact infiltration (**Bouma et al, 1977**). This concept is further elaborated in the proceeding section. Furthermore, **Patle et al. (2018)** measured infiltration rates using the double-ring infiltrometer on field for different soil size distribution and textures. They found that silt and clay caused a decline in infiltration, whereas an increase was tested for sand and organic matter occurrence. Since infiltration is altered by the type of soil classification, then considering a soil profile of different layers is a prominent justification for modifications of infiltration in such case. The alteration differs on the type of stratification, for example infiltration in a soil profile of two layers is reduced when the wetting front is in a coarse layer lied under a fine layer (**Wang et al., 1999**). **Wang et al. (1999)** found that the thickness of first layer in a case of stratified soil profile changes infiltration rates because it affects the location of the wetting front.

Research has proven that infiltration is yet a process that configures ambiguous progressions that are in need for more clarifications and simplifications. As such, preferential flow is difficult to measure and quantify. It is caused by soil heterogeneity

in which either water or solute or both be transported along preferential pathways such as earthworm burrows, cracks in soil, flow associated with soil layering, bedrocks, roots, and channels formed by buried crop residues or organic matter (**Allaire et al., 2009**). **Hendrickx and Flury (2001)** suggested that preferential flow most probably occurs at shallow depths (up to 3 meters), thus making it significant to account for its effect on infiltration. The effect depends on the position of the matter with respect to that of the preferential flow paths (**Allaire et al., 2009**). Some have found that preferential flow causes a rapid movement of mass, thus causing higher infiltration (**De Rooij, 2000; Jamieson et al., 2002; Lin and Zhou, 2008**).

As a result, it is concise to relate infiltration to various parameters that are all interdependent. The connection is a hard-evidence to relate infiltration rates to a physical-topological model.

2.2 Soil Pore Size Identification

The quality of soil is characterized mainly by its pore structure since it is considered as the domain where all hydraulic fluxes, microbial activity, root penetration and growth, nutrients transport, and all the interaction between the surface and the subsurface happen. To be able to describe such structure, it is important to characterize the pores based on their sizes. Different definitions are found in the literature: macropores are defined as pores with diameter greater than 0.015mm (**Nimmo, 2004**), 0.03mm (**Marshall, 1959; Kay and Lal, 1997**), 0.05mm (**Reichert et al., 2009; Zhang et al., 2021b**), 0.375mm (**Moret and Arrue, 2007a**), 0.5mm (**Luxmoore, 1981; Lin et al., 1996; SSSA, 2008**), 1mm (**Jury et al., 1991**), 1-5mm (**Brewer, 1964**), and 2-10mm (**Reeves, 1980**), while mesopores are those of diameter between 0.06-0.5mm (**Luxmoore, 1981; Lin et al., 1996; SSSA, 2008**), 0.0002-0.03mm (**Kay and Lal, 1997**), 0.06-1mm for coarse mesopores and 0.01-0.06mm for fine mesopores (**Jury et al., 1991**), and 0.15-0.375mm (**Moret and Arrue, 2007a**), and for micropores are those having sizes lower than 0.01mm (**Jury et al., 1991**) and 0.0002mm (**Kay and Lal, 1997**). The classification between macro-, meso- and micropores extends further into a classification that depends on matric potential limits: pores of non-available water (>1500kPa), pores of available water (33-1500kPa), slow drainage pores (10-33kPa), and fast drainage pores (<10kPa) (**Amer, 2012**). Since the

mathematical model is based on characterizing the flow between capillary-induced and flowing-free flows, the classification of pores in this research similar to that reported by **Tuller and Or (2002)** and outlined by **Kutilek and Nielsen (1964, p.20)** are determined as micropores or capillary pores including the matrix (intra-aggregate) that are pores within soil aggregates and the structural pores (inter-aggregate) that are pores between aggregates. Macropores or non-capillary pores in which flows are flown freely. The boundary size between the two categories is 12mm as reported by **Finnemore & Franzini (2002, p.39)** since the effects of capillaries become negligible for larger sizes.

2.3 Soil Management Systems

Soil management systems are of two categories: the conventional tillage including the practice of using either a moldboard plow, chisel plow, disk plow, rotary tiller, or large-disk harrow and the conservative tillage comprising the practice of either no-tillage, mulch-tillage, strip/zonal tillage, ridge-tillage, reduced/minimum tillage, cover crop, and manure tillage applications. The conventional practices involve the use of machinery or large farming implement consisting of one or more blades that are specific and unique to each type and are fixed to a sequence that rotates in the soil media causing the destruction of soil clogs. However, the conservative tillage does not focus mainly on the action of tillage but on the practice of changing the ground layout. No-tillage is the simplest form that doesn't require any operation, thus leaving the soil surface undisturbed (not removing any organic matter is also applicable), cover crop is when the undisturbed soil surface is covered with crop residues, mulch-tillage is similar to no-tillage but the soil surface is minimally disturbed to remove any evidence of soil crust while incorporating crop residues along the disruption (**as cited in Opara-Nadi, 1993**), the strip/zonal tillage is the practice of dividing the soil surface into inter-zones: the seedling zone which is mechanically tilled and the soil management zone which is left undisturbed (**as cited in Opara-Nadi, 1993**), the ridge-tillage is the practice of only disturbing the soil when planting to clean the rows (**Opara-Nadi, 1993**), and the reduced/minimum tillage is the act of reducing tillage.

2.4 Effect of Soil Management Systems

2.4.1 Effect on Infiltration

The significance behind assessing the effects of tillage on infiltration is that the latter can be altered on long-term periods due to only single tillage operation on a no-tilled soil surface (**Kettler et al, 2000**). Studies were performed to investigate the effect of different soil management systems on infiltration. Some studied the effect of tillage on infiltration with respect to no-tilled soils, others argued the efficiency of conventional and conservative practices, and even others compared the practices within each system.

2.4.1.1 Tillage vs. No-Tillage

The act of disturbing the soil provoked by tillage activities reduced infiltration as compared to undisturbed samples (**Edwards et al., 1988; Miyamoto et al., 2001; Akhtar et al., 2011**). The reason is that higher water contents were tested in tilled soils compared to no-till soils (**Fitzmaurice, 1997**). However, modifications in soils such as compaction of the upper soil layer, hindering root growth, and reduction in infiltration can be induced from no-tillage practices on the long term (**Sarauskis et al., 2012**). Tillage improves soil roughness leading to an increase in infiltration (**Mwendera and Feyen, 1993**). It was also disputed that soil bulk density, porosity, penetration resistance, and aggregation were improved by tillage practices in a manner leading to an increase in the infiltration (**Gantzer and Blake 1978; Lindstorm and Onstad, 1984; Karlen et al., 1990; Pikul et al 1990; Khurshid et al., 2006**). Thus, this was refuted by **Haghighi et al. (2010)** in which tillage destroys pore size distribution, number of macro-pores, and the continuity of pores or pathways. The controversy dispute to either consider tillage a good practice for increasing infiltration or not is obviously incessant because all the studies were examined on field, while each carrying different soil and profiles' conditions (effect of spatial variation). Consequently, the contradictions led authors to start examining the effects of different soil management systems instead of comparing infiltration in tillage and no-tillage systems.

2.4.1.2 Conservative vs. Conventional Tillage

Conflicting theories of which system is more favorable to infiltration also exist. Conservation tillage increases the soil bulk density compared to the conventional

tillage (**Afzalnia and Zabihi, 2014**). Yet, it is commonly shown that conservative soil management system provided better infiltration than the conventional system (**Tebrugge and During, 1999; Leys et al., 2007; Singh et al., 2009; VanWie et al., 2013; Alam et al., 2014; Cunha et al., 2015**). **Alam et al. (2014)** investigated the effects of four different tillage practices (zero tillage, minimum tillage, conventional tillage, and deep tillage) on soil properties. They have found that conservational tillage practices allow for an improvement in the physical and chemical properties of soil such as bulk and particle densities, organic matter accumulations, and maximum root densities. The highest organic matter accumulation, the maximum root mass density (0–15 cm soil depth), and the improved physical and chemical properties were recorded in the conservational tillage practices. Bulk and particle densities were decreased due to tillage practices. **Salem et al. (2015)** found that a combination of conventional and conservative systems called the integrated reservoir tillage system increased soil infiltration compared to each system alone producing a rate of 48% and 65% higher than the conservative and conventional systems, respectively. Within the conservative system, cover crop and mulch tillage were found beneficial in many cases as it prevents surface sealing thus reduces runoff when compared to reduced tillage (**Mannering and Meyer, 1963; Bouma et al., 1977; Radcliffe et al., 1988; Trojan and Linden, 1998; Ruan et al., 2001**). According to **Baumhardt et al. (2011)**, the retained wheat residue covers increased the mean cumulative infiltration by depths greater than 25mm compared to bare soils. **Radcliffe et al. (1988)** found that the mulch layer enhanced infiltration when added to layers either conventionally tilled or non-tilled. In Addition, **Wilhelm et al. (1989)** concluded that whatever type of management system is used, applying residues on the soil surface increased soil moisture contents due to decreased evaporation. This was proved with the addition of poultry manure to soil (**Adeyemo et al., 2019**). However, this trend is affected by the application rate of which values between 6 to 10 Mg/ha tend to reduce infiltration rates due to the formation of slurry (**Haraldsen and Sveistrup, 1994**). However, for long-term periods manure applications tend to intensify macropores through the activity of microbes (**Mubarak et al., 2009a**). On the other hand, within the conventional system, the disk harrow practice reported to increase soil porosity and reduce bulk densities thereby increasing infiltration when compared to the chisel practice (**Dahab, 2011**). Moreover, **Leghari et al. (2015)** found that both the disc plow and the cultivator enhanced infiltration, thus the disc plow is more advantageous.

2.4.2 Spatial Variation on Soil Physical Properties and Structure

As defined by **Acton and Padbury (1993)**, soil quality is attributed to any soil property that affects the potential of soil to acquire a certain function. In this section, variations of soil quality due to tillage systems are presented in this section which proves that such operations affect majorly the quality of soils in particular in agricultural land-uses. **Karlen et al. (1994)** evaluated soil physical properties of silt loam soils in a temperate area where long-term tillage was applied for 12 years. The land was left undisturbed for one year prior to moldboard plow, chisel and no-tillage operations were applied. They found that water content was significantly higher in no-till plots in the top 5cm soil profile. Water contents corresponding to soil matric potentials between -100 and -1500kPa were higher in no-till plots, between -1.3 and -100kPa no significant differences occurred while for lower potentials poorer water content was available which reflects a structure of small pore sizes in no-till plots. However, in the same plots, turbid metric measurements of water stability for aggregate of sizes 1-4mm showed that these pores were more stable. Tillage treatments accelerated the decomposition of organic matter which are incorporated with soil aggregates at greater depths (between 15 and 20cm). In these depths, results in tilled systems of higher volumetric water contents due to higher capacities of water retention of small pore aid in the decomposition of organic matter. Nitrogen concentrations at shallow depths (0 to 2.5cm) were almost twice as high in no-till plots and in chisel treatments at greater depths (7.5-15cm) while decreased in intermediate depths in the plow plots. Peak and minima concentrations of phosphorous and potassium were found at shallow depths (0-2.5cm) and deeper depths (7.5-22.5cm) in no-till plots, respectively which is not the case in subhumid region (**Buschiazzo et al., 1998**). Differences due to tillage systems affecting soil physical, chemical, and biological properties become negligible at depths greater than that at which the tillage operation was applied (**Buschiazzo et al., 1998; McVay et al., 2006**). In the modified layer, bulk density was lower in loam, sandy loam and sandy soils in conservation tillage systems when compared with conventional systems (on-going for 5-11 years) in a subhumid and semiarid region because the soil particles are loosened due to tillage effects (**Buschiazzo et al., 1998**). However, lower densities were found at deeper depths in conservation tillage (**Buschiazzo et al., 1998**) because such systems having higher organic matter contents promote soil biological activities activated by earthworms (**Lal, 1976**). A different assessment of properties was found by **Ferreras et al. (2000)**

who reported no variation in bulk density in a clay loam soil (in a humid-subhumid mesothermal region) subjected to long-term no-tillage and conventional tillage treatments due to temporal variation effects of sampling with respect to operations implementation resulting in an equilibrium state of settlement that the aggregates reach. In addition, both plots experienced a low structural stability due to the fact that the practices were initiated on a soil of low degradation condition.

While small pores in no-tillage systems were addressed as an advantage to improve water holding capacity (**McVay et al., 2006**), they can cause compaction converting pore structure to a closed system in which root growth tend to be difficult and ineffective (**Fabrizzi et al., 2005**). Additionally, compaction in the undisturbed layer in tilled soils can be induced by machinery operations (**Ess et al., 1998**). Still, resistance to compaction varies between soil types; higher values are found in soils rich in clay and organic matter contents (**McVay et al., 2006**). Aside, adding organic residues to soil is an efficient method to upgrade the quality of soil regardless of the tilled system used. In this regard, **Shirani et al. (2002)** reported that soil physical properties including organic matter content, bulk density, saturated hydraulic conductivity, and aggregate mean weight diameter are affected only by the addition of manure in arid climate to fine-loamy soils subjected to conventional tillage (moldboard plowing) and conservation tillage (reduced tillage with shallow disk harrowing). In their study, the soil exploited extensively with conventional tillage practices followed by 4 years fallowing had initially a low organic matter content. Thus, the addition of manure improved the organic content after 2 years, decreased the bulk density by 12 and 16% (applying 30 and 60 Mg.ha⁻¹ of manure, respectively), increased significantly the saturated hydraulic conductivity and the aggregate mean weight diameter. Other advantages for adding organic matter is temperature regulation. Hence, it was tested that the mean soil temperature under cover crop soil surfaces was lower than under tilled systems (**Fabrizzi et al., 2005**) due to the high solar reflectivity and low thermal conductivity of crop residues (**Al-Darby and Lowery, 1987; Cox et al., 1990; Schinners et al., 1994**). On the other hand, not the same results are obtained when adding straw instead of manure to soils. In the same type of soil reported in **Shirani et al. (2002)** but in a cool temperate environment and soils exploited on a long-term period of conventional systems. **Singh and Malhi (2006)** found that the bulk density, the aggregated size distribution, and the infiltration rate were not affected by the

addition of straw but on the type of soil and tillage systems, favoring higher values in no-till systems. However, penetration resistance was reduced to a depth of 12-15cm in no-till areas when adding the organic matter which supports the initial hypothesis stated by **McVay et al. (2006)**. This was not applicable in a different study where the penetration resistance was higher in the top 2cm in cover crop plots when compared to moldboard plowed plots with incorporated shredded residues in a clay alluvial soil located in a Mediterranean region (**Martinez et al., 2008**). Similarly, bulk density did not vary which is not consistent with the pore size distribution that resulted in more micropores in no-till plots. Besides, infiltration rates were lower in the cover crop plots since tillage increase the portion of fast draining pores. Further, the aggregate size distribution changed as the size decreased in cover crop with depth opposing to the other treatment. Aggregate sizes larger than 2mm were more abundant in cover crop plot especially in the upper layer due to the accumulation of organic residues. In fact, the mineral particles attached to clay are bonded to organic matter to form macro aggregates (**Tisdall and Oades, 1982; Bossuyt et al., 2002**). This implies that the larger the aggregate sizes are, the smaller micropores are created resulting in higher water potentials and thereby more time to unsaturated. Consequently, tightened pores filled with water for a longer time affect root respiration and growth. In this regard, no-tillage systems reported an inadequate soil aeration especially with the non-existence of cracks (**Castellini et al., 2013**).

2.4.3 Effect on Preferential Flow

Preferential flow is defined as the unequal or non-equilibrium flow path that fluids undertake hastily than others during an infiltration event in a porous media, mostly soil (**Gerke, 2006; Cheng et al., 2011; Ranjit Kumar et al., 2017**). Applicability of such flows mainly occurs in macropores and cause lateral exchange between domains in the form of adsorption and absorption (**Weiler and Naef, 2003**). It is influenced by the pore structure including pore size distribution, pore sizes and the extent of their continuity (**Jarvis, 2007**), by the physical and hydraulic properties of soil and by the impact of incorporated soil management system (**Andreini and Steenhuis, 1990**). For instance, non-tilled soils are known to be conducive for preferential flows (**Andreini and Steenhuis, 1990**) while adding vegetative cover on the soil can decrease these flows (**Stumpp and Maloszewski, 2010**). Similarly, tillage applications induce pore structure heterogeneity along the soil profile by destroying the dimension, continuity

and longevity of pores, thus decreasing preferential flow paths (**Hangen et al., 2004; Gerke et al., 2009; Badorreck et al., 2010**). However, this was reverted by **Petersen et al. (2001)** since tillage transform soil into a well-structured media, thereby creating new network of interconnected pores in which preferential flows are initiated. In addition, **Kodešová et al. (2015)** reported that organic matter affects positively dye coverages area because organic matter acts as a coating for soils and thus enhancing infiltration between the coated aggregates while preventing the flux between smaller pores (**Kodešová et al., 2012**). Accordingly, preferential flows are descriptive of the multi-moving front in a domain of several permeability. These flows, eminently found in hydrogeological simulations, can be visualized, identified, and quantified using dye tracer experiments (**Steenhuis et al., 1990; Flury and Fluhler, 1995; Flury and Wai, 2003; Ohrstrom et al., 2004; Kodešová et al., 2010; Schneider et al., 2018; Zhang et al., 2021a**). This method provides a way to reflect the hydraulic properties of the soil media through the analysis of dye coverages areas and locations (**Zhang et al., 2021a**). Therefore, it is important to choose dyes that can color the areas in which the hydraulic flux actually passes, while be able to have high tendency to travel in water and doesn't have harmful effects on recipient bodies. Thus, the dye opts to be visible, nontoxic, and to have similar hydraulic properties as the fluid (water in this case) (**Flury and Fluhler, 1994**). In this concept, visibility means reactivity, nontoxicity is referred to humans, fauna, flora, and the environment, while similarity is conservative or having low retardation (**Cao et al., 2020**). This is why Brilliant Blue FCF (C.I. Food Blue 2, Chemical Formula $C_{37}H_{34}N_2Na_2O_9S_3$) is consistently used in the dye tracer experiments (**Flury and Fluhler, 1995; Kasteel et al., 2002; Mon et al., 2006**). The method proved to be efficient in delivering images that can be assessed effortlessly either by eye observations or by image analysis software (**Mooney and Morris, 2004**). Based on the eye observation reasoning, in this study we will suggest a new methodology for preferential flow determination.

2.4.4 Macropore Significance

An extensive review of the literature proves that the structure of pores in the soil media affects undeniably hydraulic fluxes and retention (**Lin et al., 1996**), root growth, and crop productivity. This property is the most significant between properties that is altered due to tillage systems (**Hill, 1990; Tagar et al., 2017**). As it was described in many studies, tillage practices destroy macropores formed by cracks, animal burials,

and roots (**Gao et al., 2019**). Since these practices tend to ameliorate root penetration and growth (**Lal and Shukla, 2004**) and enhance crop productivity by mixing the organic matter with soil in deeper layers, adding macropores within these systems is efficient. Accordingly, **Salem et al. (2014)** studied the effect on four tillage systems (conventional tillage, minimum tillage, cover crop and reservoir tillage which is similar to minimum tillage with the addition of artificial macropores through the creation of mini-depressions or holes after planting using a hand-pushed tool with a truncated square pyramid shape) on soil physical properties. Operations resulted in higher bulk density in cover crop followed by reservoir tillage, then minimum tillage. The last two systems differed due to the effect of hand-pushed tool that was used to create the artificial macropores. Further, reservoir tillage showed a negative impact on soil temperature with respect to minimum tillage, positive results in terms of crop yields with respect to the other treatments and intermediate values of soil water potentials between cover crop and minimum tillage. The authors encouraged farmers to start using this technique especially when desired to shift from conventional to conservation systems to reduce production costs. Alternatively, **Colombi et al. (2016)** investigated the effects of artificial macropores of 1.25mm diameter using a stainless steel wire injected in compacted soils. Even though soil bulk density was not affected, such application improved oxygen concentrations, thus treating hypoxia. Discrepancies in bulk densities are caused by the increased root density occurred towards these macropores. Consequently, it reimbursed decreased robustness needed for plant growth caused by soil compaction. However, the problem with empty artificial macropores is that they tend to clog and collapse after a prolonged period of infiltration event (**Mori and Hirai 2014**). Remediation was observed when adding either clay, organic residues or natural polymers (**Mori et al., 1999**). As such, **Mori et al. (2014)** filled artificial macropores (10mm) with fibrous material (glass fiber) in poorly drained soils. Other than increasing vertical infiltration as in an empty macropore, the structure was enforced by the glass fiber. However, the artificial macropore did not function properly for rainfall intensity greater than 80mm.hr⁻¹. Artificial macropore in the literature range from 1 to 5mm (**Lamy et al., 2009; Mori et al., 2014; Mori and Hirai, 2014; Guertault and Fox, 2020**). Hence, flow in these pores are driven by capillary pressure. The only study to the knowledge of the author that used artificial macropore of size greater than 12mm (non-capillary flow conducts as it was indicated in section 2.2) is that of **Zhang et al. (2021b)**. Artificial vertical

boreholes of diameter 16mm were entrenched in bare saline soils. However, fine sandy particles were used to fill these holes for a similar objective of that of **Mori et al. (2014)**. Consequently, such fillings are not practical for usages in agricultural soils, therefore, further evaluation and application of artificial macropores not only in compacted soils is desirable to study the hydraulic fluxes and their patterns.

2.5 Infiltration Models

Infiltration models are either empirical or physical-based models. The most common and used models are: Kostiakov, Horton, Green and Ampt (GA), Richard's equation, and Philip model. **Cunha et al. (2015)** compared infiltration rates of three different soil management systems: conventional tillage, no tillage and minimum tillage measured using the classic double-ring infiltrometer method with calculated rates using different empirical models: Kostiakov, Kostiakov-Lewis, and Horton. The calculated infiltration rate that best fitted the field measured rates was Kostiakov model, in the no-tillage system, meaning that none of the empirical models was able to fit the tillage/soil management system effects. Alternatively, only physical models will be evaluated in this work in the process of choosing that best fit the suggested model.

The Green-Ampt method is a quasi-physically based model that is derived from the principle of conservation of mass with combination of Darcy's law and is applied to one-dimensional vertical flow through a soil column that is partly saturated and do not include a shallow water table (**Green and Ampt, 1911**). It assumes that two zones exist as continuous ponding is maintained at the surface: an upper saturated zone and a lower unsaturated zone that are divided by a sharp wetting front. It also assumes that infiltrated water maintains a uniform moisture content as it moves down into the lower zone (**Green and Ampt, 1911**). Just so, another physical equation is the Richards equation obtained by mass conservation and Darcy's law (**Richards, 1931**). The equation is implicit which makes it hard to use. Thus, **Philip (1957)** found an explicit solution for the Richards equation by assuming boundary conditions inspired from those imposed in the Green-Ampt model. However, Philip's model is not taken into consideration since the Green-Ampt model proves flexibility in incorporating many effects.

Other than the complications of setting the initial and boundary conditions, the implicit form of the Richards equation makes it in need for numerical solutions because of its non-linearity (**Caviedes-Voullième et al. 2013**). In addition, such solutions confront divergence issues when simulating infiltrations (**Zha et al. 2017**). **Lee. et al. (2020)** stated that solving the Green-Ampt equation for two-layered soils is less extensive than solving the nonlinear partial differential equation, the Richards equation. Subsequently, the Green-Ampt model is chosen. The flexibility of such model to incorporate different parameters affecting infiltration is described in the following section.

2.5.1 Green-Ampt Model

The simplicity of the GA allowed researchers to raise questions of whether the model can be applicable to all cases. Experimentally, it was shown in column infiltration that the pressure head at the front depends on the flow velocity (**Weitz et al., 1987; Geiger & Durnford, 2000; Annaka & Hanayama, 2005**) as this opposes to the applied assumption in the GA (the soil-water suction is constant as the wetting front advances). In this regard, **Hsu and Hilpert (2011)** adjusted the GA into a modified Green-Ampt model (MGAM) by correcting the suction head at the wetting front and including parameters of porosity, wettability, interfacial tension, water density, and soil grain size. The dynamic effect of the capillary pressure was accounted for more precisely in the MGAM than the classical GAM (**Pellichero et al., 2012; Hsu et al., 2017**). Thus, computing the infiltration using the MGAM is complicated as it includes fitting parameters which are unique to the testing media. The researchers validated the model with experimental infiltration data according to fitted parameters that were computed originally using the same experimental data. This analogy is inapplicable in this work. Alternatively, an approach named “Moving Multi-Fronts” is developed to account for the saturated and unsaturated flow dynamics by discretizing the model variables themselves including the pressure head, the water contents and the hydraulic conductivity of the soil (**Alastal & Ababou, 2019**). Meaning that the homogeneous soil profile is divided into multiple vertical zones, while each zone subsidizes its own hydraulic properties replacing the single wetting front into multi-fronts. This method can account for the non-linear behavior of the moisture content in the soil during infiltration, however gets complicated for a layered soil profile in which some wetting fronts might reach the bottom of a certain layer before other. Consequently, the

potential to have lateral infiltration is desired especially when the infiltration capacity of the underneath layer is smaller than that of the underlying layer.

In addition, derived GA models were developed for heterogeneous soils. The model of **Beven (1984)** as such for non-uniform soils is only applicable to a soil profile adhering to an exponentially decreasing saturated hydraulic conductivity with depth and to a constant storage-suction. Alternatively, **Selker et al. (1999)** proposed that the storage-suction product is not constant, as it is affected by the change in the pore size. Thus, they assumed that as the pore size decreases following the power law, the hydraulic conductivity drops with the square of the pore size and the wetting front pressure increases linearly with respect to the wetting front depth. Hence, their assumption of a linear decline in particle size might not be the case in our research. Later, heterogeneity became more generalized in the concepts of layering soils and preferential flow generated in the macropore domains. Researchers promoted the concept of macropore-micropore domains. **Stewart (2018, 2019)** accounted for the presence of macropores in the porous media. The model was the summation of infiltration corresponding to each domain (soil matrix and macropore domain). Cracks including either small-scale inter-aggregate shrinkage crack or inter-block cracks surrounding the soil matrix are inducers of preferential flow as it was mentioned in the first section of this division. Thus, the models of **Stewart (2018, 2019)** cannot be directly applied to determine the infiltration; the model included parameters that cannot be directly obtained neither experimentally nor theoretically such as the hydraulic conductivity of the aggregate and inter-aggregate domains (such parameters were experimentally fitted in this research work). Similarly, **Liu et al. (2016)** assumed that the cumulative depth of infiltration is the sum of the cumulative depth of infiltration in diffuse-flow domain and in source-responsive domain. For the purpose of developing such model, the infiltration diffuse-flow domain was based on the GA, while the other was related to the model of flux of diffuse and preferential flow by combining the Darcy–Buckingham law and the continuity equation (**Nimmo, 2010a**). **Nimmo (2010b)** assumed that the unsaturated flow in the source-responsive domains or macropores is typical to the flow in free-surface films lined by pore walls from only one side by an imaginary flat plate of a fixed length and width that are largely compared to the film thickness. However, when the macropore space is fully saturated, the assumption is no longer valid since the saturated flow of water is now completely

bounded by the pore walls. In addition, macropore flows may have different cross-sections (rectangular cracks, circular tubes, etc.) and may be tortuous. Besides, when modeling water infiltration into multi-domains, researchers don't recognize evidently the interaction between such domains, assuming no exchange of water (**Sternagel et al., 2019; Stewart, 2019**). The interaction which can be from both domains is still considered a challenge since several factors must be considered (**Simunek et al., 2003; Weiler, 2005**). As it was defined in section 2.2, the sizes of macropores are beyond 12mm. Notwithstanding, all soil management treatments applied in this research shall prove that their application inhibit the occurrence of such pores in the cover and modified layers by breakage and crop/manure macropore filling effects. Thus, the problem resides in the macropores formed by shrinkage crack at the top of no-tillage treatments (**Vogel et al., 2005**). However, these cracks are assumed to be negligible for continuously cultivated soil. In addition, these large pores are also found in the underneath unmodified layers formed by animal buries (**Li and Ghodrati, 1995**) and root penetrations (**Angers and Caron, 1998**). Such consideration is neglected as it is not in the scope of this work.

Nevertheless, GA models prove to be efficient in incorporating the most significant parameters to this research work that is the profile of the soil. The first attempt of deriving infiltration rates from the GA for a soil profile of n layers was by **Fok (1970)**, followed by **Moore and Eigel (1981)** for two layered soil. The derivation of the later was based on the modification of the GA developed by **Mein and Larson (1973)**. Both models were only valid for steady rainfall event. Hence, for unsteady rain, a model for multilayered soil was extended by **Jia and Tamai (1997)** and later modified by **Chu and Mariño (2005)** and **Liu et al. (2008)**. Later models for layered soils focused on determining equivalent values for layered soils of the physical parameters found in GA as such modifications adhere to the efficiency of determining more accurate infiltration rates. According to **Ma et al. (2010)**, the hydraulic conductivity for wetted zone is equal to the hydraulic conductivity at residual air saturation (suggested by **Bouwer (1966)** to be equal to the half of the saturated conductivity) because above the wetting front, the soil pores are not actually fully filled with water (**Bouwer, 1969; Hammecker et al., 2003**). **Ma et al. (2010)** introduced a saturation coefficient that is equal to the ratio between measured moisture volume and total saturated moisture volume of the wetted zone. It is used as a correction factor for the

hydraulic conductivity and the soil water content of the saturated zone. Additionally, the suction head at the wetting front is determined by using either the method of **Bouwer (1969)** or that of **Neuman (1976)**. Such parameters were employed in the GA model for layered soils developed by **Han et al. (2001)**. Hence, the modified model of **Ma et al. (2010)** was later improved by **Chen et al. (2019)** by introducing two saturation coefficients, one for correcting the hydraulic conductivity and the other used for the soil moisture content since using the same correction factor for both parameters induces errors. However, this model is only applicable to fine-textured soil with a coarse interlayer and induces difficulties in determining the saturation coefficients. Still, a residing problem in the model is that it replaces the original saturated hydraulic conductivity by an average value when the wetting front moves from layer i to layer $i + 1$. However, the average value is constant and is independent on the location of the wetting front location. Regardless of the accuracy to average the hydraulic conductivity rather than using an equivalent value that takes into consideration the wetting front location, the simplification is inefficient when computing the model and desiring to continue the simulation of infiltration beyond the initial chosen depth. Thus, a new average hydraulic conductivity must be calculated resulting in repeating the simulation all over again. In the same context, **Lee. et al. (2020)** developed a GA for two-layered soils. They suggested that it was more effective to determine the maximum saturated depth of the top layer, meaning to anticipate whether the wetting front will reach the bottom layer or not. In addition, this model did not consider an equivalent hydraulic conductivity for a layered soil domain in the computation of cumulative infiltration. This neglects the heterogeneity by shadowing the effects of the upper layer when water reaches the bottom layer. Nonetheless, a model was developed by **Mohammadzadeh-Habili & Heidarpour (2015)** for n-layered soil profile taking into effect the wetting front location in the computation of the hydraulic conductivity but no corrections were made to the parameters of the original GA. The model described the flow of water, the time-variance, and the depth of the wetting layer in a layered soil profile, while each layer possessing unique hydraulic parameters but only for ponded boundary conditions. Thus, no consideration was taken into account for rainfall smaller than the infiltration capacity of the layered soil. Lastly, **Chu (1985)** and **Damodhara Rao et al. (2006)** were the only researchers -to the knowledge of the author and after an extensive search for related published papers- to develop a model suitable for tilled systems. Their model similar to that of **Mohammadzadeh-Habili &**

Heidarpour (2015) targeted only three-layers: a crust, a tilled layer, and a subsoil layer. The crust layer forms either by the impact of rain drops (**McIntyre, 1958**) or after water erosion happens prior to overland flow (**Eisenhauer, 1984**). Thus, the crust layer only forms on the long-term after the operation of tillage, which is not the case here as the study is carried out on the short-term prior to tillage application. However, the methodology used to develop the model for infiltration in micropore domain driven by capillary pressures is similar to the used by **Damodhara Rao et al. (2006)**, while taking into consideration pre- and post- ponding conditions (which usually occur during irrigation events in agricultural soils) as derived similarly in the study of **Mein and Larson (1973)**.

2.5.2 Infiltration in Dual-Permeability Soil

Dual-permeability is a concept that defines a soil structure having two domains: macropores imbining spontaneous fast flow while micropores in which slower flow takes place (**Simunek and van Genuchten, 2008; Köhne et al., 2009a, 2009b**). Hydraulic fluxes in such domains were modeled (**Beven and Germann, 1981; Germann and Beven, 1982; Coppola et al., 2009a; Nimmo, 2010b; Lassabatere et al., 2013; Liu et al., 2016; Stewart, 2019**). Thus, they did not include any exchange between domains. On the other hand, the assumption that both domains obey Darcy's law is invalid in soils with macropores (**Coppola et al., 2009a**). Thus, the GA model which is a derivation of Darcy's law can be used to model the flow in micropore both vertically and horizontally (**Weiler, 2005**). Flows in macropores differ from those in micropore is when neither soil particles nor capillarity constrain the flux as if water is flowing vertically in a long-standing pipe with a certain cross-section while the boundary is formed of soil particles (**Nimmo, 2010b**). The effects of capillary as mentioned before are restricted to the sizes of pores. Hence, water particles are attracted by the surface tension formed between water and soil. However, when pore size gets bigger, the surface tension to hold all the water particles from all sides become negligible with respect to the pressure gradient of free-water flow. In this regard, the kinematic wave equation or the Hagen-Poiseuille equation is increasingly used to model flow in non-capillary pores (**Ahuja et al., 2000; Zehe and Fluhler, 2001; Malone et al., 2004; Coppola et al., 2009a, 2009b**). Yet, discrepancies were found between experimental and analytical data because macropores were not only conducts of preferential flow, but also a source of flow to the surrounding matrix (**Castiglione**

et al., 2003; Lamy et al., 2009) while the models did not take into consideration the interaction between the macropore and the surrounding domain. Nonetheless, the exchange happens laterally (**Beven and Germann, 1982**) and was numerically and experimentally simulated by **Castiglione et al. (2003)**. Thus, water exchange between domains was modeled using the first order approximation with the assumption of mobile-immobile domains which created a problem in estimating an appropriate value for the transfer rate coefficient. The exchange phenomenon is dependent on the hydraulic conditions of domains: if the macropore is saturated, water will move from this domain to micropore and vice versa (**Beven and Germann, 1982**). Since the flow in macropore domains will be more rapid than that in the matrix domain, exchange between both domains will only occur from the saturated macropore to the unsaturated micropore. **Beven and Germann (1982)** added that the process of water exchange from the macropore to the matrix and the interaction with the water present in the micropores is a function of time and geometry of both domains. When domains are saturated, exchange is limited as **Sternagel et al. (2019)** assumed that the lateral exchange becomes negligible in comparison with the vertical advection of water.

The complexity to capture the exchange moved researchers into using numerical software to compute infiltration rather than creating a complex mathematical model which will eliminate the preference of using such models over others. Exemplars used in the simulation of water flow in dual permeability soil domains are HYDRUS-1D, echoRD model, LAST-model (**Lassabatere et al., 2013; Sternagel et al., 2019**).

Chapter Three

Methodology

3.1 Physical, Structural and Hydraulic Properties

3.1.1 Testing Sites

The field experiments are located in Hasroun village situated in the district of Bcharreh in the Northern governorate of Lebanon (as shown in Figure 1-a). The study area sited along the valley of Quannoubine is exposed to a great deficit of altitude from southern highest of 2300 m above sea level (absl) to northern lowest of 1000 m absl (Figure 1-b). However, most of the lands are agriculturally exploited (Figure 1-c) through the application of ground leveling due to the adequacy of soil for cultivation usages (Figure 1-d). The region is characterized by a Mediterranean climate. Annual mean snow precipitation of 500mm extends from December to early March having a mean temperature of -5°C . This period is known as the resting period in which cultivation halts. Warmer periods prolong from April to June (sowing period) and from September to November (harvest period) with a mean rain precipitation of 10mm and a mean temperature of 15°C . The remaining months are exposed to a dry spell, thus conveying the highest annual temperatures, around 35°C . Agricultural systems in that area depends on the type of soil, the type of cultivation, and the production costs. The common practices are rotary tillage, manure tillage, manure cover (especially after harvest period before winter), and no-tillage. Two experimental sites having different soil textural and hydraulic properties are chosen from disparate agricultural fields. The first testing site, denoted by "Tawbe" (Lat. $34^{\circ}13'17.65''\text{N}$, Long. $35^{\circ}57'36.10''\text{E}$) and having the highest altitude of 1900 m absl, is formed of loamy sand soil (USCS: well-graded sand, LL=54.63, PL=44.06, PI=10.57). The site was converted from a heath to a cultivated land of sweet cherry (*Prunus avium*) and Firecracker™ Red Flesh Apple (*Malus domestica*) trees and in-between leaf vegetables, common bean (*Phaseolus vulgaris*) and potatoes (Irish potato, white potato, *Solanum tuberosum* L.) almost fifteen years ago. Rotary tillage and the application of manure and fertilizers was annually implemented. The second testing site (Lat. $34^{\circ}14'35.03''\text{N}$, Long.

35°58'0.25"E) designated by “Aren” is at 1355m absl and formed of clay loam (USCS: sandy fat clay, LL=61.41, PL=32.42, PI=28.99). The area was cultivated by a wheat/potato yearly rotation and managed using traditional tillage methods for more than 20 years after which pear trees with no-tillage system was instigated. Thereafter, the abandoned region was turned into a heath in the late 90s until 2019 in which wheat cultivation was realized again with no-tillage system.

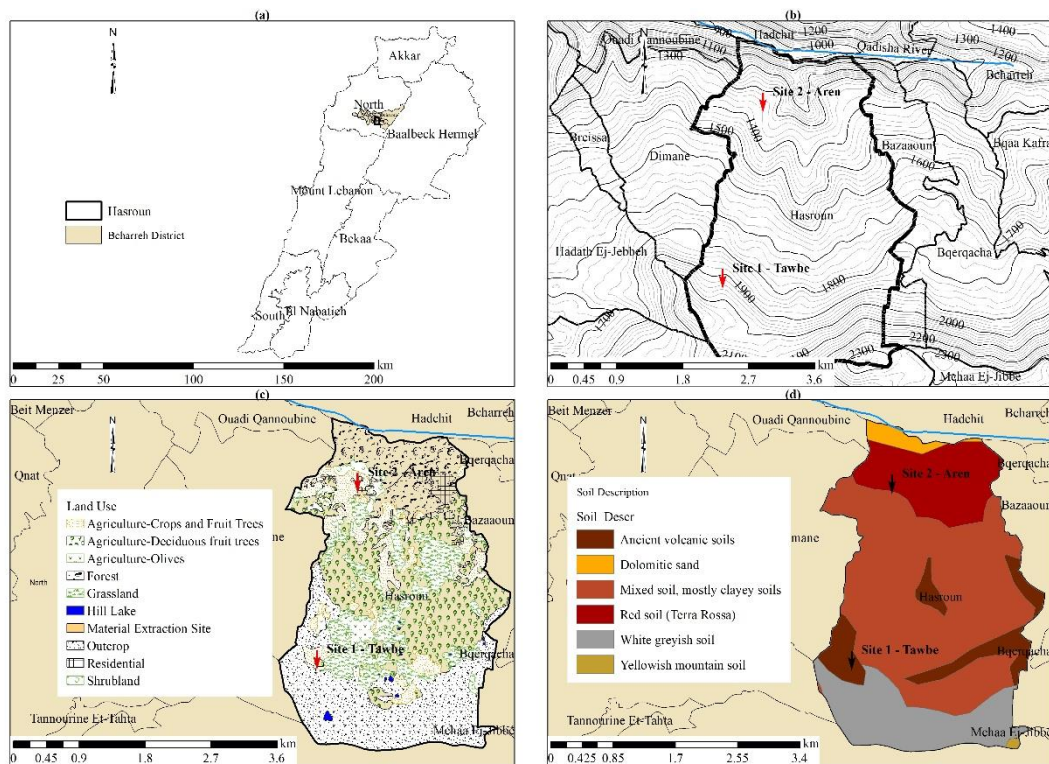


Figure 1: (a) Geographical position, (b) Topography map, (c) Land-use map and (d) Soil description map of Hasroun village

3.1.2 Experimental Design and Land Preparation

The experiment is arranged in randomized design block (Adeyemo et al., 2019) with 6 plots (as shown in Figure 2 first row). Each plot size is 2m x 2m (~4m²) buffered from the next plot by a 2m x 1m zone. Samples were only removed from the top layers, hence the studied depths differed from one plot to other. Six treatments are evaluated: No Tillage (NT), Rotary Tillage (RT), Chicken Manure Tillage Application (MTA), Mulch Tillage (MT), Crop Residues Cover (CC), and Chicken Manure Cover (MC). The conventional tillage methods (RT, MTA and MT) are implemented both using a

rotary tiller. A chain of rotary blades is fixed at the front-bottom of the tractor which rotates when the engine is turned on allowing the blades to cut the soil. In addition, a rail secured at the backward-bottom of the machine is embedded in the soil allowing a mass balance between the farmer holding the dynamic instrument and the machine itself. The only difference between RT and the other methods is that a layer of 5cm chicken manure is added to the soil for the MTA plot so that the tilled soil layer is mixed with the manure (equivalent to an application rate of ~173tons/ha) while a layer of 5cm crop residues is added to the MT plot (equivalent to an application rate of ~42tons/ha). Physical, structural and hydraulic properties of the cover layers' materials are found in Table 2. The conservative methods require less physical work in that the NT plot is left completely undisturbed. In the CC plot, a 5cm layer of residues mixed of straw, hay and stubble are added to the top soil surface. Duplicate to CC, chicken manure is used instead of residues for MC plot. Such notations will only be used to objectify the type of application used on the corresponding layer. As such, CC+NT would be defined as the soil profile formed of a top layer CC which are crop residues resided on an intact/unmodified layer (NT). As this stands, all layers have a bottom intact/unmodified infinite layer designated as NT. The depths of layers are fixed as 5cm for covers, 20cm for modified layers. Table 1 summarizes the different combinations used to determine the infiltration rate.

Table 1: Soil treatment combinations used in this research work

Treatment Designation	Number of layers	Depth of layer above NT (cm)	Description (above NT layer)
NT	1	0	The soil is left as is
CC+NT	2	5	The soil is covered by crop residues
MC+NT	2	5	The soil is covered by chicken manure
RT+NT	2	20	The soil upper layer is tilled
MTA+NT	2	20	The soil upper layer is tilled while mixed with chicken manure
MT+NT	2	20	The soil upper layer is tilled while mixed with crop residues
CC+RT+NT	3	5+20	The tilled upper layer is covered with crop residues
MC+RT+NT	3	5+20	The tilled upper layer is covered with chicken manure
CC+MTA+NT	3	5+20	The mixed tilled and manure layer is covered with crop residues
CC+MT+NT	3	5+20	The mixed tilled and crop residues layer is covered with crops
MC+MT+NT	3	5+20	The mixed tilled and crop residues layer is covered with chicken manure
CC+MC+NT	3	5+5	A chicken manure layer is overlaid by a crop residues layer
MC+CC+RT+NT	4	2.5+2.5+20	The tilled upper layer is covered with crop residues then with manure

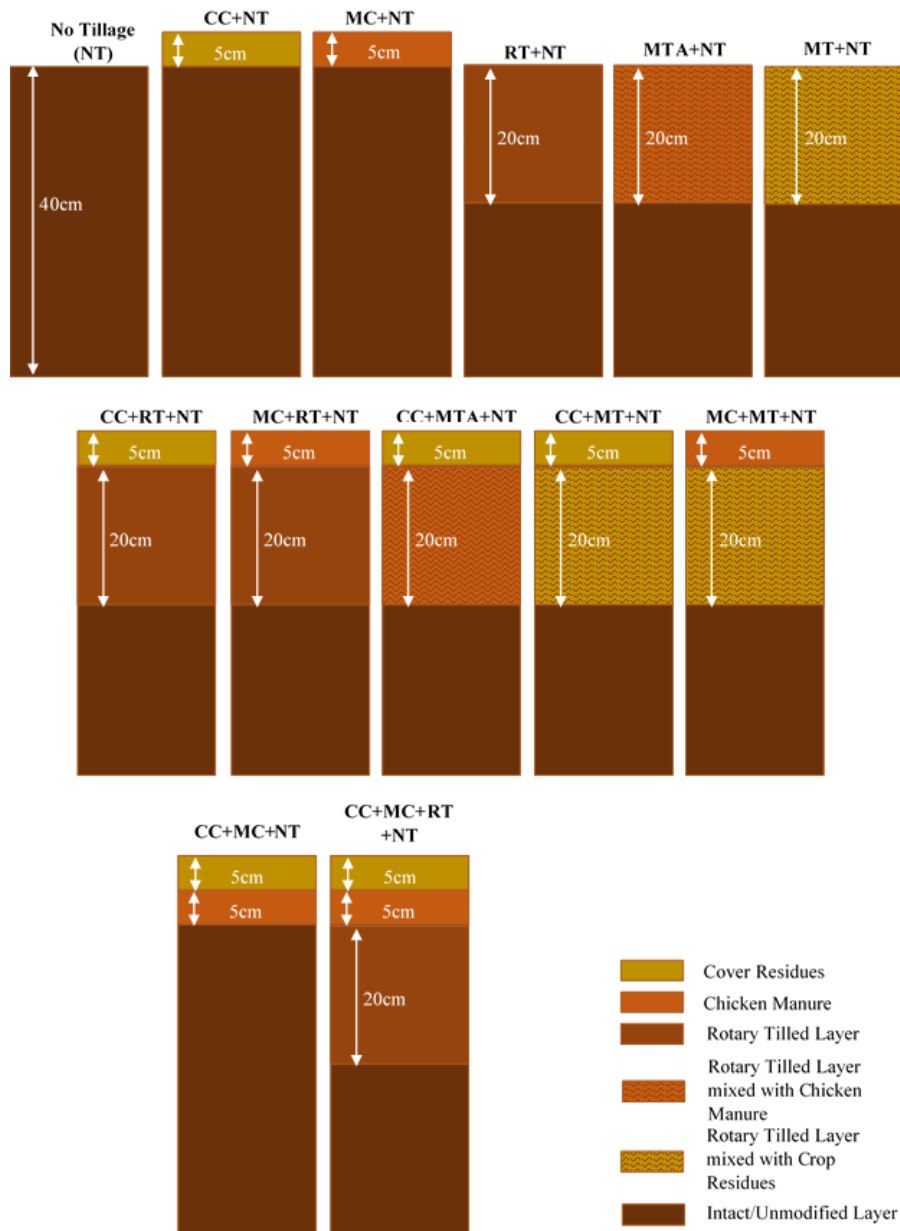


Figure 2: Soil profiles variation with respect to the soil management systems (not to scale)

Table 2: Physical, hydraulic and structural properties of cover layer materials

	BD (g.cm^{-3})	DD (g.cm^{-3})	SD (g.cm^{-3})	n ($\text{cm}^3.\text{cm}^{-3}$)	Θ_r ($\text{cm}^3.\text{cm}^{-3}$)	OMC (g kg^{-1})	MWD (mm)	K_s (cm/day)
Crop Residues	0.0837 \pm 0.0005	0.0837 \pm 0.0005	0.9772	0.8935 \pm 0.0006	0.04509 \pm 0.0006	912.5 \pm 5.2	5.032	2752.9 \pm 77.6
Chicken Manure	0.3446 \pm 0.0023	0.2726 \pm 0.0036	1.0141	0.7415 \pm 0.0036	0.3358 \pm 0.0036	414.8 \pm 12.2	4.951	30.245 \pm 0.245

3.1.3 Sample Collection and Preparation

Table 3 summarizes the characteristics to be tested, the depth at which the samples were removed, the number of replicates for each measurement in each soil plot, the total number of measurements in each study area and the method used to determine the corresponding property. Undisturbed (UD.S.) and disturbed (D.S.) samples are removed from the study area for the analysis of soil physical, structural and hydraulic properties. A disturbed soil sample from each study area used to determine soil classification is collected using a shovel. In the same area, undisturbed soil samples are removed from each plot using an epoxy cylinder having exact dimensions of the apparatus used in the hydraulic conductivity test. Other undisturbed and disturbed samples are removed using metallic rings and spoons, respectively, to compute the dry and bulk densities, the organic matter content, and the aggregate size distribution. After measuring the dry density, samples were saturated for 24hr period and then measured for saturated densities and left to drain water for subsequent days. Other UD.S. are removed using a polyvinyl chloride (PVC) pipe for CT-scanning. The soil columns are carefully removed by gently pushing the tubes into the soil (4.5cm inner diameter tube, 1cm thick, 10cm long) (Filipovic et al., 2020).

Table 3: Summary of parameters and properties tested for each tillage system in each site

Characteristic	Resulted parameter	Type of sample	Depth-increment (cm)					R.*	Σ'	Method	
			NT	CC	MC	MT	RT				MTA
			Maximum depth (cm)								
			40cm	-5cm [^]			20cm				
Soil classification	Soil type	D.S						1	1	Sieve analysis USDA, USCS	
Organic matter content	OMC	UD.S	10cm	-5cm			20cm	3	33	Loss on ignition	
Density	<i>BD, DD, SD, n, θ_r</i>	UD.S	10cm	-5cm			20cm	3	33	Core method	
Aggregate size distribution	<i>(f)</i> MWD	UD.S			in the upper 0-20cm			1	6	Sieve analysis	
Saturated hydraulic conductivity	<i>K_s</i>	UD.S			in the upper 0-20cm			1	6	Constant head Permeability Test	
Pore Structure	SWRC, PVD, AC, PAWC, RFC S-value	UD.S			in the upper 0-20cm			3	18	X-ray computed tomography scanning analysis	

* R. means replicate number

' Σ means the total number of measurement in each study area

[^] The negative sign in front of the 5cm corresponds to the direction of depth measurement with respect to the soil surface; the positive sign corresponds to depth measured downward from the soil surface.

3.1.4 Soil Pore Structure

The undisturbed soil samples were scanned at an energy level of 120kV and current of 60mAs using an Aquilion Prime SP medical CT scanner (Canon Medical Systems) at LAU Medical Center – Saint John’s Hospital, Jounieh, Lebanon. A rate of 1slice/0.3mm was set and produced in an axial view for each sample (capturing the whole cross-sectional area in every slice). The scanned images were analyzed with ImageJ software (version 1.48) and the ImageJ plugin BoneJ (**Doube et al., 2010**). The images (600 x 600 pixels) were cut near the edges to minimize the analysis of any artificial feature that might occur due to beam hardening (**Schneider et al., 2012**). For simplicity, an area comprising a circle of diameter 40mm was selected for each core data. Subsequently, the images were processed using a 1.0 Guassian filter and a 2.0 median filter that is widely used to reduce noise (**Jassogne et al., 2007**) and were analyzed using the processed binary images of 0 and 255 color thresholds. The quantification of soil pore structure was assessed for ranges of pixels’ areas to determine the percentage of areal content in the x-y plane of each range mean pore size. The data were transferred to an excel sheet in which the areal content was converted to a volumetric content $V(h)$ by using 0.3mm increments in the z-direction. The real total porosity n which is assumed to equal θ_s was used as a reference to determine $\theta(h)$ for each pore size and treatment by subtracting θ_s from $V(h)$ corresponding to the lowest pressure head h . The result was further subtracted from $V(h)$ corresponding to the second lowest h and the sequence continues until reaching the $\theta(h)$ corresponding to the highest h .

3.1.5 Soil Properties

3.1.5.1 Soil Classification

Soil Size Distribution

The soil size distribution is determined using the sieve analysis method (**Das and Sohban, 2014**). The method consists of placing the disturbed soil samples in an oven at $110 \pm 5^{\circ}C$ for 24hrs. Then, the soil is completely crushed so that all particles are alienated and placed on a set of sieves having progressively smaller openings from top to bottom (from top to bottom US. sieves No. 4, 8, 16, 30, 40, 50, 60, 100, 200, and a pan equivalent to diameters of 4.75, 2.36, 1.18, 0.6, 0.43, 0.36, 0.25, 0.15, 0.08, and 0mm). The set is mechanically shaken for 10mins. After determining the mass of the soil retained on each sieve, the particle size distribution curve is drawn in a plot of the

percent finer with respect to the particle diameter (log-scale) from which two parameters valuable in the determination of soil classification can be determined:

- The uniformity coefficient C_u which is expressed as: $C_u = \frac{D_{60}}{D_{10}}$ (1), where D_{10} and D_{60} are the diameters corresponding to 10% and 60% finer, respectively;
- The coefficient of gradation C_c which is expressed as: $C_c = \frac{D_{30}^2}{D_{60} \times D_{10}}$ (2), where D_{30} is the diameter corresponding to 30% finer;

Soil Classification

Two classification systems are used to define the soil class for each testing site: the textural classification system developed by the U.S. Department of Agriculture (USDA) and the Unified Soil Classification System (USCS). Each requires a specific guideline. Table 4 compare the definitions of the aforementioned systems for soil sizes: gravel, sand, silt and clay. The percentages of these soil types are only required to classify the soil on the USDA textural classification chart. In addition to the percentages passing U.S. NO. 4 and 200 sieves, the Atterberg limits are needed and determined according to ASTM in test designation D-4318. The USCS is the most extensive system (ASTM Test Designation D-2487) which requires in addition to all the above-mentioned parameters the following: C_u , C_c , location on the plasticity chart (Das and Sohban, 2014, p.132) and the organic matter content (OMC).

Table 4: Soil particle size definitions

%	USDA	USCS
Gravel	100 - %passing U.S. No. 10 sieve	100 - %passing U.S. No. 4 sieve
Sand	%passing U.S. No. 10 sieve - %finer than 0.05mm	%passing U.S. No. 4 sieve - %passing U.S. No. 200 sieve
Silt	%finer than 0.05mm - %finer than 0.002mm	%passing U.S. No. 200 sieve *
Clay	%finer than 0.002mm	

Note: U.S. No. 4, 10, and 200 sieves corresponds to sieve openings of 4.75mm, 2mm, and 0.075mm, respectively.

***Silt and clays are combined in the Unified Soil Classification systems and are denoted as fines.**

Organic Matter Content

The organic matter content is determined based on the loss on ignition method (**Stockdale, 2018**). The method consists of measuring the weight loss from a dried soil sample that is oven-heated at $110 \pm 5^{\circ}\text{C}$ for 24hrs. Accordingly, the samples are placed in a furnace at a temperature of 550°C for one hour allowing the organic matter to be burnt and are weighted again. The organic matter content OMC is determined by:

$OMC(\%) = \frac{m_d - m_{d-550}}{m_d} \times 100$ (3), where m_d is the mass of the oven-heated solid $[M]$ and m_{d-550} is the mass of the dry soil burnt at 550°C $[M]$.

3.1.5.2 Aggregate Size Distribution

The undisturbed soil sample is set to air-dry for 3days. Then the soil is placed in a set of US. sieves no. – (38.1mm), - (25mm), $\frac{3}{4}$ (19mm), $\frac{1}{2}$ (12.5mm), $\frac{3}{8}$ (9.5mm), $\frac{1}{4}$ (6.3mm), 4 (4.75mm), 8 (2.36mm), 10 (2mm), 20 (0.85mm), 40 (0.43mm), 100 (0.15mm), 200 (0.075mm) and a pan underneath. The set is mechanically shaken for 10mins. The soil retained on each pan is oven-dried at $110 \pm 5^{\circ}\text{C}$ for a 24hr period and weighed. The weights are then expressed as percentages of the total dry weight and converted into a mean weight diameter (MWD) from the frequency density function of the aggregate distribution (f) in the same manner as calculated in **van Bavel (1950)**.

3.1.5.3 Saturated Hydraulic Conductivity

The saturated hydraulic conductivity of the micropore domain is measured using the constant-head permeability test (**Klute and Dirksen, 1986**). The undisturbed soil samples are placed in the specimen tube. After allowing the sample to saturate, the supply of water to the specimen is adjusted at a constant rate. The saturated hydraulic conductivity is calculated using Eq. (4):

$K_s = \frac{Vl}{AHt}$ (4), where $V[L^3]$ is the quantity of water collected in time $t[T]$; l is the length of the soil sample $[L]$; A is the cross-section area of the soil sample; and H is the constant head elevation at which the water flows into the saturated specimen $[L]$.

3.1.5.4 Soil Water Retention Curve

Micropore sizes are expressed in terms of the capillary forces in the form of pressure head potential h $[m]$ by the capillary rise equation (**Hillel, 1980**):

$h = \frac{2T_s \cos \zeta}{\rho g r}$ (5a), where T_s is the surface tension between water and air [M/T^{-2}] (0.0727 kg.s⁻² at 20⁰C); ζ is the contact angle taken as 0 for a wetted surface [-]; ρ is water density (998 kg.m⁻³ at 20⁰C); g is the acceleration due to gravity [L/T^{-2}] (9.81 m.s⁻²); and r is the equivalent cylindrical pore radii [L]. Accordingly, a pore radius corresponding to a certain water pressure is expressed from Eq. (5a):

$$r = \frac{2T_s}{\rho g r h} \quad (5b)$$

The **van Genuchten (1980)** water release function, $\theta(h)$, can be written as:

$\theta(h) = \theta_r + \frac{(\theta_s - \theta_r)}{[1 + (\alpha h)^n]^m}$ (6), where $\theta(h)$ is a volumetric water content [L^3/L^3] correspondent to a pressure head h [L], θ_s is the saturated volumetric water content [L^3/L^3] assumed to equal the total porosity of soil n , θ_r is the residual volumetric water content [L^3/L^3] measured after the soil has been left to drain for three days, α [L^{-1}], n [-] and m [-] are to-be-determined parameters. In Eq. (6), h is set to be positive. In addition:

$$m = 1 - \frac{1}{n} \quad (7)$$

Accordingly, the soil water retention curve (SWRC) is dependent on volumetric water content that is corresponding to a pore water pressure. Thus, the volumetric water content is determined from the image analysis followed by pore quantification performed on undisturbed soil samples using CT scanning (which is explained in section 3.1.4). SWRC is fitted on a semi-log plot (volumetric water content [L^3/L^3] vs. natural logarithmic of the pressure head $\ln(h)$ [L]) from which α and n are fitted from the SWRC curve using Retention Curve Computer Program (RETC) with the aid of unfitted θ_r , θ_s and K_s (**van Genuchten et al., 1991**).

3.1.5.5 Pore Volume Distribution Function

The pore volume distribution function *PVD* is a curve on a plot having y-axis the pore volume density $S_v(h)$ [-] and x-axis (log scale) the equivalent pore diameter, $d = 2r$ [L], where r is determined from Eq. (5b) (**Jena and Gupta, 2002**). $S_v(h)$ is derived from the **van Genuchten (1980)** fitted $\theta(h)$ by **Dexter (2004a)** which equals the slope of the volumetric water content $\theta(h)$ vs. $\ln(h)$:

$$S_v(h) = \frac{d\theta(h)}{d(\ln h)} = -mn(\theta_s - \theta_r)(\alpha h)^n [1 + (\alpha h)^n]^{-(m+1)} \quad (8)$$

In addition, the peak point of the PVD curve corresponds to the inflection point $S_{vi}(h)$ [–] found in the van Genuchten fitted $\theta(h)$ vs. $\ln(h)$ and having the coordinates $(\theta_{vi}(h), \ln h_i)$ and has the following magnitude:

$$S_{vi}(h) = \frac{d\theta_{vi}(h)}{d(\ln h_i)} = \left| -n(\theta_s - \theta_r) \left[1 + \frac{1}{m} \right]^{-(m+1)} \right| \quad (9), \quad \text{where } \theta_{vi}(h) = \theta_r + \frac{(\theta_s - \theta_r)}{\left[1 + \frac{1}{m} \right]^m}$$

$$\text{and } h_i = \frac{1}{\alpha} \left(\frac{1}{m} \right)^{\frac{1}{n}}$$

The pore volume distribution function is characterized and compared by shape and location parameters (**Reynolds et al., 2009**) which can be calculated based on an equivalent diameter:

$$d_{\theta} = \frac{2980\alpha}{(\theta^{-1/m} - 1)^{1/n}} \quad (10)$$

Location Parameters

Location parameters include the mode (the most frequent d_{θ} , which corresponds to the inflection point in the SWRC), the median, and the mean (central tendency) diameter:

$$d_{\text{mode}} = \frac{2980\alpha}{m^{-1/n}} \quad (11)$$

$$d_{\text{median}} = d_{0.5} = \frac{2980\alpha}{(0.5^{-1/m} - 1)^{1/n}} \quad (12)$$

$$d_{\text{mean}} = e^{\left(\frac{\ln(d_{0.16}) + \ln(d_{0.5}) + \ln(d_{0.84})}{3} \right)} \quad (13)$$

Shape Parameters

Shape parameters comprise standard deviation SD (spread), skewness (asymmetry), kurtosis (peakedness). As reported by **Blott and Pye (2001)**, the parameters are expressed as:

$$SD = e^{\left(\frac{\ln(d_{0.84}) - \ln(d_{0.16})}{4} + \frac{\ln(d_{0.95}) - \ln(d_{0.05})}{6.6} \right)} \quad (14), \quad \text{where } SD \geq 1$$

$$\text{Skewness} = \frac{1}{2} \left[\frac{\ln(d_{0.16}) + \ln(d_{0.84}) - 2\ln(d_{0.5})}{\ln(d_{0.84}) - \ln(d_{0.16})} + \frac{\ln(d_{0.05}) + \ln(d_{0.95}) - 2\ln(d_{0.5})}{\ln(d_{0.95}) - \ln(d_{0.05})} \right] \quad (15), \quad \text{where } -1 \leq \text{Skewness} \leq +1$$

$$\text{Kurtosis} = \frac{\ln(d_{0.05}) - \ln(d_{0.95})}{2.44[\ln(d_{0.25}) - \ln(d_{0.75})]} \quad (16), \quad \text{where } \text{Kurtosis} \geq 0.41$$

3.1.5.6 Soil Physical Quality Indicators

Reynolds et al. (2009) propose a set of soil physical quality indicators with threshold levels recommended for agricultural soils. The thresholds are summarized for different parameters in Table 5.

Table 5: Optimal ranges or critical limits for soil physical quality indicators (Reynolds et al., 2009)

Parameter	Critical Lower Limit	Optimal Range	Critical Upper Limit	Soil Type
Bulk density, BD	< 0.9 g.cm ⁻³ inadequate plant anchoring and a reduction in PAWC	0.9-1.2 g.cm ⁻³ for maximum crop production	> 1.3 g.cm ⁻³ productivity decreases due to inadequate soil aeration	Medium or fine texture
Air capacity, AC		AC ≥ 0.14 cm ³ .cm ⁻³ is required. AC > 0.10 cm ³ .cm ⁻³ to reduce the incidence of crop-damage or yield-reducing aeration deficits in the root zone.		Sandy loam or clay soils Agricultural soils
Plant-available water capacity, PAWC	PAWC < 0.1 cm ³ .cm ⁻³ is poor or droughty	PAWC ≥ 0.2 cm ³ .cm ⁻³ is ideal for root growth and functions 0.15 ≤ PAWC < 0.2 cm ³ .cm ⁻³ is good	0.1 ≤ PAWC < 0.15 cm ³ .cm ⁻³ is limited	
Relative field capacity, RFC	RFC < 0.6 water limited soils	0.6 ≤ RFC ≤ 0.7 optimal balance between AC and PAWC: desirable water and air content needed for a better microbial production of nitrogen more recurrently and for extended periods (Reynolds et al., 2002; Castellini et al., 2013)	RFC > 0.7 aeration limited soils	Agricultural soils
S-value (Dexter, 2004b; Dexter and Czyz, 2007; Tormena et al., 2008)	0.020 ≤ S _f < 0.035 poor physical quality S _f < 0.020 very poor or degraded physical quality	S _f ≥ 0.05 very good soil physical or structural quality, 0.035 ≤ S _f < 0.050 good physical quality		Temperate and tropical soils
		Common range 0.007 ≤ S _f ≤ 0.14 (Dexter and Czyz, 2007)		Agricultural soils
Field saturated hydraulic conductivity, K_{sf}	< 8.6 cm.d ⁻¹ (Reynolds et al., 2007)	43.2-432 cm.d ⁻¹ ideal to increase infiltration, drainage of excess soil water and distribution of PAWC and decrease surface runoff and soil erosion (Reynolds et al., 2008)	864 cm.d ⁻¹ droughty soils (i.e., soils with coarse texture or excessive cracks and biopores (Topp et al., 1997; Reynolds et al., 2007))	Agricultural soils

Bulk, Dry and Saturated Densities

Densities are determined according to the core method (**Blake & Hartge, 1986**). Cylindrically cores of well-known dimensions are used to remove the undisturbed soil samples at the assigned depths by applying gentle pressure by hand. The cores are

weighted prior and after the soil sampling. The bulk density $BD[M/L^3]$ is expressed as:

$BD = \frac{m_m}{V}$ (17), where m_m is the mass of the moist solid removed using the metallic ring (which is the difference of the mass of the ring filled with soil and the mass of the ring prior to sampling) $[M]$ and V is the volume of the metallic ring $[L^3]$.

Later, the samples are placed in an oven at a temperature of $110 \pm 5^{\circ}C$ for 24hr and are weighed again to have a dry mass $m_d[M]$ (Hartge and Horn, 2009). Accordingly, the dry density DD is:

$$DD = \frac{m_d}{V} \text{ (18)}$$

Afterwards, the dry samples are saturated for 24 hrs and weighed again to have a mass of $m_s[M]$. Thus, SD is defined as:

$$SD = \frac{m_s}{V} \text{ (19)}$$

Porosity

The total porosity n is determined by the relationship between densities, where ρ is the density of water $[M/L^3]$:

$$n = \frac{SD-DD}{\rho} \text{ (20)}$$

Residual Volumetric Content

The residual volumetric moisture content θ_r equals the volumetric content of water in a saturated soil sample that has been left to drain for three consecutive days after which the soil sample is weighed as $m_r [M]$. The sample is placed in an oven for 24 hrs at a temperature of $110 \pm 5^{\circ}C$ and is weighed again to have the dry mass of $m_d [M]$.

$$\theta_r = \frac{m_r - m_d}{\rho V} \text{ (21)}$$

Air Capacity

As defined in Castellini et al. (2013), air capacity or soil aeration is the ability of soil to store and transmit air and is defined as:

$AC = \theta_s - \theta_{FC}$ (22), where θ is the volumetric water content $[L^3/L^3]$ and the subscripts s and FC correspond to the field capacity of water pressure under saturation

and at $h = 100\text{cm}$ (equivalent to $2.97\mu\text{m}$ pore diameter), respectively determined from the SWRC.

Plant-available Water Capacity

As defined by its name, the plant-available water capacity is the ability of soil to store and provide water necessary for root uptake and plant growth (**Castellini et al., 2013**). It is expressed as:

$PAWC = \theta_{FC} - \theta_{PWP}$ (23), where θ is the volumetric water content [L^3/L^3] and the subscripts FC and PWP correspond to the field capacity of water pressure at $h = 100\text{cm}$ and to the permanent wilting point at $h = 15,300\text{cm}$ (equivalent to $0.0195\mu\text{m}$ pore diameter), respectively determined from the SWRC.

Relative Field Capacity

The dimensionless relative field capacity is the ability of soil to store water and air with respect to the soil's total pore volume represented by the saturated volumetric water content θ_s (**Castellini et al., 2013**):

$$RFC = \frac{\theta_{FC}}{\theta_s} \quad (24)$$

S theory

The S-value is the magnitude of the slope at the inflection point expressed in Eq. (9) which is derived by **Dexter (2004a)**.

3.1.6 Preferential flow

Preferential flow patterns are evaluated only for loamy sand soil in a rainfall simulation experiment of which the setup is sketched in Figure 3 similarly as that applied by **Andreini & Steenhuis (1990)**. The application rate didn't create runoff or ponding as referred by **Andreini & Steenhuis (1990)**. The soil was obtained from Site 1 from plots that were subjected to rotary tillage without any addition of any agricultural waste. After placement in large bags, the soil was placed on ground near the laboratory setup in an open space not to allow the soil to crumble in the bags. The same soil layers' combinations used in section 3.1.3 as presented in Table 1 are applied. RT layers and covers of either crops or chicken manure were poured into the box and leveled without any pressure to a certain depth. Similarly, MTA and MT layers were placed after preparation of soil and either crop residues or manure mixes of 2:1 volume ratio. In addition, it was not applicable to remove an undisturbed sample of NT to fit

in the experimental glass box. Therefore, it was practical to compact the soil by placing it in 5cm increments and using a 10x5x5cm wood box to apply a pressure on the air-dried soil. Prior to the experiments, batch tests of NT were measured for dry densities and compared with those measured for the field undisturbed samples resulting in a fair P-value of 0.15 (fail to reject the hypothesis of equal means). As a result, the soil was placed in 5cm increments which were compacted for NT layers and only free-pressure leveled for the others. Each increment was tested for its initial moisture content using TEROS 12 (TEROS12, METER Group) (Singh et al., 2020). It consists of three parallel needles 5.5cm long. The rods are embedded into the soil in which electromagnetic field is generated by an oscillator in the sensor head running at 70MHz and is transmitted into the soil media. As a response, the oscillator measures the dielectric constant in the soil which is converted into the apparent permittivity and later into the volumetric moisture content. A pro-check handheld meter is connected to the sensor for measurements' readings.

Nonetheless, the setup consists of a transparent glass box 40x40x40cm (1). The later was placed on a flat steel table (2) in which soil was placed in different layers to simulate all the treatments. Water in a tank (7) was pumped at the delivery of 2m at a constant rate (6) during the entire time of the irrigation period. A pressure gage (5) was connected to the pipes after the pumping action to assure a constant pressure of 25kPa from which water is moved through the closing valve (4) into a sprinkler (3) centered and fixed above the box by 50cm. Surface runoff was collected from one side of the box on an aluminum sheet attached to the box from one side while suspended to the outside where a graduated cylinder is placed underneath (8). A low constant flow of $1.2 \pm 0.0207 \text{ m}^3/\text{day}$ equivalent to an irrigation rate of $0.518 \pm 0.008984 \text{ mm}/\text{min}$ was chosen for all experiments. The nozzle sprayed over a circular area diameter of 35cm. Time is recorded at the beginning of each irrigation experiment after which the wetting front locations L_{exp_i} along the back (L_{exp1}), front (L_{exp2}), and right (L_{exp3}) sides of the box are monitored and logged through observation along the transparent sides of the box. The objective is to compare the experimental wetting front L_{exp_i} and the theoretical wetting front depth L to assess the presence of preferential flows PF. As a result, three conditions arise: if $L_{exp} = L$, this means that there are no PFs. If $L_{exp} > L$, then PF is assumed to be in the vertical direction and its length would be $L_{exp} - L$. Similarly, if $L_{exp} < L$, then the length of PF is $L - L_{exp}$ but measured in

the horizontal (lateral) direction. The irrigation rate Irr ($0.518\text{mm}/\text{min}$) is the sum of the infiltration Inf and surface runoff SR rate. Therefore, $Inf = Irr - SR = 0.518 - SR$. Nevertheless, the theoretical wetting front depth L is determined in the set of Eq. (25) in Table 6.

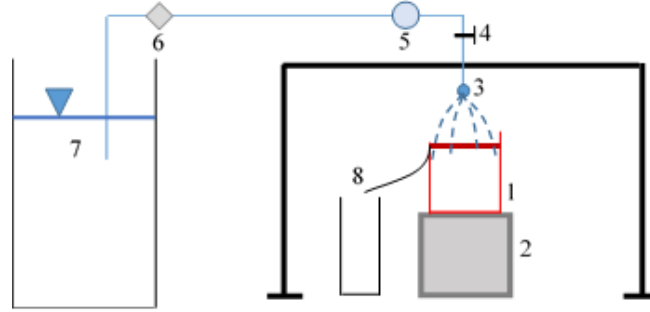


Figure 3: Scheme of the device for wetting front location and surface runoff with volume reading in calibrating cylinder (not to scale)

Table 6 [Eq. (25)]: Wetting front depth, L for preferential flow experimental study

Profile		Subscript Designation	Wetting front Depth, L	Condition	Time variables
1-layer		-	$\frac{Inf \times t}{\Delta\theta}$		
2-layers	1 st layer	'mo'	$\frac{Inf \times t}{\Delta\theta_{mo}}$	$t \leq t_{z_{mo}}$	$t_{z_{mo}}$ $= \frac{z_{mo} \times \Delta\theta_{mo}}{Inf}$
	2 nd layer	'umo'	$z_{mo} + \frac{Inf \times (t - t_{z_{mo}})}{\Delta\theta_{umo}}$	$t > t_{z_{mo}}$	
3-layers	1 st layer	'c'	$\frac{Inf \times t}{\Delta\theta_c}$	$t \leq t_{z_c}$	$t_{z_c} = \frac{z_c \times \Delta\theta_c}{Inf}$
	2 nd layer	'mo'	$z_c + \frac{Inf \times (t - t_{z_c})}{\Delta\theta_{mo}}$	$t_{z_c} < t \leq t_{z_{mo}}$	$t_{z_{mo}}$ $= t_{z_c}$ $+ \frac{z_{mo} \times \Delta\theta_{mo}}{Inf}$
	3 rd layer	'umo'	$z_c + z_{mo} + \frac{Inf \times (t - t_{z_{mo}})}{\Delta\theta_{umo}}$	$t > t_{z_{mo}}$	
4-layers	1 st layer	'c1'	$\frac{Inf \times t}{\Delta\theta_{c1}}$	$t \leq t_{z_{c1}}$	$t_{z_c} = \frac{z_{c1} \times \Delta\theta_c}{Inf}$
	2 nd layer	'c2'	$z_{c1} + \frac{Inf \times (t - t_{z_{c1}})}{\Delta\theta_{c2}}$	$t_{z_{c1}} < t \leq t_{z_{c2}}$	$t_{z_{c2}}$ $= t_{z_{c1}}$ $+ \frac{z_{c2} \times \Delta\theta_{c2}}{Inf}$
	3 rd layer	'mo'	$z_{c1} + z_{c2} + \frac{Inf \times (t - t_{z_{c2}})}{\Delta\theta_{mo}}$	$t_{z_{c2}} < t \leq t_{z_{mo}}$	$t_{z_{mo}}$ $= t_{z_{c2}}$ $+ \frac{z_{mo} \times \Delta\theta_{mo}}{Inf}$
	4 th layer	'umo'	$z_{c1} + z_{c2} + z_{mo} + \frac{Inf \times (t - t_{z_{mo}})}{\Delta\theta_{umo}}$	$t > t_{z_{mo}}$	

3.1.7 Statistical Analysis

A completely randomized design is set to implement the field testing experiments of several response variables y_i . Each experiment is analyzed using the analysis of variance (ANOVA – 1 and 2-way interaction) (in which the test statistic for the hypothesis of no differences in treatment means is two-sided) after checking for model and normality assumption adequacy with a 95% confidence of interval. Further, for 2-way ANOVA, experiments depend on two factors: the two factors F1 & F2 are the soil treatment systems and the soil type. F1 entails 6 qualitative levels: (1) NT, (2) CC, (3) MC, (4) MT, (5) RT, (6) MTA while F2 combines 2 qualitative levels: (1) Site 1-Tawbe (loamy sand) and (2) Site 2-Aren (clay loam). Nuisance factors such as sampling soil disturbances, and temperature variations cannot be neglected, hence they are not taken into consideration (no blocking). In case of statistical difference occurrence, least significant difference method was used to compare means pairs. Minitab19 was used to simulate the aforementioned statistical analysis.

3.2 Mathematical Model

In this section, the theory behind developing the model of infiltration for agricultural soils is listed in details. Prior to derivation, the model must opt to certain criteria that were previously described in the literature review section such as the heterogeneity of the soil, physical properties, and water supply conditions. As a result, Table 7 entails a schematic that assists in the methodology for developing the model. The involved properties are those specific to the soil media and to the source and intensity of water. In this regard, three cases arise, where P is the rate fall of water on the soil surface (the source of water might be from rainfall and irrigation water either from sprinkles, or furrow/strip water), I is the infiltration capacity of the soil horizon, and K_{seq} is the equivalent saturated hydraulic conductivity of the soil profile. In this work, we are only interested in case 2.

- 1) $P < K_{seq} < I$
- 2) $K_{seq} < P < I$
- 3) $K_{seq} < I < P$

The infiltration in the micropore system is driven by capillary pressure induced by micro-porosities. Hence, it is modeled according to the Green-Ampt model for layered

soils similar to that derived by **Damodhara Rao et al. (2006)**. In each layer, the soil is considered homogeneous, having a constant initial soil moisture, constant matric potential and a uniform hydraulic conductivity pertaining to the assumptions of the original Green-Ampt model. The wetting-front moves vertically and uniformly from one layer to the other. In addition, the water supply is assumed to be constant and at steady state resembling to the irrigation systems.

3.2.1 Infiltration in one-layer micropore domain

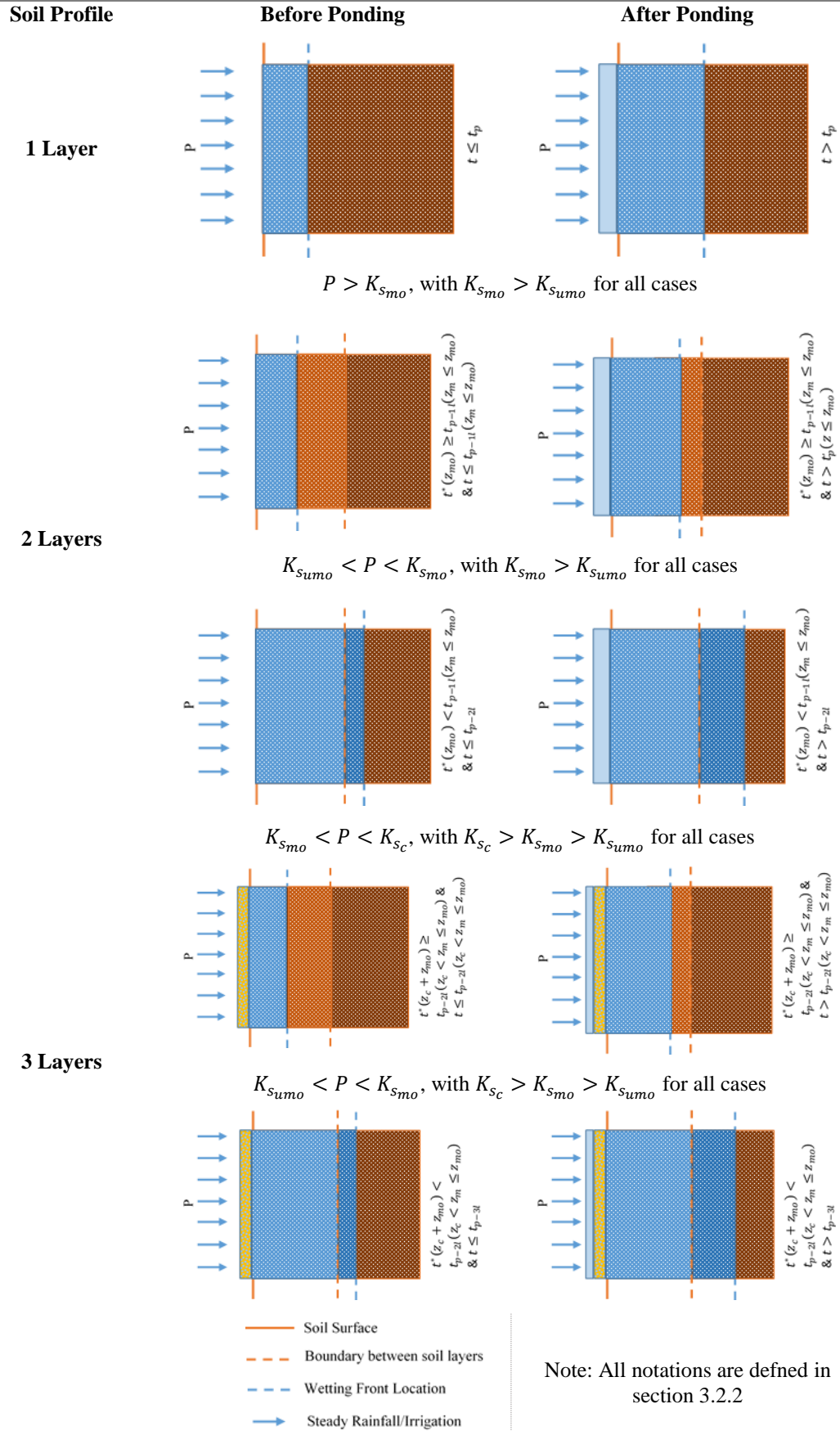
According to Darcy's law (**Darcy, 1856, pp. 590–594**), the discharge velocity of water in a micropore domain v_m determined at right angles to the direction of flow is the volume of water flowing in unit time through a unit gross cross-sectional area of soil which is the infiltration rate of water into soil. It is determined using Eq. (26) where K_s is the saturated hydraulic conductivity of the transmission zone [L/T] and i is the unitless total hydraulic gradient which is the head loss Δh between the starting and ending boundaries of the area in which the water flows [L] divided by the length L perpendicular to the flow over which the head loss occurs [L] as written in Eq. (27).

$$v_m = K_s i \quad (26)$$

$$i = \frac{\Delta h}{L} \quad (27)$$

The total head at any point in flowing water is the summation of the pressure head h_p , velocity head h_v , and elevation head h_e according to the Bernoulli's equation. Hence, the velocity head is negligible in the case of flowing water in porous media in comparison with the remaining heads (**Das and Sohban, 2014**). For downward infiltration in a soil column floated by a ponding water, the head loss in the micropore domain in which flow of water is driven by capillary forces is determined between the soil surface at point A and the Green-Ampt sharp wetting front at point B as shown in Figure 4. Δh can be written as Eq. (28) where h_A and h_B are the total heads at point A and B, respectively [L]; h_0 is the ponded depth above the soil surface [L]; ψ_f is the initial suction head at the wetting front [L] and z_m is the vertical length of the wetting front in the micropore domain measured positively downwards from the top surface of the soil [L]. For calculation purposes, a datum is set at the wetting front location.

Table 7: Infiltration into layered agricultural soil with and without ponding



Thus, the total head at B is equal to the pressure head driven by the weight of the water carried by capillary forces, while the total head at A is equal to the elevation head measured vertically from the reference datum and the pressure head formed from the ponded water above the soil surface.

$$\Delta h = |h_A - h_B| = |h_0 + z_m - \psi_f| = |h_0 - \psi_f| + z_m \quad (28)$$

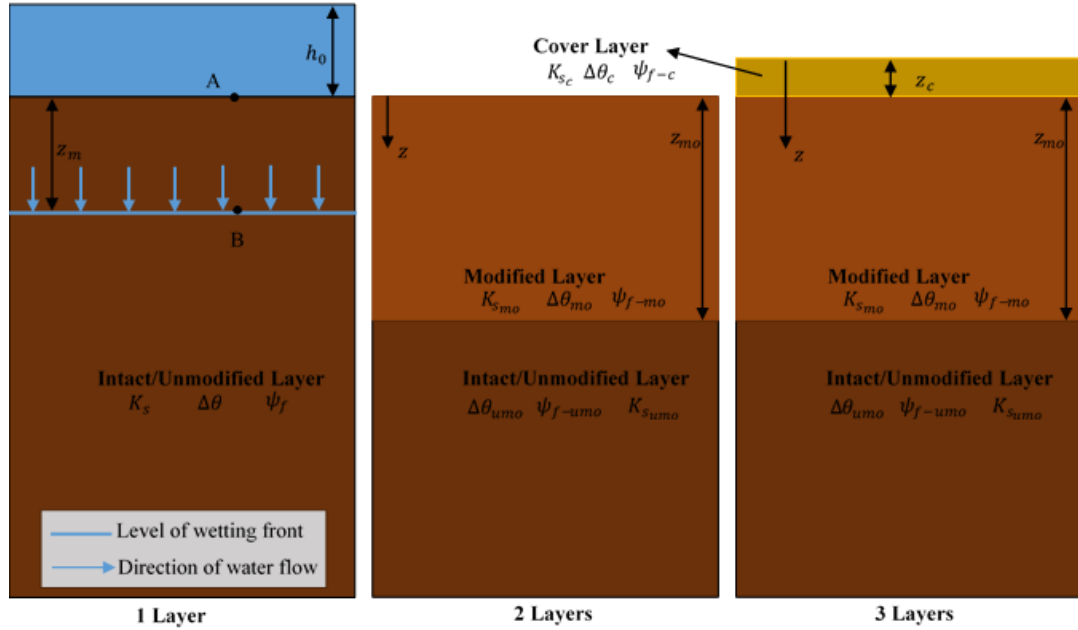


Figure 4: Water Infiltration in layered soil media

In cases where there is no ponding water at the surface, h_0 would be zero. Using Eqs. (27) and (28), Eq. (26) is re-written as

$$v_m(z_m) = K_s \frac{|h_0 - \psi_f| + z_m}{z_m} \quad (29)$$

In addition, the aforementioned discharge velocity equals the multiplication of effective porosity nS (n is the porosity [L^3/L^3] and S is the difference of degree of saturations after and before wetting [L^3/L^3]) and the actual velocity of the water defined as the seepage velocity v_{m-a} ($v_m = nSv_{m-a}$). The seepage velocity is the quantity of water flowing in unit time through the void spaces of the porous media. Thus, it is equivalent to the gradient in wetting front location with respect to time t [T] ($v_{m-a} = \frac{dz_m}{dt}$). Consequently, we can replace v_m by:

$$v_m = nS \frac{dz_m}{dt} \quad (30)$$

The first two factors of Eq. (30) can be replaced by $\Delta\theta = \theta_s - \theta_i$ where θ_s is the saturated volumetric moisture content [L^3/L^3] and θ_i is the initial volumetric moisture content [L^3/L^3]:

$$v_m = \Delta\theta \frac{dz_m}{dt} \quad (31)$$

Combining Eqs. (29) and (31) yields

$$\frac{dz_m}{dt} = K_s \frac{|h_0 - \psi_f| + z_m}{\Delta\theta z_m} \quad (32)$$

The integration of Eq. (32) on both sides with initial condition $(z_m, t) = (0, 0)$ yields either an implicit form to determine the wetting front location in the partially saturated soil column in terms of time or an explicit solution for the time in terms of the wetting front location as shown in Eqs. (33a) and (33b), respectively.

$$z_m \Delta\theta - |h_0 - \psi_f| \Delta\theta \ln \left(\frac{|h_0 - \psi_f| + z_m}{|h_0 - \psi_f|} \right) = K_s t \quad (33a)$$

Or

$$t(z_m) = \frac{1}{K_s} \left[z_m \Delta\theta - |h_0 - \psi_f| \Delta\theta \ln \left(\frac{|h_0 - \psi_f| + z_m}{|h_0 - \psi_f|} \right) \right] \quad (33b)$$

The cumulative infiltration Z_m is

$$Z_m = z_m \Delta\theta \quad (34)$$

Substituting Eq. (34) into Eq. (33a) yields an implicit equation for the cumulative infiltration in the micropore domain with respect to time t .

$$Z_m - |h_0 - \psi_f| \Delta\theta \ln \left(1 + \frac{Z_m}{|h_0 - \psi_f| \Delta\theta} \right) = K_s t \quad (35a)$$

$$t(Z_m) = \frac{1}{K_s} \left[Z_m - |h_0 - \psi_f| \Delta\theta \ln \left(1 + \frac{Z_m}{|h_0 - \psi_f| \Delta\theta} \right) \right] \quad (35b)$$

Eq. (35) is the conventional Green-Ampt model (GA) which is derived for a one-layer homogeneous soil profile. As such, Figure 5 illustrates conceptually the flow in unsaturated micropore domain taking into consideration the basic assumptions of the

GA model which consists of shifting from the actual non-linear profile to a more-stable rectangular shaped that moves immediately from unsaturation to full saturation.

The infiltration rate v_m in Eq. (29) for pre-ponding conditions equals the waterfall rate P . Ponding occurs when $t = t_p$, where t_p is the time for the water to pond at the surface of the soil which is inferred when the infiltration rate is greater than the infiltration capacity of the soil profile. At the time of ponding, the cumulative infiltration Z_m is denoted as Z_p . Hence Eq. (29) can be re-written as:

$$P = K_s \frac{|h_0 - \psi_f| + \frac{Z_p}{\Delta\theta}}{\frac{Z_p}{\Delta\theta}} \quad (36)$$

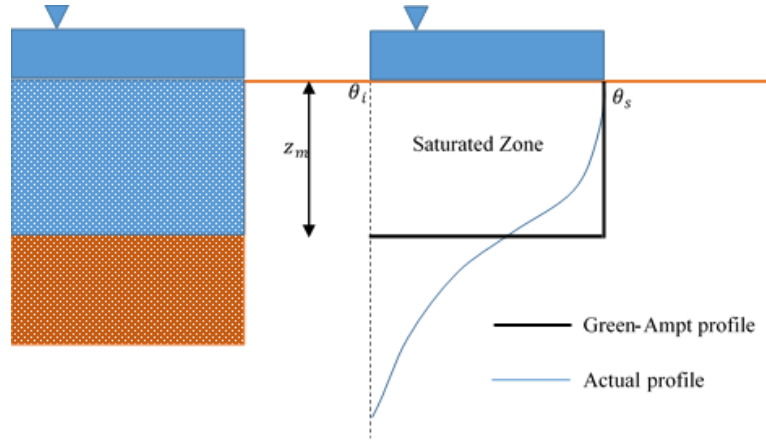


Figure 5: Infiltration profile in an unsaturated micropore domain (not to scale)

In addition, the vertical cumulative infiltration depths in micropore domains Z_m and Z_p equal $P \times t$ and $P \times t_p$ for pre- and at ponding conditions, respectively. So Eq. (36) becomes:

$$P = K_s \frac{|h_0 - \psi_f| + \frac{P \times t_p}{\Delta\theta}}{\frac{P \times t_p}{\Delta\theta}} \quad (37)$$

Re-arranging Eq. (37) to have t_{p-1l} where $t_p = t_{p-1l}$ for one-layer soil profile or when ponding occurs while the wetting front is still in the first layer for a layered soil profile

$$t_{p-1l} = \frac{K_s(|h_0 - \psi_f|)\Delta\theta}{P(P - K_s)} \quad (38)$$

The integration of Eq. (32) on both sides with initial condition $(z_m, t) = (z_p, t_{p-1l})$, where z_p is calculated using Eq. (34) by replacing Z_m with Z_p yields:

$$(z_m - z_p)\Delta\theta + |h_0 - \psi_f|\Delta\theta \ln\left(\frac{|h_0 - \psi_f| + z_p}{|h_0 - \psi_f| + z_m}\right) = K_s(t - t_{p-1l}) \quad (39a)$$

Re-arranging Eq. (41a) to implicitly determine the time for post-ponding conditions:

$$t(z_m) = t_{p-1l} + \frac{1}{K_s} \left[(z_m - z_p)\Delta\theta + |h_0 - \psi_f|\Delta\theta \ln\left(\frac{|h_0 - \psi_f| + z_p}{|h_0 - \psi_f| + z_m}\right) \right] \quad (39b)$$

According to Eqs. (31) and (34), the infiltration rate can be re-written as:

$$v_m = \Delta\theta \frac{dz_m}{dt} = \frac{dZ_m}{dt} \quad (40)$$

Substituting Eqs. (34) and (39) in Eq. (29), we get:

$$\frac{dZ_m}{dt} = K_s \frac{|h_0 - \psi_f| + \frac{Z_m}{\Delta\theta}}{\frac{Z_m}{\Delta\theta}} \quad (41)$$

The integration of Eq. (41) on both sides with initial condition $(Z_m, t) = (Z_p, t_{p-1l})$ yields the modified GA adjusted for post-ponding conditions:

$$Z_m - Z_p + |h_0 - \psi_f|\Delta\theta \ln\left(\frac{|h_0 - \psi_f|\Delta\theta + Z_p}{|h_0 - \psi_f|\Delta\theta + Z_m}\right) = K_s(t - t_{p-1l}) \quad (42a)$$

Re-arranging Eq. (41a) to implicitly determine the time for post-ponding conditions:

$$t(Z_m) = t_{p-1l} + \frac{1}{K_s} \left[Z_m - Z_p + |h_0 - \psi_f|\Delta\theta \ln\left(\frac{|h_0 - \psi_f|\Delta\theta + Z_p}{|h_0 - \psi_f|\Delta\theta + Z_m}\right) \right] \quad (42b)$$

3.2.2 Infiltration in multi-layered micropore domain

The different soil management systems prompt alterations to the soil profile homogeneous structure resulting in two homogeneous layer profile by either adding a cover or disturbing the top soil layer. Three-layers profile is also applicable by adding a cover to the tilled/modified layer. As this stands, we are only interested in 1-, 2-, and 3-layers soil profile. Each layer is assumed to be homogeneous, has distinctive hydraulic and physical properties, and flow moves from one layer to the other downward and vertically.

The derivation in section 3.2.1 was employed for 1-layer soil profile. In this section, derivation is performed for 2 and 3-layers profile taking also into account pre- and post-ponding conditions. The subscripts ‘c’, ‘mo’ and ‘umo’ are added to all

parameters to define those measured in the top cover layer, the second modified layer and the subsoil intact/unmodified layer, respectively. The model is referred to the re-structured Green-Ampt Model for Agricultural layered soils model (**GARALS**).

3.2.2.1 2-layers profile

When the wetting front is within the upper modified layer ($z_m \leq z_{mo}$), all equations stated in 3.2.1 can be used by replacing all the parameters by those adhering the subscript 'mo'. However, when the wetting front reaches the subsoil intact layer ($z_m > z_{mo}$), K_s is replaced by an equivalent hydraulic conductivity K'_c for vertical flow (**Damodhara Rao et al., 2006**).

$$K'_c = \frac{z_m \Delta\theta_{umo}}{\frac{z_{mo} \Delta\theta_{mo}}{K_{smo}} + \frac{(z_m - z_{mo}) \Delta\theta_{umo}}{K_{sumo}}} \quad (43)$$

Replacing Eq. (43) in Eq. (32)

$$\Delta\theta_{umo} \frac{dz_m}{dt} = \frac{z_m \Delta\theta_{umo}}{\frac{z_{mo} \Delta\theta_{mo}}{K_{smo}} + \frac{(z_m - z_{mo}) \Delta\theta_{umo}}{K_{sumo}}} \times \frac{|h_0 - \psi_{f-umo}| + z_m}{z_m} \quad (44)$$

Eq. (44) is reduced into

$$\frac{dz_m}{dt} = \frac{|h_0 - \psi_{f-umo}| + z_m}{\frac{z_{mo}(\Delta\theta_{mo} - \Delta\theta_{umo})}{(K_{smo} - K_{sumo})} + \frac{z_m \Delta\theta_{umo}}{K_{sumo}}} \quad (45a)$$

Or

$$\frac{dz_m}{dt} = \frac{|h_0 - \psi_{f-umo}| + z_m}{A' + B' z_m} \quad (45b) \text{ where } A' = \frac{z_{mo}(\Delta\theta_{mo} - \Delta\theta_{umo})}{(K_{smo} - K_{sumo})} \text{ and } B' = \frac{\Delta\theta_{umo}}{K_{sumo}}$$

The integration of Eq. (45b) on both sides with initial condition $(z_m, t) = (z_{mo}, t(z_{mo}))$, where $t(z_{mo})$ is the time for the wetting front to reach the bottom of the modified layer and by replacing z_m with z_{mo} , yields either an implicit form to determine the wetting front location in terms of time or an explicit solution for the time in terms of the wetting front location as shown in Eq. (46):

$$t(z_m) = t(z_{mo}) + (A' - B' |h_0 - \psi_{f-umo}|) \left[\ln \left(\frac{z_m + |h_0 - \psi_{f-umo}|}{z_{mo} + |h_0 - \psi_{f-umo}|} \right) \right] + B' (z_m - z_{mo}) \quad (46)$$

The cumulative infiltration in this case is

$$Z_{m-umo} = z_{mo} \Delta\theta_{mo} + (z_m - z_{mo}) \Delta\theta_{umo} \quad (47)$$

Using Eq. (47) to determine explicitly z_m :

$$z_m = \frac{Z_{m-umo} - z_{mo}(\Delta\theta_{mo} - \Delta\theta_{umo})}{\Delta\theta_{umo}} \quad (48)$$

As well, integrating Eq. (45b) by replacing z_m by its value in Eq. (48) on both sides with initial condition $(Z_{m-umo}, t) = (Z(z_{mo}), t(z_{mo}))$, where $Z(z_{mo})$ is calculated using Eq. (34), meanwhile assuming that $\frac{dZ_{m-umo}}{dt} = \frac{d}{dt}[z_{mo}\Delta\theta_{mo} + (z_m - z_{mo})\Delta\theta_{umo}] = \frac{d(z_m\Delta\theta_{umo})}{dt} + \frac{d[z_{mo}(\Delta\theta_{mo} - \Delta\theta_{umo})]}{dt} = \frac{d(z_m\Delta\theta_{umo})}{dt} + 0 = \Delta\theta_{umo} \frac{dz_m}{dt}$, Eq. (45) becomes:

$$t = t(z_{mo}) + \frac{1}{\Delta\theta_{umo}} \left\{ (C' - B \cdot D') \left[\ln \left(\frac{Z_{m-umo} + D'}{Z(z_{mo}) + D'} \right) \right] + B' [Z_{m-umo} - Z(z_{mo})] \right\} \quad (49),$$

$$\text{where } C' = A' \Delta\theta_{umo} - B' z_{mo} (\Delta\theta_{mo} - \Delta\theta_{umo}) \text{ and } D' = \Delta\theta_{umo} |h_0 - \psi_{f-umo}| - z_{mo} (\Delta\theta_{mo} - \Delta\theta_{umo})$$

Additionally, the time to pond exerts some modification with the replacement of the saturated hydraulic conductivity with its equivalency for wetting fronts located in the second layer ($z_m > z_{mo}$).

To identify whether ponding occurs before or after the wetting front moves into the second layer, we shall determine the time for the wetting front to reach the bottom of the first layer $t^*(z_{mo})$ (without taking into effect any ponding yet) and the time to pond if the wetting front is still in the first layer $t_{p-1l}(z_m \leq z_{mo})$ using Eq. (38):

$$t^*(z_{mo}) = \frac{z_{mo}}{P} = \frac{z_{mo}\Delta\theta_{mo}}{P} \quad (50)$$

$$t_{p-1l}(z_m \leq z_{mo}) = \frac{K_{s_{mo}}(|h_0 - \psi_{f-mo}|)\Delta\theta_{mo}}{P(P - K_{s_{mo}})} \quad (51)$$

If $t^*(z_{mo}) \geq t_{p-1l}(z_m \leq z_{mo})$, then ponding occurs when the wetting front is in the first layer, thus having $t_p = t_{p-1l}(z_m \leq z_{mo})$. In this case, $t(z_{mo})$ in Eq. (46) is calculated using Eq. (39b). However, when $t^*(z_{mo}) < t_{p-1l}(z \leq z_{mo})$, then the wetting front reaches the second layer prior to ponding. $t(z_{mo})$ in this case would be equal to $t^*(z_{mo})$. In addition, when the wetting front reaches the unmodified layer, we ought to use the equivalent hydraulic conductivity K'_c ; a situation that alters the computation of the ponding time, the infiltration rate, the wetting front location and the cumulative infiltration. Thus, the time of ponding is equal to the time the wetting

front reaches the bottom of the first layer $t^*(z_{mo})$ in addition to the time it takes to pond in the second layer computed using Eq. (38):

$$t_{p-2l} = t^*(z_{mo}) + \frac{K_{s_{umo}}(|h_0 - \psi_{f-umo}|)\Delta\theta_{umo}}{P(P - K_{s_{umo}})} \quad (52)$$

The integration of Eq. (45b) on both sides with initial condition $(z_m, t) = (z_p, t_{p-2l})$, where z_p is calculated using Eq. (48) by replacing Z_{m-umo} with Z_p yields:

$$t(z_m) = t_{p-2l} + (A' - B'|h_0 - \psi_{f-umo}|) \left[\ln \left(\frac{z_m + |h_0 - \psi_{f-umo}|}{z_p + |h_0 - \psi_{f-umo}|} \right) \right] + B'(z_m - z_p) \quad (53)$$

As well, integrating Eq. (45b) by replacing z_m by its value in Eq. (48) on both sides with initial condition $(Z_{m-umo}, t) = (Z_p, t_{p-2l})$, meanwhile assuming that:

$$\frac{dZ_{m-umo}}{dt} = \frac{d}{dt} [Z_{mo}\Delta\theta_{mo} + (z_m - z_{mo})\Delta\theta_{umo}] = \frac{d(z_m\Delta\theta_{umo})}{dt} + \frac{d[z_{mo}(\Delta\theta_{mo} - \Delta\theta_{umo})]}{dt} = \frac{d(z_m\Delta\theta_{umo})}{dt} + 0 = \Delta\theta_{umo} \frac{dz_m}{dt}:$$

$$t(Z_m) = t_{p-2l} + \frac{1}{\Delta\theta_{umo}} \left\{ (C' - B'D') \left[\ln \left(\frac{Z_m - umo + D'}{Z_p + D'} \right) \right] + B'(Z_m - umo - Z_p) \right\} \quad (54),$$

$$\text{where } C' = A'\Delta\theta_{umo} - B'z_{mo}(\Delta\theta_{mo} - \Delta\theta_{umo}) \text{ and } D' = \Delta\theta_{umo} |h_0 - \psi_{f-umo}| - z_{mo}(\Delta\theta_{mo} - \Delta\theta_{umo})$$

3.1.2.1 3-layers profile

When the wetting front is within the upper cover layer ($z_m \leq z_c$), all equations stated in 3.2.1 can be used by replacing all the parameters by those adhering to the subscript 'c'. However, when the wetting front reaches the subsoil intact layer ($z_c < z_m \leq z_c + z_{mo}$), Eqs. (43) to (49) and Eqs. (52) to (54) are to be used by replacing the subscripts 'mo' by 'c' and 'umo' by 'mo'. In addition, when the water moves into the unmodified layer ($z_m > z_c + z_{mo}$), the equivalent hydraulic conductivity becomes (**Damodhara Rao et al., 2006**):

$$K_c'' = \frac{z_m\Delta\theta_{umo}}{\frac{z_c\Delta\theta_c}{K_{sc}} + \frac{z_{mo}\Delta\theta_{mo}}{K_{smo}} + \frac{(z_m - z_c - z_{mo})\Delta\theta_{umo}}{K_{sumo}}} \quad (55)$$

Replacing Eq. (55) in Eq. (32):

$$\Delta\theta_{umo} \frac{dz_m}{dt} = \frac{z_m\Delta\theta_{umo}}{\frac{z_c\Delta\theta_c}{K_{sc}} + \frac{z_{mo}\Delta\theta_{mo}}{K_{smo}} + \frac{(z_m - z_c - z_{mo})\Delta\theta_{umo}}{K_{sumo}}} \times \frac{|h_0 - \psi_{f-umo}| + z_m}{z_m} \quad (56)$$

Eq. (56) is reduced into

$$\frac{dz_m}{dt} = \frac{|h_0 - \psi_{f-umo}| + z_m}{\frac{z_c(\Delta\theta_c - \Delta\theta_{umo})}{(K_{s_c} - K_{s_{umo}})} + \frac{z_{mo}(\Delta\theta_{mo} - \Delta\theta_{umo})}{(K_{s_{mo}} - K_{s_{umo}})} + \frac{z_m \Delta\theta_{umo}}{K_{s_{umo}}}} \quad (57a)$$

Or

$$\frac{dz_m}{dt} = \frac{|h_0 - \psi_{f-umo}| + z_m}{A'' + B'' z_m} \quad (57b), \text{ where } A'' = \frac{z_c(\Delta\theta_c - \Delta\theta_{umo})}{(K_{s_c} - K_{s_{umo}})} + \frac{z_{mo}(\Delta\theta_{mo} - \Delta\theta_{umo})}{(K_{s_{mo}} - K_{s_{umo}})} \text{ and } B'' = \frac{\Delta\theta_{umo}}{K_{s_{umo}}}$$

The integration of Eq. (57b) on both sides with initial condition $(z_m, t) = (z_c + z_{mo}, t(z_c + z_{mo}))$, where $t(z_c + z_{mo})$ is the time arrival of the wetting front to the bottom of the modified layer, yields either an implicit form to determine the wetting front location in terms of time or an explicit solution for the time in terms of the wetting front location as shown in Eq. (58).

$$t(z_m) = t(z_c + z_{mo}) + (A'' - B'' |h_0 - \psi_{f-umo}|) \left[\ln \left(\frac{z_m + |h_0 - \psi_{f-umo}|}{z_c + z_{mo} + |h_0 - \psi_{f-umo}|} \right) \right] + B''(z_m - z_c - z_{mo}) \quad (58)$$

The cumulative infiltration is

$$Z_{m-umo} = z_c \Delta\theta_c + z_{mo} \Delta\theta_{mo} + (z_m - z_c - z_{mo}) \Delta\theta_{umo} \quad (59)$$

Using Eq. (59) to determine explicitly z_m :

$$z_m = \frac{Z_{m-umo} - z_c(\Delta\theta_c - \Delta\theta_{umo}) - z_{mo}(\Delta\theta_{mo} - \Delta\theta_{umo})}{\Delta\theta_{umo}} \quad (60)$$

As well, integrating Eq. (57b) by replacing z_m by its value in Eq. (60) on both sides with initial condition $(Z_{m-umo}, t) = (Z(z_c + z_{mo}), t(z_c + z_{mo}))$, where $Z(z_c + z_{mo})$ is calculated using Eq. (59) by replacing z_m with $z_c + z_{mo}$, meanwhile assuming that:

$$\frac{dZ_{m-umo}}{dt} = \frac{d}{dt} [z_c \Delta\theta_c + z_{mo} \Delta\theta_{mo} + (z_m - z_c - z_{mo}) \Delta\theta_{umo}] = \frac{d(z_m \Delta\theta_{umo})}{dt} + \frac{d[z_c(\Delta\theta_c - \Delta\theta_{umo}) + z_{mo}(\Delta\theta_{mo} - \Delta\theta_{umo})]}{dt} = \frac{d(z_m \Delta\theta_{umo})}{dt} + 0 = \Delta\theta_{umo} \frac{dz_m}{dt} :$$

$$t(Z_m) = \frac{1}{\Delta\theta_{umo}} \left\{ (C'' - B'' D'') \left[\ln \left(\frac{Z_{m-umo} + D''}{D''} \right) \right] + B'' Z_{m-umo} \right\} \quad (61), \text{ where } C'' = A'' \Delta\theta_{umo} - B'' z_c (\Delta\theta_c - \Delta\theta_{umo}) - B'' z_{mo} (\Delta\theta_{mo} - \Delta\theta_{umo}) \text{ and } D'' = \Delta\theta_{umo} |h_0 - \psi_{f-umo}| - z_c (\Delta\theta_c - \Delta\theta_{umo}) - z_{mo} (\Delta\theta_{mo} - \Delta\theta_{umo})$$

It is critical to identify the wetting front location during the initiation of ponding. Using Eqs. (50) and (51) and by substituting the subscript ‘mo’ by ‘c’, we compare the time for the wetting front to reach the bottom of the first layer with the time for ponding to occur as if the wetting front is still in the top layer:

$$t^*(z_c) = \frac{z_c}{P} = \frac{z_c \Delta \theta_c}{P} \quad (62)$$

$$t_{p-1l}(z_m \leq z_c) = \frac{K_{s_c}(|h_0 - \psi_{f-c}|) \Delta \theta_c}{P(P - K_{s_c})} \quad (63)$$

If $t^*(z_c) \geq t_{p-1l}(z_m \leq z_c)$, then ponding occurs when the wetting front is in the first layer, thus resulting in $t_p = t_{p-1l}(z_m \leq z_c)$. In this case, $t(z_c + z_{mo})$ in Eq. (58) is calculated using Eq. (46) while substituting the subscripts ‘mo’ and ‘umo’ with ‘c’ and ‘mo’ respectively and z_m with $z_c + z_{mo}$. Consequently, $t(z_{mo})$ in Eq. (46) becomes $t(z_c)$ which is calculated using Eq. (39b) which is computed by replacing z_m with z_c . However, when $t^*(z_c) < t_{p-1l}(z_m \leq z_c)$, then the wetting front moves beyond the top layer. We proceed to identify whether ponding occurs before or after the wetting front moves into the third layer, we shall determine the time for the wetting front to reach the bottom of the second layer $t''(z_{mo})$ (without taking into effect any ponding yet) and the time to pond if the wetting front is still in the second layer $t_{p-2l}(z_c < z_m \leq z_{mo})$ using Eq. (51):

$$t^*(z_c + z_{mo}) = \frac{z_c \Delta \theta_c}{P} + \frac{z_{mo} \Delta \theta_{mo}}{P} \quad (64)$$

$$t_{p-2l}(z_c < z_m \leq z_{mo}) = t^*(z_c) + \frac{K_{s_{mo}}(|h_0 - \psi_{f-mo}|) \Delta \theta_{mo}}{P(P - K_{s_{mo}})} \quad (65)$$

If $t^*(z_c + z_{mo}) \geq t_{p-2l}(z_c < z_m \leq z_{mo})$, then ponding occurs when the wetting front is in the second layer, thus resulting in $t_p = t_{p-2l}(z_c < z_m \leq z_{mo})$. In this case, $t(z_c + z_{mo})$ is calculated using Eq. (53) while substituting the subscripts ‘mo’ and ‘umo’ with ‘c’ and ‘mo’ respectively. However, when $t^*(z_c + z_{mo}) < t_{p-2l}(z_c < z_m \leq z_{mo})$, then the wetting front reaches the third layer prior to ponding then $t(z_c + z_{mo})$ is equal to $t^*(z_c + z_{mo})$. Thus, Thus, the time of ponding is equal to the time the wetting front will reach the bottom of the second layer $t^*(z_c + z_{mo})$ in addition to the time it takes to pond in the third layer computed using Eq. (38):

$$t_{p-3l} = t^*(z_c + z_{mo}) + \frac{K_{s_{umo}}(|h_0 - \psi_{f-umo}|) \Delta \theta_{umo}}{P(P - K_{s_{umo}})} \quad (66)$$

The integration of Eq. (57b) on both sides with initial condition $(z_m, t) = (z_p, t_{p-3l})$, where z_p is calculated using Eq. (60) by replacing Z_{m-umo} with Z_p yields:

$$t(z_m) = t_{p-3l} + (A'' - B''|h_0 - \psi_{f-umo}|) \left[\ln \left(\frac{z_m + |h_0 - \psi_{f-umo}|}{z_p + |h_0 - \psi_{f-umo}|} \right) \right] + B''(z_m - z_p) \quad (67)$$

As well, integrating Eq. (57b) by replacing z_m by its value in Eq. (60) on both sides with initial condition $(Z_{m-umo}, t) = (Z_p, t_{p-3l})$, meanwhile assuming that:

$$\frac{dZ_{m-umo}}{dt} = \frac{d}{dt} [z_c \Delta\theta_c + z_{mo} \Delta\theta_{mo} + (z_m - z_c - z_{mo}) \Delta\theta_{umo}] = \frac{d(z_m \Delta\theta_{umo})}{dt} + \frac{d[z_c(\Delta\theta_c - \Delta\theta_{umo}) + z_{mo}(\Delta\theta_{mo} - \Delta\theta_{umo})]}{dt} = \frac{d(z_m \Delta\theta_{umo})}{dt} + 0 = \Delta\theta_{umo} \frac{dz_m}{dt} :$$

$$t(Z_m) = t_{p-3l} + \frac{1}{\Delta\theta_{umo}} \left\{ (C'' - B''D'') \left[\ln \left(\frac{Z_{m-umo} + D''}{Z_p + D''} \right) \right] + B''(Z_{m-umo} - Z_p) \right\} \quad (68)$$

where $C'' = A''\Delta\theta_{umo} - B''z_c(\Delta\theta_c - \Delta\theta_{umo}) - B''z_{mo}(\Delta\theta_{mo} - \Delta\theta_{umo})$ and $D'' = \Delta\theta_{umo}|h_0 - \psi_{f-umo}| - z_c(\Delta\theta_c - \Delta\theta_{umo}) - z_{mo}(\Delta\theta_{mo} - \Delta\theta_{umo})$

3.2.3 Model Validation

The same experimental setup described in section 3.1.6 is applied to run irrigation simulation for 2 and 3 layers of soils takes from Site 1 only. For each profile, the experiment is duplicated but each time using different irrigation rate: P_1 (1.875 cm/min) to observe ponding while the wetting front is still in the modified layer and P_2 (0.25 cm/min) resulting in the initiation of surface runoff when the wetting front reaches the unmodified layer. For 3-layers profile in particular, the pressure needed to have ponding in the first layer having the largest hydraulic conductivity and shallow depth is high and cannot be performed using the setup described. Since all treatments will be later analyzed for infiltration simulation after model validation, we will choose only one 2-layers profile and one 3-layers profile to run. The 2-layers profile includes a rotary tilled layer on the top and a compacted layer in the bottom while the 3-layers profile is formed of 5cm crop residues cover, a rotary tilled layer and a compacted layer. Table 8 summarizes the properties of each soil profile. Initial conditions of moisture content and matric potential are measured for each layer using real-time monitoring sensors TEROS12 (TEROS12, METER Group) (Singh et al., 2020) and TEROS21 (TEROS 21, METER Group) (Wang et al., 2020a), respectively. The working suction range of the tensiometer is limited between -9 and -2000kPa.

Nevertheless, a pro-check handheld meter is connected to each sensor for measurements' readings.

The validation is achieved by evaluating the performance of the model through the calculation of the Nash–Sutcliffe Efficiency (NSE; Nash & Sutcliffe, 1970).

$$NSE = 1 - \frac{\sum_{i=1}^N (\text{predicted}_i - \text{actual}_i)^2}{\sum_{i=1}^N (\text{predicted}_i - \bar{\text{actual}})^2} \quad (64),$$
 where $NSE \leq 1$. The upper limit corresponds to a perfect model, while values above 0.75, 0.65 and 0.5 results in a very good, good, and acceptable model (Moriassi et al., 2007).

Table 8: Initial, boundary and physical properties of the experiments for model validation

Soil Profile	Formation	Depth (cm)	K_s [cm/min]	θ_s [cm^3/cm^3]	θ_i [cm^3/cm^3]	ψ_f [cm]
Irrigation Rate = 1.875 cm/min						
2-layers	RT	0-20	0.04803 ± 0.00819	0.57549 ± 0.02992	0.06613 ± 0.00432	113.80 ± 2.23
	NT	20-40	0.00847 ± 0.00031	0.43342 ± 0.03791	0.07837 ± 0.00561	562.05 ± 8.90
3-layers	CC	0-5	1.91176 ± 0.05392	0.89354 ± 0.00060	0.01225 ± 0.00025	14409.73 ± 74.28
	RT	5-25	0.04803 ± 0.00819	0.57549 ± 0.02992	0.07867 ± 0.00167	60.13 ± 0.62
	NT	25-40	0.00847 ± 0.00031	0.43342 ± 0.03791	0.08513 ± 0.00350	550.08 ± 9.64
Irrigation Rate = 0.25 cm/min						
2-layers	RT	0-10	0.04803 ± 0.00819	0.57549 ± 0.02992	0.08425 ± 0.00125	113.80 ± 2.23
	NT	10-40	0.00847 ± 0.00031	0.43342 ± 0.03791	0.09133 ± 0.00276	5530.91 ± 107.19
3-layers	CC	0-5	1.91176 ± 0.05392	0.89354 ± 0.00060	0.01250 ± 0.00065	14296.9 ± 111.80
	RT	5-15	0.04803 ± 0.00819	0.57549 ± 0.02992	0.0735 ± 0.00238	83.01 ± 2.35
	NT	15-40	0.00847 ± 0.00031	0.43342 ± 0.03791	0.075 ± 0.00207	555.70 ± 8.82

3.3 Optimal Soil Management System

3.3.1 Model Simulation

GARALS is applied to a different combinations of soil management systems of two and three layers of Site 1 – Loamy sand. The model only tolerates a decreasing saturated hydraulic conductivity from top to bottom, hence MC is not chosen as a cover except for MC+NT since it has a saturated hydraulic conductivity smaller than those of the other layers.

Since each layer is treated as a homogeneous and independent layer, in this section the combinations of soil layers' profiles found in Table 1 are chosen so that the underlying layer has always a smaller saturated hydraulic conductivity (CC+NT, MC+NT, RT+NT, MTA+NT, MT+NT, CC+RT+NT, CC+MTA+NT, CC+MT+NT, CC+MC+NT). Each soil management system is simulated for water infiltration under steady irrigation rates (0.01, 0.05, 0.1, 0.5, 1, 2, 5, 10, 20, and 40 cm/min) to evaluate which profile is able to move water to deeper depths faster in study area of Site 1 regardless of the irrigation rate. The depths of layers are fixed as 5cm for covers, 20cm for modified layers and infinite depth for intact/unmodified NT layer. Initial conditions shown in Table 9 of moisture content and matric potential are measured for each layer using TEROS12 and TEROS21, respectively, on site in the randomized design block applied in section 3.1.2.

Table 9: Initial properties of the different soil management systems for water infiltration simulation

Formation	Depth (cm)	K_s [cm/min]	θ_s [cm^3/cm^3]	θ_i [cm^3/cm^3]	ψ_f [cm]
CC	0-5	1.91176 ±	0.89354 ±	0.01 ±	17654.21 ±
		0.05392	0.00060	0.00026	84.13
MC	0-5	0.02100 ±	0.74150 ±	0.0357 ±	84076.20 ±
		0.00012	0.00361	0.00072	112.72
RT	0-20	0.04803 ±	0.57549 ±	0.05 ±	113.80 ± 2.23
		0.00819	0.02992	0.00252	
MTA	0-20	0.12054 ±	0.54843 ±	0.078 ±	54879 ±
		0.00975	0.06989	0.00457	91.64
MT	0-20	0.04703 ±	0.60725 ±	0.0579 ±	26534.97 ±
		0.00185	0.05220	0.00641	86.72
NT	>20	0.00847 ±	0.43342 ±	0.07837 ±	1363.59 ±
		0.00031	0.03791	0.00561	38.11

3.3.2 Soil Treatment Optimization

The ultimate purpose is to identify the best soil management system that when implemented in Site 1, can drain water faster and to greater depths. The system is optimized by introducing the concept of artificial macropores. Additionally, the system will opt covers to assess the ability of soil to preserve the water while protecting it from extreme evaporation. Initially, to assess the best management system, an irrigation rate equal to that used on field is used (0.04cm/min). The type of cultivation in Site 1 is a mixture of vegetables and apple trees. So, after an investigation to determine an acceptable and moderate subsurface soil depth to irrigate, 40 cm of

saturated soil is ideal for Site 1 as referred by the farmers. Therefore, the first criteria involve choosing all systems having wetting front depth larger than 40cm prior to ponding not to have any waste in water. For the chosen systems, a further identification is set to determine the treatment that insures the least amount of cumulative water (since we want to use the least amount of water for preservation purposes) while having fastest times to reach 10, 20, 30 and 40 cm depths. It is noteworthy to mention that the aforementioned depths are measured from the initial soil surface so that the additional depths of added covers are taken into consideration. After identification of the best soil management system using the initial properties listed in Table 8, the treatment is applied on field in Site 1 over a total area of 2.2m x 1.5m (~3.3m²). The treatments are implemented on 3 plots identically twice (plot 1 [1a & 1b], plot 2 [2a & 2b], and plot 3 [3a & 3b]), while each 90 cm x 60 cm plot is buffered from the next plot by a 90 cm x 10 cm zone as shown in Figure 6. A soil moisture sensor TEROS10 placed in each soil plot in the soil at 20 cm depth and left during and after the entire study period for real-time monitoring. Hence, the TEROS10 indicates moisture contents larger than 0.4 m³/m³ when the voids start to fill with water. After the application of the system, artificial macropores (AM) are only placed in plot 2 and plot 3. In plot 3, the AM are filled with crop residues (CC-AM) while those in plot 2 are left empty (AM). They are created vertically into the soil using a steel rod of 2 cm diameter (**Mori and Hirai, 2014**). The rod is pushed into the soil with light pressure at depths of 20 cm and equally spaced of 15cm with 15cm margins transversely, and 20 cm with 20cm margins longitudinally resulting in 9 AM in total in each plot. Notwithstanding, since the soil was initially dry, the AM collapsed after the removal of the rods. Therefore, we irrigated the plots for 15 minutes after which the simulation was stopped to insert the AM after which the irrigation was resumed.

On the other hand, the irrigation event was applied similarly to how local farmers apply it without any alteration of the system. The irrigation system consists of primary and secondary pipes that are connected to a centralized system which only holds filters for suspended solids. The source of water comes from a water pond elevated from the land by 40 m. Sprinkles are connected to secondary pipes and are installed for every 50 cm x 50 cm plot. A steady state rate of 7.3m³/day ± 0.22 was naturally maintained. The plots were irrigated for 6 hours and a half in the morning starting at 9:00am. Real-time monitoring data were recorded along 5 minutes' increments in the first one hour and a

half followed by 10 minutes' intervals and later 30 minutes during the irrigation period and for 2 hours following the irrigation event the same day of irrigation event while the monitoring continued on the next six days in the morning and the evening. It is also noted that after the irrigation event, crop residues were placed at 5cm depth to cover plots 1b, 2b, and 3b. The resultant data of moisture are then evaluated by comparing the moisture content at 20 cm below the soil surface. The optimized treatment would have the highest moisture contents in shorter times during the irrigation period and will maintain higher moisture content for longer times following the irrigation event.

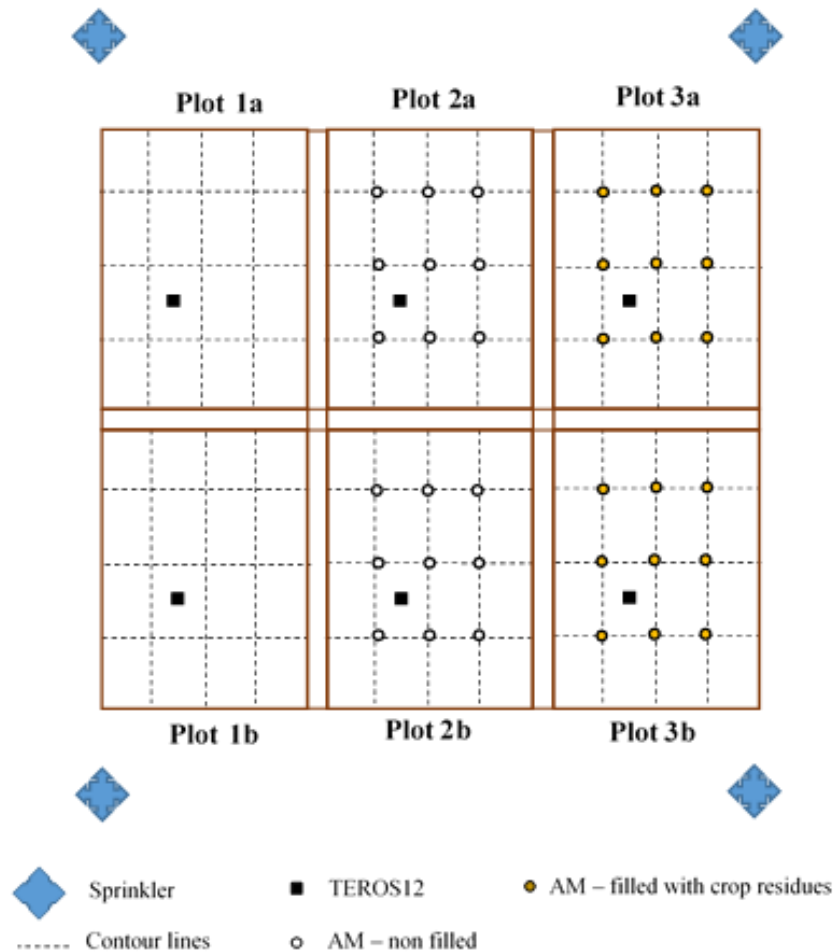


Figure 6: Field experimental setup to optimize the optimal management system with the creation of artificial macropores

Chapter Four

Results and Discussion

4.1 Soil Properties

4.1.1 Organic Matter Additives

4.1.1.1 Densities

Bulk, dry, and saturated density of chicken manure ($0.3446 \text{ g.cm}^{-3} \pm 0.0023$, $0.2726 \text{ g.cm}^{-3} \pm 0.0036$, 1.0141 g.cm^{-3} , respectively) are significantly greater (**P<0.001) than those of straw residues ($0.0837 \text{ g.cm}^{-3} \pm 0.0006$, $0.0837 \text{ g.cm}^{-3} \pm 0.0006$, 0.9772 g.cm^{-3} , respectively) (as shown in Figure 7). It was reported by **Khater (2015)** that the bulk densities of cattle manure, herbal plants residues, and sugar cane plants residues are 0.655 g.cm^{-3} , 0.582 g.cm^{-3} , and 0.420 g.cm^{-3} , respectively while having moisture contents of 25.6%, 31.2%, and 32.1%, respectively. Compared to our values, the moisture contents of chicken manure and straw residues when measuring the bulk density were $26.44 \% \pm 2.17$ and $0\% \pm 0$, respectively. The bulk density of chicken manure is less than that of cattle manure and the bulk density of straw residues is less than those of herbal plants residues and sugar cane plants residues. This is because the material in **Khater (2015)** was compacted in opposition to the materials tested in this study in which the organics were filled in the containers as if they are thrown on the ground. Notwithstanding, similar results for chicken manure were obtained for farmyard manure made from cow dung having a bulk density of 0.3462 g.cm^{-3} with a moisture content of 23.55% (**Sahu et al., 2020**). Comparing the bulk densities with the optimal values indicated by **Reynolds et al. (2009)** found in Table 5, both organic additives are not suitable for plant anchoring while their capacities to hold water for plants are limited. The inappropriateness of having these substances as a replacement for medium cultivation is ample to drive farmers to only use them either as soil cover of shallow depths or as organic additives to soil. However, it is essential to mention that the compaction of organic matter increased the bulk densities as found in **Khater (2015)**, hence organic matter in particular chicken manure is highly predicted to be adequate to replace soil when it is appropriately compacted. In addition, it was referred by **Caron et al. (2015b)** that mixing different components of organic matter can result

in a mixture suitable to physically support root growth thereby be used as growing medium. For instance, the bulk density of a green waste compost ($0.64 \text{ g.cm}^{-3} \pm 0.0045$) was increased to the optimal range of 0.9-1.2 for maximum crop production when ground bricks was added in different mixing ratios (Willaredt & Nehls, 2021).

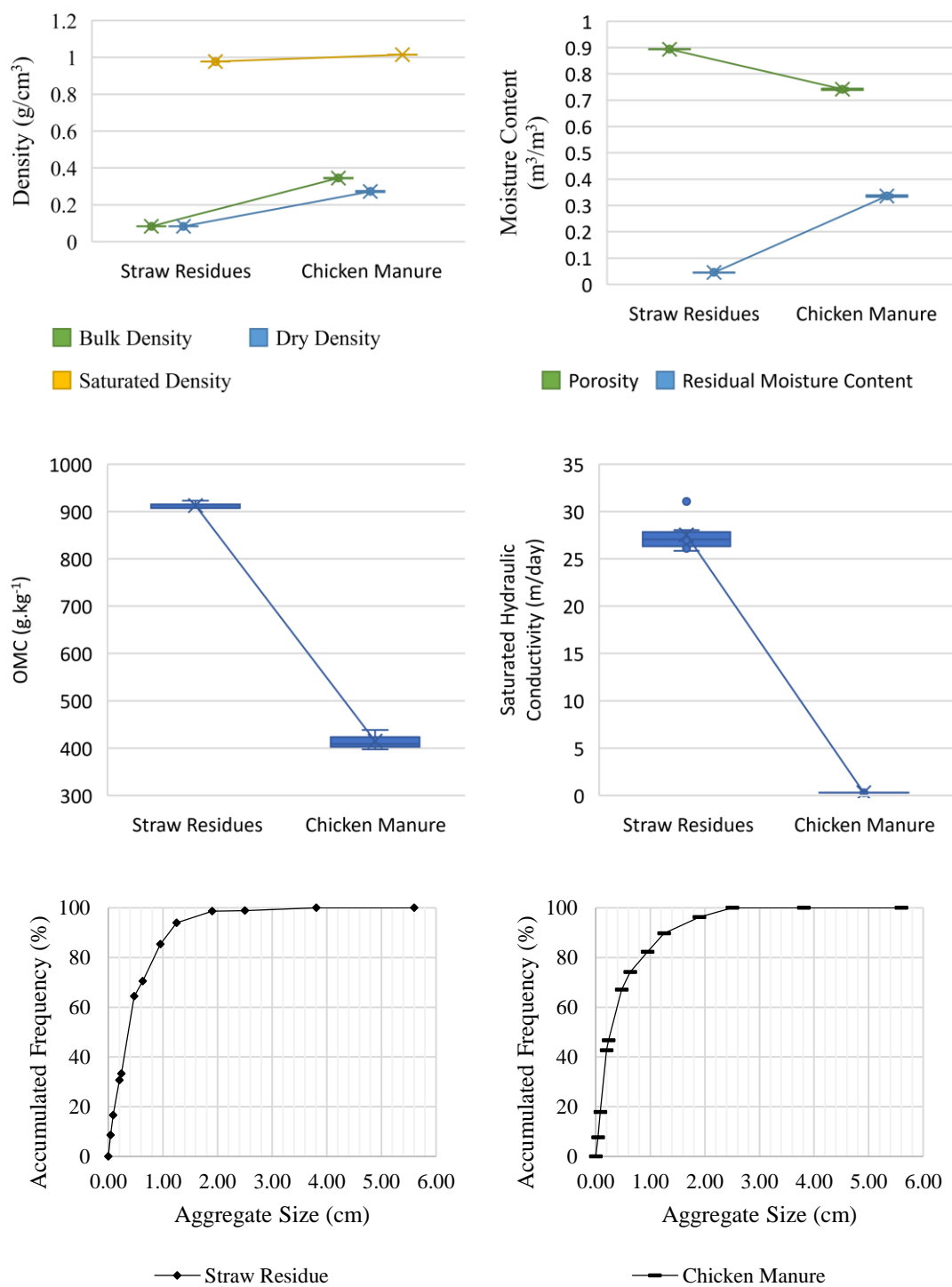


Figure 7: Physical properties of straw residues and chicken manure

4.1.1.2 Organic Matter Content

The organic matter content in chicken manure ($414.75 \text{ g.kg}^{-1} \pm 12.20$) is significantly less ($***P < 0.001$) than that in straw residues ($912.45 \text{ g.kg}^{-1} \pm 5.20$) (as shown in Figure 7). Lower organic matter contents were reported in **Khater (2015)** for cattle manure (313 g.kg^{-1}) than chicken manure and for herbal plants residues and sugar cane plants residues (431 g.kg^{-1} and 613 g.kg^{-1} , respectively) than straw residues. Nonetheless, cow dung (OMC = 510.3 g.kg^{-1}) has higher OMC than chicken manure (**Khaing et al., 2019**). Yet, straw residues are found to have the highest organic matter content even greater than green waste composts reported by **Willaredt and Nehls (2021)** ($0.268 \text{ g.kg}^{-1} \pm 0.0052$) and higher than agricultural wastes as cited by **Khaing et al. (2019)**. Notwithstanding, **Khaing et al. (2019)** reported organic matter contents for sesame husk (899.7 g.kg^{-1}), saw dust (911.8 g.kg^{-1}), chaff (234.9 g.kg^{-1}), cow dung (510.3 g.kg^{-1}), and rice husk (793.6 g.kg^{-1}). When these agricultural wastes are mixed while each having a mass of 250g, the organic matter content of the resultant compost becomes 228.9 g.kg^{-1} . Further, the organic matter content drops when green waste composts are mixed with ground bricks (**Willaredt & Nehls, 2021**). The alteration in organic matter between different organic substrates and organic mixtures is important to consider since changes in organic matter contents imply different soil structures and thereby affecting moisture drainage and maintenance in the pore system of the medium (**Panagea et al., 2021**).

4.1.1.3 Porosity and Residual Moisture Content

Higher porosities are significantly ($***P < 0.001$) stated in straw residues ($0.8935 \text{ m}^3.\text{m}^{-3} \pm 0.0006$ equivalent to $10.6780 \text{ g H}_2\text{O.g}^{-1}$ straw residues ± 0.0828) then chicken manure ($0.7415 \text{ m}^3.\text{m}^{-3} \pm 0.0036$ equivalent to $2.7212 \text{ g H}_2\text{O.g}^{-1}$ chicken manure ± 0.0493) (as shown in Figure 7). On the contrary, higher residual moisture contents ($***P < 0.001$) were found for chicken manure ($0.3359 \text{ m}^3.\text{m}^{-3} \pm 0.0036$ equivalent to $1.2327 \text{ g H}_2\text{O.g}^{-1}$ chicken manure ± 0.0296) than for straw residues ($0.0451 \text{ m}^3.\text{m}^{-3} \pm 0.0006$ equivalent to $0.5390 \text{ g H}_2\text{O.g}^{-1}$ straw residues ± 0.0109). Green waste composts are found to have intermediate values of saturated and residual moisture content between chicken manure and straw residues ($\theta_s \sim 0.64 \text{ m}^3.\text{m}^{-3}$, $\theta_r \sim 0.22 \text{ m}^3.\text{m}^{-3}$) (**Willaredt & Nehls, 2021**). Notwithstanding, **Quemada and Cabrera (2002)** found that the maximum water contents for clover leaves, rye leaves, clover stems, and rye stems are $4.5 \text{ g H}_2\text{O.g}^{-1}$, $2.9 \text{ g H}_2\text{O.g}^{-1}$, $3.7 \text{ g H}_2\text{O.g}^{-1}$ and $2.1 \text{ g H}_2\text{O.g}^{-1}$, respectively,

while the residual water contents are $0.2 \text{ g H}_2\text{O.g}^{-1}$, $0.1 \text{ g H}_2\text{O.g}^{-1}$, $0.2 \text{ g H}_2\text{O.g}^{-1}$ and $0.2 \text{ g H}_2\text{O.g}^{-1}$ for clover leaves, rye leaves, clover stems, and rye stems, respectively. Albeit the aforementioned organics are cut, they have lower residual contents with smaller pore sizes than the straw residues. It is noteworthy to highlight the effect of the hydrophobicity that is positively correlated with some organic matter (**MataixSolera and Doerr 2004; Nakaya 1981**) as reflected in the low residual contents (**Quemada and Cabrera, 2002**) which impedes the storage capacities. On the other hand, values of porosities reported by **Quemada and Cabrera (2002)** are closer to those of chicken manure than the straw residues. Similarly, other studies reported near porosity values to chicken manure than straw residues for oat straw (2.5g.g^{-1}) (**Bartholomew & Norman, 1946**) and for wheat straw (slightly over 3g.g^{-1}) (**Myrold et al., 1981**). While it seems paradoxical, the straw used in those researches were either cut (**Quemada & Cabrera, 2002**), chopped (**Myrold et al., 1981**) or grounded to pass 2-mm sieve (**Bartholomew & Norman, 1946**) so that their pore structure resembles that of the chicken manure and not the straw residues which are not chopped in this study. Hence, the capacity of a porous medium to hold and maintain water depends on the pore-size distribution of the medium in addition to the composition since the presence of organic matter doesn't always signify water repellency (**Nakaya et al., 1977**). This hypothesis is verified by the residual moisture content obtained by **Khater (2015)** for cattle manure (3.5g.g^{-1}), herbal plant residues (3.9g.g^{-1}), and sugar cane plants residues (4.4g.g^{-1}) which are significantly larger than those of chicken manure and straw residues as cited in this study while smaller porosities were reported ($0.61 \text{ m}^3.\text{m}^{-3}$ for cattle manure, 0.67 for herbal plants residues, and 0.72 for sugar cane plants residues). The discrepancies are due to the compaction application applied in **Khater (2015)** that increased the capacity of soil substrate to hold more water for longer periods by decreasing the pore sizes.

4.1.1.4 Aggregate Size Distribution

From the aggregate size distribution found in Figure 7, chicken manure partakes 40%, 40% and 20%, while straw residues endure 30%, 55%, and 15% of aggregates of sizes finer than 2mm, between 2mm and 10mm, and greater than 10mm, respectively. Consequently, both organic substrates have a range in their pore sizes distribution. It is noteworthy to mention that through observation the large aggregates ($>10\text{mm}$) found in straw residues are due to the longitudinal shape of straws that couldn't pass the

coarser sieves due to the position of displacement. Yet, such aggregates found in chicken manure are due to very fine organics bounded to each other during composting period (wetting and drying processes) to form large aggregate. Such distributions resulted in near values for the mean weight diameter (5.03mm for straw residues and 4.95mm for chicken manure). Hence, higher MWD was reported for cow dung farmyard manure (22mm) (**Sahu et al., 2020**) even though both chicken manure (344.56 kg.m⁻³) and cow dung (346.25 kg.m⁻³) had close bulk densities. This means that the inconsistency in the MWD is caused by dependence of aggregate formation and the pore-size distribution of the medium rather than on the total volume of pores.

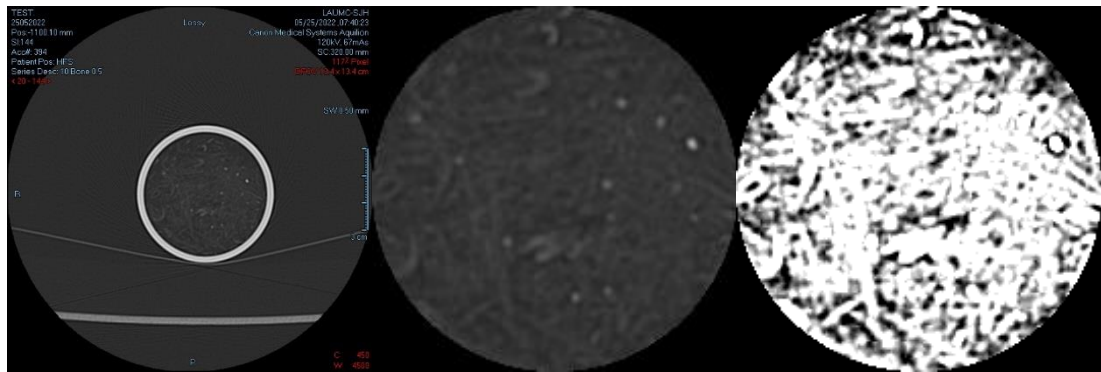
4.1.1.5 Saturated Hydraulic Conductivity

As expected, the straw residues (27.5290 m/day \pm 0.7764) acquired a significant larger (**P<0.001) saturated hydraulic conductivity than chicken manure (0.3025 m/day \pm 0.0024) (as shown in Figure 7). This is because a wider range of moisture contents was observed between the residual and saturated moisture content for straw residues ($\theta_s - \theta_r = 0.8484 \text{ m}^3.\text{m}^{-3}$) than chicken manure ($\theta_s - \theta_r = 0.4057 \text{ m}^3.\text{m}^{-3}$). This means that water is better drained in straw residues than chicken manure while keeping in mind that the aggregate size distribution of straw residues endures a wider range of coarser pores. In addition, the large aggregates in the straw residues are dry and thirsty so that when they are saturated, the aggregates themselves become conductive due to the high organic matter content in opposition to the large aggregate found in chicken manure. Such aggregates get clogged so that water passage becomes only applicable in larger pores. According to **Reynolds et al. (2009)**, the saturated hydraulic conductivity of chicken manure is almost within the range of optimal infiltration while impeding surface runoff (if it was compacted, then higher K_s would have been recorded). However, the saturated hydraulic conductivity of straw residues indicate that the medium has an excessive of coarse pores which results in having a high conductive medium but subjective to fast droughts.

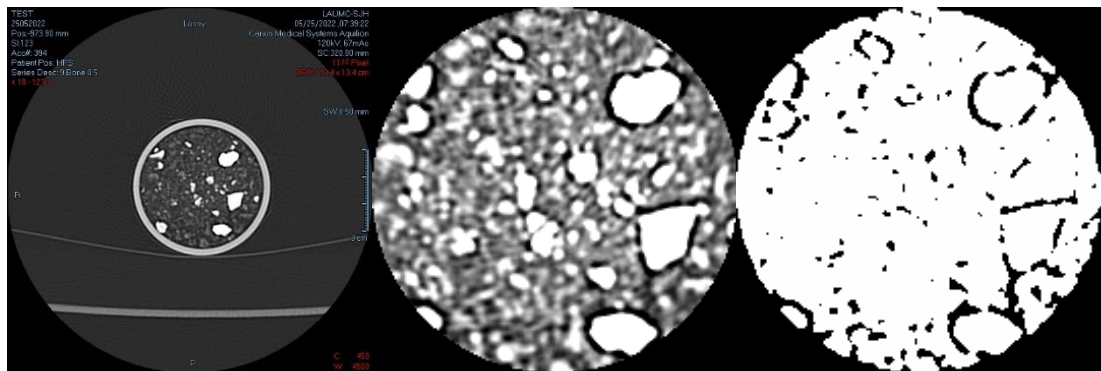
4.1.1.6 Pore Structure and WRC

The pore structure as illustrated in Figure 8 from CT-scans differ by shape, size, and distribution. Large pore sizes exist on the boundary of large aggregates in straw residues and chicken manure samples, while their shape changes between wide and longitudinal pores in straw residues and curved and circular in chicken manure. The connectivity of pores in straw residues is better than that in chicken manure, since the

pores in the formed are more distributed over the entire surface area of the samples while those are only found around aggregation formations. Hence, such aggregation may not be distributed along the same vertical plane in the chicken manure.



(a)



(b)

Figure 8: CT scanning images for (a) straw residues and (b) chicken manure. On the left, the picture is the result of the CT-scan which is cropped to a diameter of 4cm, after which brightness and contrast are adjusted while filters are applied to convert the picture into 8-bit image with a threshold of two colors 0 (matter) and 255 (pore space).

The observational interpretation is further juxtaposed by the volumetric content distribution of pore sizes in these two soil substrates (as shown in Figure 9). Hence, straw residues have 0.046, 0.095, 0.727, and 0.025 $\text{m}^3 \cdot \text{m}^{-3}$ porosities corresponding to pore sizes finer than 0.1mm, between 0.1 and 1mm, between 1 and 5mm, and larger than 5mm, respectively. In opposition, porosities of chicken manure of the same pore sizes are 0.367, 0.252, 0.118, and 0.004 $\text{m}^3 \cdot \text{m}^{-3}$. Higher volumetric contents of medium and large pores exist in the straw residues, while finer pores ($<0.1\text{mm}$) are more

profuse in the chicken manure that are mainly found in the large aggregates (also observed in the CT-scan images: there are no black dots in the large aggregates of the chicken manure which explains that the pores are so fine ($<0.1\text{mm}$) that the resolution of CT-scan couldn't detect them). In addition, it is evident that the pores in straw residues have almost the same size which explains the well sorting behavior of WRC. This means that the chicken manure is better graded than the straw residues since it has abundant porosities of different pore sizes.

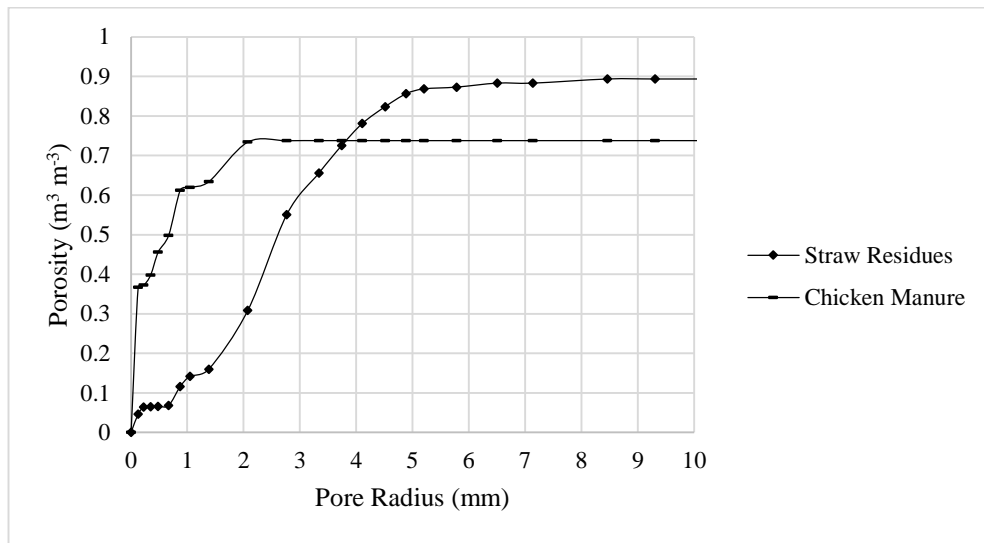


Figure 9: Porosity Distribution for straw residues and chicken manure from the analysis of volumetric contents of pore sizes in ImageJ

Figure 10a and 10b exemplifies the observed and fitted moisture content with respect to the matric potential. Both model fittings using RETC software are good-fit models with R-squared greater than 0.99. α and n are higher for straw residues ($\alpha=0.1875\text{mm}^{-1}$, $n=3.8837$) than chicken manure ($\alpha=0.064\text{mm}^{-1}$, $n=2.6971$). The fitted van Genuchten parameters α and n are used to simulate the soil water retention curves developed in Figure 10c. Chicken manure drains over a large range of matric potential in opposition to straw residues which drains over a smaller range of potentials. This means that the straw residues is better sorted than the chicken manure. Notwithstanding, chicken manure can hold more water while straw residues can convect more rapidly. For instance, at 100kPa (equivalent to 10mm matric potential), the WRC is higher for chicken manure than straw residues, while between 10kPa

(~1mm) and 980kPa (~100mm) potential pressure, $0.69 \text{ m}^3 \cdot \text{m}^{-3}$ of porosity is activated in straw residues while $0.15 \text{ m}^3 \cdot \text{m}^{-3}$ of porosity allow water drainage. Similar results of fast drainage for straw residues were observed in other studies for clover stems, rye stems, clover leaves and rye leaves (Quemada & Cabrera, 2002). In addition, a correlation between bulk density and the SWR curve was reported by many researchers (Husz, 1967; Gupta & Larson, 1979; Arya & Paris, 1981; Vereecken et al., 1989) in which the higher the bulk density, the more stretched is the SWRC. Hence, this hypothesize is verified with our study.

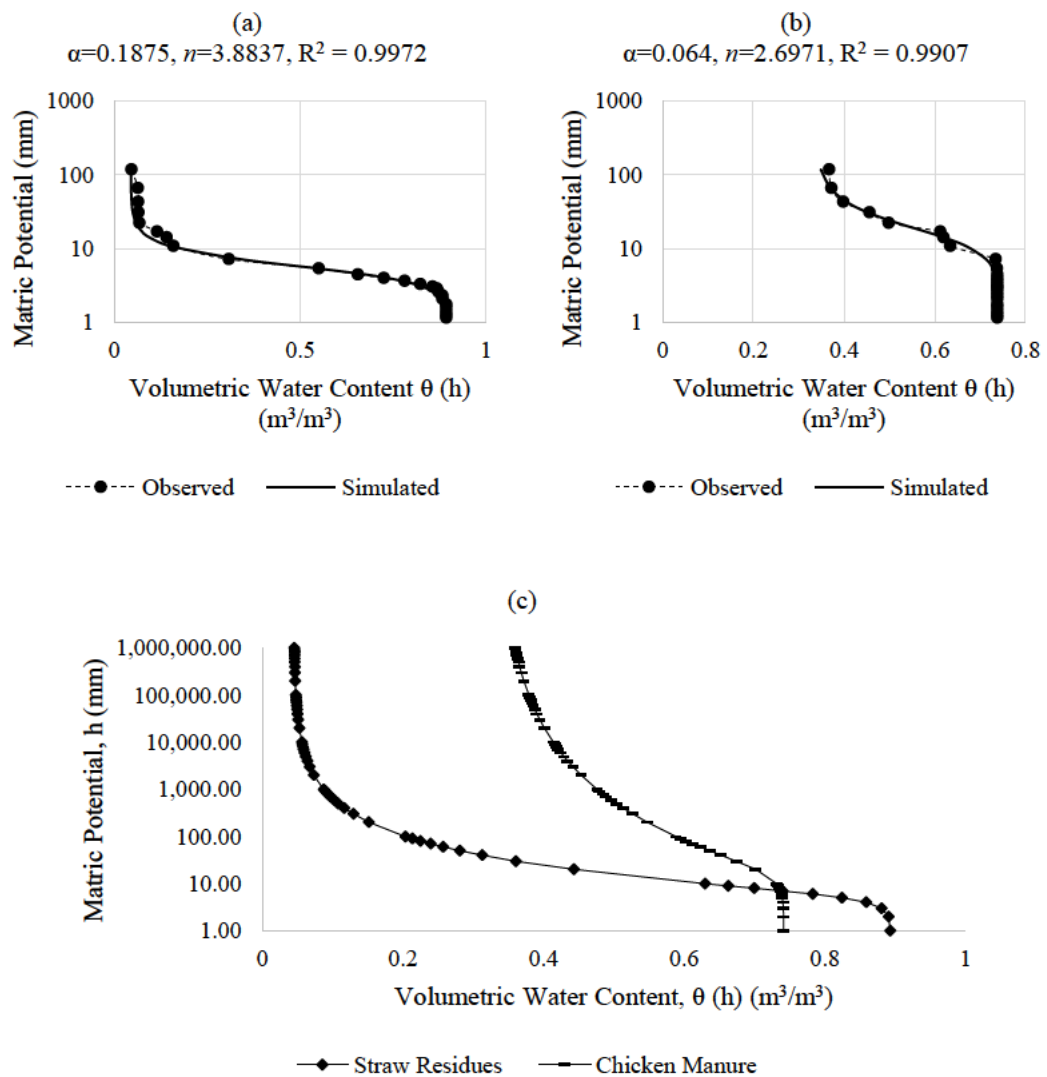


Figure 10: Soil water retention curve for straw residues and chicken manure (a) and (b) are the simulated SWRC using RETC software vs the calculated values using CT-scans for straw residues and chicken manure, respectively and (c) predicted characteristics moisture of straw residues and chicken manure. Units of α : 1/mm

4.1.1.7 Physical Quality Indicators

According to Table 10, both soil substrates have optimal air capacity and S theory values, meaning they both have adequate capacities for root and microbial activity aeration in a satisfactory medium of good physical and structural quality. However, PAWC is limited in chicken manure while droughty conditions are appeared in straw residues making it limited with water. Yet, chicken manure indicates an optimal balance between AC and PAWC as an indication for a better microbial production due to the balanced water and air content availability for longer time periods. Hence the limitation of water storage in straw residues and better capacities of water maintenance in chicken manure were also observed in the WRC.

Table 10: Soil physical quality indicators for straw residues and chicken manure

Soil Physical Quality Indicators	Straw Residues	Chicken Manure
$\theta(FC)$	0.0875	0.4765
$\theta(PWP)$	0.0474	0.3749
Air Capacity AC	0.8059	0.2649
PAWC	0.0401	0.1015
RFC	0.0980	0.6426
S theory	0.3126	0.0749

4.1.2 Site 1 – Loamy Sand

4.1.2.1 Densities

Tillage application decreases significantly the bulk density (*P-value = 0.018) from $1.149 \text{ g/cm}^3 \pm 0.047$ (NT) to $0.954 \text{ g/cm}^3 \pm 0.037$ (RT) to $0.852 \text{ g/cm}^3 \pm 0.084$ (MTA) to $0.809 \text{ g/cm}^3 \pm 0.065$ (MT) and the dry density (*P-value = 0.024) from $0.899 \text{ g/cm}^3 \pm 0.037$ (NT) to $0.729 \text{ g/cm}^3 \pm 0.029$ (RT) to $0.679 \text{ g/cm}^3 \pm 0.069$ (MTA) to $0.629 \text{ g/cm}^3 \pm 0.052$ (MT) (as shown in Figure 11). Accordingly, NT layer proves to be more compacted and evidently is denser with grains and finer with pores (Ball-Coelho et al., 1998; Schønning and Rasmussen, 2000) but proves to be efficient for maximum crop production in loamy sand soil while not causing any harm to root growth (critical range between 0.9 and 1.2 g/cm^3) (Singh & Malhi, 2006). The tillage application reduced the bulk density by 17%, yet the reduction didn't affect the quality for crop production. The reduction of bulk density from NT to RT was the result of soil loosening (Buschiazzo et al., 1998), hence this was observed in many studies (Taser

& Metinoglu, 2005; Fabrizzi et al., 2005; Afzalnia & Zabihi, 2014; Salem et al., 2014). Within the tilled layer, the addition of crops and manure to soil decrease the bulk of RT by 15% and 11% and the dry density of RT by 14% and 7%, respectively to produce a body that is inadequate for plant anchoring and water storage, thereby causing a dilution effect on the soil (Zhang et al., 2014). The decrease is due to the low dry and bulk densities of CC and MC. Further, the addition of crops generates a larger decrease than manure on the short-run because CC has smaller bulk and dry densities (BD=DD=0.083 g/cm³ ± 0.0006) than MC (BD=0.344 g/cm³ ± 0.00234, SD=0.272 g/cm³ ± 0.00361). Similar decrease in the bulk density with the addition of organics in sandy soils was reported on the long term and was due to the high earthworm activity (Lal, 1976; Buschiazzi et al., 1998). Consequently, the addition of organic matter decreased the tendency for soil to compact (Mosaddeghi et al., 2000).

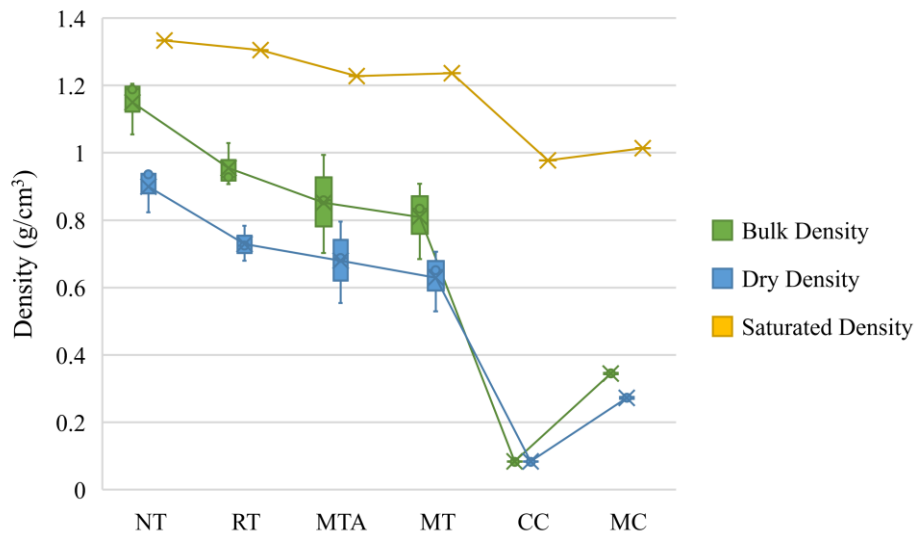


Figure 11: Bulk, dry, and saturated densities of individual homogeneous layers of different soil management systems in Site 1 – Loamy Sand

It is also perceptible that the bulk and dry densities of CC increase by 10 times and 7.5 times respectively when added to soil while that of MC increases by 2.5 times. Hence, their low density ranges indicate that the cover layers formed of organic matter have much smaller bulk and dry densities than the others, thereby they are not suitable for

plant growth (as their density is much smaller than the optimal range set by **Reynolds et al. (2009)**), yet they are only used either as covers along a shallow depth or as mixture components. In addition, even though when added to soil didn't improve the bulk density to a value in the optimal range proposed by **Reynolds et al. (2009)**, however, the problem might be in the ratio mixture chosen in this study. Hence, it was shown in **Willaredt and Nehls (2021)** that the bulk density improved when the ratio on volume basis of loamy sand/organic matter additive (in their case green waste compost) was increased. Consequently, the application rate of straw residues and chicken manure (42 tons/ha and 173tons/ha, respectively) must be further reduced to reach an optimal range for bulk density.

On the other hand, SD decreases from 1.332 g/cm³ (NT) to 1.304 g/cm³ (RT) to 1.236 g/cm³ (MT) to 1.227 g/cm³ (MTA). The only difference is that MT has a higher saturated density than MTA due to the higher volumes of voids that are filled with water created by the crops. In addition, since crops are initially dry (SD=DD) more water is needed since the dry crop residues will prove in later section to be very adsorptive to water; meaning not only the air voids are saturated but also the crops themselves absorb the water creating higher volumes of filled water. This is also reflected in the increase in the dry density of CC by 11.7 times to reach saturation. For the others, DD is increased by 1.5, 1.79, 1.8, 1.96, and 2.8 times to saturate for NT, RT, MTA, MT and MC, respectively. This finding results in having more pore spaces in crop residues, followed by chicken manure, then the tilled layers and finally NT. The author couldn't find any study that compared the pore structure of CC, MC, NT, RT, MT, and MTA, but the literature is abundant with findings of tillage systems altering the fine pores found in NT to coarser pores (**Gantzer and Blake 1978; Lindstorm and Onstad, 1984; Karlen et al., 1990; Pikul et al 1990; Mwendera and Feyen, 1993; Khurshid et al., 2006; García-Orenes et al., 2009**) due to the formation of cracks and large pores from animal buries and wormholes.

4.1.2.2 Porosity and Residual Volumetric Content

NT layer provokes the least porosity (0.433 m³/m³ ± 0.038) which is defined here as the saturated moisture content, with respect to other treatments also reported by **Salem et al. (2014)** (as shown in Figure 12). Tillage practices results in higher porosities (**P-value<0.001) by the breakage application of soil aggregates to alter fine into coarser pores: the tillage application, the addition of manure, and the incorporation of

crops increases the porosity by 32%, 26%, and 40%, respectively. The addition of crops to tilled soils increases the porosity by only 5% while the addition of manure decreases it by 4.7%. According to Tukey’s test, such difference is not significant since 95%CI of RT, MTA, and MT overlap. Hence, the addition of organic matter doesn’t affect the porosity of tilled layer since the voids which are filled by these organic matter residues are recovered by voids created on their boundaries. However, numerically, the addition of crop residues increased the total porosity of soil. Another study found similar patterns in porosity variations between NT, RT and MT (**Eden et al., 2011**). In their study, the total porosity of NT was increased from 0.452 to 0.462 for RT and 0.467 for MT on the long term. Hence, higher increase rates can be observed on the short-term (**Bamberg et al., 2011**).

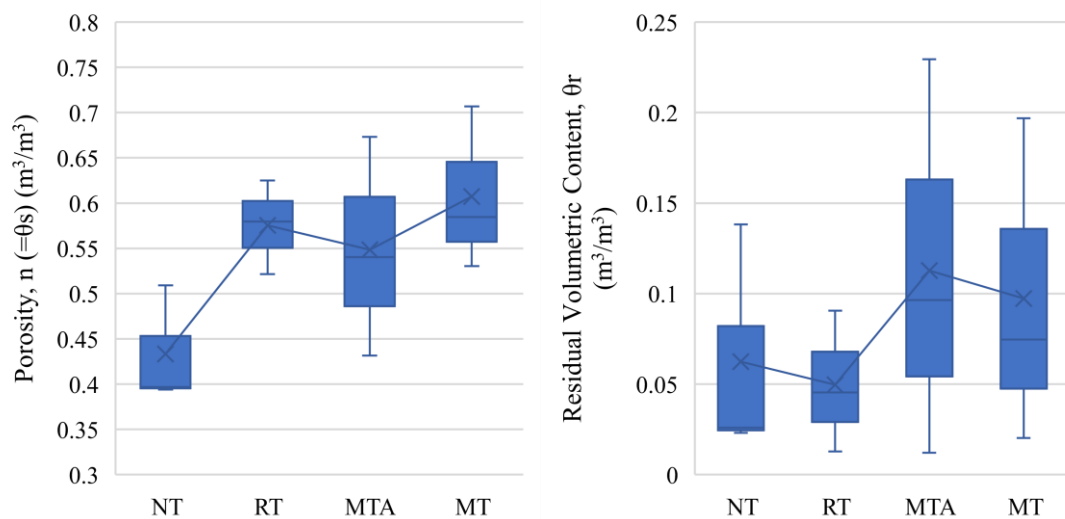


Figure 12: Moisture volumetric contents for NT, RT, MTA, MT, CC, and MC in Site 1 – Loamy Sand, (a) porosity or saturated volumetric moisture content θ_s , (b) residual volumetric moisture content θ_r .

On the other hand, the residual water content does not differ between the layers NT, RT, MTA, MT and CC while only that of MC is significant (P-value= 0.002) (NT: $0.0624 \text{ m}^3/\text{m}^3 \pm 0.0379$, RT: $0.04105 \text{ m}^3/\text{m}^3 \pm 0.02992$, MTA: $0.1046 \text{ m}^3/\text{m}^3 \pm 0.06989$, MT: $0.09726 \text{ m}^3/\text{m}^3 \pm 0.0522$, CC: $0.04509 \text{ m}^3/\text{m}^3 \pm 0.0006$). This means that the tillage application doesn’t affect the residual moisture content since the later depends on the amount of clay particles in the sample which are relatively small in compacted

and tilled soils (0% USDA, 13.28% USCS) (Lund, 1959; Kivisaari, 1971). Albeit statistically is not significant, NT has a larger residual moisture content than RT due to its smaller mean pore sizes which allow soil to maintain water (Martinez et al., 2008; Salem et al., 2014). In addition to the scarcity of fine pore volumes, RT's larger pores can induce higher evaporation rate by allowing heat to percolate within its larger pores' pathways (Buschiazzo et al., 1998). On the other hand, the addition of organic matter enhanced the ability of soil to maintain water. From one side, MC contains large aggregates formed of fine particles that are resilient in withstanding water and containing the moisture for longer times to have the highest residual moisture content of $0.335 \text{ m}^3/\text{m}^3 \pm 0.0036$. The addition of manure to loamy sand soil was efficient by raising the residual moisture content by 60% with respect to tilled soils, even though the large aggregates of MC were crushed during tillage application. This is also supported by Haynes and Naidu (1998) who noted that the addition of organic manure decreased the bulk densities (as seen in section 4.1.1.1) and enhances the water holding capacity of soils by increasing the residual moisture content while improving water drainage as well. In addition, several studies substantiate higher water contents measurements in systems that incorporated organic matter (Puricelli et al., 1976; Thomas, 1985; Smika & Unger (1986).

4.1.2.3 Organic Matter Content

The incorporation of chicken manure in tilled soil results in the highest organic matter content ($137.7 \text{ g.kg}^{-1} \pm 5.2$) following the mulch tilled layer in which crop residues are added ($11.847 \text{ g.kg}^{-1} \pm 0.41$), the tilled layer RT ($102.27 \text{ g.kg}^{-1} \pm 1.3$) and lastly the NT layer ($86.07 \text{ g.kg}^{-1} \pm 0.7$) (Figure 13-a). A one-way ANOVA indicates that the organic matter content in NT, RT, MTA, and MT layers is significant (***P-value <0.001) which means that organic matter content increases by 20% when the soil is disturbed by rotation and further rises by 40% and 60% when organic crops and chicken manure are added, respectively. This was also proved using the paired Dunnett's, Fisher's and Tukey's test in which all 95%CI do not contain 0 while adhering to the percentages of increase by the CI shifts from zero (Figure 13-d). In addition, the MTA treatment proves to have the highest 95%CI in all pairs' comparisons, which indicates that the chicken manure alone has a higher organic matter content than the crop residues. However, this is not retained as shown in Figure 7 since the crop residues layer ($912.7 \text{ g.kg}^{-1} \pm 5.2$) contain much higher OMC than the

chicken manure layer ($414.87 \text{ g.kg}^{-1} \pm 12.2$) ($P\text{-value} < 0.001$). This is because the OMC is obtained by mass rather than volume measures, hence the crops are much lighter than the chicken manure.

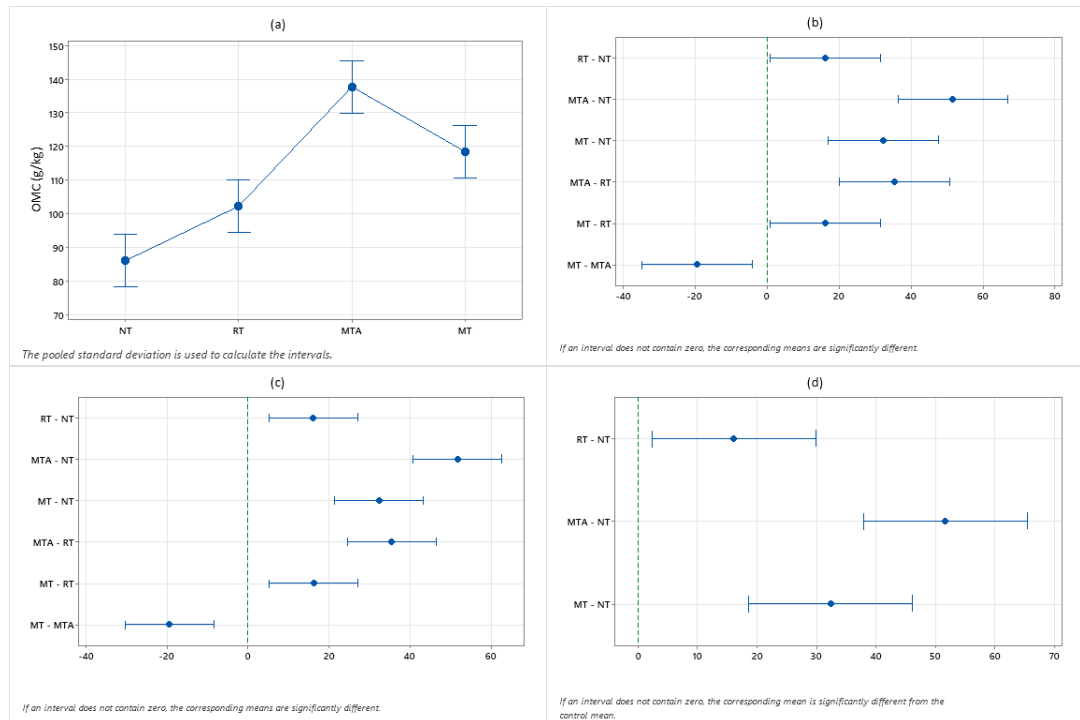


Figure 13: OMC Statistical Analysis for NT, RT, MTA, MT in Site 1 (a) Interval plot with 95% CI for the mean, (b) Tukey 95% CI, (c) Fisher LSD pairwise comparison with 95% CI, (d) Dunnett 95% CI with a control treatment NT

Nonetheless, it is important to imply that the rotary tillage layer has a higher OMC than the unmodified layer albeit that none organic matter is added while tillage application. This can be explained by the short-term application of crushing and mixing tree and plant debris that are found on the top of the soil surface which are not included in the NT testing samples. However, on the long term, it was shown that NT has a higher OMC in sandy soils than tilled layers (**Buschiazzo et al., 1998**) since the tillage application rotates the soil while pushing the organics into deeper depths (**Dick, 1983; Rosell & Andriulo, 1989; Standley et al., 1990; Unger, 1991; Schomberg et al., 1994**). Meanwhile organics found at the surface of NT are preserved. Notwithstanding, the addition of crop residues to the tilled layer impose nearly the same effect on OMC that RT implies on NT (same 95% CI in Figure 13-b and 13-c).

Similarly, the addition of chicken manure to the tilled layer create a same effect on OMC that when adding crops to an unmodified layer. This can be interpreted that the addition of chicken manure has a double effect on the rise of OMC when compared to the mulch tillage layer. Lastly, each individual homogeneous layer has a different organic matter content which makes it different that the other in its composition.

4.1.2.4 Aggregate Size Distribution

The frequency density functions found in Appendix A are used to determine the mean weight diameter of individual homogeneous layers which form the different soil profiles of different soil management systems. The MWD (Figure 14) of the NT layer soil sample is the highest (0.68cm) following MT (0.44cm), then RT (0.39) and later MTA (0.38cm). The cover layers (CC 0.5cm, MC 0.49cm) have a MWD smaller than that of NT but greater than the tilled layers. This means that the compaction of soil in the NT layer removed excess voids to allow soil particles to adhere together to form larger soil aggregates (**Marti´nez et al., 2008**).

On the other hand, the tillage application broke down the aggregates by disturbing the binding agent of macro-aggregates formed by binding recalcitrant-humified organic matter with mineral particles (clay–humus complexes) and activated by compaction to tolerate the entry of air in soil and move the particles away resulting in the formation of smaller aggregates by almost 40% (**Marti´nez et al., 2008**) and in the reduction of aggregate stability (**García-Orenes et al., 2009**). Thus, in the process of adding chicken manure to the tilled soil, the MWD didn't quite change from that of the tilled soil while the addition of crop residues increased the MWD of RT by almost 15% as similarly found by **Singh & Malhi (2006)** in loam textured soils in NT plots covered with crop residues in which the retention of crop residues caused the increase in the aggregate distribution (**Rolda´n et al., 1994; Lax et al., 1997**).

Hence, the addition of organic matter enhances the aggregate stability of soil. This is absurd to the MWD values of CC and MC. Nevertheless, MWD is measured by mass portions. Paradoxically, CC and MC have much smaller bulk densities than their counter layers of mixed tilled layers (MT and MTA, respectively). In particular, CC is really light compared to the other treatments which allow the addition of manure to the tilled layer more effective than the addition of crops. As this stands, the initial MWD of the compacted soil decreases 44% due to manure amalgamation while 35%

due to crop addition might be due to two reasons: (1) crop residues comprise longitudinal shapes of particles which might either got stuck or was standing in position that hinder its passage from one sieve to the other, (2) during tillage application, the large aggregated particles formed in the chicken manure might be crushed in the rotation process to have an amalgam of soil aggregates similar to that of the RT layer. Consequently, the MWD of CC could have been lower if the longitudinal shapes crops were passed through the sieves vertically (their cross-section). Then, the manure chicken would have the highest MWD following the NT layer. Regardless, the highest MWD means that the soil has large aggregates which are formed of very fine soils adhered together during the wetting and drying events. Yet, in accordance with the results obtained for MT, the addition of straw mulch to soil results in a medium mean weight diameter that improves aggregate stability (Mulumba & Lal, 2008; Jordán et al. 2010) and soil strength (Pervaiz et al., 2009) by increasing soil porosity, moisture retention and drainage capacities.

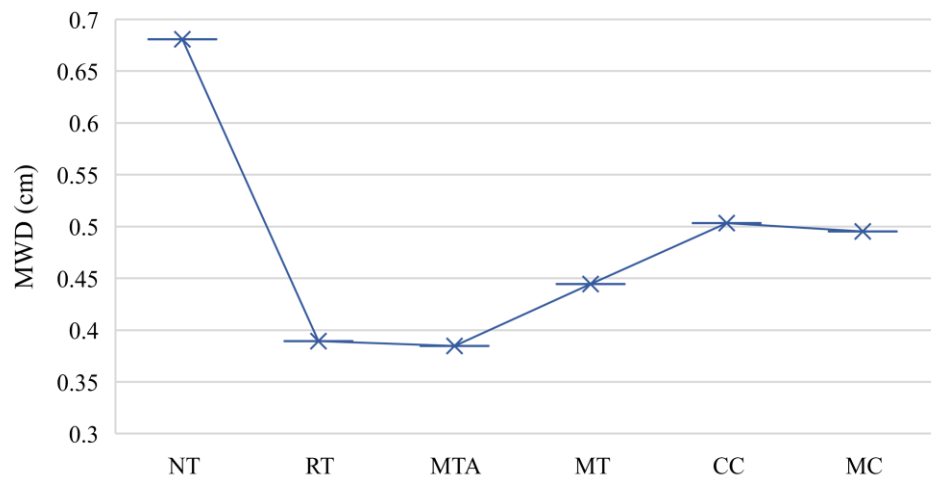


Figure 14: Mean weight diameter (MWD) from the frequency density function of the aggregate distribution (f) in Site 1 for NT, RT, MTA, MT

4.1.2.5 Saturated Hydraulic Conductivity

NT layer has the lowest saturated hydraulic conductivity of $1.31 \text{ cm/day} \pm 0.044$ (a critical value as referred to Reynolds et al. (2007) while greater and significant values (**P-value<0.001) are reported for tilled layers (MT: $67.7 \text{ cm/day} \pm 2.66$, RT: 69.1

cm/day \pm 11.79, MTA: 173.6 cm/day \pm 14.04 illustrated in Figure 15). This means that the tillage application created a larger space for voids so that water would pass through to have optimal saturated hydraulic conductivity as advised by **Reynolds et al. (2008)** for better infiltration, thereby reducing surface runoff and soil erosion while allowing space for water distribution and penetration into the finer pores. This is shown by the increase of K_s by 52 times from NT to RT. Similar findings were determined on coarse loamy over sandy by **Martinez et al. (2008)** and **Reyes et al. (2002)**. However, this finding is opposed when NT comprises cracks or macropores from animal boreholes (**Karlen et al., 1994**). When comparing the tilled layers, the addition of crop residues didn't affect the saturated hydraulic conductivity of RT similarly as found by other studies (**Blevin 1983; Ahamefule and Mbagwu, 2007**) because the predicted additional water would be assumed to pass in the preferential paths that the crops created along the longitudinal shaped residues in the shape of fingered flows that would be longer than the vertical path (**Liu et al., 1994**). Another reason could be due to the high adsorption capacity of crop residues to water especially for air-dried straws that can absorb water up to 4.8 times its original weight (**Wu et al, 1995**). Here again the crop residues prove to be highly adsorptive to water. Thus, such effect is neglected for CC since the convection effect is highly substantial due to the large volumetric content of void spaces that exist in the structure of crop residues. The high saturated hydraulic conductivity (2753cm/day) indicates that the large pores make the soil in a droughty state much faster than the others. This concept is additionally justified in loamy soil plots where tilled and no-tilled fields were covered with straw mulch. Consequently, **Singh and Malhi (2006)** reported that the organic cover increased the infiltration of water, hence proving that the crop residues are highly conductive when left solo.

Nonetheless, the addition of chicken manure to tilled soils was significant (according to Tukey's and Fisher LSD tests) and increased the saturated hydraulic conductivity of the tilled layer by 2.5 times as it was reported in other studies where the infiltration was affected positively by the addition of organic matter (**Lal & Vandoren, 1990; Shukla et al., 2003; Ghuman & Sur, 2001**). **de Jonge et al. (2009)** interpreted that high-carbon medium endure a "sponge-like" effect for water conductivity. Such effect is altered into a "pipe-like" effect when the organic matter is decreased. Hence, the chicken manure with high organic matter had a lower hydraulic conductivity reflecting

the sponge-like effect while its incorporation with loamy sand soil reflected a better conductive soil similar to the pipe-like effect. On the other hand, MC had the lowest saturated hydraulic conductivity among layers other than NT but an optimal value for an efficient infiltration. As it was mentioned earlier, MC had the largest MWD following the NT layer, meaning that water tends to only pass between the large aggregates of manure which decreased its hydraulic conductivity. However, when the manure is mixed with soil, the rotary tiler crushes the aggregates which creates more spaces for water flow. This is revealed in the increase of the hydraulic conductivity of tilled soils when manure is added. In addition, **Jiao et al. (2006)** found that the addition of manure increased the stability of the soil structural quality in sandy soils which enhanced the water retention capacity of the soil.

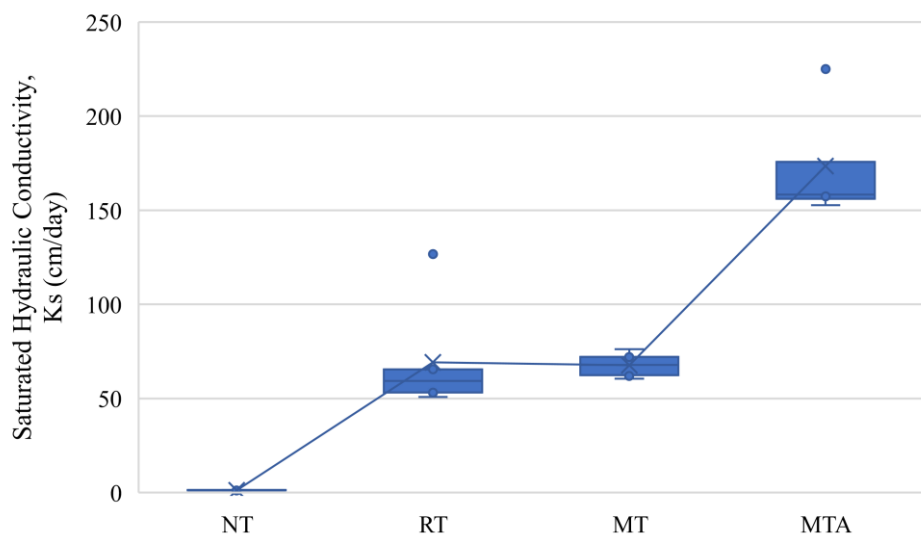
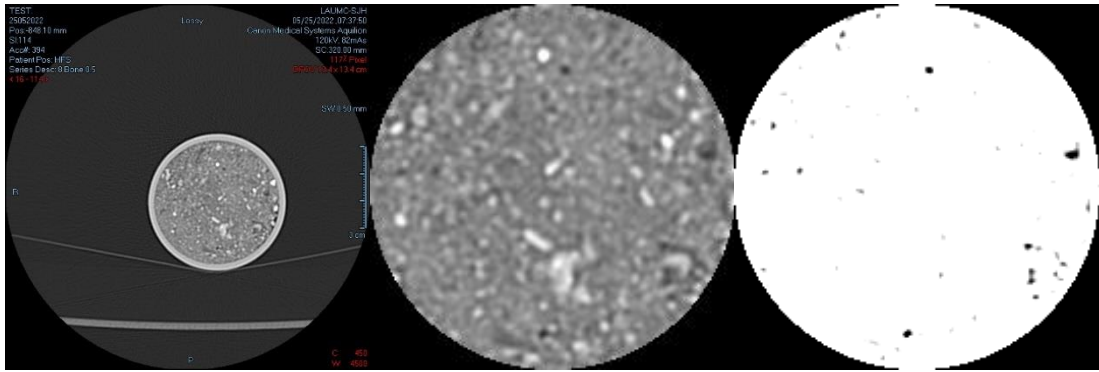


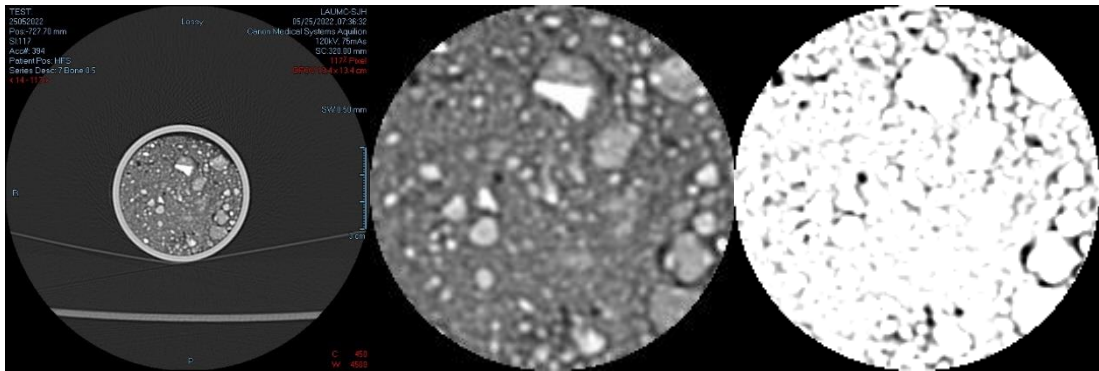
Figure 15: Saturated Hydraulic Conductivity, K_s for individual layer in Site 1 for NT, RT, MTA, MT

4.1.2.6 Soil Pore Structure and SWRC

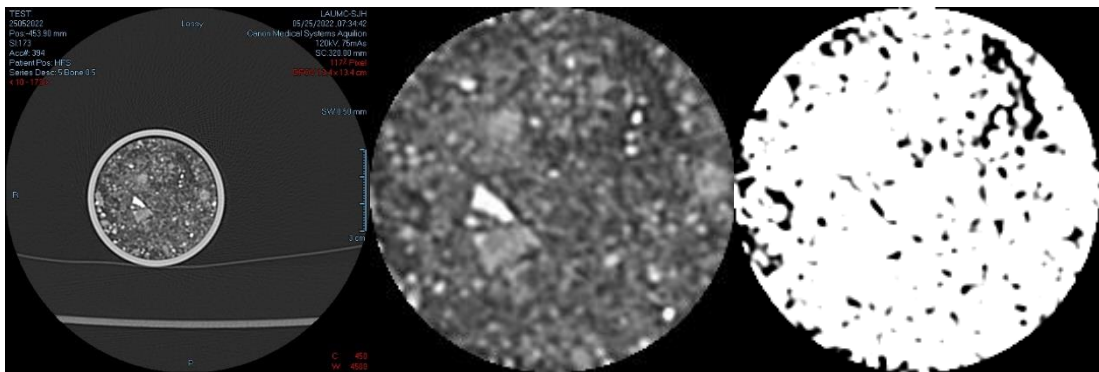
The structure of individual layers forming the different soil management systems are illustrated in Figure 8 and 16. From left to right of Figures 16 in (a), (b), (c), and (d), the first picture is the CT-scan image result, the second is the one cropped in ImageJ and the last is the one filtered and color thresholded. Figure 16 demonstrates that the pores are smaller and lesser in NT and larger and abundant in tilled layers.



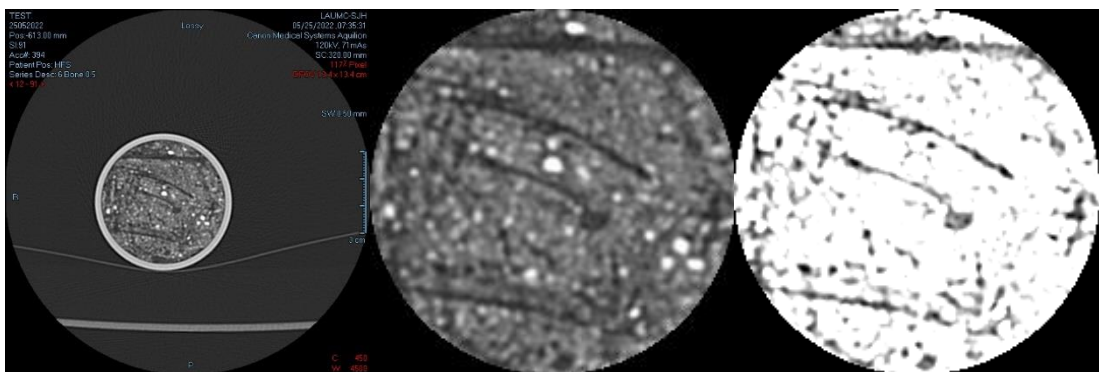
(a)



(b)



(c)



(d)

Figure 16: CT scanning images for (a) NT, (b) RT, (c) MTA, and (d) MT in Site 1

On the other hand, Figure 8 proves that CC induces the largest areal content of voids while the large aggregates in MC as discussed in 4.1.2.4 are shown through their surrounding void spaces. In addition, the cross-sectional shape of pores differ from one layer to the other, depending on the soil aggregates and organic content. As this stands, the NT acquirnig the highest MWD have small circular pores, while RT and MTA have larger circular pores due to the smaller MWD. However, MT's pores are partially longitudinal where crop residues are found and partially circular surrounding the soil aggregates.

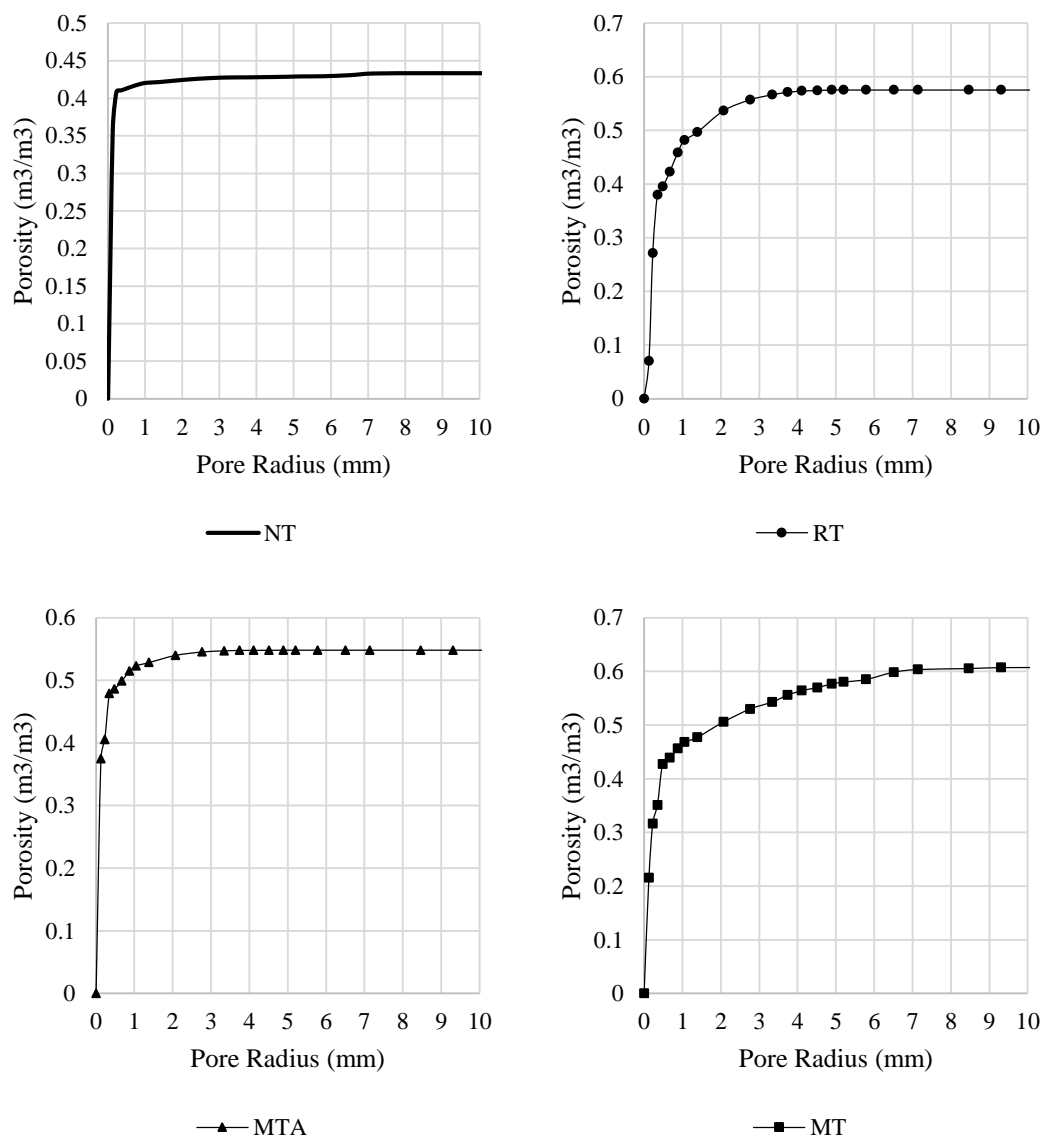


Figure 17: Porosity Distribution for NT, RT, MTA, and MT from the analysis of volumetric contents of pore sizes in ImageJ in Site 1

The porosity distribution for the different individual layers with respect to pore sizes are shown in Figure 17. Pores of radius greater than 5mm are the least present in NT (<7%) followed by MTA (<18%), MT (<37%), MC (<38%), RT (<51%), and lastly CC (<83%). This again shows that NT (mean pore radius = 50 μ m) is a compacted soil layer that only permits very small pores to exist. The compaction is disturbed by tillage practices so that soil particles move away from each other to create new and larger void spaces (Mean pore radius of RT = 234 μ m). A finding that supports the hypothesis of **Castellini et al. (2013)** stating that tillage practices allow to drain excess water and ease root penetration by providing a satisfactory pore structure. Thus, the more the tillage application is intensive, the larger the pore sizes ought to be (**Ren et al., 2019**). Similarly, organic covers (CC and MC) endure larger void spaces than NT. Yet, the crop residues have a much larger mean pore radius than the chicken manure. Porosities for (*NT, RT, MTA, and MT*) corresponding to pore sizes smaller than 0.1mm, between 0.1 and 1mm, between 1 and 5mm and larger than 5mm are (0.358, 0.070, 0.375, 0.215 $m^3.m^{-3}$), (0.062, 0.411, 0.149, 0.253 $m^3.m^{-3}$), (0.008, 0.094, 0.025, 0.112 $m^3.m^{-3}$), and (0, 0, 0, 0.027 $m^3.m^{-3}$), respectively. Hence, fine pores (<0.1mm) are more profuse in NT, following MTA, MT and RT. Pores between 0.1-1mm are more abundant in RT following MT, MTA, and NT. For pores between 1-5mm, MT is favorable following RT, MTA, and NT while MT only contains pores larger than 5mm. It is evident that the incorporation of straw residues in the loamy sand soil increase volumetric contents of large pores, while the addition of chicken manure increases the content of fine pores of tilled soils. Hence, it is fair to indicate that the incorporation of organic matter has altered the soil into a well graded soils (having pores of different radius). Notwithstanding, the manure is crushed resulting in a decrease of pore sizes so that the manure replaces the large pores of RT to have a smaller mean pore radius. On the other hand, CC evidently has the largest volumetric content of pores. However, when adding crop to tilled layers, the observation of Figure 8 remarks that there is no increase in the total volumetric pore content. This means that the large pores existed in the crop residues are decreased by the tillage practice. Hence, the crushed crops fill the large voids found in RT and create new but smaller spaces than those found in CC. When comparing the mean pore radius obtained in the CT-scans, MT has a larger mean pore radius than RT since the crop form void spaces juxtaposing to their boundaries which are longitudinal and more connected so that the area gets bigger.

Figure 18 exemplifies the observed and fitted moisture content with respect to the matric potential. All model fittings are good-fit models with R-squared greater than 0.89. α lying between 0.013 and 0.188 for all layers shows an increase from NT to MTA following RT, MC, MT, and CC while n lying between 1.238 and 3.884 increases from NT, MT, MTA, RT, MC, and lastly CC. The fitted van Genuchten parameters α and n are used to simulate the soil water retention curves developed in Figure 18. For instance, at 0.45kPa, the SWRC differ from one treatment to the other in the order NT>MTA>MT>RT above 2000kPa, the soil water retention is greater for MTA>NT>MT>RT before saturation and MT>RT>MTA>NT during saturation.

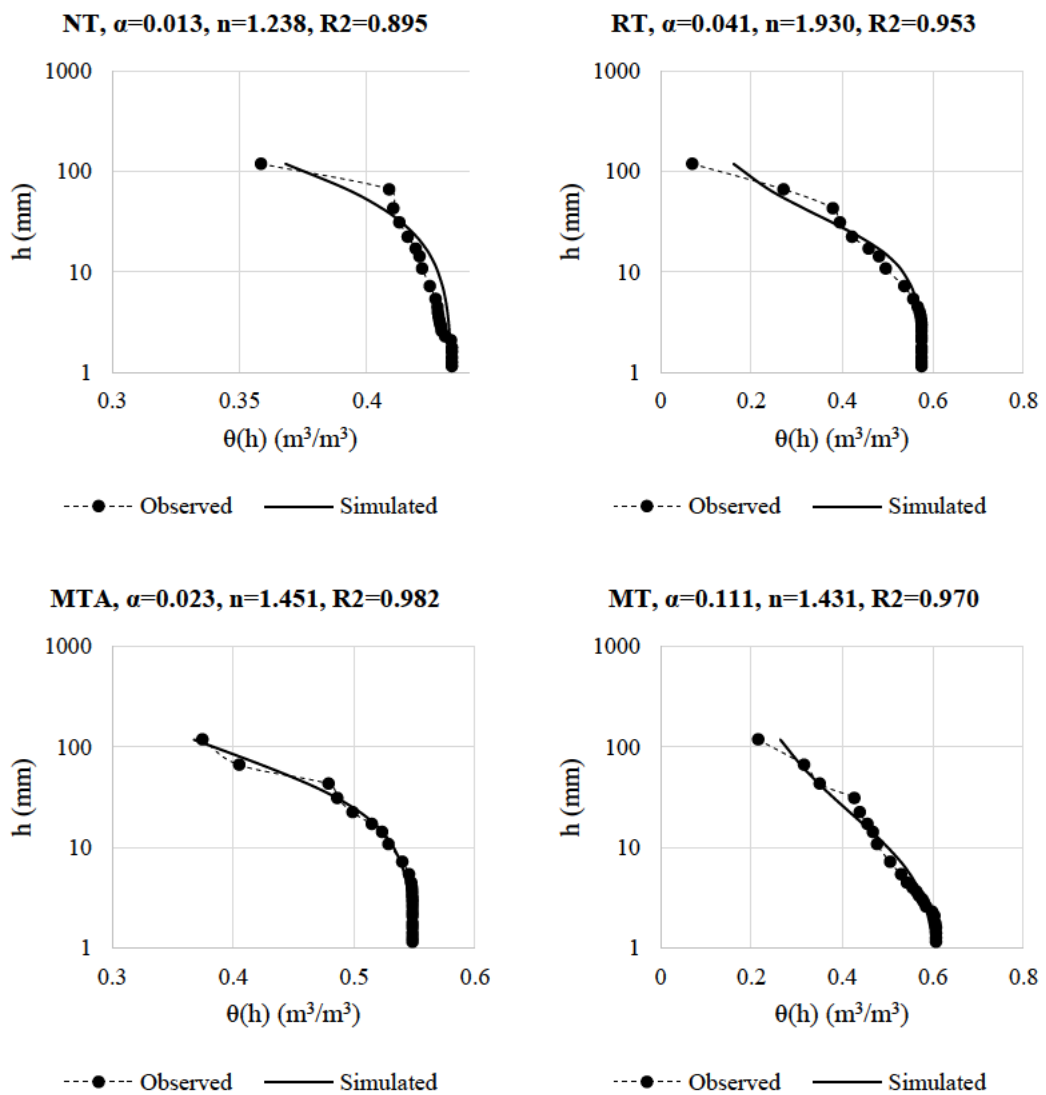


Figure 18: Fitted van Genuchten parameters for NT, RT, MTA, MT, CC, and MC in Site 1 (α in [1/mm])

Similar findings were reported in **Kumar et al. (2012)**. Accordingly, more energy is required for water to drain the undisturbed layer when compared to the tilled layers while the undisturbed soil can maintain more water for longer time. The soil water retention curve SWRC of NT decreases the SWRC similarly as in **Ciollaro and Lamaddalena (1998)** and **Kumar et al. (2012)** and indicates that the soil is poorly sorted and drains over a long range of matric potential due to its compacted state in comparison with the other layers due to the heterogeneity of soil pore sizes and their discontinuities (**Castellini et al., 2013**) (as shown in Figure 19). Further, the number of pores finer than $3\mu\text{m}$ is higher in NT analogous to that found in **Eden et al. (2011)** where volumes of pores larger than $10\mu\text{m}$ are limited. In contradiction, the tilled layers show to be better-sorted than NT which supports the hypothesis that tillage practice change soil structure in more advantageous way to drain water (**Ciollaro & Lamaddalena, 1998**). Being more precise, the NT had more fine pores ($<10\mu\text{m}$) than the other layers while the tilled layer had medium to large pores ($>10\mu\text{m}$) similar to that found in **Francis & Knight (1993)**, **Karlen et al., (1994)**, **Startsev & McNabb (2001)** and **Kumar et al. (2012)**. On the other hand, the addition of organic matter produces a good sorting for smaller pore sizes than those found in RT. Similarly, in **Eden et al., (2011)**, the porosity was higher for pores less than $30\mu\text{m}$ in MT than both RT and NT while for pores greater than $30\mu\text{m}$ the porosities were smaller than RT but greater than NT. In this regard, comparing the air-entry value ($1/\alpha$), MT has the lowest air-entry value following RT, MTA and NT. This means that MT has the largest volumetric contents with coarse pores ($>10\text{mm}$) following RT, MTA and NT. However, when the SWRC move beyond their inflection points and prior to dryness ($<30\mu\text{m}$), more profuse fine pores are activated in NT following MTA, MT and RT.

Notwithstanding, there are no studies to the knowledge of the author that compare the amalgamation of crop residues and chicken manure to tilled soils. Hence, in this study, the addition of both crop residues and chicken manure increases the range of finer pores than RT and the range of coarse pores than NT. However, coarser pores are reported in MT while finer pores are found in MTA. This is because MT has a higher mean pore radius than RT and MTA as it was shown in the earlier section while they all have a mean pore radius greater than that of NT. Consequently, as the three layers (RT, MT, MTA) have near values of porosities, it is logical to interpret that the sizes of their pore contents change with the addition of organic matter.

It is also worthy to mention that the saturation of MT is observed for matric potential smaller than 0.1MPa while larger values were reported for wheat straw (0.38MPa) (Myrold et al., 1981), clover leaves (0.31MPa), clover stems (0.19MPa), rye leaves (0.94MPa), and rye stems (0.88MPa) (Quemada & Cabrera, 2002). Hence, the residues were cut into piece of 5mm while those used in this study were left as. The MWD for CC was ~5mm meaning that larger sizes of residues existed in the CC samples. The distribution in aggregate sizes led to a coarser pore structure which decreased the matric potential at saturation in opposition to the other cut residues.

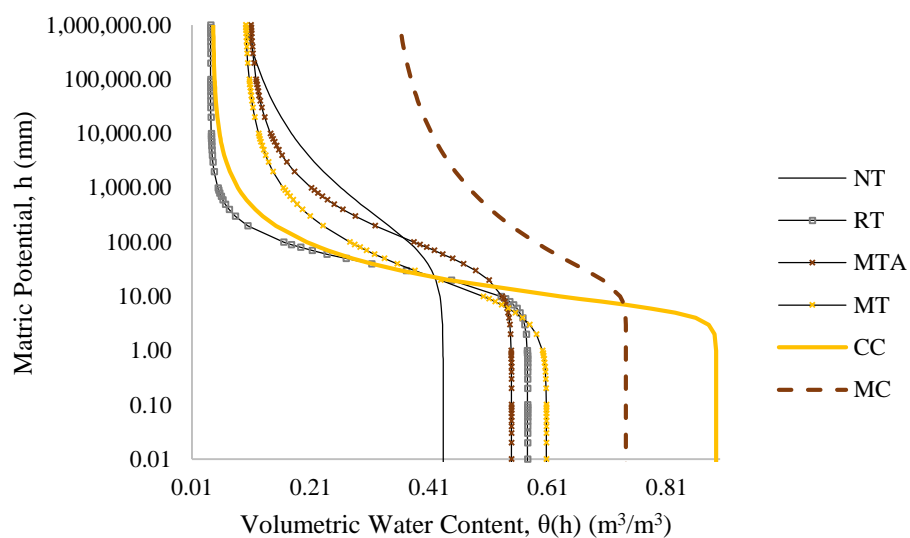


Figure 19: Fitted soil water retention curves for NT, RT, MTA, MT, CC, and MC in Site 1

Further, the addition of organic matter in particular chicken manure placed additional stress on water to either retain or drain in tilled soils. However, such addition will prove to be balanced by other advantageous alterations to the soil physical and structural quality that would together enhance water infiltration. Nevertheless, it is remarkable to mention that even though RT has the highest bulk density following MTA and MT meaning wider curve for RT than MTA and MT, this doesn't omit the fact that soil water retention curve relies on pore size distribution rather than on the total porosity of the soil whilst neglecting the effect of bulk density. This is also reflected in the curve of MC which has a smaller bulk density than the tilled layers but drains over a long range of pressure. In contrast to this finding, Hebb et al., (2017)

reported an indifference in α parameter for native grassland which had a higher total porosity than the others, introduced pasture and annual cropland plots due to the change in the sizes of macropores. However, the bulk density parameter is significant when evaluating the SWRC for undisturbed, disturbed and crop residues cover layer. Consequently, CC having the lowest bulk density shows to be the best sorted layer, thus it drains quickly due to its lightness and its large pore sizes. A correlation between bulk density and the SWR curve was reported by many researchers (Husz, 1967; Gupta & Larson, 1979; Arya & Paris, 1981; Vereecken et al., 1989) in which the higher the bulk density, the more stretched is the SWRC.

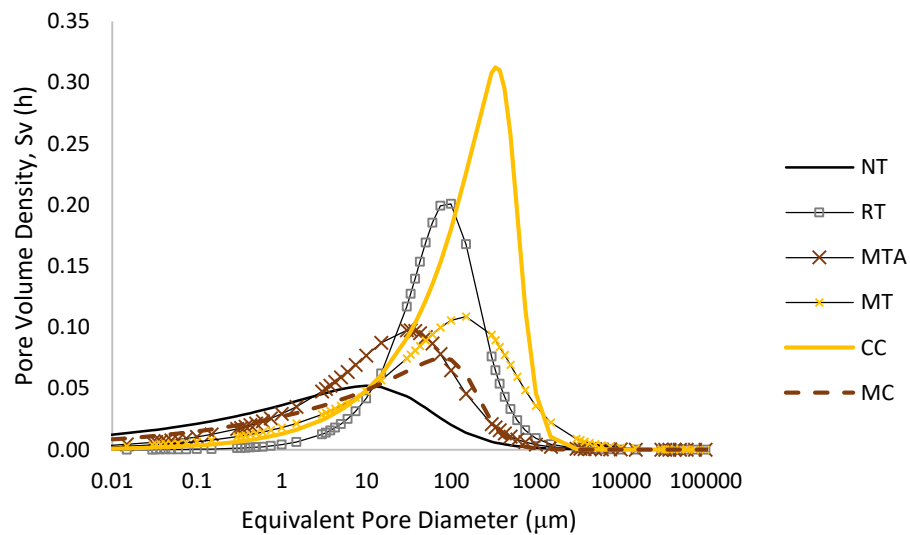


Figure 20: Pore volume distribution PVD functions for NT, RT, MTA, MT, CC, and MC in Site

1

4.1.2.7 Pore Volume Distribution

A further analysis for the pore structure is established by evaluating the pore volume distribution function *PVD* for each individual layer NT, RT, MTA, MT, CC, and MC as shown in Figure 20. The manipulation of the *PVD* functions is carried by analyzing the location and shape parameters which describes the layout of each function. These are reported in Table 10. The mean pore diameter is the least for NT, followed by MC, MTA, MT, RT, and CC. It is important to mention that for each soil layer the corresponding mean equivalent diameter is not equal to the double of the matching

mean pore radius obtained when analyzing the CT-scans. This is due to the limitation of the CT-scans to capture pores smaller than 10 μm . Thus, the fitting of the SWRC using the measured saturated and residual moisture content allowed the prediction of matric potential with their equivalent volumetric content for pores smaller than 10 μm . Therefore, when incorporating all the micropores, the mean diameter decreased by 90%, 20%, 45%, 67.5%, and 90.5% for NT, MTA, MT, CC and MC, respectively, while it increased by 29% for RT. Consequently, all layers except for RT had larger volumes of micropores ($<10 \mu\text{m}$). In particular, NT and MC had their highest portions of such micropores since NT is a compacted layer while those in MC are located in the large aggregates that were formed after wetting and drying of highly organic soils. For MTA and MT, the additional micropores are justified by the very fine organic matter that fills in larger pores and thereby creating smaller void spaces. Notwithstanding, CC have the highest total pore volume and the largest mean diameter which hinders ImageJ from capturing the finest pores even when the brightness and contrast are adjusted since the large pores tend to overshadow the smaller ones. In addition, the median diameters are spaced from the mean diameter by almost 11.5, 61.5, 44.1, 205.1, 470.8, and 68.6 μm for NT, RT, MTA, MT, CC, and MC, respectively. The significance of the spacing is analyzed using the shape parameters. Additionally, the modal equivalent diameter measures the most frequent diameter found in a layer. Accordingly, it is apparent that CC endures the largest frequent diameter ($\sim 3.4\text{mm}$). The addition of crops to tilled soils also results in the largest frequent diameter ($\sim 1.4\text{mm}$) among the tilled soils equivalent to an increase of 63% from that of RT. In opposition, the addition of chicken manure lowers the most frequent diameter with respect to RT by 65% since chicken manure alone has a lower (by 10%) most frequent diameter than that of RT. As this stands, chicken manure is further crushed during tillage application so that fine particles are able to fill more pores in tilled soils. Yet, NT remains the layer of smallest frequent diameter due to its compaction state.

Blott and Pye (2001) suggested a descriptive terminology reported in Table 11 for the shape parameters of grain size distribution. In the same manner, the terminology is used to assess the PVD function's parameter. NT and CC are extremely poorly sorted since they are abundant with very fine pores. This presumption was also predicted by the shape of their SWRC and by the low saturated hydraulic conductivity. Conversely,

the tillage practices enhanced the gradation of pores in loamy sand soil, while the addition of organic matter perturbed the improvement. Additionally, CC layer is poorly sorted since it is copious with large pores which is reflected by the high saturated hydraulic conductivity and large pore diameters. On the other hand, the PVD functions show asymmetries with the negative values of skewness, which reflect the difference in mean, mode and median measures. This assumption is yet to be predicted since the pore volume density $S_v(h)$ on the y-axis of the PVD functions are predicted using the fitted van Genuchten parameters for pores smaller than 10 μm . For that reason, the distribution of all the functions is to the right where the large pores occur.

Table 11: Location and shape parameters of the PVD functions for NT, RT, MTA, MT, CC, and MC in Site 1

	Site 1				Common	
	NT	RT	MTA	MT	CC	MC
Location Parameters						
d(mode) [μm]	104.5366	881.1139	312.8602	1437.63	3412.349	794.8183
d(median) [μm]	22.12005	728.5891	162.8979	717.5824	1667.24	125.4404
d(mean) [μm]	10.52729	667.0206	118.7816	512.5015	1196.395	56.86205
Shape Parameters						
SD	48.90005	3.309002	9.479236	10.32303	4.835167	31.31386
Skewness	-0.36692	-0.1466	-0.27363	-0.28063	-0.40364	-0.44133
Kurtosis	1.254473	1.236305	1.258721	1.259198	1.244247	1.224738
Descriptive Terminology (Blott and Pye, 2001)						
SD	<1.27	Very well sorted				
	1.27-1.41	Well sorted				
	1.41-1.62	Moderately well sorted				
	1.62-2.00	Moderately sorted				
	2.00-4.00	Poorly sorted				
	4.00-16.00	Very poorly sorted				
	>16.00	Extremely poorly sorted				
Skewness	-1.0 – -0.3	Very fine skewed				
	-0.3 – -0.1	Fine skewed				
	-0.1 – 0.1	Symmetrical				
	0.1 – 0.3	Coarse skewed				
	0.3 – 1.0	Very coarse skewed				
Kurtosis	<0.67	Very platykurtic				
	0.67-0.90	Platykurtic				
	0.90-1.11	Mesokurtic				
	1.11-1.50	Leptokurtic				
	1.50-3.00	Very leptokurtic				
	>3.00	Extremely leptokurtic				

That's why the skewness gets finer thereby generating a surfeit in small pores to reimburse the low resolution of CT-scans in capturing very fine pores. Lastly, all layers have leptokurtic distributions since the functions are more peaked in the center with flatter tails in the extremes as shown in Figure 20. This means that the degree of concentration of pore diameters lies within the centered 95% of the distribution and neglects the upper 5% due to unmeasured very fine pores (<10 μm). Thus, a similar leptokurtic distribution was observed in **Castellini et al. (2013)** who used a Buchner funnel apparatus for the measurement of water retention data. Herein, the range is measured from left and right of the modal diameter since it corresponds to the peak of the PVD functions (inflection point of the SWRC). So, RT has the narrower range of [877.8; 884.42] following CC [3407.5; 3417.2], MTA [303.38; 322.34], MT [1427.3; 1448], MC [763.5; 826.13], and NT [55.64; 153.44]. The narrower the range the more the soil is sorted as this was proved earlier.

4.1.2.8 Soil Physical Quality Indicators

Referring to the optimal and critical ranges of soil physical indicators reported in Table 5, all the layers of the different soil management systems possess an air capacity higher than $0.1 \text{ cm}^3/\text{cm}^3$ which is needed for agricultural soils to allow soil aeration in the root zone for healthier yields (Refer to Table 12). This means that the volumetric content of pores greater than $\sim 3\mu\text{m}$ allowing for air to penetrate is enough even for the compacted soil layer NT which has the smallest pore diameters. However, the volumetric contents of pores smaller than $0.0195\mu\text{m}$ are scarce for all the layers. Therefore, limited water is available for storage for root uptake for NT layers, while the other layers are poor (**Fabrizzi et al., 2005**). Consequently, the cover layers' role of maintaining the water is not applicable. On the other hand, the tillage application widened the soil-pore structure in loamy sand soils so that the soil's ability to store water for longer times is not an option as when the soil is left undisturbed in loamy sand. A similar finding was reported by **Castellini et al. (2013)**. Albeit the addition of crops (1:4 volume ratio) raised the PAWC of tilled soil, still it is not efficient. Future investigations are recommended for different ratios of soil-organic matter mixes. Similarly, the relative field capacity shows water storage limitation under tillage practices with respect to undisturbed soils. Likewise, CC cannot store water since it proved that it drained quickly. However, chicken manure having fine pores have optimal relative field capacity. Also NT but smaller than MC, has an optimal RFC

(between 0.6 and 0.7) which indicates a good pore structure for microbial production of nitrogen more often and over a prolonged time. Notwithstanding, the addition of organic matter (either crops or chicken manure) increased the RFC but in the same manner it did with the PAWC. Although RT and CC didn't prove to maintain and store water (as was also found in **Castellini et al (2013)** for tilled soils), they have a very good soil physical and structural quality as they have the highest S theory values which is similar to the findings of **Castellini et al. (2013)**. Thus, all the other layers have the optimum range for physical and structural quality. The S-index was also found statistically similar to forests natural and disturbed plots with and without pasture in a Mediterranean region (**Cullotta et al., 2016**).

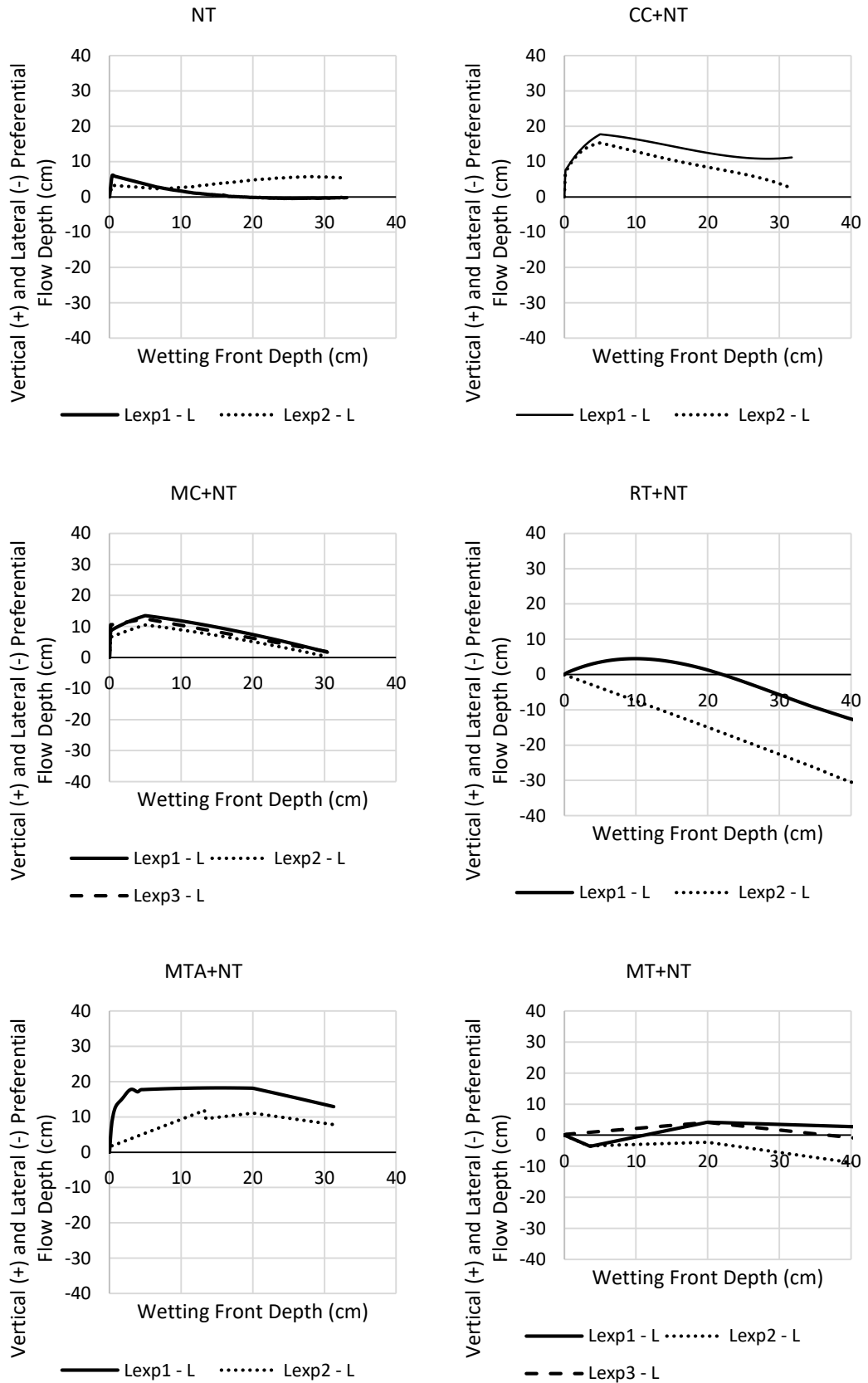
Table 12: Soil physical quality indicators for NT, RT, MTA, MT, CC, and MC in Site 1

	SITE 1				Common	
	NT	RT	MTA	MT	CC	MC
Air Capacity AC	0.172281	0.522048	0.337347	0.443302	0.805945	0.264994
PAWC	0.138396	0.012322	0.095449	0.059078	0.04011	0.101597
RFC	0.602509	0.092867	0.384886	0.269984	0.098033	0.642626
S theory	0.052235	0.202687	0.097669	0.108799	0.312647	0.074903

4.1.2.9 Preferential Flow

The experimental vertical (VPF) and lateral (LPF) preferential flow depths are illustrated with respect to the simulated wetting front depth in Figure 21. Among the different soil profiles, only RT+NT, MT+NT, and MC+CC+RT+NT provoked LPF while water flow in all layers traveled some VPF of different depths and times. NT and MTA experienced an almost steady VPF along the experiment, while VPF increased rapidly to reach its maximum when water was passing in the systems having organic matter as covers (either crop residues or chicken manure i.e. CC+NT, MC+NT, CC+RT+NT, MC+RT+NT, CC+MTA+NT, MC+MT+NT, MC+CC+RT+NT). Such PF starts to decrease when reaching the undisturbed layer to reach the real wetting front (CC+NT, MC+NT) or when intermediately passing through the tilled layer to follow the simulated wetting front and either start new PF (CC+RT+NT, MC+RT+NT, MC+CC+RT+NT) or move along a uniform front (CC+MTA+NT, MC+MT+NT). Consequently, the wetting front of layers having RT

as the modified layer moves into LPF after it reaches the bottom of that layer. Hence, when the wetting front reaches its bottom, its infiltration rate decrease while infiltrating into NT. Thereafter, water particles tend to move laterally to resume its saturation in the tilled layer while slowing the rate of infiltration moving into the undisturbed layer. Notwithstanding, the addition of organic matter to tilled soils better regulated the tendency for PF formations as reflected in those having MT or MTA as tiller layers. VPF is activated at the beginning of the irrigation event but becomes either steady (in the case of MTA) or unsteady with minimal fluctuations with respect to the real wetting front (in the case of MT). Hence, water particles find a balance while moving in fine and coarse pores so when they reach other layers, their speed is better adjusted so they are motivated to continue rather than finding other easier paths. This is reflected in the PF variations in MT+NT and MTA+NT profiles. For instance, in MTA+NT profile VPF initially appears but later shows a uniform change between the experimental and simulated wetting fronts. This means that after the initial VPF, the pore structure was well sorted so that water starts to infiltrate in the same speed as it started but with a delay. Nonetheless, the wetting front in the MT+NT profile shows discrepancies between lateral and vertical PF that reflects the ranges of pore size in the mixture of crop and loamy sand soil and the placement of longitudinal crop observed in CT-scans (if the longitudinal crops are parallel to the flow, VPF are favored; if they are perpendicular, fronts are likely to move into LPF). Consequently, it is fair to judge that the movement in tilled layers is not directed by preferential flow except when water hits the interface between the tilled and non-tilled layer. As this stands, tillage practices change the soil-pore structure so that preferential flow become not favorable (**Fan et al., 2013**). Similar to that occurred in NT with negligible PF, other studies have found that NT and RT excluded macropores that could attenuate to the occurrence of PF (**Sasal et al., 2006; Capowicz et al., 2009**). Hence, the observation of PFs in tilled profiles is due to the low velocity of water that was applied while no PFs could have been neglected for higher velocities (**Andreini & Steenhuis, 1990**). However, the movement along the pores in cover layers especially CC is surely induced by PF along the longitudinal walls of crop residues. As it was shown in earlier sections, CC has the largest modal diameter, the smallest air water entry, and the largest total porosity. Hence this layer has more macropores than all the others. Consequently, these macropores serve as conductors for PF paths (**Fan et al., 2013; Zhang et al., 2021a**) similar to those found in natural compacted soils.



(Figure 21 to be continued on next page)

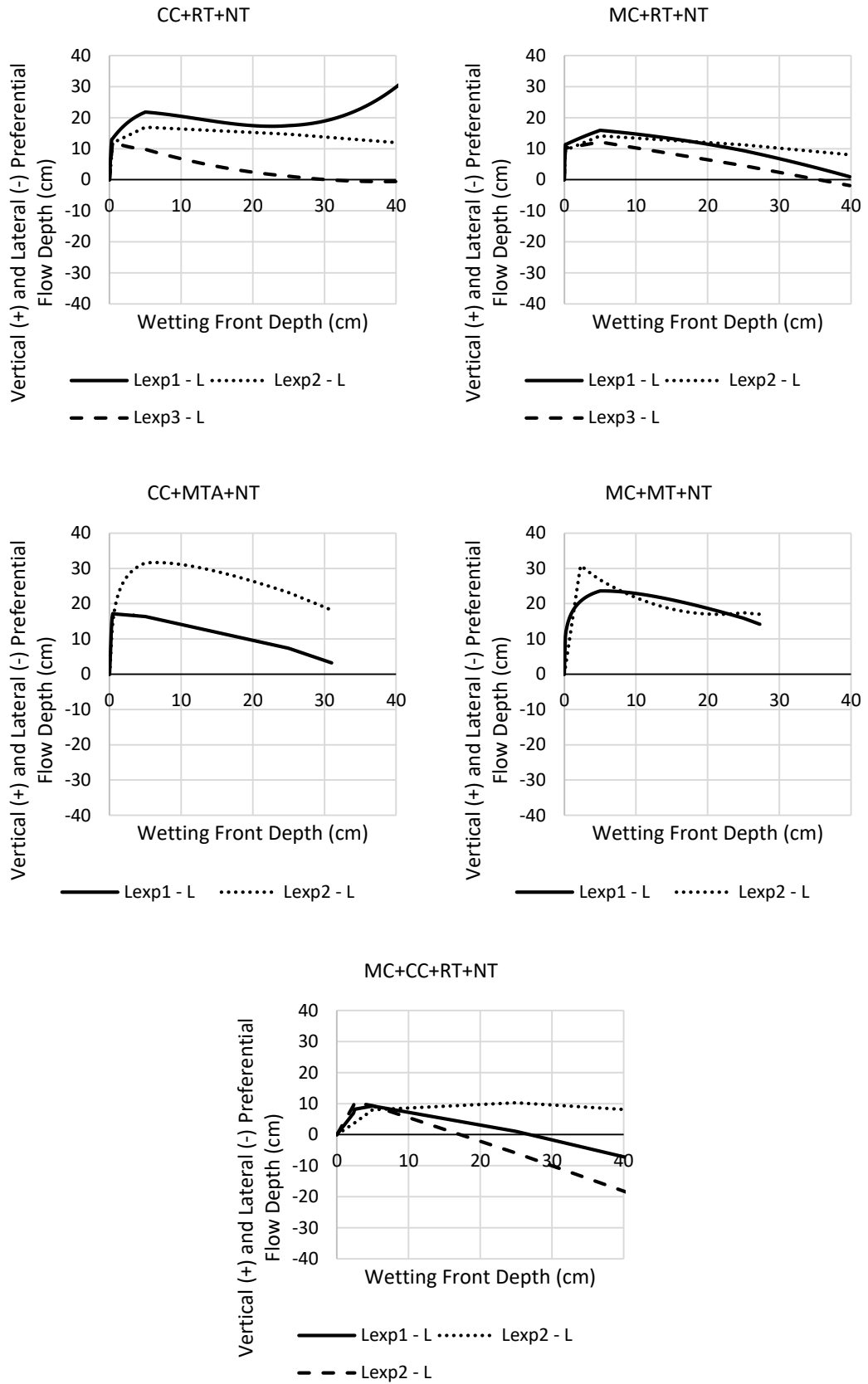


Figure 21: Vertical and lateral preferential flow variation along a 40cm soil profile of different soil management systems and under an irrigation rate of 0.518mm/min

4.1.3 Site 2 – Clay Loam

4.1.3.1 Densities

Referring to Figure 22, the bulk density of NT ($1.91 \text{ g/cm}^3 \pm 0.0298$) in clay loam soil indicates that this layer has degraded and became inadequate for crop productivity due to the inaccessibility of soil aeration needed for root and plant growth which is opposed to that found by **Castellini et al., (2019)** in clay loam soil under similar climatic conditions (Mediterranean) after 24 years of continuous no-tillage practices but similar to that found by **Reynolds et al. (2007)** on the same type of soil in Canada. The inconsistency with **Castellini et al., (2019)** is corroborated by large pores enclosed in the NT samples that are created by animal buries and roots, while samples in this study were abundant with such pores since no cultivation were taken place during the last 30 years. However, the application of rotary tillage decreases the bulk density of compacted soil to an optimal density to have maximum crop production ($0.95 \text{ g/cm}^3 \pm 0.0647$) since tillage applications allow soil to lose their structure and increase pore volume contents thereby affecting their resistance to compact (**Nawaz et al., 2013**) mirrored in the lower penetration resistance values (**Ferreras et al., 2000**). Similar manner of bulk density drop between no-tillage and conventional tillage systems was obtained in clay loam soils (**Grant and Lafond, 1993; Singh et al., 2014; Gao et al., 2016; Bogunovic et al., 2018**) for the top soil layer on the short-term. However, a settling state was reported for tilled layers on the long-term along which the soil is given time to consolidate back resulting in increase in bulk densities (**Bogunovic et al., 2018**). Similar to **Zhang et al. (2014)**, the addition of crop residues and chicken manure to tilled clay loam decreases further the bulk density by ~25% (MTA: $0.7061 \text{ g/cm}^3 \pm 0.0259$, MT: $0.7066 \text{ g/cm}^3 \pm 0.0305$) to a critical value that affects the anchorage of plants. Other researchers reported smaller drop rates when manure is added but with smaller application rates in silty clay loam soils (**Shirani et al., 2002**). Hence, the type of organic matter is not substantial since the bulk densities of CC and MC were close when compared using Tukey's test. An analogous variation for dry and saturated density is observed in Figure 21: tillage application decreases the density of NT which is further decreased by the addition of organic matter regardless of the type) (P-value<0.0001).

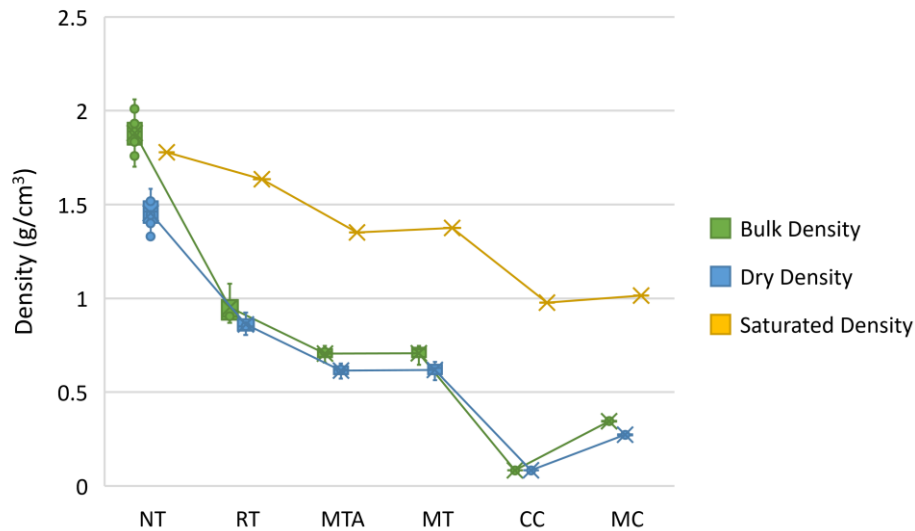


Figure 22: Bulk, dry, and saturated densities of individual homogeneous layers of different soil management systems in Site 2 – Clay Loam

4.1.3.2 Porosity and Residual Volumetric Content

The most compacted layer, NT has the lowest total volumetric content of pores ($0.325 \text{ m}^3/\text{m}^3 \pm 0.023$). The latter is enhanced by 2.385, 2.268 and 2.333 times due to tillage application RT, MTA and MT respectively as illustrated in Figure 23. Such incongruities in porosities between NT and CT treatments are also reported by **Castellini et al. (2019)**. Thus, the addition of organic content was not significant (almost similar 95%CI in Tukey’s test for RT, MTA, MT) as the application of tillage. This is justified by the unimportance in porosity between MC and the tilled layers. Even though the porosity of CC is higher than that of the tilled layers, yet the crops are crushed in the rotation so that it doesn’t affect the total porosity of RT. On the other hand, the addition of manure and mulch increased the residual moisture content of the disturbed layer by 57.66% and 21.02% respectively. Such increase was also observed by **Zhang et al. (2014)** in silty loam soils. Even though the crop residues had a really low residual content, its addition to tilled soil enhance its capacity to hold water since smaller mean pore were generated than RT while keeping in mind that the clay in these soils overrules all other grains to maintain water. On the other hand, the compacted soil when crushed during tillage application will endure some aggregates in which the finest pores and grains exist (as will be shown in later sections) that protects bonded clay together so that when any type of organic matter is added to tilled soil, the organics

will fill in the pores between the aggregates and won't affect the functionality of clay particles. This also reflects in the triviality in residual moisture content between the NT layer and the other tilled layers in which the finest soil grains of main function to store and maintain water are intact.

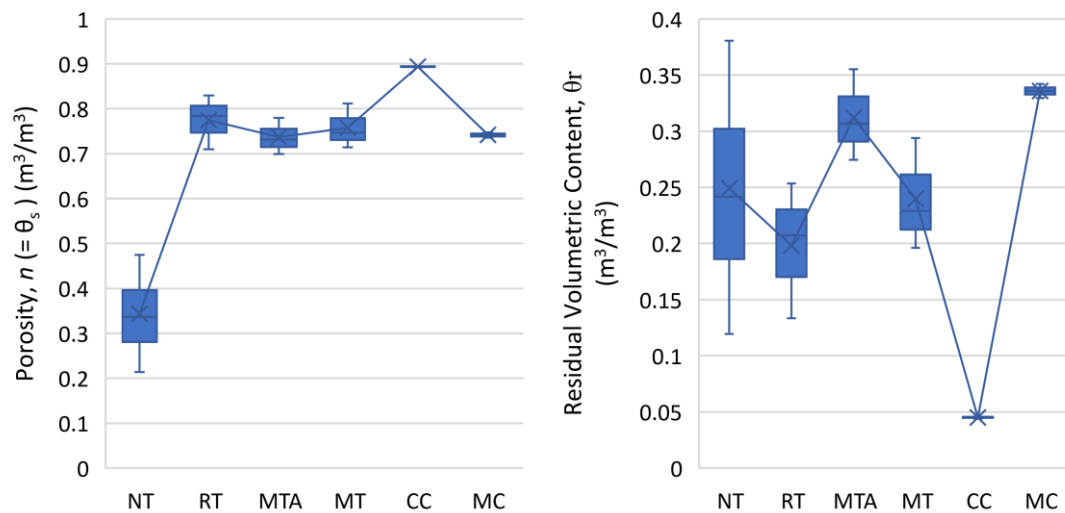


Figure 23: Porosity and residual moisture content of individual homogeneous layers of different soil management systems in Site 2 – Clay Loam

4.1.3.3 Organic Matter Content

The organic matter content doesn't change significantly between the different treatments of the soil management systems ($P\text{-value}=0.225$) (as shown also in Figure 24), which means that neither the application of tillage nor the addition of organic matter content (crop residues and chicken manure) affect OMC since CC and MC have very low dry bulk density with respect to clay loam soil. So when CC or MC are incorporated in the tillage application, their bulk densities don't vary and ultimately OMC will remain unchanged. The negligible short-term effect of manure application on OMC in clay loam terrains was opposed to the long-term effect of OMC on silty clay loam as reported by **Shirani et al. (2002)**. Albeit the manure application rate used in **Shirani et al. (2002)** ($<0.0001\text{kg}/\text{m}^2$) was much lower than that used in this work ($17.22\text{kg}/\text{m}^2$) while the organic matter content existed in the manure was smaller by 85% than that used in the work, the manure addition increased the OMC by 4 times on

the long-run, while for the short term it was only raised by 50% (from NT to MTA) and by 35% (from RT to MTA). Thus, OMC was measured after harvesting of corn in the second year which indicates that the effect of OMC was not attributed to the manure application completely when compared to the short-term effects. Also **Shirani et al. (2002)** reported an increase in OMC due to manure addition after two years in fine-loamy soils. This is because manure provides the necessary nutrients which improves the crop yield, thereby leaving behind after harvest periods good quality of crop residues and ultimately increasing the OMC (**Shirani et al., 2002**). Crop residues having high OMC ($912.45 \text{ g.kg}^{-1} \pm 5.20$) that are formed during this long period are decayed on the soil surface while contributing to the organic contents.

It is worthy to mention that if NT and RT were only compared, tillage application hence decreases the organic matter content significantly (**P-value <0.001). The organic matter loss due to tillage application was similarly conveyed by other studies (**Elliott, 1986; Six et al., 2000; Reynolds et al., 2007; Troldborg et al., 2013; Castellini et al., 2019**).

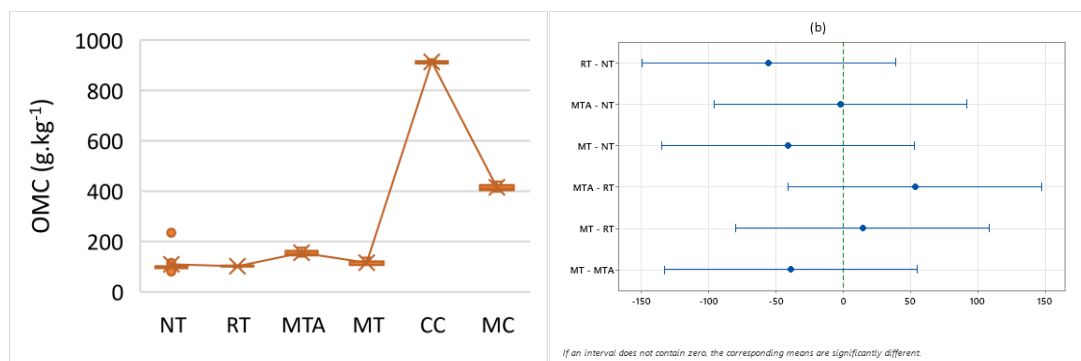


Figure 24: OMC Statistical Analysis for NT, RT, MTA, MT in Site 2 (a) Interval plot with 95% CI for the mean, (b) Tukey 95%CI

4.1.3.4 Aggregate Size Distribution

The mean weight diameter determined from the frequency density functions in Appendix A are shown in Figure 25 in which NT has the largest MWD (4.55cm) following MT (1.14cm), then RT (0.96cm), MTA (0.935cm), CC (0.50cm), and lastly MC (0.49cm). The MWD are the mean size of aggregates that are formed of the finest grains while consisting of the finest pores. Approximately, each compacted aggregate

is divided between 5 identical aggregates after tillage. Thus, it is logical to interpret that the volumetric content of fine pore didn't change with tillage but only additional volumetric contents are added for larger pores that exist between the aggregates. In addition, when adding the organics to the tilled soils, insignificant change to the MWD with respect to RT exist since larger aggregates of clay loam are already formed.

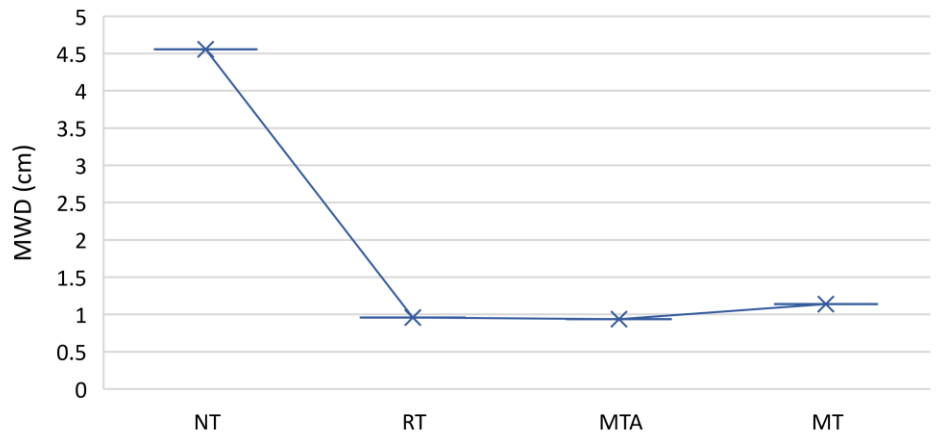


Figure 25: Mean weight diameter (MWD) from the frequency density function of the aggregate distribution (f) in Site 2 for NT, RT, MTA, MT

4.1.3.5 Saturated Hydraulic Conductivity

The saturated hydraulic conductivity of an undisturbed clay loam soil from Figure 26 is much smaller than the threshold ($0.0294 \text{ cm/day} \pm 0.0059$) which indicates that the soil is suitable for usage in ponds for restriction of subsurface water infiltration. Opposing to other studies, higher K_s values were detected for NT than CT since large macropore created by animal buries which are larger than the pores creates between the aggregates of tilled soils must have contributed to the conductivity of water (Vogeler et al., 2009; Castellini et al., 2019). In this study, the tillage application increases this value by 3 and a half order of magnitude (RT: $48.165 \text{ cm/day} \pm 6.209$) due to the large void spaces between the 1cm aggregates' sizes. In accordance, tillage application reduced the densities of NT soils and thereby increased the water conductivity on the short-term (Hu et al., 2009; Blanco-Canqui et al., 2017) especially during the beginning of agricultural season before seeding (Villarreal et al., 2017). It is noteworthy that such enhancement provoked immediately after tillage

decreases with time due to the consolidation of loosened tilled soil caused from overburden pressure and raindrop impacts (Strudley et al., 2008). Thus, the aggregates have an angular shape which creates large pores in between. The addition of crop residues to tilled soils is not statistically significant however the decrease by 37.5% is due to the drop in the large pore sizes created in RT between the aggregates since the organics fill these pores and thereby dividing the large pores into individual smaller pores. Further, crop residues have higher sorption capacities than soil by 10 to 60 times (Boyd et al., 1990; Reddy et al., 1995); hence the adsorption effect might be still active during the measurement of the hydraulic conductivity. On the other hand, the addition of manure to tilled soil increases the hydraulic conductivity of RT which is not consistent with the pore structure change that the manure imposes on RT. Thus, chicken manure in this case is hydrophobic and can pass water easily and faster in opposition to the crop residues which tend to be highly adsorptive to water. Similar results were reported by Shirani et al. (2002) when manure was added to silty clay loam and by Zhang et al. (2014) using farmyard manure in silty loam soils where much lower manure rates were applied resulting in 2 times increase while here it was increased by 7 folds.

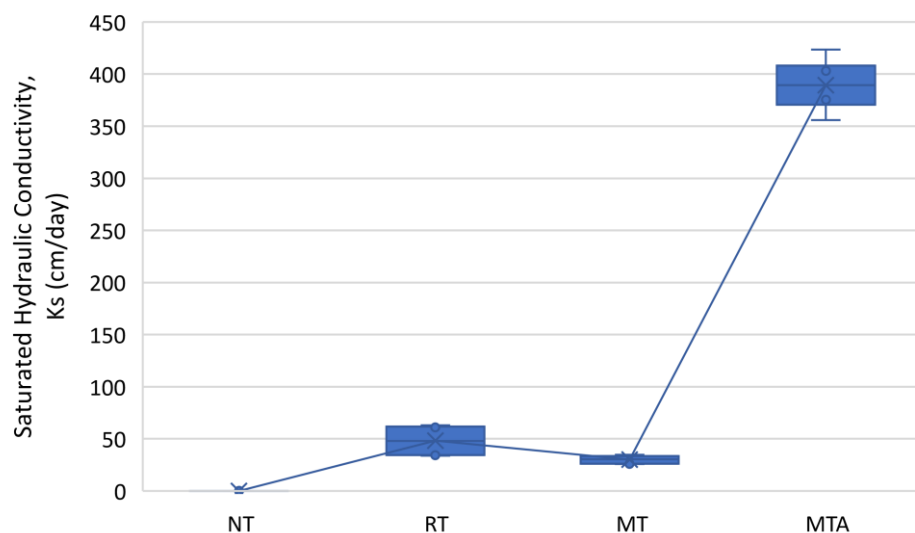
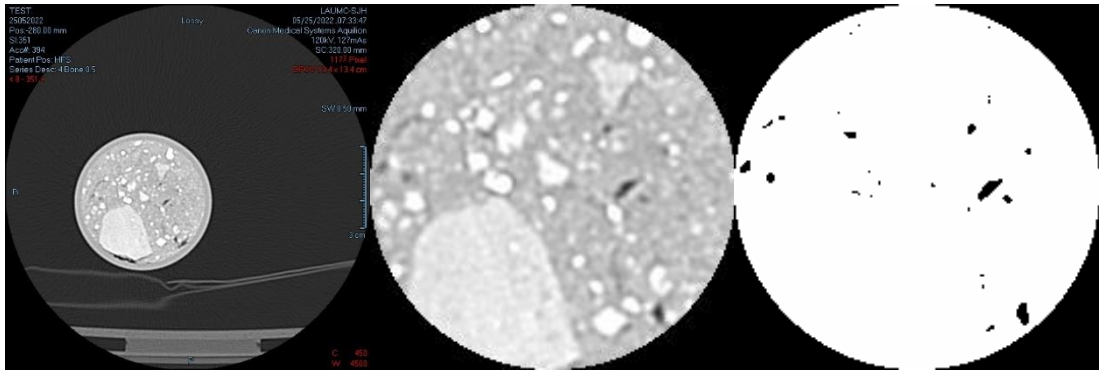
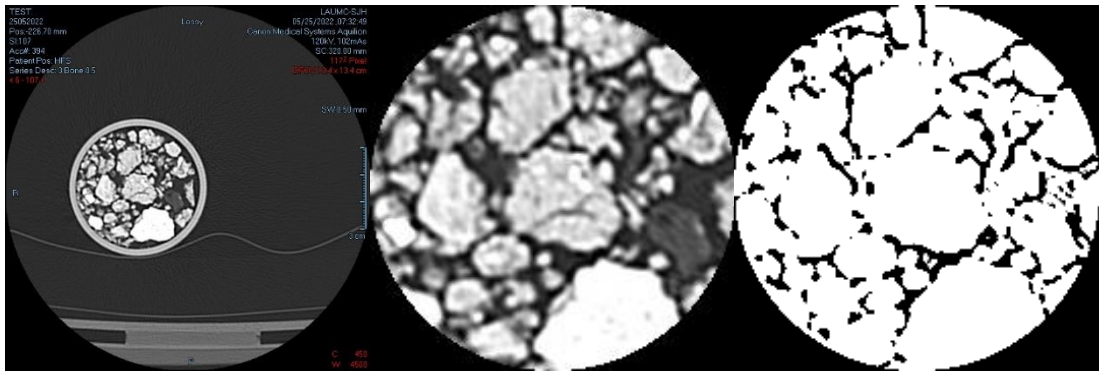


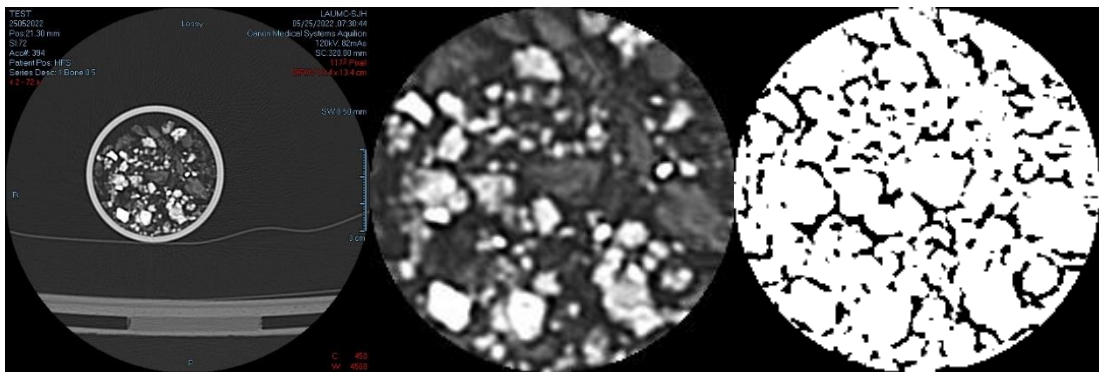
Figure 26: Mean weight diameter (MWD) from the frequency density function of the aggregate distribution (f) in Site 2 for NT, RT, MTA, MT



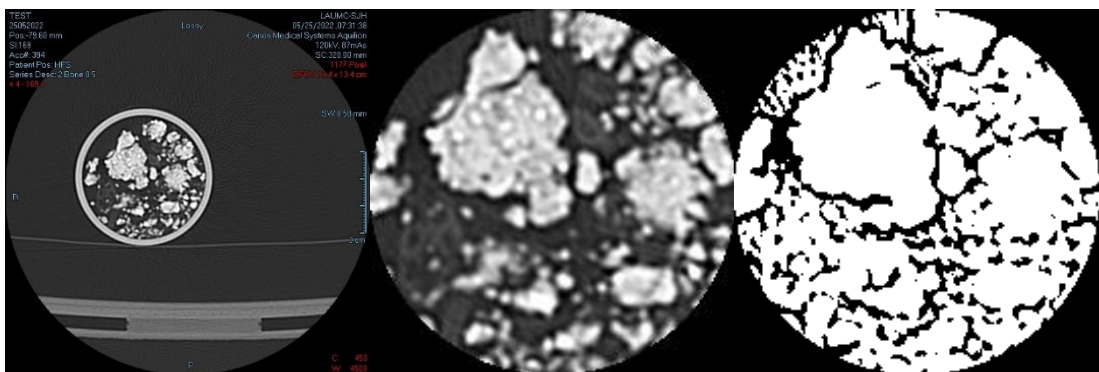
(a)



(b)



(c)



(d)

Figure 27: CT scanning images for (a) NT, (b) RT, (c) MTA, and (d) MT in Site 2

4.1.3.6 Soil Pore Structure, SWRC & PVD

The CT-scans of soil samples from clay loam fields for NT, RT, MTA, and MT illustrated in Figure 27 corroborate the results of the parameters discussed earlier. For instance, scans for NT shows the scarcity of volumetric pore contents which reflects the low porosity, small hydraulic conductivity, the high residual content and the large aggregates (the pores are so small to allow for the soil grains to desiccate which tightens the soil grains more to result in larger aggregates). Smaller aggregates are formed after soil crushing during tillage application as shown in Figure 27 – b where the pores are produced in between these aggregates. Furthermore, the pore spaces are filled by chicken manure in Figure 27 – c and with crop residues in Figure 27 – d so that more sorted body is formed. Porosities for (*NT, RT, MTA, and MT*) corresponding to pore sizes smaller than 0.1mm, between 0.1 and 1mm, between 1 and 5mm and larger than 5mm are ($0.324, 0.599, 0.678, 0.600 \text{ m}^3.\text{m}^{-3}$), ($0.0002, 0.0481, 0.0538, 0.0852 \text{ m}^3.\text{m}^{-3}$), ($0, 0.1262, 0.0050, 0.0355 \text{ m}^3.\text{m}^{-3}$), and ($0, 0.0011, 0, 0.0365 \text{ m}^3.\text{m}^{-3}$), respectively. Hence, it is paradoxical that RT have a higher porosity than NT of pores smaller than 0.1mm. This is refuted since the percentage of porosity carrying these fine pores with respect to the total porosity is smaller for RT (77.34%) than NT (99.93%). This means that almost all the porosity residing in the undisturbed soils include these fine pores, whereas 77.34% of the pores are activated by fine pores. These fine pores exist in the large aggregates formed in RT. In addition, the incorporation of chicken manure to the tilled soil increases the volumetric content of fine pores with a reduction in the coarser pores, while the addition of organic matter improved the volumetric content of pores larger than 5mm. However, pores improvements are not as significant since the organic matter content was not significant between all treatments due to the high density of the particle grains of soil.

The fitted van Genuchten parameter are resulted from good models with R-squared greater than 0.8 (Figure 29). α shows a humongous increase from NT to MTA, then RT and lastly MT while n is lowest for NT and increases in MT, then MTA and finally RT. The fitted van Genuchten parameters are used to draw the soil water retention curves for NT, RT, MTA, and MT as shown in Figure 30. NT drains over a large range of matric potential while the tilled layers become better sorted meaning lower values of pressure are depicted for the inflection point similarly reported by **Castellini et al. (2019)**. **Kay and Vanden Bygaart (2002)** reported that the gap between fine and

coarse pores increase in no-tilled soils as it was observed in this study since the fine and coarse pores become finer and coarser, respectively. Thus, on the long-term it has been identified a better sorted pore structure in NT than CT (Castellini et al., 2019), since pores in NT become well-connected due to their large aggregation (Wahl et al., 2004).

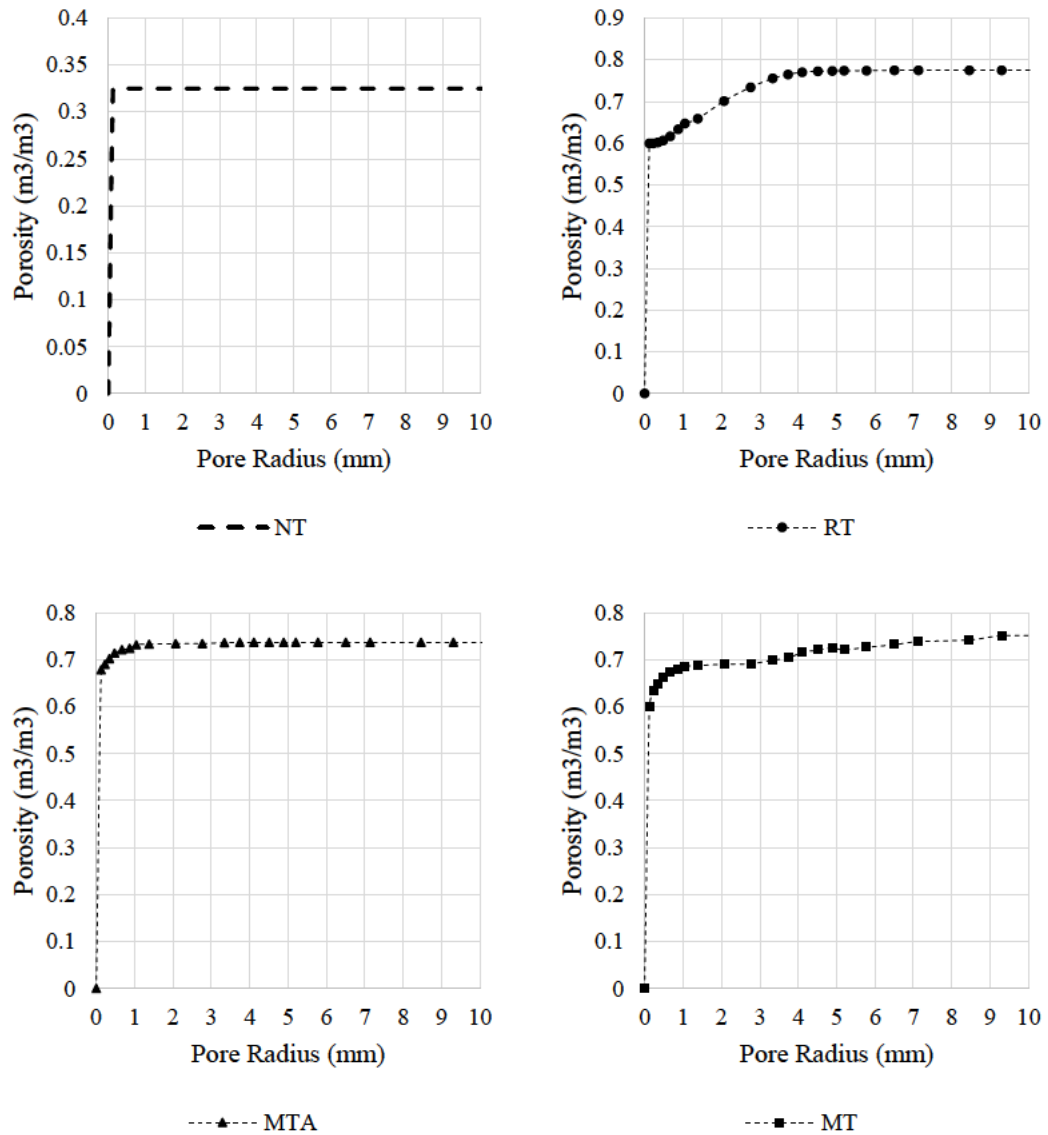


Figure 28: Porosity Distribution for NT, RT, MTA, and MT from the analysis of volumetric contents of pore sizes in ImageJ in Site 2

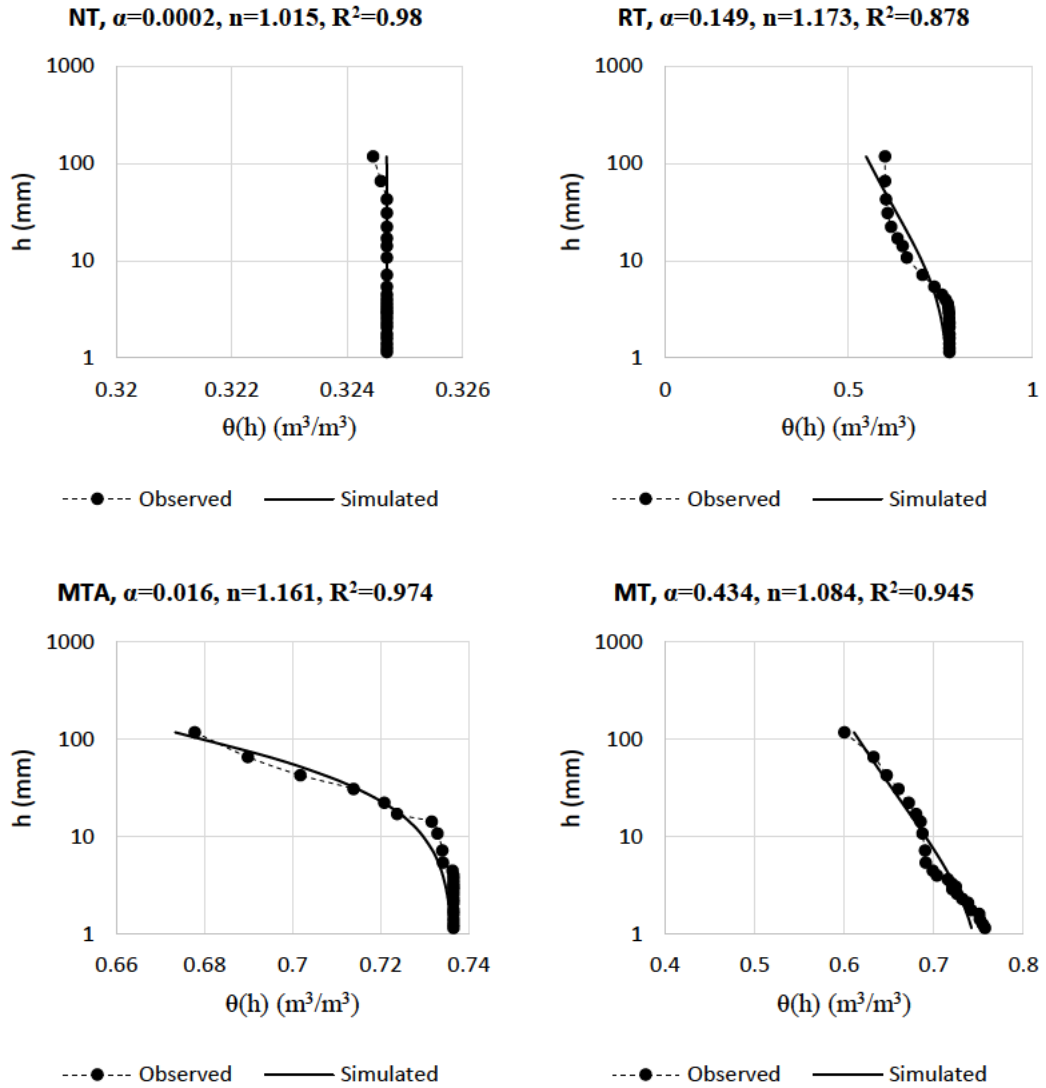


Figure 29: Fitted van Genuchten parameters for NT, RT, MTA, MT, CC, and MC in Site 2 (α in [1/mm])

The treatments' order of pressure to drain or retain water is $NT > MTA \geq MT > RT$. Through observation, the curves of tilled layers show that they drain after saturation over a small range of matric potential due to the large pores existing between the aggregates, and further drains after a longer range when the curve moves beyond the inflection to the residual moisture content. This is because when all the large pores are drained, the drainage for the finer pores requires higher pressures for water removals. This can be also seen as an advantage in having large pores and very fine one to maintain water for longer periods for root uptake. However, when analyzing the pore volume distribution function's parameters from Figure 31, all layers show to be

extremely poorly sorted, very fine skewed while the shape is leptokurtic as indicated by the shape and location parameter determined in Table 13. This means that all layers have excess in fine pores due to the large aggregation. However, the results of the saturated hydraulic conductivity contradict with the fitting parameters of tilled layers (RT, MT, and NT) in which very fine pores are overestimated. This is why the functions were negatively skewed.

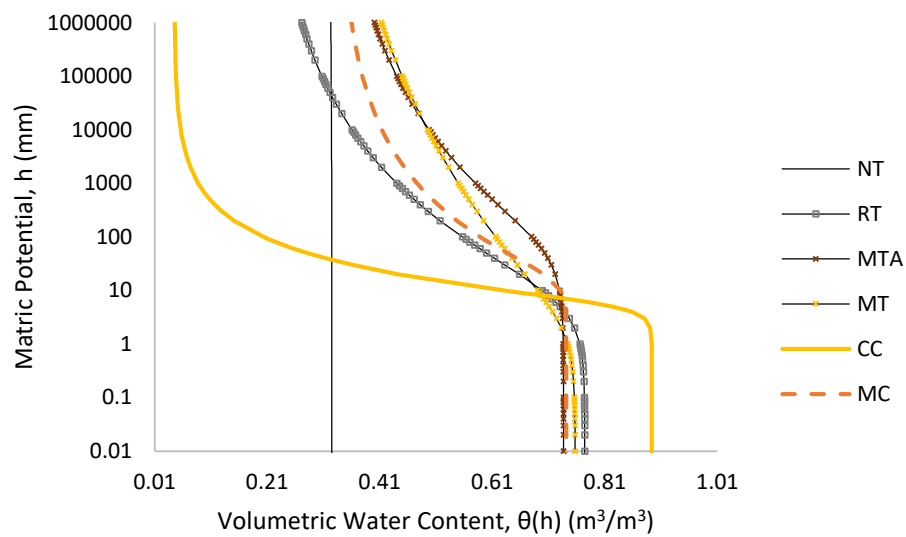


Figure 30: Fitted soil water retention curves for NT, RT, MTA, MT, CC, and MC in Site 2

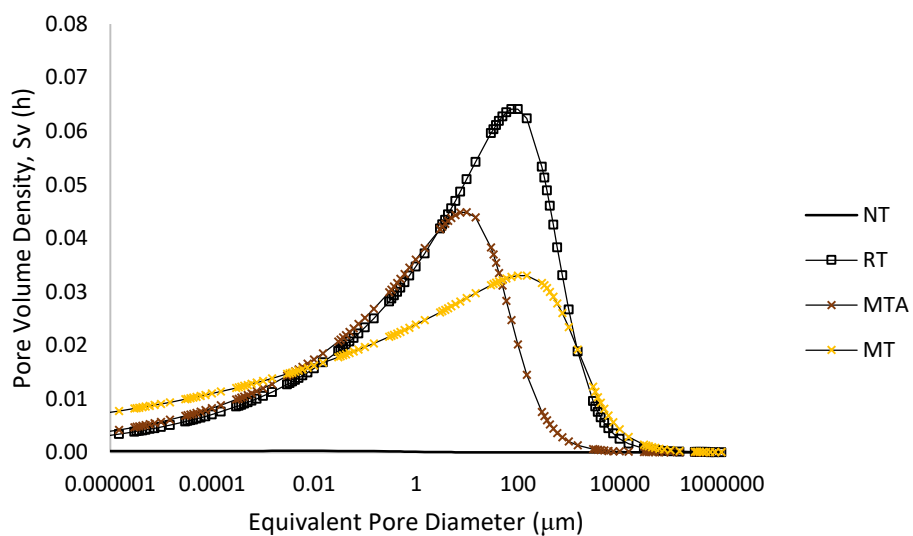


Figure 31: Pore volume distribution PVD functions for NT, RT, MTA, and MT in Site 2

On the other hand, larger modal diameters were depicted for tilled layers than those found in NT as opposed to those detected in CT and NT plots in clayey soils by **Castellini et al. (2019)** since macro-pores were more abundant in NT than CT. This is caused by the large pores created by animal buries that were taken into consideration while plotting the SWRC opposing to the negligence of such pores in this study since the purpose was mainly to compare the structure of micropores. In the support of our results, **Ferreras et al. (2000)** reported that soils in tilled layers had larger volumes of pore sizes higher than 20 μm than NT. In accordance with this study, modal diameters were greater than 20 μm in tilled soils (RT, MTA, and MT) while less than 1 μm in NT. This means that more than 50% of the pore volume in tilled soils had pore sizes larger than 20 μm .

Table 13: Location and shape parameters of the PVD functions for NT, RT, MTA, MT, CC, and MC in Site 2

	Site 2				Common	
	NT	RT	MTA	MT	CC	MC
Location Parameters						
d(mode) [μm]	0.081763	870.2335	91.05387	1226.476	3412.349	794.8183
d(median) [μm]	1.35E-19	81.5427	6.82465	3.483077	1667.24	125.4404
d(mean) [μm]	1.95E-25	27.21926	2.076304	0.310102	1196.395	56.86205
Shape Parameters						
SD	2.02E+24	183.4906	259.9517	30753.5	4.835167	31.31386
Skewness	-0.46901	-0.4035	-0.41014	-0.45081	-0.40364	-0.44133
Kurtosis	1.196705	1.244298	1.241686	1.217338	1.244247	1.224738
Descriptive Terminology (Blott and Pye, 2001)						
SD		<1.27				Very well sorted
		1.27-1.41				Well sorted
		1.41-1.62				Moderately well sorted
		1.62-2.00				Moderately sorted
		2.00-4.00				Poorly sorted
		4.00-16.00				Very poorly sorted
Skewness		>16.00				Extremely poorly sorted
		-1.0 – -0.3				Very fine skewed
		-0.3 – -0.1				Fine skewed
		-0.1 – 0.1				Symmetrical
		0.1 – 0.3				Coarse skewed
Kurtosis		0.3 – 1.0				Very coarse skewed
		<0.67				Very platykurtic
		0.67-0.90				Platykurtic
		0.90-1.11				Mesokurtic
		1.11-1.50				Leptokurtic
		1.50-3.00				Very leptokurtic
	>3.00				Extremely leptokurtic	

4.1.3.7 Soil Physical Quality Indicators

Referring to Table 14, the air capacity of undisturbed soil in clay loam soil is smaller than the volumetric content needed for soil aeration. Thus, tillage practices tolerate higher AC values through the application of soil crushing and allowing air to fill in between the aggregates.

Table 14: Soil physical quality indicators for NT, RT, MTA, MT, CC, and MC in Site 2

SITE 2				
	NT	RT	MTA	MT
Air Capacity AC	4.37E-05	0.334007	0.156375	0.207555
PAWC	0.000888	0.14079	0.148369	0.107237
RFC	0.999865	0.568678	0.78771	0.725974
S theory	0.006811	0.064199	0.044883	0.033024

In particular, RT has a large value of AC, even larger than that of MC. However, RFC values show that RT only tolerates good soil aeration while the rest doesn't due to the scarcity of pores in NT and due to large pores fillings of tilled soils with organic matter for MTA and MT (limited capacities) while taking into consideration that MTA is a better pore-filling component than MT. The decrease in RFC between RT and NT is opposing to that reported by **Reynolds et al. (2007)** since treatments were evaluated over a longer period which results in having macropores in NT larger than those found in RT due to animal buries and root penetrations. The presence of macropores would increase the porosity and the PAWC at the same time. Thus, their results show that the tillage application destroys those macropores and thereby increasing the RFC so that the soil would have smaller pores to reach soil aeration limitations. Hence, this is not the case in our study which demonstrates that the tillage application increases the volume of larger pores. Anyhow, the tilled layers can hold water for storages for subsequent root functioning and crop growth while having lower RFC values than NT. This is advantageous since the less the soil is limited in aeration, the better the microbial activity is, which enhances root growth and crop yield (**Reynolds et al., 2007**). Even though NT has larger aggregates meaning large storage for water and higher ability to maintain water (**Ferreras et al., 2000**), but this is not the case in this study (PAWC<0.1) where soil is highly compacted (larger bulk density than optimal) thereby reducing the volumetric content of pores needed for water storages. Overall, RT is hypothesized to have a better soil physical and structural quality than the other

tilled layers (referring to S theory values) while NT is assumed to be very poor or in other words has a very degraded physical quality opposing to the assessment of NT and RT on clay soils by **Castellini et al, (2013)** who found that NT entailed a better physical quality suggesting that RT acquires low heterogeneity of pore diameters. Hence, the more homogeneous the pore size are, the better the sorting is which boosts the movement of water especially when the sorted pores have adequate size for smooth water flow as it is the case in the tilled soils. In our study, the tilled soils proved to have better soil physical quality than NT.

4.1.4 Spatial Variation Analysis

Two-way ANOVA analysis is run for each property illustrated in Figure 32. Statistically, the location of tested soil samples each having different soil classification is significant in terms of affecting the physical (except for OMC), structural and hydraulic properties of the different layers of soil management systems (NT, RT, MTA and MT) but doesn't disturb the effect that tillage practices and the addition of organic matter impose. Initially, treatments regardless of the soil type reveal an increase in their organic matter content after the addition of either manure and mulch straw as seen for other research (**Bolan et al., 2004; Zhao et al., 2009; Thangarajan et al., 2013**). In addition, all NT and RT densities and saturated densities for MT and MTA (P-value<0.001) are larger for clay loam than loamy sand soil, while bulk and dry MTA and MT densities are smaller for clay loam than loamy sand. Therefore, the clay loam has higher particle density. When tilled, higher volumetric contents are recorded in tilled layers for clay loam soils than loamy soils since they fit into higher mass of water so that their saturation density gets bigger in clay loam soils. On the other hand, the tillage application decreases the densities for both sites similarly to that found in **Singh & Malhi (2006)** on loamy textured soils due to decrease in soil penetration resistance (**Fabrizzi et al., 2005**) while the addition of organic matter lowers the densities of RT for both sites similarly to that found by **Adeyemo et al. (2019)**. It is noteworthy to mention that when organic matter is retained on the surface rather than amalgamated with the soil, no significant change in the bulk density is identified (**Singh & Malhi, 2006**). Hence, the addition of organic matter improved the degradation of aggregates that the tillage application induced on NT (smaller MWD for RT) and reflected the enhancement in structure by increasing its pore structure sorting.

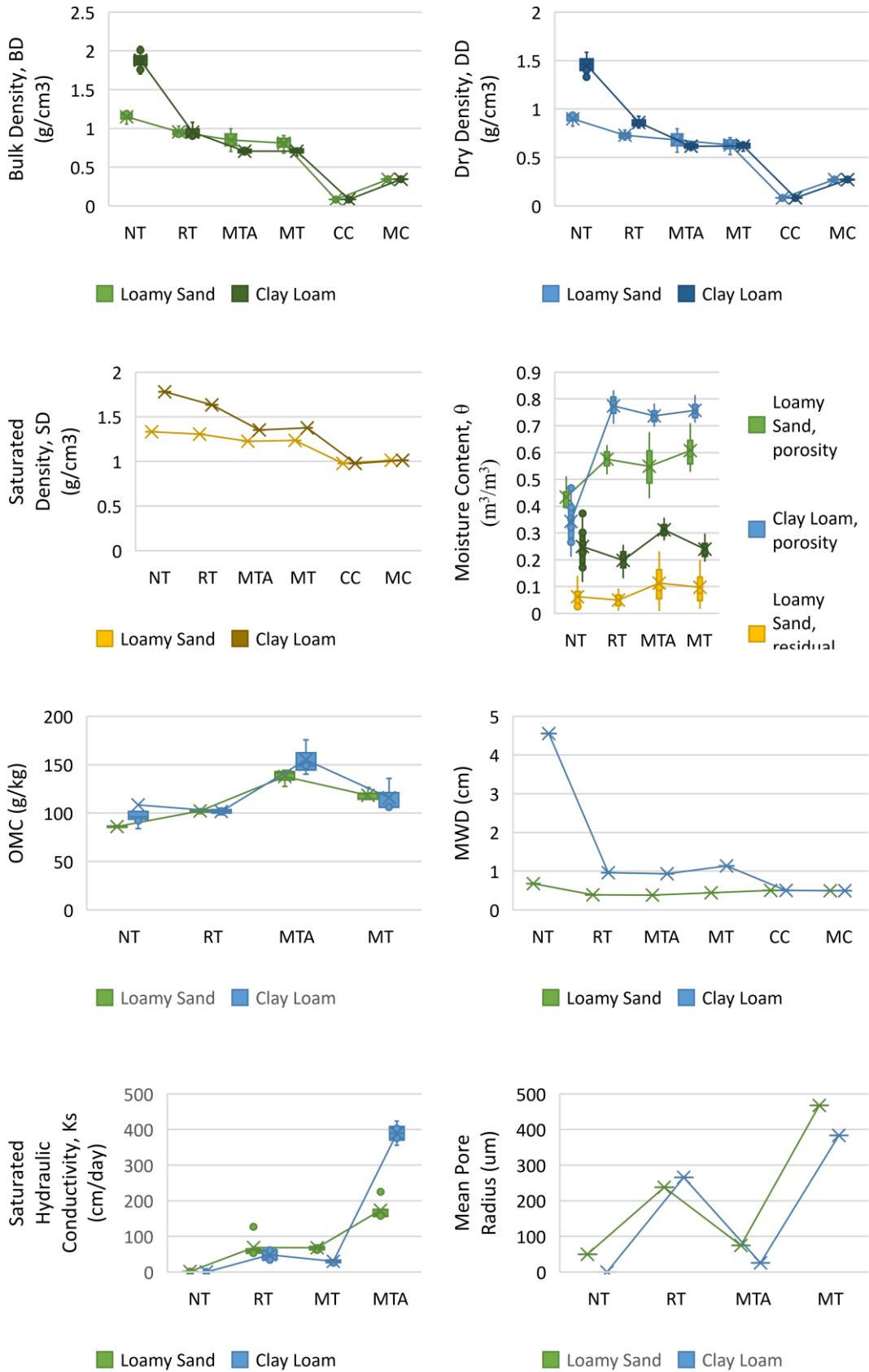


Figure 32: Physical, structural and hydraulic properties for NT, RT, MTA, and MT in Sites 1 and 2

The total and residual moisture contents of clay loam soils is lower for NT layers than loamy sands. However, the tillage application for clay loam soils tolerate higher volumetric contents than loamy sands while maintaining higher residual content. This is because the mean weight diameter for tilled clay loam soils is higher than that of tilled loamy sand which means that the clay loam have larger aggregates of which larger volumetric pore contents are formed in between while protecting the clay inside the aggregates for water storage. On the contrary, loamy sand soils has lower clay content and smaller aggregates in which smaller volumetric contents exist between their boundaries (**Buschiazzo et al., 1998**). Notwithstanding, both soil types shows drop in the mean weight diameter when compacted soil is tilled which focuses on the impact of tillage practice to induce soil structure deterioration (**Elliott, 1986; Six et al., 2000; Troldborg et al., 2013**). However, such deterioration can be advantageous to root growth and penetration when comparing the soil physical quality indicators of RT layers with NT compacted soils. Notwithstanding, the addition of organic matter lowers the porosity and increase the residual moisture content in both sites thereby it consistently pertains to a pore-filling function. The alteration in structural components improves and better stabilizes the soil structure of tilled soils against physical deterioration regardless of the soil type (**Adeyemo et al., 2019**).

It is also noteworthy to mention that the range of moisture content that each layer has between θ_s and θ_r is not significant between soil type and tilled layers except for clay loam NT layer ($0.02\text{m}^3/\text{m}^3$). It only differs between compacted and tilled soils of which the range increases since the porosity of tilled layers proliferates while having an almost unchanged residual moisture content.

Additionally, clay loam soils possess lower saturated hydraulic conductivities than loamy sand since the latter pore structure is better sorted which makes it easier for water to infiltrate. Further, the hydraulic conductivity of MTA in both soils is remarkably higher than the other layers while having in parallel smaller mean pore diameter than the tilled layers which justify the hydrophobicity of chicken manure in which it is largely shown in clay loam soils. This is because the water penetrating clays is harder than passing through sand due to the decrease of flow velocity at wall boundaries of soil. Thus, water percolating in clay loam MTA layer passes along the manure particles while in loamy sand soil, water may favor its passage between sand particles and thereby will have slower speed. Similar findings were reported by

Mubarak et al. (2009b) and **Adeyemo et al. (2019)** where an appropriate justification for long-term effect was pointed towards the favoring of activation of microbial activity in clayey soils (in comparison to sandy clay loam in a tropical environment of Sub-Sahara Africe) which results in an increase in the volumetric contents following the application of manure. Regardless of the soil type, chicken manure has proved its effectiveness on increasing the hydraulic conductivity. Other studies reported analogous outcomes for poultry manure application (**Adeyemo et al., 2019**) and for other types of animal manure (**Martens & Frankenberger, 1992**).

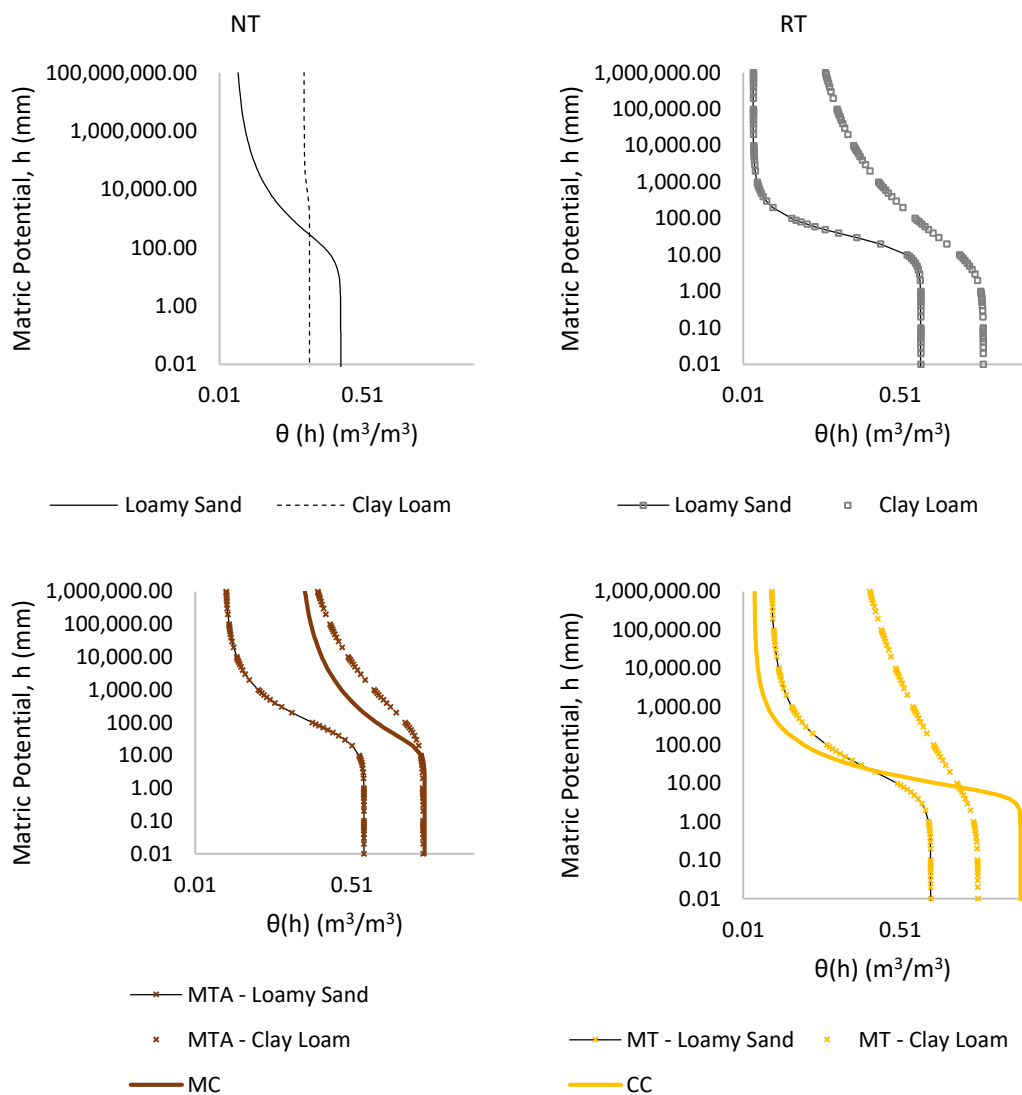


Figure 33: Soil water retention curves for contrasting individual layers in Sites 1 and 2

Comparing the soil water retention curves by observation in Figure (33) indicates that loamy sand soils is better sorted than clay loam regardless of the management system applied. It is also worth mentioning that crop residues are more sorted than when they are mixed with soil regardless of the type, whereas chicken manure behaves more like the loamy sand MT layer which drains over a short range of pressure in opposition to clay loam MT layer. This means that when incorporating chicken manure to low storage soil capacity, it enhances its storativity while not significantly affecting the passage of water. On the other hand, the addition of crop residues to a very fine dense soil enhance water infiltration while not disturbing the soil to acquire its storativity functions. Furthermore, regardless of the soil type, NT in both sites had the smallest α value which indicates a higher air-entry value ($1/\alpha$). Meaning that water requires more time to drain (**Martínez et al., 2008**).

Nevertheless, **Cullotta et al. (2016)** suggested that when the intention is to describe the soil pore system, location and shape parameters are used. Hence, location parameters (mode, median and mean diameters) are larger for loamy sand soil than for clay loam in NT, RT, MT, and MTA plots, respectively. Therefore, larger pore size exist in loamy sand soils regardless of the soil management system. However, a wider range of pore sizes is identified for clay loam soils than loamy sand soils. This reflects the softness in pore arrangement in clay loam soils with respect to loamy sand soils. On the other hand, when the intention is to assess the ability of soil to store and maintain water, the soil physical quality indicators are used. Consequently, loamy sand soil has greater potential to allow for soil aeration than clay loam while clay loam is preferable to maintain and properly store water regardless of the soil treatment type. Notwithstanding, loamy sand soils have a better soil physical and structural quality (higher S-theory values) than clayey soil which its quality is enhanced only with the application of tillage practices without the need to add any organic matter.

4.2 GARALS Model

The validation of GARALS model is accepted by the high limits of the Nash-Sutcliffe Efficiency which are greater than 0.75 when estimating the wetting front location resulting in a very good model (**Moriasi et al., 2007**) (as shown in Figure 34). However, when it comes to estimate the infiltration rate, good NSE ranges were

recorded in the case of ponding occurring in the unmodified layer while acceptable values were recorded for the case when ponding occurred in the modified layer (higher irrigation rate) (as shown in Figure 35). The validation incorporated four different cases in which 2 layers and 3 layers' soil profile were taken into consideration for different ponding locations. Therefore, the model can be used to explicitly estimate the different times that different wetting front could reach and then use the time for comparison at fixed wetting front locations to compare the efficiency of different soil management systems.

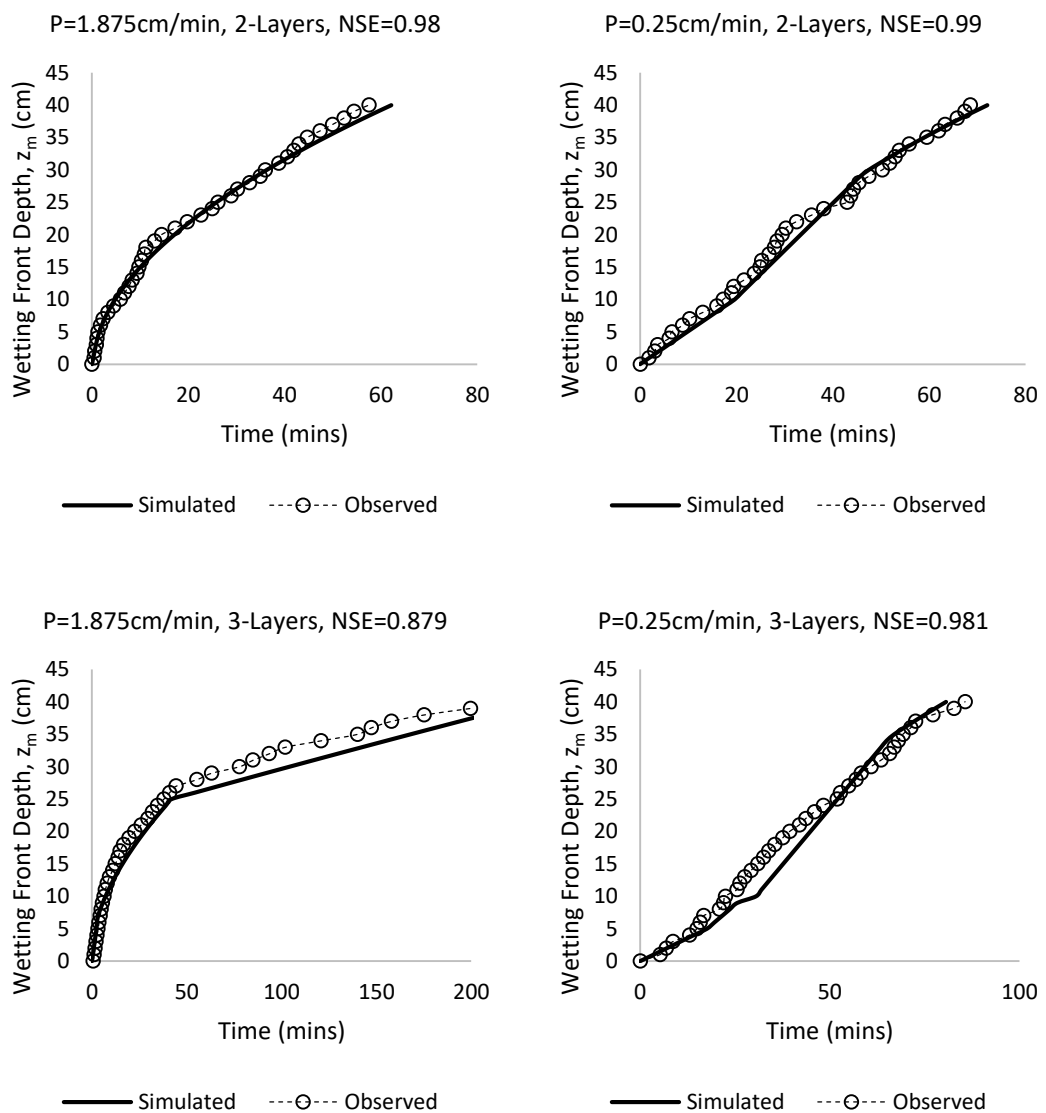


Figure 34: GARALS validation of wetting front depth z_m with experimental observed data

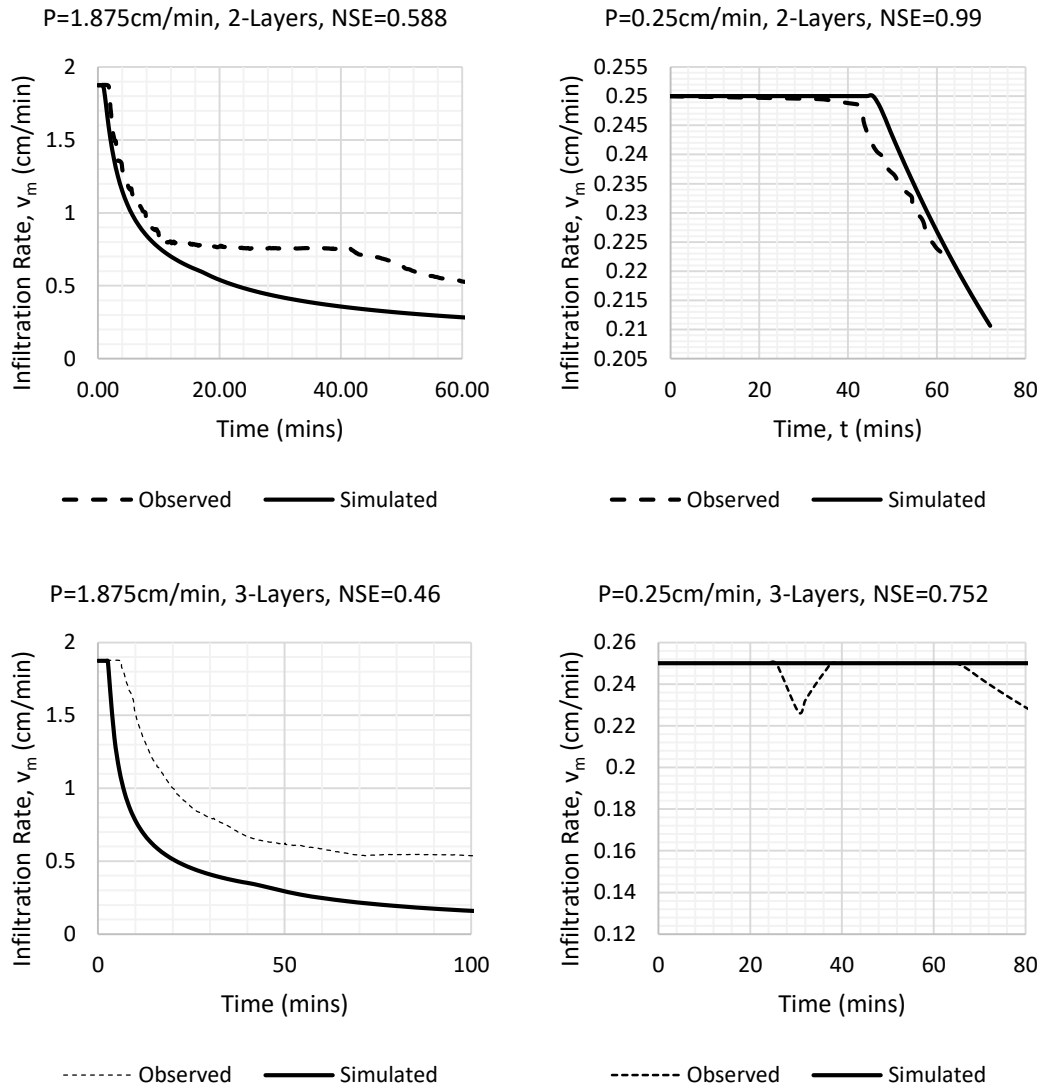


Figure 35: GARALS validation of infiltration rate v_m with experimental data computed from observed surface runoff data

4.3 Model Simulation

The simulation of the different soil management systems resulted in time variations along different wetting front depths (as shown in Figure 36). Thus, the movement of wetting fronts are divided between 5 categories combining different soil management treatments that have similar water flow pattern with some time delays: (C1) NT which is a 1-layer soil profile, (C2) CC+NT and MC+NT which consists of 5cm cover under lied by NT, (C3) RT+NT, MTA+NT, and MT+NT which are 20cm disturbed soil laying on NT, (C4) CC+RT+NT, CC+MTA+NT, and CC+MT+NT which consists of

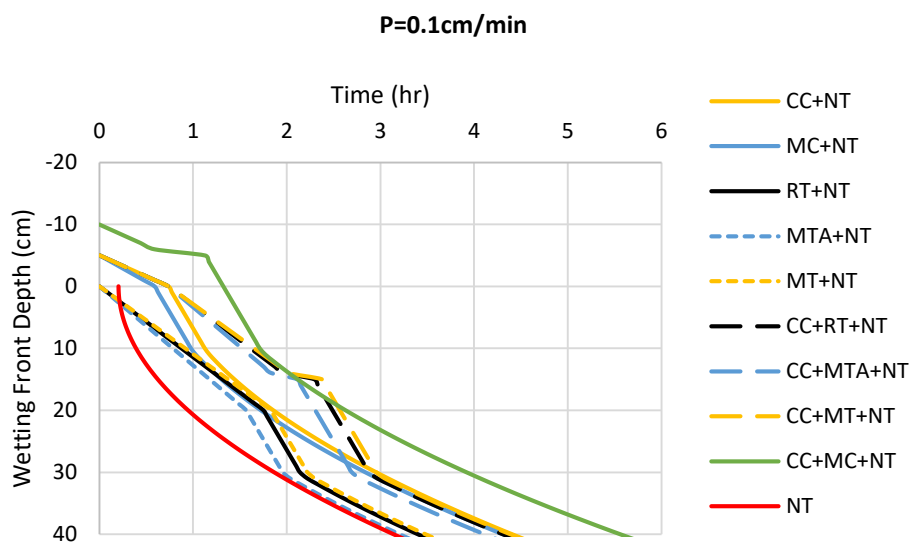
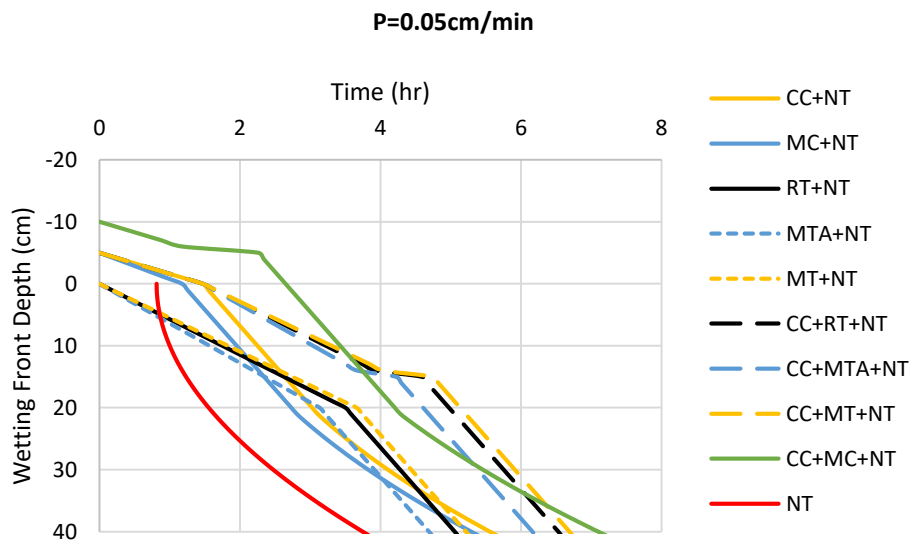
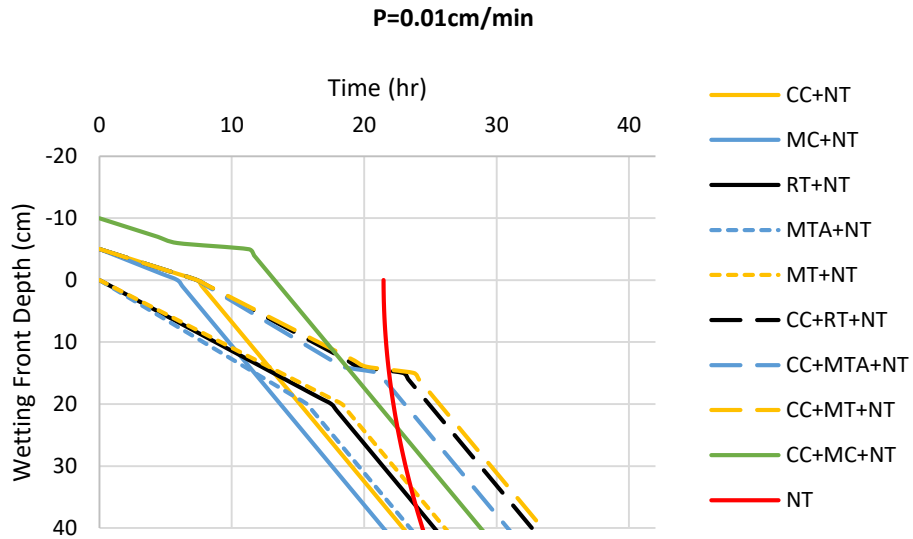
5cm cover, 20cm disturbed soil layer and NT, (C5) CC+MC+NT which involves of two 5cm covers above NT. Almost each category moves together in the same manner with some discrepancies. For irrigation rate smaller than 0.05cm/min, NT moves faster since the rate is so small that it infiltrates completely into NT without ponding while for the other profiles, higher porosities are found at shallow depths in which more water is needed to saturate the pores so that a wetting front is generated. The second category follows since it only has 5cm cover of porous medium to saturate. (C3) comes next having a deeper porous layer of 20cm (tilled/modified layer) than (C2), then followed by (C5) (having 10cm of coarser porous layers than (C3)) and later (C4) (having the largest shallow depth of porous medium – 25cm). As this stands, no-tillage systems proved to be efficient in increasing water infiltration in many studies (**Alvarez & Steinbach, 2009; Kahlon et al., 2013; Roper et al., 2013**). Therefore, NT a system that is economical, time and resources efficient (**Deen & Katakai 2003; Lankoski et al. 2004**) would be recommended in case of irrigation rates smaller than 0.05cm/min. Nevertheless, for irrigation rates between 0.05 and 0.1cm/min, (C3) starts to infiltrate faster than (C2) while (C5) becomes the last. Between 0.1 and 2cm/min, wetting fronts moves faster in (C3), then (C4), (C1), (C2), and lastly (C5). The same manner of infiltration carries on for higher irrigation rate but with a delay of CC+RT+NT only. Notwithstanding, the simulation shows that (C3) infiltrates water faster than (C4) for higher irrigation rates even though (C4) possess a cover layer of very high saturated hydraulic conductivity and large porosity and well-sorted pore structure. In this regard, going-in-depth in the crop residues cover advantages, many became eminent: they protect the soil surface from direct impacts of raindrops resulting in the reduction of soil erosion, soil detachment (**Schwab et al., 1993; Lal, 1979; Gholami et al., 2013; García-Orenes et al., 2009; Mwangi et al., 2016; Prosdocimi et al., 2016**) and soil surface sealing, compaction and crusting (**Cook et al., 2006; Jordan et al., 2010; Montenegro et al., 2013; Zonta et al., 2012**). However, the capacities of cover crops to decrease water infiltration is investigated to prove that cover crops inhibit water flow while increasing the ability of soil to maintain water after infiltration (**Clark et al., 1997; Waggener and Mengel, 1988; Unger and Vigil, 1998; Qi and Helmers, 2010; Rahma et al., 2019**). Further, the addition of crop residues on the soil surface increases the latter hydraulic roughness resulting in reducing the surface water velocity (**Montenegro et al., 2013; Shi et al., 2013; Foster & Meyer, 1975; Cruse et al., 2011; Jordan et al., 2010; Miyata et al., 2009; Rahma et al., 2013**). Thus, the

efficiency of using cover crops depends on the timing, the water holding capacity of the soil beneath the cover crop and the rate of precipitation (**Frye et al., 1988**). Hence, when using cover crop as soil covers, additional water to replace the water used by these residues must be taken into consideration (**Kaspar & Singer, 2011**), thus it is not recommended to be used in places of low precipitation or irrigation rates (**Unger and Vigil, 1998**), since under light irrigation rates, water is unlikely to reach the soil surface underneath CC unless the cover layer is fully saturated which will occur after adsorption is almost at steady state (**Pérez, 2000**).

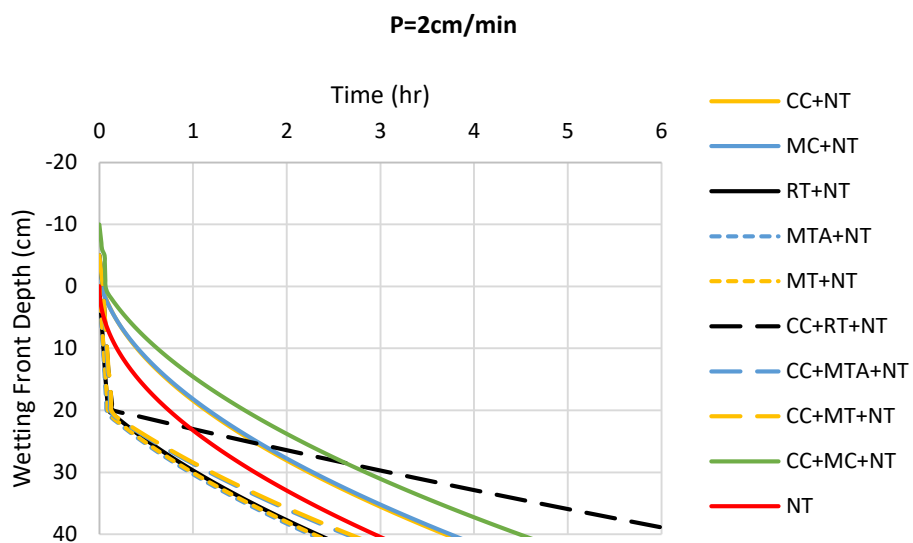
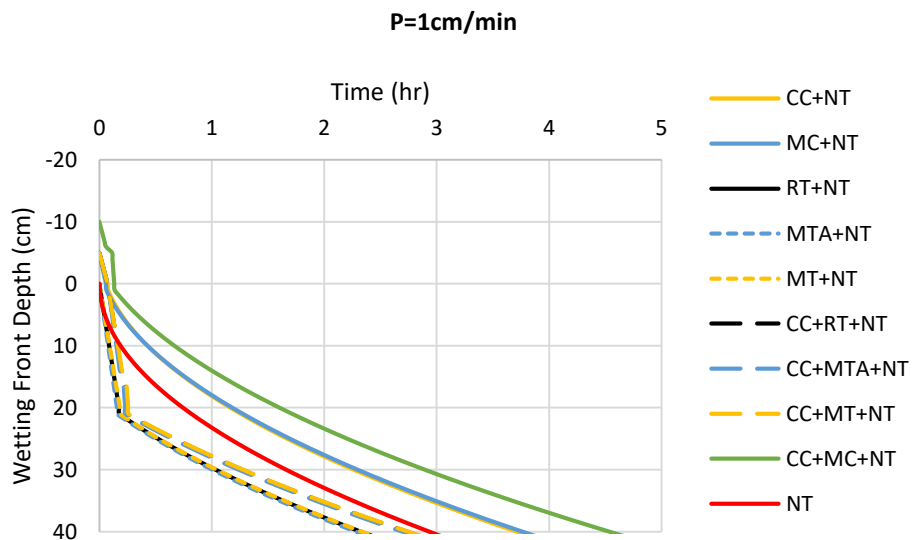
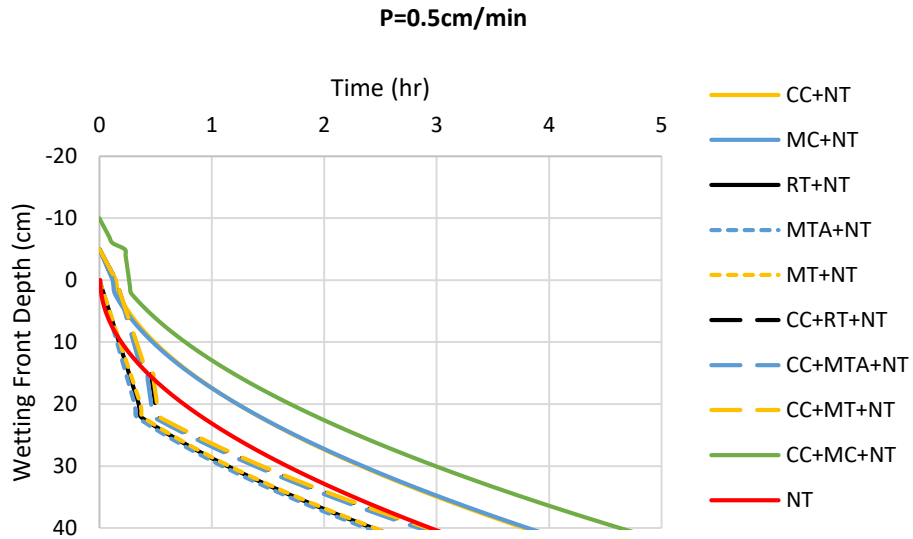
At high irrigation rates (C4) becomes faster than (C2) due to the presence of the modified layer in (C4) that has a suitable pore structure to maintain the high rate of water in opposition to the NT layer in (C2). Therefore, the tillage application through the crushing action that imposes on the 20cm soil depth forms a homogeneous layer that is well-sorted (in pores and aggregates) which are more or less connected to those in the underlying layer (**Ciollaro & Lamaddalena, 1998**). Between (C1), (C2) and (C5) the wetting front in the soil profile with cover layers is delayed from that of NT. This is because the addition of cover layers increased the depth of the soil profile by either 5 or 10cm. Thus, if we want to compare the arrival time to reach 20cm below the soil surface, the reference line for measurement should always be the original soil surface. Hence, if the measurement line for profiles with covers was at the surface of the cover, then the wetting front would seem to move faster in profiles with covers especially in those having cover crop residues. Similarly, if we changed the reference line of measurement in profiles having CC, the wetting fronts would be faster for all those having either crop covers or tilling layer or both meaning: C4>C3>C5>C2>C1. However, the increase in infiltration is not significant due to the absorption effects of the cover layer (**Unger, 1971; Lightfoot & Eddy, 1994; Pérez, 2000**). In accordance, the results would be similar to other studies who found that the addition of soil organic layer increases water infiltration (**Cook et al., 2006; Jordan et al., 2010; Montenegro et al., 2013; Zonta et al., 2012; Shi et al., 2013**). However, none of these studies took into consideration the change in the location of the reference line of the wetting front depth. Therefore, the organic matter addition seems to allow water to reach deeper fronts but in reality it is not. In accordance, **Rahma et al. (2019)** reported that infiltration rates are maintained with the addition of crop residues but only the surface runoff was reduced. In fact, an interesting advantage that CC induce on the soil-water

infiltration in this simulation is that it delays the time (dependent on the intensity of irrigation rate) to have surface runoff which is consistent with other studies' findings (**Cook et al., 2006; García-Orenes et al., 2009; Jordan et al., 2010; Montenegro et al., 2013; Zonta et al., 2012; Shi et al., 2013; Rahma et al., 2019**). Thus, using crop residue cover when the irrigation rate is high (as in the case of conventional irrigation along ponded furrows) is recommended.

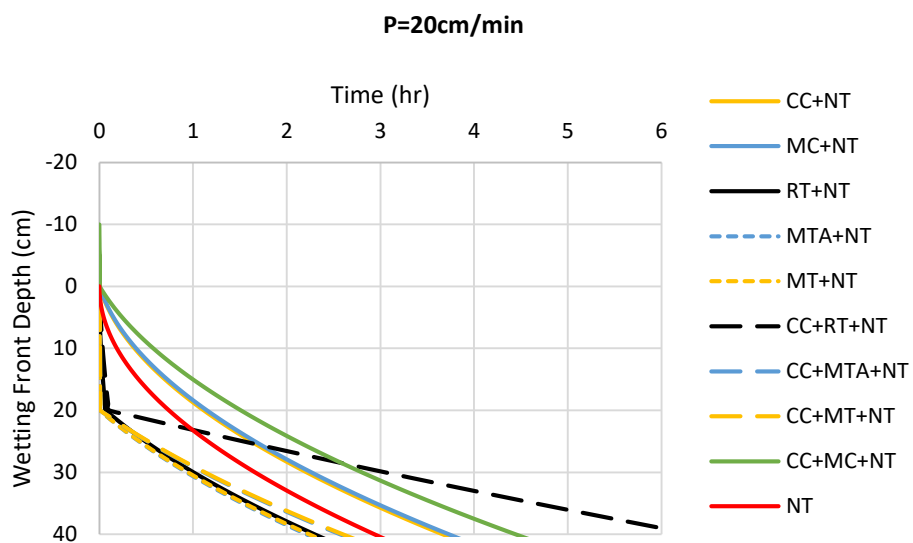
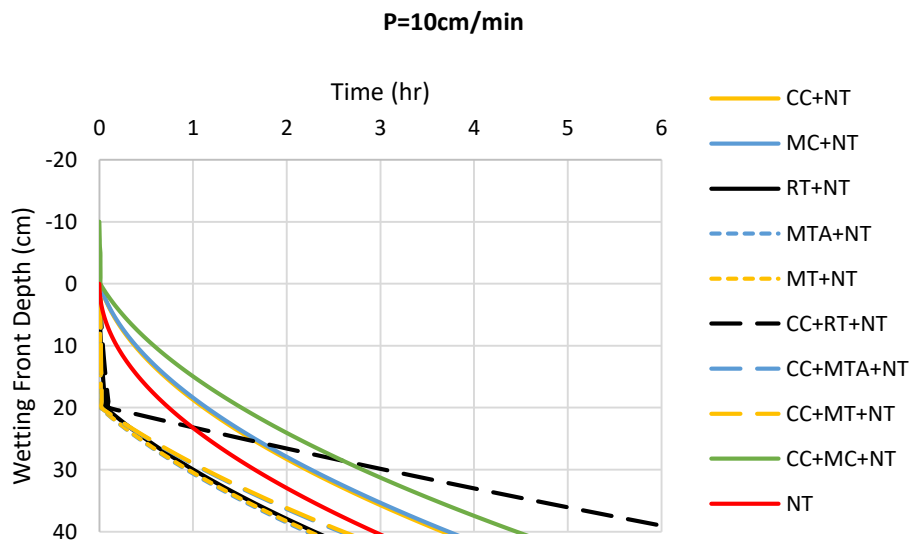
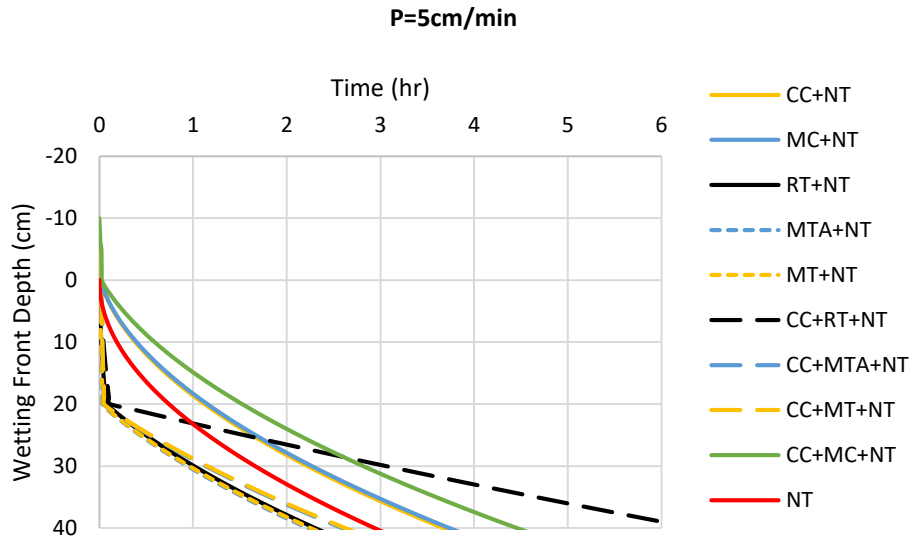
Notwithstanding, at higher rates, adding the tilling layer into the soil profile enhance the infiltration rate. A finding that is commonly reported by studies (**Gantzer and Blake 1978; Lindstorm and Onstad, 1984; Karlen et al., 1990; Pikul et al 1990; Mwendera and Feyen, 1993; Khurshid et al., 2006; García-Orenes et al., 2009**). Additionally, when crop residues are amalgamated with the soil during the tillage application, a faster infiltration is observed through deeper wetting fronts in shorted times (**Radcliffe et al., 1988; Wilhelm et al., 1989; Baumhardt et al., 2011**), even sometimes inhibiting ponding generated from RT plots (**García-Orenes et al., 2009**). Manure also is advantageous in increasing water infiltration (**Adeyemo et al., 2019**). As it was shown in earlier section, the aggregate stability was improved by the addition of organic matter. Even though the RT layers showed to have a more-sorted pore-size distribution, however the addition of organic content caused higher infiltration rates since MT had greater modal pore diameter than RT while MTA had higher saturated hydraulic conductivity. Between the crop residues and chicken manure, the latter enhanced the infiltration since the crop residues were shown to have higher sorptive capacities than soil (**Wu et al, 1995**). However, treatments with tilled and mixed soil with any type of organics prove to drain water better tilling the soil alone.



(Figure 36 to be continued on next page)



(Figure 36 to be continued on next page)



(Figure 36 to be continued on next page)

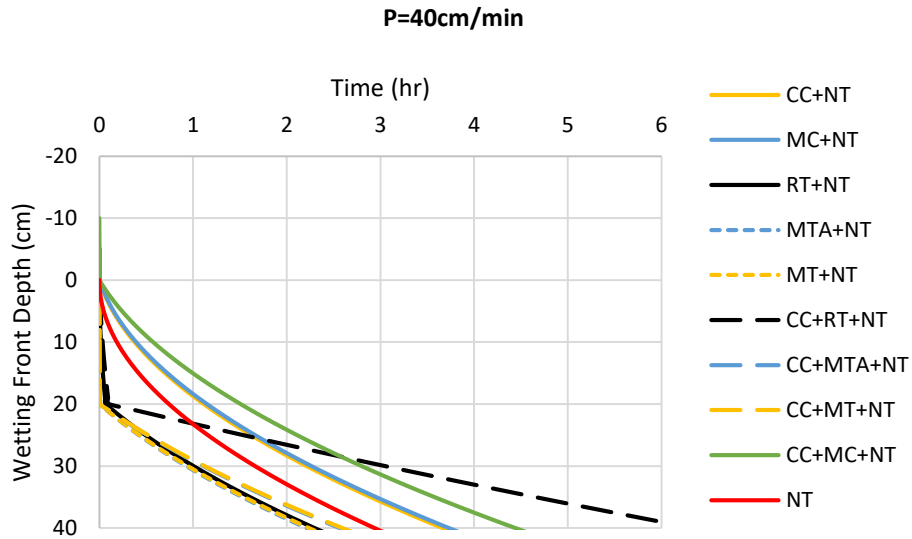


Figure 36: GARALS simulation for different soil profiles exhibiting different combinations of soil management systems under different irrigation rates (0.01, 0.05, 0.1, 0.5, 1, 2, 5, 10, 20, 40cm/min)

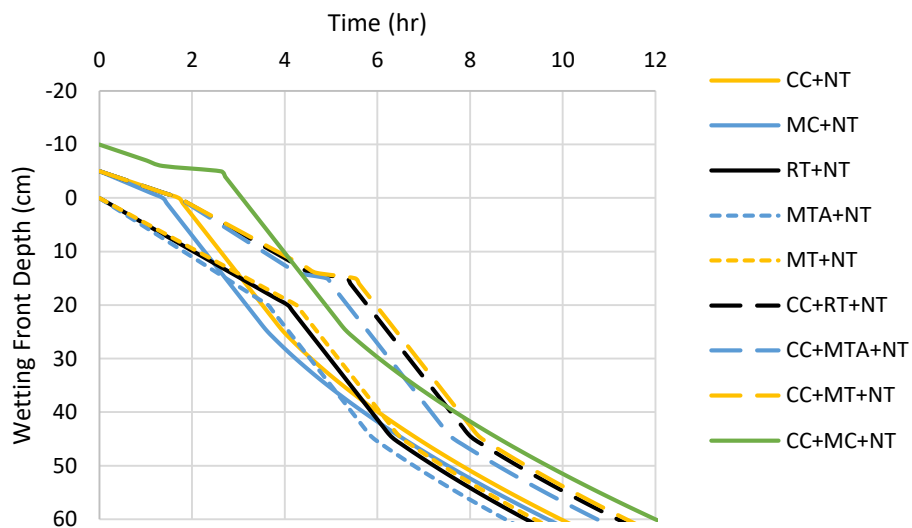


Figure 37: GARALS simulation for different soil profiles exhibiting different combinations of soil management systems under Site 1 field irrigation rate (0.04cm/min)

4.4 Soil Management System Optimization in Site 1

The simulation of GARALS of the different soil management systems under the irrigation rate using field real data is presented in Figure 37. Saturated wetting fronts

are reached faster by different treatments depending on the depths, meaning that MTA+NT is faster for depths smaller than 15cm and greater than 40cm while MC+NT is quicker for depths between 15 and 40cm. The first elimination level of treatments include those having wetting fronts smaller than 40cm prior to ponding ($z_p \leq 40\text{cm}$) which includes: CC+NT ($z_p = 29.6\text{cm}-5\text{cm}$ cover), MC+NT ($z_p = 29.6\text{cm}-5\text{cm}$ cover), NT, CC+MC+NT ($z_p = 34.6\text{cm}-10\text{cm}$ cover). Hence, the rest of the layers are evaluated for the shortest times of arrival to 10, 20, 30, 40cm and to ponding depth which are reported in Table 15. Consequently, MTA+NT is chosen for its higher speed to infiltrate water while using smaller amount of water. After applying the treatment in field, Figure 38 illustrates the change in moisture content at depth beyond 20cm between the plots (1a, 1b, 2a, 2b, 3a, 3b) during and after the irrigation event. Referring to Figure 38, the time needed for moisture to reach the moisture sensor, meaning when the moisture increases rapidly from initial state to more than $0.4 \text{ m}^3/\text{m}^3$ is approximately between 370 and 390 minutes in plots 1a and 1a, between 380 and 390 minutes in plots 2a and 2b, while ranges from 190 and 195 minutes in plots 3a and 3b.

Table 15: Cumulative infiltration (Z_p) prior to ponding and time of arrivals of wetting fronts to 10, 20, 30, 40cm and z_p measured from the initial surface soil for treatments having wetting front depths larger than 40cm prior to ponding in Site 1 using the field irrigation rate (0.04cm/min)

Soil Management System	z_p (cm)	Z_p (cm)	Time to reach (hrs)				
			10cm	20cm	30cm	40cm	44.6cm
RT+NT	44.6	16.25	2.03	4.06	4.97	5.87	6.29
MTA+NT	44.6	15.15	1.82	3.64	4.54	5.45	5.86
MT+NT	44.6	16.73	2.12	4.25	5.15	6.06	6.47
CC+RT+NT	49.6 (-5cm cover)	20.67	3.74	5.78	6.68	7.58	8.00
CC+MTA+NT	49.6 (-5cm cover)	19.57	3.53	5.35	6.25	7.16	7.57
CC+MT+NT	49.6 (-5cm cover)	21.15	3.83	5.96	6.86	7.77	8.18

Notwithstanding, **Salem et al. (2014)** investigated the effects of reservoir tillage on soil physical properties in loam soils. Such method consists of chisel ploughing the land to a depth of 20cm and later create mini-depression or holes using a hand-pushed tool with a truncated square pyramid shape similar to the herein design. The method induced positive physical properties' alteration that lead to high crop yields. However, the method was not assessed for its capacity to drain water.

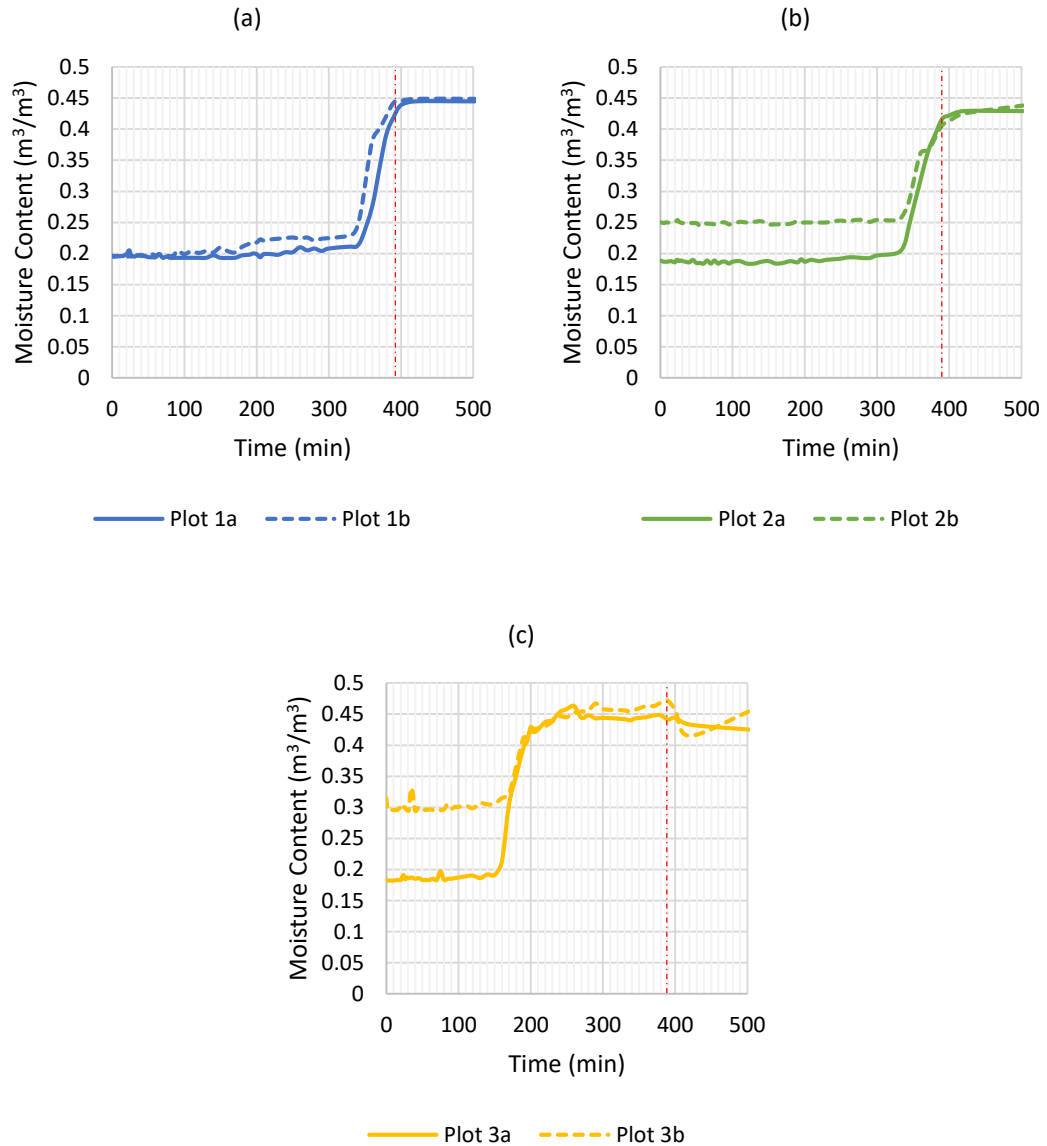


Figure 38: Moisture content variation at depth between 20 and 40cm for MTA+NT soil management system (a) MTA+NT replicated in plots 1a and 1b, (b) MTA+NT with empty AM replicated in plots 2a and 2b, (c) MTA+NT with filled AM + crop residues replicated in plots 3a and 3b (the dashed red line is the boundary that indicates the end of the irrigation event)

Hence, a one-way ANOVA reveals that the addition of crop residues in the artificial macropore is significant in increasing the infiltration while the insertion of empty artificial macropores didn't affect the infiltration process according to Tukey's test of pairwise comparisons (in addition, plots 1 and 2 have overlapped 95%CI: plot 1 [360.25;400.75] and plot 2 [364.75;405.25]). Consequently, the addition of crop residue in the AM decreased the time to reach 20cm by 49.4% and 50% from plots 1

and 2, respectively. As this stands, the crop residues were shown to be good sorted with large pore contents and well-connected pores. So the water could easily infiltrate within irregular preferential flow, thereby moving water into deeper depths in the vertical direction. The preferential flow is likely to occur in this case since the irrigation rate was smaller than the saturated hydraulic conductivity of the crop residues ($0.04 < 1.91 \text{ cm/min}$). Thus, preferential flow in the form of “fingered flow” can ensue in this artificial macropore of coarse-grained pores (Liu et al., 1994). However, water falling into the empty macropore might reaches the side walls of the AM and immediately getting absorbed due to difference in moisture contents, in other words, the water particles will flow along the walls of the artificial macropores with a “slip” boundary condition (Barrat & Bocquet, 1999; Li et al., 2018). Thus, the water will move horizontally from the walls of the macropores while not being able to percolate vertically. This is why the empty macropores plot was similar in infiltrating water to that lacking the AM.

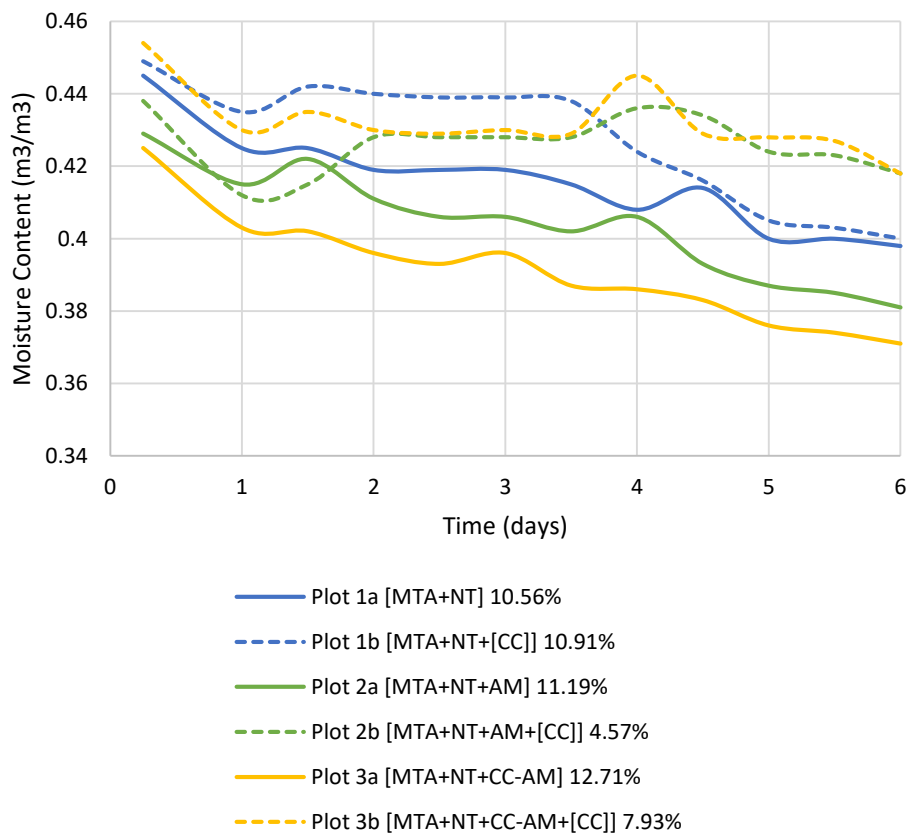


Figure 39: Moisture content variation at depth between 20 and 40cm for MTA+NT soil management system after the end of irrigation experiment

Furthermore, the monitoring of the moisture content in the upcoming days post the irrigation event is illustrated in Figure 39. Accordingly, after four days, the moisture content in the uncovered plots (1a, 2a, 3a) is the lowest where AM are inserted and then filled with crop residues (3a) (removal of 12.71%) following the plot where the AM is left empty (2a) (removal of 11.19%) following the plot with no AM (1a) (removal of 10.56). Therefore, the uncovered plots do not maintain subsurface moisture in the presence of AM since the macropores can absorb heat from the sun while transporting it to deeper depth and thereby increasing the evaporation rate. In addition, it is noticeable that the injection of crop residues in the AM was able to capture the moisture from deeper depths since the crop residues are highly adsorptive to water. This is reflected in the highest moisture content removal of 12.71%. That's why lower moisture contents were observed in plot 3a.

On the other hand, when plots are covered with crop residues post-irrigation test, moisture was better maintained than the uncovered plots in the presence of AM. In opposition to uncovered plots, those with AM (2b and 3b) maintained moisture better than 1b justified by the low removal of moisture (4.57% in plot 2b and 7.93% in plot 3b). Consequently, the cover layer functioned properly in securing the moisture in the subsurface while inhibiting heat exchange at the air-soil interface. The crop residues are illustrious of their high solar reflectivity and low thermal conductivity which prevent an increase of temperature in the subsurface (**Fabrizzi et al., 2005; Schinners et al., 1994**) by limiting the penetration of solar radiation (**Salem et al., 2014**). Nonetheless, since plot 3b had the highest initial moisture content after the irrigation stopped, it should maintain moisture better than plot 2b. Thus, the crop residues filled in the AM could have absorbed some moisture since the crops are initially dry when inserted. Another solution is to place wetted crop residues instead of thirsty dry crops. This issue was also seen when comparing plots 1a and 1b. 1b had a higher removal rate albeit it was covered and protected from evaporation. So any additional removal was due to the adsorption effect of crops.

Chapter Five

Conclusion

Inferences about the soil management systems can be summed up between advantages and malfunctions: the undisturbed soil endures a poorly sorted system with very fine pores while tilled layers carry coarser and better-sorted pores. The addition of organic matter results in a soil body that is intermediate between NT and RT having a wider range of fine and coarse pores. However, their effects change with the soil type. In addition, the different soil management systems present alterations to the soil physical, structural, and pore system which results in different trends for water infiltration and storage capacities. Therefore, the more the properties are identified, the better the judgement is to choose an appropriate system. For instance, the soil physical quality indicated that the undisturbed soil in loamy soil is better than the tilled layers, even those having organic matter. However, the infiltration of water stands to be effective in these layers. So the judgement is inferred based on the purpose of using the corresponding soil management system. It is also recommended for future investigators to assess different combination of soil management systems with the implication of having different application rates of organic matter since the latter was shown to enhance the quality of the soil. It is also remarkable that the inferences that we had on tillage practices were not all similar in both sites. Meaning, it would be a gaffe to generalize the effects of soil management systems on soil. Therefore, for farmers to achieve better results of crop residues, site-specific assessment is encouraged. On the other hand, using mathematical-coded simulations can be efficient in terms of time and resources consumption. However, it is not applicable in all cases where the real-system is complex. For instance, modelling the infiltration in the heterogeneous system of MTA+NT chosen for optimization while coupled with artificial macropore is not simple to elaborate mathematically, hence numerical simulations for dual-domain permeability systems can be used instead.

Bibliography

- Acton, D.F. & Padbury, G.A. (1993). A conceptual framework for soil quality assessment and monitoring. In: O.F. Acton (Editor), A Program to Assess and Monitor Soil Quality in Canada: Soil Quality Evaluation Program Summary (interim). Centre for Land and Biological Resources Research, No. 93-49, Agriculture Canada, Ottawa.
- Adeyemo, A.J., Akingbola, O.O., & Ojeniyi, S.O. (2019). Effects of poultry manure on soil infiltration, organic matter contents and maize performance on two contrasting degraded alfisols in southwestern Nigeria. *Int. J. Recycl.*, 8 (Suppl 1), S73–S80. <https://doi.org/10.1007/s40093-019-0273-7>
- Afzalnia, S. & Zabihi, J. (2014). Soil compaction variation during corn growing season under conservation tillage. *Soil Tillage Res.*, 137, 1–6.
- Ahamefule, H.E. & Mbagwu, J.S. (2007). Effects of phosphorus and four tillage mulch systems on the physico-chemical properties of an ultisol in Eastern Nigeria. *Agro-Sci.*, 6(1). doi:10.4314/as.v6i1.1553
- Ahuja, L.R., Rojas, K.W., Hanson, J.D., Shaffer, M.J., & Ma, L. editors. (2000). The Root Zone Water Quality Model. *Water Resour. Publ.*, Highlands Ranch, CO.
- Akhtar, M.S., Stüben, D., Norra, S., & Memon, M. (2011). Soil structure and flow rate-controlled molybdate, arsenate and chromium(III) transport through field columns. *Geoderma*, 161, 126–137.
- Al-Darby, A.M. & Lowery, B. (1987). Seed zone soil temperature and early corn growth with three conservation tillage systems. *Soil Sci. Soc. Am. J.*, 51, 768–774.
- Alam, K.M., Islam, M.M., Salahin, N., & Hasanuzzaman, M. (2014). Effect of Tillage Practices on Soil Properties and Crop Productivity in Wheat-Mungbean-Rice Cropping System under Subtropical Climatic Conditions. *Sci. World J.* ID 437283, 15 pp. <http://dx.doi.org/10.1155/2014/437283>
- Alastal, K. & Ababou, R. (2019). Moving Multi-Front (MMF): A generalized Green-Ampt approach for vertical unsaturated flows. *J. Hydrol.*, 579, 124184. <https://doi.org/10.1016/j.jhydrol.2019.124184>.
- Allaire, S.E., Roulier, S., & Cessna, A.J. (2009). Quantifying preferential flow in soils: A review of different techniques. *J. hydrol.*, 378, 179-204. doi:10.1016/j.jhydrol.2009.08.013
- Alletto, L. & Coquet, Y. (2009). Temporal and spatial variability of soil bulk density and near-saturated hydraulic conductivity under two contrasted tillage management systems. *Geoderma*, 152, 85–94. doi:10.1016/j.geoderma.2009.05.023

- Allmaras, R.R., Burrows, W.C. & Larson, W.E. (1964). Early growth of corn as affected by soil temperature. *Soil Sci. Soc. Am. Proc.*, 28, 271–275.
- Alvarez R., Alvarez, CR., & Lorenzo, G. (2001). Carbon dioxide fluxes following tillage from a mollisol in the Argentine Rolling Pampa. *Eur. J. Soil Biol.*, 37, 161–166.
- Alvarez, R., & Steinbach, H.S. (2009). A review of the effects of tillage systems on some soil physical properties, water content, nitrate availability and crops yield in the Argentine Pampas. *Soil Till. Res.*, 104 (1), 1–15. doi: 10.1016/j.still.2009.02.005
- Alvaro-Fuentes, J., López, M.V., Cantero-Martinez, C., & Arrúe, J.L. (2008). Tillage Effects on Soil Organic Carbon Fractions in Mediterranean Dryland Agroecosystems. *Soil Sci. Soc. Am. J.*, 72 (2), 541. doi:10.2136/sssaj2007.0164
- Amer, A.M. (2012). Water flow and conductivity into capillary and non-capillary pores of soils. *J. Soil Sci. Plant Nutr.*, 12 (1), 99-112.
- Amézketa, E. (1999). Soil aggregate stability: a review. *J. Sustain. Agric.*, 14, 83–151.
- Anderson, D.T. & Russell, G.C. (1964). Effects of various quantities of straw mulch on the growth and yield of spring and winter wheat. *Can. J. Soil Sci.*, 44, 109–118.
- Andreini, M. S. & Steenhuis, T. S. (1990). Preferential paths of flow under conventional and conservation tillage. *Geoderma*, 46, 85–102. doi: 10.1016/0016-7061(90)90009-x
- Angers, D.A. & Caron, J. (1998). Plant-induced changes in soil structure: Processes and feedbacks. *Biogeochemistry*, 42, 55–72. doi:10.1023/A:1005944025343
- Angulo-Jaramillo, R., Moreno, F., Clothier, B.E., Thony, J.L., Vachaud, G., Fernandez-Boy, E., & Cayuela, J.A. (1997). Seasonal variation of hydraulic properties of soils measured using a tension disk infiltrometer. *Soil Sci. Soc. Am. J.*, 61, 27-32.
- Annaka, T. & Hanayama, S. (2005). Dynamic water-entry pressure for initially dry glass beads and sea sand. *Vadose Zone J.*, 4, 127–133.
- Arya, L.M. & Paris, J.F. (1981). A physicoempirical model to predict the soil moisture characteristics from particle-size distribution and bulk density data. *Soil Sci. Soc. Am. J.*, 45, 1023-1030.
- Azevedo, A.S., Kanwar, R.S., & Horton, R. (1998). Effect of cultivation on hydraulic properties of an Iowa soil using tension infiltrometers. *Soil Sci.*, 163, 22–29.
- Badorreck, A., Gerke, H. H., & Vontobel, P. (2010). Noninvasive observations of flow patterns in locally heterogeneous mine soils using neutron radiation. *Vadose Zone J.*, 9, 362–372. doi: 10.2136/vzj2009.0100
- Ball-Coelho, B.R., Roy, R.C., & Swanton, C.J. (1998). Tillage alters corn root distribution in coarse-textured soil. *Soil Till. Res.*, 45, 249–273.

- Bamberg, A.L., Cornelis, W.M., Timm, L.C., Gabriels, D., Pauletto, E.A. & Pinto, L.F.S. (2011). Temporal changes of soil physical and hydraulic properties in strawberry fields. *Soil Use Manag.*, 27, 385–394.
- Barrat, J. & Bocquet, L. (1999). Large slip effect at a nonwetting fluid-solid interface. *Phys. Rev. Lett.*, 82, 4671–4674.
- Bartholomew, W.V. & Norman, A.G. (1946). The threshold moisture content for active decomposition of some mature plant materials. *Soil Sci. Soc. Amer. Proc.*, 11, 270–279.
- Baumhardt, R.L., Keeling, J.W., & Wendt, C.W. (1993). Tillage and residue effects on infiltration into soils cropped to cotton. *Agron. J.*, 85, 379–383.
- Baumhardt, R.L., Johnson, G.L., & Schwartz, R.C. (2011). Residue and Long-Term Tillage and Crop Rotation Effects on Simulated Rain Infiltration and Sediment Transport. *Soil Sci. Soc. Am. J.*, 76:1370–1378. doi:10.2136/sssaj2011.0331
- Baumhardt, R.L., Unger, P.W., & Dao, T.H. (2004). Soil and crop management — seedbed surface geometry effects on soil crusting and seedling emergence. *Agron. J.*, 96, 1112–1117.
- Bechara, E., Papafilippaki, A., Doupis, G., Sofu, A., & Koubouris, G. (2018). Nutrient dynamics, soil properties and microbiological aspects in an irrigated olive orchard managed with five different management systems involving soil tillage, cover crops and compost. *J. Water Climate Change*, 9(4), 736-747. <https://doi.org/10.2166/wcc.2018.082>
- Beven, K. (1984). Infiltration into a class of vertically non-uniform soils. *Hydrol. Sci. J.*, 29(4), 425-434. DOI: 10.1080/02626668409490960
- Beven, K. & Germann, P. (1981). Water Flow in Soil Macropores II. A Combined Flow Model. *J. Soil Sci.*, 32, 15-29.
- Beven, K.J. & Germann, P. (1982). Macropores and water flow in soils. *Water Resour. Res.*, 18, 1311–1325.
- Bharati, L., Lee, K.H., Isenhardt, T.M., & Schultz, R.C. (2002). Soil water infiltration under crops, pasture, and established riparian buffer in Midwestern USA. *Agrofor. Syst.* 56, 249–257.
- Blake, G. & Hartge, K. (1986). Bulk Density, in *Methods of Soil Analysis*, Klute, A., Editor (pp. 363-375).
- Blanco-Canqui, H., Gantzer, C.J., Anderson, S.H., & Alberts, E.E. (2004). Tillage and Crop Influences on Physical Properties for an Epiaqualf. *Soil Sci. Soc. Am. J.*, 68 (2), 567-576. <https://doi.org/10.2136/sssaj2004.5670>
- Blanco-Canqui, H., Wienhold, B.J., Jin, V.L., Schmer, M.R., & Kibet, L.C. (2017). Long-term tillage impact on soil hydraulic properties. *Soil & Till. Res.*, 170, 38-42. <http://dx.doi.org/10.1016/j.still.2017.03.001>

- Blevin, R.L., Smith, M.S., Thomas, G.W., & Frye, W.W. (1983). Influence of conservation tillage on soil properties. *J. Soil Water Conserv.*, 38, 301–305.
- Blevins, R.L. & Frye, W.W. (1993). Conservation tillage: an ecological approach to soil management. *Adv. Agron.*, 51, 33–78.
- Blott, S.J. & Pye, K. (2001) Gradistat: A Grain Size Distribution and Statistics Package for the Analysis of Unconsolidated Sediments. *Earth Surf. Process. Landf.*, 26, 1237-1248. <http://dx.doi.org/10.1002/esp.26>
- Bogunovic, I., Pereira, P., Kistic, I., Sajko, K., & Sraka, M. (2018). Tillage management impacts on soil compaction, erosion, and crop yield in Stagnosols (Croatia). *Catena*, 160, 376–384. <https://doi.org/10.1016/j.catena.2017.10.009>
- Bogunovic, I., Telak, L.J., Pereira, P., Filipovic, V., Filipovic, L., Percin, A., Durdevic, B., Birkás, M., Dekemati, I., & Rodrigo-Comino, J. (2020). Land management impacts on soil properties and initial soil erosion processes in olives and vegetable crops. *J. Hydrol. Hydromech.*, 68(4), 328–337. DOI: 10.2478/johh-2020-0033
- Bolan, N., Adriano, D., & Mahimairaja, S. (2004). Distribution and Bioavailability of Trace Elements in Livestock and Poultry Manure By-Products. *Crit. Rev. Environ. Sci. Technol.*, 34(3), 291–338. doi:10.1080/10643380490434128
- Bormann, H. & Klaassen, K. (2008). Seasonal and land use dependent variability of soil hydraulic and soil hydrological properties of two Northern German soils. *Geoderma*, 145, 295–302.
- Bossuyt, H., Six, J., & Hendrix, P.F. (2002). Aggregate-protected carbon in no-tillage and conventional tillage agroecosystems using carbon- 14 labeled plant residue. *Soil Sci. Soc. Am. J.*, 66, 1965–1973.
- Bouma, J., Jongerius, A., Boersma, O., Jager, A., & Schoonderbeek, D. (1977). The function of different types of macropores during saturated flow through four swelling soil horizons. *Soil Sci. Soc. Am. J.* 41, 945-950.
- Bouwer, H. (1966). Rapid field measurement of air-entry value and hydraulic conductivity of soil as significant parameters in flow system analysis. *Water Resour. Res.*, 2, 729–738.
- Bouwer, H. (1969). Infiltration of water into nonuniform soil. *J. Irr. Drainage Division*, 95 (IR4), 451–462.
- Boyd, S.A., Xiangcan, J., & Lee, J.F. (1990). Sorption of nonionic organic compounds by corn residues from a no-tillage field. *J. Environ. Qual.*, 19, 734–738.
- Brewer, R. (1964). *Fabric and Mineral Analysis of Soils*, John Wiley, New York.
- Bronick, C.J. & Lal, R. (2005). Soil structure and management: a review. *Geoderma*, 124, 3–22.

- Buschiazzo, D.E., Panigatti, J.L, & Unger, P.W. (1998). Tillage effects on soil properties and crop production in the subhumid and semiarid Argentinean Pampas. *Soil Till. Res.*, 49, 105-116. P I I : S0167- 1 9 8 7 (9 8) 0 0 1 6 0- 3
- Cao,V., Schaffer, M., Taherdangkoo, R., & Licha, T. (2020). Solute Reactive Tracers for Hydrogeological Applications: A Short Review and Future Prospects. *Water*, 12, 653. doi:10.3390/w12030653
- Capowiez, Y., Cadoux, S., Bouchant, P., Ruy, S., Roger-Estrade, J., Richard, G., & Boizard, H. (2009). The effect of tillage type and cropping system on earthworm communities, macroporosity and water infiltration. *Soil Till. Res.*, 105 (2), 209–216. doi:10.1016/j.still.2009.09.002
- Caron, J., Pepin, S., & Póriard, Y. (2010). Physics of growing media in a green future. *Acta Hortic*, 1034, 309–318
- Caron, J., Heinse, R., & Charpentier, S. (2015a). Organic materials used in agriculture, horticulture, reconstructed soils, and filtering applications. *V. Z. J.*, 14 (6)
- Caron, J., Price, J., & Rochefort, L. (2015b). Physical properties of organic soil: adapting mineral soil concepts to horticultural growing media and histosol characterization. *V. Z. J.*, 14 (6).
- Castellini, M., Fornaro, F., Garofalo, P., Giglio, L., Rinaldi, M., Ventrella, D., Vitti., C., & Vonella, A. (2019). Effects of No-Tillage and Conventional Tillage on Physical and Hydraulic Properties of Fine Textured Soils under Winter Wheat. *Water*, 11 (3), 484. doi:10.3390/w11030484
- Castellini, M., Pirastru, M., Niedda, M., & Ventrella, D. (2013). Comparing physical quality of tilled and no-tilled soils in an almond orchard in southern Italy. *Ital. J. Agron.*, 8:e20. doi:10.4081/ija.2013.e20
- Castellini, M. & Ventrella, D. (2012). Impact of conventional and minimum tillage on soil hydraulic conductivity in typical cropping system in Southern Italy. *Soil Till. Res.*, 124, 47-56. <http://dx.doi.org/10.1016/j.still.2012.04.008>
- Castiglione, P., Mohanty, B. P., Shouse, P. J., Šimůnek, J., van Genuchten, M. Th., & Santini, A. (2003). Lateral water diffusion in an artificial macroporous system. *V. Z. J.*, 2, 212– 221. <http://doi.org/10.2136/vzj2003.2120>
- Caviedes-Voullième, D., A-Navarro, P. G., & Murillo, J. (2013). Verification, conservation, stability, and efficiency of a finite volume method for the 1D Richards equation. *J. Hydrol.*, 480, 69–84. <https://doi.org/10.1016/j.jhydrol.2012.12.008>
- Chen, S., Mao, X., & Wang, C. (2019). A Modified Green-Ampt Model and Parameter Determination for Water Infiltration in Fine-textured Soil with Coarse Interlayer. *Water*, 11, 787. doi:10.3390/w11040787.
- Cheng, J., Zhang, H., Wang, W., Zhang, Y., & Chen, Y. (2011). Changes in Preferential Flow Path Distribution and Its Affecting Factors in Southwest China. *Soil Sci.*,176, 652Y660. DOI: 10.1097/SS.0b013e31823554ef

- Chenu, C., Le Bissonais, Y., & Arrouays, D. (2000). Organic matter influence on clay wettability and soil aggregate stability. *Soil Sci. Soc. Am. J.*, 64, 1479–1486.
- Chu, S.T. (1985). Modeling infiltration into tilled soil using non-uniform rain. *Trans. ASAE*, 28:1226–1232.
- Chu, X. & Marino, M. (2005). Determination of ponding condition and infiltration into layered soils under unsteady rainfall. *J. Hydrol.*, 313, (3–4), 195–207. <https://doi.org/10.1016/j.jhydrol.2005.03.002>.
- Ciollaro, G. & Lamaddalena, N. (1998). Effect of Tillage on the Hydraulic Properties of a Vertic Soil. *J. Agric. Eng. Res.*, 71, 147–155.
- Clark, A.J., Decker, A.M., Meisinger, J.J., & McIntosh, M.S. (1997). Kill date of vetch, rye, and vetch–rye mixture: I. Cover crop and corn nitrogen. *Agron. J.*, 89:427–434.
- Colombi, T., Braun, S., Keller, T., & Walter, A. (2016). Artificial macropores attract crop roots and enhance plant productivity on compacted soils. *Sci. Total Environ.*, 574, 1283–1293. <https://doi.org/10.1016/j.scitotenv.2016.07.194>
- Coppola, A., Comegna, V., Basile, A., Lamaddalena, N., & Severino, G. (2009a). Darcian preferential water flow and solute transport through bimodal porous systems: Experiments and modelling. *J. Contam. Hydrol.*, 104, 74–83. doi:10.1016/j.jconhyd.2008.10.004
- Coppola, A., Kutílek, M., & Frind, E.O. (2009b). Transport in preferential flow domains of the soil porous system: Measurement, interpretation, modelling, and upscaling. *J. Contam. Hydrol.*, 104:1–3. doi:10.1016/j.jconhyd.2008.05.011
- Cook, H.F., Valdes, G.S.B., & Lee, H.C. (2006). Mulch effects on rainfall interception, soil physical characteristics and temperature under *Zea mays* L. *Soil Till. Res.*, 91, 227e235.
- Coutadeur, C., Coquet, Y., & Roger-Estrade, J. (2002). Variation of hydraulic conductivity in a tilled soil. *Eur. J. Soil Sci.*, 53, 619–628.
- Cox, W.J., Zobel, R.W., van Es, H.M., & Otis, D.J. (1990). Tillage effects on some soil physical and corn physiological characteristics. *Agron. J.*, 82, 806–812.
- Cruse, R.M., Mier, R., & Mize, C.W. (2011). Surface residue effects on erosion of thawing soils. *Soil Sci. Soc. Am. J.*, 65, 178e184.
- Cullotta, S., Bagarello, V., Baiamonte, G., Gugliuzza, G., Iovino, M., La Mela Veca, D. S., Maetzke, F., Palmeri, V., & Sferlazza, S. (2016). Comparing Different Methods to Determine Soil Physical Quality in a Mediterranean Forest and Pasture Land. *Soil Sci. Soc. Am. J.*, 80 (4), 1038. doi:10.2136/sssaj2015.12.0447
- Cunha, J.L.X.L., Coelho, M.E.H., Albuquerque, A.W., Silva, C.A., Silva-J, A.B., & Carvalho, I.D.E. (2015). Water infiltration rate in Yellow Latosol under different soil management systems. *R. Bras. Eng. Agríc. Ambiental.*, 19(11), 1021–1027.

- Dahab, M.H. (2011). Effect of Selected Tillage Implements on Physical Properties of Two Types of Soils in Khartoum Area. *AMA*, 42(2).
- Damodhara Rao, M., Raghuwanshi, N. S., & Singh, R. (2006). Development of a physically based 1D-infiltration model for irrigated soils. *Agric. Water Manage.*, 85(1-2), 165–174.
- Darcy, H. (1856). *Détermination des lois d'écoulement de l'eau à travers le sable*. Les Fontaines Publiques de la Ville de Dijon: Victor Dalmont, Paris.
- Das, B.M. & Sobhan, K. (2014). *Principles of geotechnical engineering*. 8th edition, Cengage Learning: Stamford, USA.
- Datiri, B.C. & Lowery, B. (1991). Effects of conservation tillage on hydraulic properties of a Griswold silt loam soil. *Soil Till. Res.*, 21, 257–271
- de Jonge, L.W., Moldrup, P. & Schjønning, P. (2009). Soil infrastructure, interfaces & translocation processes in inner space (“Soil-it-is”): towards a road map for the constraints and crossroads of soil architecture and biophysical processes. *Hydrol. Earth System Sci.*, 13, 1485–1502.
- de Rooij, G.H. (2000). Modeling fingered flow of water in soils owing to wetting front instability: a review. *Journal of Hydrology*, 231, 277–294.
- Deen, W. & Katakai, P.K. (2003). Carbon Sequestration in a Long-Term Conventional Versus Conservation Tillage Experiment. *Soil Till. Res.*, 74(2), 143-150.
- Dexter, A.R. (2004a). Soil physical quality: Part I. Theory, effects of soil texture, density, and organic matter, and effects on root growth. *Geoderma*, 120, 201–214.
- Dexter, A.R. (2004b). Soil physical quality: Part II. Friability, tillage, tillage and hard-setting. *Geoderma*, 120, 215–225.
- Dexter, A.R. & Czyz, E.A. (2007). Applications of S-theory in the study of soil physical degradation and its consequences. *Land Degrad. & Dev.*, 18, 369–381.
- Dick, W.A. (1983). Organic carbon, nitrogen and phosphorus concentrations and pH in soil profiles as affected by tillage intensity. *Soil Sci. Soc. Am. J.*, 47, 102-107
- D’Haene, K., Vermang, J., Cornelis, W.M., Leroy, B.L.M., Schiettecatte, W., De Neve, S., Gabriels, D., & Hofman, G. (2008). Reduced tillage effects on physical properties of silt loam soils growing root crops. *Soil Till. Res.*, 99, 279–290.
- Doube, M., Kłosowski, M.M., Arganda-Carreras, I., Cordelières, F.P., Dougherty, R.P., Jackson, J.S., Schmid, B., Hutchinson, J.R., & Shefelbine, S.J. (2010). BoneJ: Free and extensible bone image analysis in ImageJ. *Bone*, 47, 1076-1079. doi:10.1016/j.bone.2010.08.023
- Drury, C.F., Tan, C., Welacky, T.W., Olaya, T.O., Hamill, A.S., & Weaver, S.E. (1999). Red clover and tillage influence on soil temperature, water content, and corn emergence. *Agron. J.*, 91, 101–108.

- Eden, M., Schjønning, P., Moldrup, P., & de Jonge, L.W. (2011). Compaction and rotovation effects on soil pore characteristics of a loamy sand soil with contrasting organic matter content. *Soil Use Manag.*, 27, 340–349, doi: 10.1111/j.1475-2743.2011.00344.x
- Edwards, W.M., Norton, L.D., & Redmond, C.E. (1988). Characterizing macropores that affect infiltration into non-tilled soil. *Soil Sci. Soc. Am. J.*, 52, 483–437.
- Elliott, E.T. (1986). Aggregate structure and carbon, nitrogen, and phosphorus in native and cultivated soils. *Soil Sci. Soc. Am. J.*, 50, 627–633. <http://dx.doi.org/10.2136/sssaj1986.03615995005000030017x>.
- Eisenhauer, D.E. (1984). Surface sealing and infiltration with surface irrigation. PhD dissertation, Colorado State University, Ft. Collins, CO.
- Emerson, W.W., Bond, R.D., & Dexter, A.R. (1978). Modification of soil structure. New York : Wiley.
- Ess, D.R., Vaughan, D.H., & Perumpral, J.V. (1998). Crop residue and root effects on soil compaction. *Trans. ASAE*, 41,1271–1275.
- Fabrizzi, K.P., Garcia, F.O., Costa, J.L., & Picone, L.I. (2005). Soil water dynamics, physical properties and corn and wheat responses to minimum and no-tillage systems in the southern Pampas of Argentina. *Soil Till. Res.*, 81, 57-69. doi:10.1016/j.still.2004.05.001
- Fan, R., Zhang, X., Yang, X., Liang, A., Jia, S., & Chen, X. (2013). Effects of tillage management on infiltration and preferential flow in a black soil, Northeast China. *Chin. Geogr. Sci.*, 23 (3), 312–320. doi:10.1007/s11769-013-0606-9
- Ferreras, L.A., Costa, J.L., Garcia, F.O., & Pecorari., C. (2000). Effect of no-tillage on some soil physical properties of a structural degraded Petrocalcic Paleudoll of the southern "Pampa" of Argentina. *Soil Till. Res.*, 54, 31-39. PII: S0 1 6 7 - 1 9 87 (9 9) 0 0 1 0 2 – 6
- Filipović, V., Defterdarović, J., Šimůnek, J., Filipović, L., Ondrašek, G., Romić, D., Bogunović, I., Mustać, I., Čurić, J., & Kodešová, R. (2020). Estimation of vineyard soil structure and preferential flow using dye tracer, X-ray tomography, and numerical simulations. *Geoderma*, 380, 114699. doi:10.1016/j.geoderma.2020.114699
- Findeling, A., Ruy, S., & Scopel, E. (2003). Modeling the effects of a partial residue mulch on runoff using a physically based approach. *J. Hydrol.*, 275, 49–66.
- Finnemore, E.J. & Franzini, J.B. (2002). *Fluid Mechanics with Engineering Applications* (10th Edition). McGraw-Hill Education.
- Fitzmaurice, J.L. (1997). The effect of tillage practices and soil compaction on the physical properties and productivity of a clay soil. The University of Manitoba, Winnipeg Manitoba. ProQuest Dissertations Publishing. MM16130.

- Flury, M. & Fluhler, H. (1994). Brilliant Blue FCF as a Dye Tracer for Solute Transport Studies-A Toxicological Overview. *J. Environ. Qual.*, 23, 1108-1112.
- Flury, M. & Fluhler, H. (1995). Tracer Characteristics of Brilliant Blue FCF. *Soil Sci. Soc. Am. J.*, 59, 22-27.
- Flury, M. & Wai, N.N. (2003). Dyes as tracers for vadose zone hydrology. *Rev. Geophysics*, 41, 1-24.
- Fok, Y.-S. (1970). One-dimensional infiltration into layered soils. *J. Irrig. Drain. Div.*, 96 (2), 121-129.
- Foster, G.R., & Meyer, L.D. (1975). Mathematical simulation of upland erosion by fundament erosion mechanics. In Present and prospective technology for predicting sediment yields and sources, 190-204. U.S. Dep. Agric. ARS-S-40.
- Francis, G.S. & Knight, T.L. (1993). Long-term effects of conventional and no-tillage on selected soil properties and crop yields in Canterbury, New Zealand. *Soil Till. Res.*, 26, 193-210.
- Frye, W.W., Blevins, R.L., Smith, M.S., Corak, S.J., & Varco, J.J. (1988). *Role of annual legume cover crops in efficient use of water and nitrogen*. p. 129-154. In W.L. Hargrove (ed.) *Cropping strategies for the efficient use of water and nitrogen*. ASA, CSSA, and SSSA, Madison, WI.
- Gantzer, C.J. & Blake, G.R. (1978). Physical characteristics of Le Sueur clay loam soils following no-till and conventional tillage. *Agron. J.* 70, 853-857. <https://doi.org/10.2134/agronj1978.00021962007000050035x>
- Gao, L., Wang, B., Li, S., Wu, H., Wu, X., Liang, G., Gong, D., Zhang, X., Cai, D., & Degre, A. (2019). Soil wet aggregate distribution and pore size distribution under different tillage systems after 16 years in the Loess Plateau of China. *Catena*, 173, 38-47. <https://doi.org/10.1016/j.catena.2018.09.043>
- Gao, W., Whalley, W.R., Tian, Z., Liu, J., & Ren, T. (2016). A simple model to predict soil penetrometer resistance as a function of density, drying and depth in the field. *Soil Tillage Res.*, 155, 190-198. <http://dx.doi.org/10.1016/j.still.2015.08.004>.
- García-Orenes, F., Cerda, A., Mataix-Solera, J., Guerrero, C., Bodí, M.B., Arcenegui, V., Zornoza, R., & Sempere, J.G. (2009). Effects of agricultural management on surface soil properties and soil water losses in eastern Spain. *Soil Till. Res.*, 106, 117e123.
- Geiger, S. & Durnford, D. (2000). Infiltration in homogeneous sands and a mechanistic model of unstable flow. *Soil Sci. Soc. Am. J.*, 64 (2), 460-469.
- Gerke, H.H., & van Genuchten, M.T. (1993). A dual-porosity model for simulating the preferential movement of water and solutes in structured porous-media. *Water Resour. Res.*, 29 (2), 305-319.

- Gerke, H.H. (2006). Preferential-flow descriptions for structured soils. *J. Plant Nutr. Soil Sci.*, 169, 1–19.
- Gerke, H.H., Badorreck, A., & Einecke, M. (2009). Single- and dual-porosity modelling of flow in reclaimed mine soil cores with embedded lignitic fragments. *J. Cont. Hydrol.*, 104, 90–106. doi: 10.1016/j.jconhyd.2008.10.009
- Gholami, L., Sadeghi, S.H., & Homae, M. (2013). Straw mulching effect on splash erosion, runoff, and sediment yield from eroded plots. *Soil Sci. Soc. Am. J.*, 77 (1), 268e278. <https://doi.org/10.2136/sssaj2012.0271>.
- Ghuman, B.S. & Sur, H.S. (2001). Tillage and residue management effects on soil properties and yields on rainfed maize and wheat in a subhumid subtropical climate. *Soil Till. Res.*, 58, 1–10.
- Gómez, J.A., Guzman, M.G., Giráldez, J.V., & Fereres, E. (2009a). The influence of cover crops and tillage on water and sediment yield, and on nutrient, and organic matter losses in an olive orchard on a sandy loam soil. *Soil Till. Res.*, 106, 137–144. doi:10.1016/j.still.2009.04.008.
- Gómez, J.A., Romero, P., Giráldez, J.V., & Fereres, E. (2004). Experimental assessment of runoff and soil erosion in an olive grove on a vertic soil in southern Spain as affected by soil management. *Soil Use Manage.*, 20, 426–431. DOI: 10.1079/SUM2004275.
- Gómez, J.A., Sobrinho, T.A., Giráldez, J.V., & Fereres, E. (2009b). Soil management effects on runoff, erosion, and soil properties in an olive grove of Southern Spain. *Soil Till. Res.*, 102(1), 5–13.
- Govers, G., Lobb, D.A., & Quine, T.A. (1999). Tillage erosion and translocation: emergence of a new paradigm in soil erosion research. *Soil Till. Res.*, 51, 167–174.
- Grant, C.A. & Lafond, G.P. (1993). The effects of tillage systems and crop sequences on soil bulk density and penetration resistance on a clay soil in southern Saskatchewan. *Can. J. Soil Sci.*, 73, 223–232.
- Greb, B.W. (1966). Effect of surface-applied wheat straw on soil water losses by solar distillation. *Soil Sci. Soc. Am. Proc.*, 30, 786–788.
- Green, W. H., & G. A. Ampt. (1911). Studies in soil physics: 1. Flow of air and water through soils. *J. Agric. Sci.*, 4(1): 1–24. <https://doi.org/10.1017/S0021859600001441>
- Gregory, J.H., Dukes, M.D., Jones, P.H., & Miller, G.L. (2006). Effect of urban soil compaction on infiltration rate. *J. Soil Water Conserv.* 61(3), 117–124.
- Guertault, L. & Fox, G.A. (2020). Performance of preferential flow models in predicting infiltration through a remolded soil with artificial macropores. *V. Z. J.*, 19:e20055. <https://doi.org/10.1002/vzj2.20055>

- Gupta, S.C. & Larson, W.E. (1979). Estimating soil water retention characteristics from particle size distribution, organic matter percent, and bulk density. *Water Resour. Res.*, 15, 1633-1635.
- Hacısalihoglu, S., Oktan, E., & Yucesan, Z. (2010). Predicting soil erosion in oriental spruce (*picea orientalis* (L.) link.) stands in Eastern Black Sea Region of Turkey. *African Journal of Agricultural Research*, 5(16), 2200-2214. <https://doi.org/10.5897/AJAR10.613>
- Haghighi, F., Gorji, M., & Shorafa, M. (2010). A study of the effects of land use changes on soil physical properties and organic matter. *Land Degrad. Develop.*, 21, 496–502. DOI: 10.1002/ldr.999
- Haynes, R.J. & Naidu, R. (1998). Influence of lime, fertilizer and manure applications on soil organic matter content and soil physical conditions: A review. *Nutr. Cycl. Agroecosys.*, 51, 123-137.
- Hammecker, C., Antonino, A.C.D., Maeght, J.L., & Boivin, P. (2003). Experimental and numerical study of water flow in soil under irrigation in northern Senegal: evidence of air entrapment. *European Journal of Soil Science*, 54, 491–503.
- Han, Y., Luo, Y., Yu, Q., & Zhang, H. (2001). The Green–Ampt model for heterogeneous soil profiles. *Chinese Journal of Eco-Agriculture.*, 9 (1), 31–37 (in Chinese).
- Hangen, E., Gerke, H. H., Schaaf, W., & Hüttl, R. F. (2004). Flow path visualization in a lignitic mine soil using iodine–starch staining. *Geoderma*, 120, 121–135. doi: 10.1016/j.geoderma.2003.08.011
- Haraldsen, T.K. & Sveistrup, T.E. (1994). Effects of cattle slurry and cultivation on infiltration in sandy and silty soils from northern Norway. *Soil Till. Res.*, 29(4),307–321. [https://doi.org/10.1016/0167-1987\(94\)90105-8](https://doi.org/10.1016/0167-1987(94)90105-8)
- Harisuseno, D., Khaeruddin, D.N., & Haribowo, R. (2019). Time of concentration-based infiltration under different soil density, water content, and slope during a steady rainfall. *J. Water Land Dev.*, 41(IV–VI), 61–68. DOI: 10.2478/jwld-2019-0028
- Hartge, R. & Horn, R. (2009). Measuring the physical parameters of soils: Methods, Application, and Assessment. Schweizerbart Verlag.
- Hatfield, J.L., Sauer, T.J., & Prueger, J.H. (2001). Managing soils to achieve greater water use efficiency: A review. *Agron. J.*, 93 (2), 271-280. <https://doi.org/10.2134/agronj2001.932271x>
- Hebb, C., Schoderbek, D., Hernandez-Ramirez, G., Hewins, D., Carlyle, C.N., & Bork, E. (2017). Soil physical quality varies among contrasting land uses in Northern Prairie regions. *Agr. Ecosyst. Environ.*, 240, 14–23.

- Hendrickx, J. M. & Flury, M. (2001). Uniform and preferential flow mechanisms in the vadose zone. In *Conceptual models of flow and transport in the fractured vadose zone* (pp. 149–187). Washington, D.C.: National Academy Press. National Research Council.
- Hill, R.L. (1990). Long-term conventional and no-tillage effects on selected soil physical properties. *Soil Sci. Soc. Am. J.*, 54, 161–166.
- Hillel, D. (1980). *Fundamentals of soil physics*. Academic press, New York.
- Holtz, W.G. (1959). Expansive Clays – Properties and Problems. *Quarterly of the Colorado School of Mines*, 54(4). pp. 89-125.
- Horton, R., Thompson, M.L., & McBride, J.F. (1987). Method of estimating the travel time of noninteracting solutes through compacted soil material. *Soil Sci. Soc. Am. J.* 51, 48–53. DOI 10.2136/sssaj1987.03615995005100010009x.
- Hsu, S.Y. & Hilpert, M. (2011). Incorporation of dynamic capillary pressure into the green-ampt model for infiltration. *Vadose Zone J.*, 10, 642–653.
- Hsu, S.Y., Huang, V., Park, S.W., & Hilpert, M. (2017). Water infiltration into prewetted porous media: Dynamic capillary pressure and Green-Ampt modeling. *Adv. Water Resour.*, 106, 60-67. <http://dx.doi.org/10.1016/j.advwatres.2017.02.017>
- Hu, W., Shao, M., Wang, Q., Fan, J., & Horton, R. (2009). Temporal changes of soil hydraulic properties under different land uses. *Geoderma*, 149, 355–366. <https://doi.org/10.1016/j.geoderma.2008.12.016>.
- Husz, G. (1967). Determination of the pF curve from texture, using multiple regressions. *Z. Pflanzenernaehr. Bodenk.*, 116, 115-125.
- Jamieson, R.C., Gordon, R.J., Sharples, K.E., Stratton, G.W., & Madani, A. (2002). Movement and persistence of fecal bacteria in agricultural soils and subsurface drainage water: a review. *Canadian Biosystems Engineering*, 44, 1.01–1.09.
- Jarvis, N.J. (2007). A review of non-equilibrium water flow and solute transport in soil macropores: principles, controlling factors and consequences for water quality. *Eur. J. Soil Sci.*, 58, 523–546.
- Jassogne, L., McNeill, A., & Chittleborough, D. (2007). 3D-visualization and analysis of macro- and meso-porosity of the upper horizons of a sodic, texture-contrast soil. *Eur. J. Soil Sci.*, 58 (3), 589–598. doi:10.1111/j.1365-2389.2006.00849.x
- Jena, A. & Gupta, K. (2002). Determination of pore volume and pore distribution by liquid extrusion porosimetry without using mercury. *Ceramic Eng. & Sci. Pr.*, 23 (4), 277–284.
- Jia, Y. & Tamai, N. (1997). Modeling infiltration into a multilayered soil during a unsteady rain. *Ann. J. Hydraul. Eng.*, 41, 31–36.

- Jiao, C.J., Xu, Q.L., Wang, C.Y., Li, F.M., Li, Z.X., & Wang, Y. F. (2006). Accumulation pattern of toxin β -ODAP during lifespan and effect of nutrient elements on β -ODAP content in *Lathyrus sativus* seedlings. *J. Agric. Sci.*, 144 (3), 543-549
- Jordan, A., Zavala, L.M., & Gil, J. (2010). Effects of mulching on soil physical properties and runoff under semi-arid conditions in southern Spain. *Catena*, 81, 77e85.
- Jury, W.A., Gardner, W.R., & Gardner, W.H. (1991). *Soil physics*. John Wiley & Sons, New York.
- Kahlon, M.S., Lal, R., & Ann-Varughese, M. (2013). Twenty-two years of tillage and mulching impacts on soil physical characteristics and carbon sequestration in Central Ohio. *Soil Till. Res.*, 126, 151–158. doi: 10.1016/j.still.2012.08.001
- Karlen, D., Erbach, D., Kaspar, T., Colvin, T., Berry, E., & Timmons, D. (1990). Soil Tillage: A Review of Past Perceptions and Future Needs. *Soil Sci. Soc. Am. J.*, 54(1), 153-161.
- Karlen, D.L., Wollenhaupt, N.C., Erbach, D.C., Berry, E.C., Swan, J.B., Eash, N.S., & Jordahl, J.L. (1994). Long-term tillage effects on soil quality. *Soil Till. Res.*, 32, 313-327.
- Kasteel, R., Vogel, H., & Roth, K. (2002). Effect of non-linear adsorption on the transport behavior of brilliant blue in a field soil. *Eur. J. Soil Sci.*, 53, 231Y240.
- Kaspar, T. C. & Singer, J. W. (2011). *The Use of Cover Crops to Manage Soil*. Publications from USDAARS / UNL Faculty. 1382. <https://digitalcommons.unl.edu/usdaarsfacpub/1382>
- Kay, B. & Lal, R. (1997). Soil structure and organic carbon: a review. *Soil Process. Carbon Cycle*, 198, 169–197.
- Kay, B.D. & VandenBygaart, A.J. (2002). Conservation tillage and depth stratification of porosity and soil organic matter. *Soil Till. Res.*, 66, 107–118.
- Kefi, M., Yoshino, K., Zayani, K., & Isoda, H. (2009). Estimation of Soil Loss by Using Combination of Erosion Model and GIS-Case of Study Watersheds in Tunisia-. *J. Arid Land Studies*, 19(1), 287-290.
- Kettler, T.A., Lyon, D.J., Doran, J.W., Powers, W.L., & Stroup, W.W. (2000). Soil quality assessment after weed-control tillage in a no-till wheat-fallow, cropping system. *Soil Sci. Soc. Am. J.* 64,339-346.
- Khaing, T., Win, S.S., & Win, N.N. (2019). Physical and Chemical Properties of Compost Made from Agricultural Wastes. *IJERD*, 10, 2.
- Khater, El-S.G. (2015). Some Physical and Chemical Properties of Compost. *J. Waste Resour.*, 5: 172. doi:10.4172/2252-5211.1000172

- Khurshid, K., Iqbal, M., Arif, M.S., & Nawaz, A. (2006). Effect of Tillage and Mulch on Soil Physical Properties and Growth of Maize. *Int. J. Agric. Biol.*, 8(5), 593-596.
- Kivisaari, S. (1971). Influence of texture on some moisture constants. *Acta Agr. Fennica*, 123, 217-222.
- Klute, A. & Dirksen, C. (1986). Hydraulic conductivities and diffusivity: laboratory methods. Methods of soil analysis. Part 1. In: Klute, A. (Ed.), *Physical and Mineralogical Methods*. 2nd ed. ASA-SSSA, Madison, WI, pp. 687–734
- Kodešová, R., Šimůnek, J., Nikodem, A., & Jirků, V. (2010). Estimation of the Dual-Permeability Model Parameters using Tension Disk Infiltrometer and Guelph Permeameter. *Vadose Zone J.*, 9, 213–225. doi:10.2136/vzj2009.0069
- Kodešová, R., Němeček, K., Kodeš, V., & Žigová, A. (2012). Using Dye Tracer for Visualization of Preferential Flow at Macro- and Microscales. *Vadose Zone J.*, 11(1), 0. doi:10.2136/vzj2011.0088
- Kodešová, R., Němeček, K., Žigová, A., Nikodem, A., & Fer, M. (2015). Using dye tracer for visualizing roots impact on soil structure and soil porous system. *Biologia*, 70 (11), 1439–1443.
- Köhne, J.M., Köhne, S., & Simunek, J. (2009a). A review of model applications for structured soils: a) Water flow and tracer transport. *J. Contam. Hydrol.*, 104, 4–35. doi:10.1016/j.jconhyd.2008.10.002
- Köhne, J.M., Köhne, S., & Simunek, J. (2009b). A review of model applications for structured soils: b) Pesticide transport. *J. Contam. Hydrol.*, 104: 36–60. doi:10.1016/j.jconhyd.2008.10.003
- Köhne, J.M. & Mohanty, B.P. (2005). Water flow processes in a soil column with a cylindrical macropore: experiment and hierarchical modeling. *Water Resour. Res.*, 41, W03010, <http://dx.doi.org/10.1029/2004WR003303>.
- Kumar, S., Kadono, A., Lal, R., & Dick, W. (2012). Long-Term Tillage and Crop Rotations for 47–49 Years Influences Hydrological Properties of Two Soils in Ohio. *Soil Sci. Soc. Am. J.*, 76(6), 2195. doi:10.2136/sssaj2012.0098
- Kutilek, M. & Nielsen, D.R. (1964). *Soil Hydrology*. Catena Verlag, Cremlingen Destedt, Germany
- Kutilek, M. (2004). Soil hydraulic properties as related to soil structure. *Soil Till. Res.*, 79, 175–184.
- Lal, R. (1976). No-tillage Effects on Soil Properties under Different Crops in Western Nigeria. *Soil Sci. Soc. Am. J.*, 40(5), 762-768. <https://doi.org/10.2136/sssaj1976.03615995004000050039x>

- Lal, R. (1979). Physical characteristics of soils of the tropics: Determination and management. In R. Lal, & Greenlan (Eds.), *Soil physical properties and crop production in the tropics*. New York: John Wiley and Sons.
- Lal, R. (2018). Accelerated Soil erosion as a source of atmospheric CO₂. *Soil & Tillage Res.*, 188. DOI:10.1016/j.still.2018.02.001
- Lal, R., & Shukla, M.K. (2004). *Principles of Soil Physics*. CRC Press.
- Lal, R. & Vandoren, D.M.J. (1990). Influence of 25 years of continuous corn production by three tillage methods on water infiltration for two soils in Ohio. *Soil Till. Res.*, 16, 71–84.
- Lamy, E., Lassabatere, L., Bechet, B., & Andrieu, H. (2009). Modeling the influence of an artificial macropore in sandy columns on flow and solute transfer. *J. Hydrol.*, 376, 392-402. doi:10.1016/j.jhydrol.2009.07.048
- Lankoski, J., Ollikainen, M., & Uusitalo, P. (2004). No-Till Technology: Benefits to Farmers and the Environment? Discussion paper 1, Helsinki, Finland. University of Helsinki. March.
- Lascano, R.J. & Baumhardt, R.L. (1996). Effects of crop residue on soil and plant water evaporation in a dryland cotton system. *Theor. Appl. Climatol.*, 54, 69–84. <http://dx.doi.org/10.1007/BF00863560>.
- Lassabatere, L., Pu, J.H., Bonakdari, H., & Joannis, C. (2013). Velocity Distribution in Open Channel Flows: Analytical Approach for the Outer Region. *J. Hydraul. Eng.*, 139 (1), 37-43. doi:10.1061/(asce)hy.1943-7900.0000609
- Lax, A., Rolda'n, A., Caravaca, F., & Garcí'a-Orenes, F. (1997). Relationships between aggregate improvement, microbiological activity and organo-mineral formation in soil from semiarid areas. In: Pandalai, S.G. (Ed.), *Recent Research Developments in Soil Biology and Biochemistry*. Research Signpost, India, pp. 77–92.
- Lee, S., Chu, M.L., & Schmidt, A.R. (2020). Effective Green-Ampt Parameters for Two-Layered Soils. *J. Hydrol. Eng.*, 25(4), 04020004. DOI: 10.1061/(ASCE)HE.1943-5584.0001897
- Leghari, N., Ali, A., & Mangrio, M.A. (2015). Relative efficiency of different tillage practices and their effect on soil physical properties under semi-arid climate of Tandojam, Pakistan. *J. Eng. Tech.*, 35(2), 239-246.
- Leys, A., Govers, G., Gillijns, K., & Poesen, J. (2007). Conservation tillage on loamy soils: explaining the variability in interrill runoff and erosion reduction. *Eur. J. Soil Sci.*, 58(6), 1425–1436
- Li, C., Shen, Y., Ge, H., Zhang, Y., & Liu, T. (2018). Spontaneous imbibition in fractal tortuous micro-nano pores considering dynamic contact angle and slip effect: phase portrait analysis and analytical solutions. *Sci. Rep.*, 8, 3919. DOI:10.1038/s41598-018-21002-y

- Li, Y. & Ghodrati, M. (1995). Transport of nitrate in soils as affected by earthworm activities. *J. Environ. Qual.*, 24, 432–438. doi:10.2134/jeq1995.00472425002400030006x
- Liu, Y., Steenhuis, T. S., & Parlange, J.-Y. (1994). Closed-form solution for finger width in sandy soils at different water contents. *Water Resour. Res.*, 30(4), 949–952. doi:10.1029/94wr00068
- Lightfoot, D.R. & Eddy, F.W. (1994). The agricultural utility of lithic-mulch gardens: past and present. *Geojournal*, 34.4, 425–437.
- Lindstorm, M.J. & Onstad, C.A. (1984). Influence of tillage systems on soil physical parameters and infiltration after planting. *J. Soil Water Conserv.*, 39, 149–152
- Lin, H.S., McInnes, K.J., Wilding, L.P., & Hallmark, C.T. (1996). Effective porosity and flow rate with infiltration at low tensions in a well-structured subsoil. *Trans. ASAE*, 39, 131–133.
- Lin, H., & Zhou, X. (2008). Evidence of subsurface preferential flow using soil hydrologic monitoring in the Shale Hills catchment. *Eur. J. Soil Sci.*, 59, 34–49.
- Liu, D., Xu, Y., Guo, S., Liu, P., & Rheinheimer, D.E. (2016). A modified Green–Ampt model for water infiltration and preferential flow. *Hydrol. Res.*, 47(6), 1172–1181. <https://doi.org/10.2166/nh.2016.160>
- Liu, J., Zhang, J., & Feng, J. (2008). Green-Ampt model for layered soils with nonuniform initial water content under unsteady infiltration. *Soil Sci. Soc. Am. J.*, 72(4), 1041–1047. <https://doi.org/10.2136/sssaj2007.0119>.
- Liu, Y., Steenhuis, T. S., & Parlange, J.-Y. (1994). Formation and persistence of fingered flow fields in coarse grained soils under different moisture contents. *J. Hydrol.*, 159 (1-4), 187–195. doi:10.1016/0022-1694(94)90255-0
- López, M.V., Moret, D., Gracia, R., & Arrúe, J.L. (2003). Tillage effects on barley residue cover during fallow in semiarid Aragon. *Soil Till. Res.*, 72, 53–64.
- Lund, Z. F. (1959). Available water-holding capacity of alluvial soils in Louisiana. *Soil Sci. Soc. Amer. Proc.*, 23, 1-3.
- Luxmoore, R.J. (1981). Micro-, meso-, and macroporosity of soil. *Soil Sci. Soc. Am. J.*, 45, 671–672.
- Lyon, D.J., Stroup, W.W., & Brown, R.E. (1998). Crop production and soil water storage in long-term winter wheat-fallow tillage experiments. *Soil Tillage Res.*, 49, 19–27.
- Ma, Y., Feng, S., Su, D., Gao, G., & Huo, Z. (2010). Modeling water infiltration in a large, layered soil column with a modified Green-Ampt model and HYDRUS-1D. *Supplement, Comput. Electron. Agric.*, 71 (S1), S40–S47. <https://doi.org/10.1016/j.compag.2009.07.006>.

- Malone, R.W., Shipitalo, M.J., & Meek, D.W. (2004). Relationship between herbicide concentration in percolate, percolate breakthrough time, and number of active macropores. *Trans. ASAE*, 47, 1453–1456. doi:10.13031/2013.17625
- Mamedov, A.I., Shainberg, I., & Levy, G.J. (2000). Rainfall energy effects on runoff and interrill erosion in effluent irrigated soils. *Soil Sci.*, 165, 535–544.
- Mannering, J.V. & Meyer, L.D. (1963). The effects of various rates of surface mulch on infiltration and erosion. *Soil Sci. Soc. Am. J.*, 27(1), 84–86.
- Marshall, T. J. (1959). Relations between water and soil, Tech. Comm. 50, Commonwealth Bur. Soils, Harpenden, U.K.
- Martens, D.A. & Frankenberger, W.T. (1992). Modification of infiltration rates in an organic-amended irrigated soil. *Agro. J.*, 84:707. <https://doi.org/10.2134/agronj1992.00021962008400040032x>
- Martínez, E., Fuentes, J.-P., Silva, P., Valle, S., & Acevedo, E. (2008). Soil physical properties and wheat root growth as affected by no-tillage and conventional tillage systems in a Mediterranean environment of Chile. *Soil Till. Res.*, 99, 232-244. doi:10.1016/j.still.2008.02.001
- Martino, D.L. & Shaykewich, C.F. (1994). Root penetration profiles of wheat and barley as affected by soil penetration resistance in field conditions. *Can. J. Soil Sci.*, 74 (2), 193-200. <https://doi.org/10.4141/cjss94-027>
- MataixSolera, J. & Doerr, S.H. (2004). Hydrophobicity and aggregate stability in calcareous top soils from fire-affected pine forests in southeastern Spain. *Geoderma*, 118, 77–88.
- McIntyre, D.S. (1958). Permeability measurements of soil crust formed by raindrop impact. *Soil Sci.*, 85, 185–189.
- McVay, K.A., Budde, J.A., Fabrizzi, K., Mikha, M. M., Rice, C.W., Schlegel, A.J., Peterson, D. E., Sweeney, D. W., & Thompson, C. (2006). Management Effects on Soil Physical Properties in Long-Term Tillage Studies in Kansas. *Soil Sci. Soc. Am. J.*, 70:434–438. doi:10.2136/sssaj2005.0249
- Mein, R.G. & Larson, C.L. (1973). Modeling infiltration during a steady rain. *Water Resour. Res.*, 9(2), 384-394.
- Messing, I. & Jarvis, N.J. (1993). Temporal variation in the hydraulic conductivity of a tilled clay soil as measured by tension infiltrometers. *J. Soil Sci.*, 44, 11–24.
- Miyamoto, T., Kobayashi, R., Annaka, T., & Chikushi, J. (2001). Applicability of multiple length TDR probes to measure water distributions in an Andisol under different tillage systems in Japan. *Soil Tillage Res.*, 60, 91–99.
- Miyata, S., Kosugi, K., Gomi, T., & Mizuyama, T. (2009). Effects of forest floor coverage on overland flow and soil erosion on hillslopes in Japanese cypress

- plantation forests. *Water Resour. Res.*, 45, W06402. <https://doi.org/10.1029/2008WR007270>.
- Mohammadzadeh-Habili, J. & Heidarpour, M. (2015). Application of the Green–Ampt model for infiltration into layered soils. *J. Hydrol.*, 527, 824–832. <http://dx.doi.org/10.1016/j.jhydrol.2015.05.052>
- Mon, J., Flury, M., & Harsh, J. B. (2006). Sorption of four triarylmethane dyes in a sandy soil determined by batch and column experiments. *Geoderma*, 133, 217Y224.
- Montenegro, A.A.A., Abrantes, J.R.C.B., de Lima, J. L.M.P., Singh, V.P., & Santos, T.E.M. (2013). Impact of mulching on soil and water dynamics under intermittent simulated rainfall. *Catena*, 109, 139e149. <https://doi.org/10.1016/j.catena.2013.03.018>.
- Mooney, S.J. & Morris, C. (2004). Quantification of preferential flow in undisturbed soil columns using dye tracers and image analysis. SuperSoil 2004: 3rd Australian New Zealand Soils Conference, 5 – 9 December 2004, University of Sydney, Australia. Published on CDROM.
- Moore, I. D. & Eigel, J. D. (1981). Infiltration into two-layered soil profiles. *Trans. ASAE*, 24, (6), 1496–1503. <https://doi.org/10.13031/2013.34480>.
- Moret, D. & Arrue, J.L. (2007a). Characterizing soil water-conducting macro- and mesoporosity as influenced by tillage using tension infiltrometry. *Soil Sci. Soc. Am. J.*, 71, 500–506.
- Moret, D. & Arrue, J.L. (2007b). Dynamics of soil hydraulic properties during fallow as affected by tillage. *Soil Till. Res.*, 96, 103–113.
- Mori, Y., Fujihara, A., & Yamagishi, K. (2014). Installing artificial macropores in degraded soils to enhance vertical infiltration and increase soil carbon content. *Prog. Earth Planet. Sci.*, 1,30. <http://www.progearthplanetosci.com/content/1/1/30>
- Mori, Y. & Hirai, Y. (2014). Effective Vertical Solute Transport in Soils by Artificial Macropore System. *J. Hazard. Toxic Radioact. Waste*, 18. s. DOI: 10.1061/(ASCE)HZ.2153-5515.0000192
- Mori, Y., Maruyama, T., & Mitsuno, T. (1999). Soft X-ray radiography of drainage patterns of structured soils. *Soil Sci. Soc. Am. J.*, 63(4),733–740.
- Moriasi, D.N., Arnold, J.G., Van Liew, M.W., Bingner, R.L., Harmel, R.D., & Veith, T.L. (2007). Model evaluation guidelines for systematic quantification of accuracy in watershed simulations. *Trans. ASABE*, 50, 885–900. <http://doi.org/10.13031/2013.23153>
- Mosaddeghi, M.R., Hajabbasi, M.A., Hemmat, A., & Afyuni, M. (2000). Soil compactibility as affected by soil moisture content and farmyard manure in central Iran. *Soil Till. Res.*, 55, 87-97.

- Mrabet, R., Saber, N., El-Brahli, A., Lahlou, S., & Bessam, F. (2001). Total, particulate organic matter and structural stability of a Calcixeroll soil under different wheat rotations and tillage systems in a semiarid area of Morocco. *Soil Till. Res.*, 57, 225–235.
- Mubarak, A.R., Omaima, E.R., Amal, A.A., & Nemat, E.H. (2009a). Short-term studies on use of organic amendments for amelioration of a sandy soil. *AJAR*, 4(7), 621–627.
- Mubarak, I., Mailhol, J.C., Angulo-Jaramillo, R., Ruelle, P., Boivin, P., & Khaledian, M. (2009b). Temporal variability in soil hydraulic properties under drip irrigation. *Geoderma*, 150, 158–165.
- Mulumba, L.N. & Lal, R. (2008) Mulching Effects on Selected Soil Physical Properties. *Soil & Till. Res.*, 98, 106-111. <https://doi.org/10.1016/j.still.2007.10.011>
- Mwango, S.B., Msanya, B.M., Mtakwa, P.W., Kimaro, D.N., Deckers, J., & Poesen, J. (2016). Effectiveness of mulching under miraba in controlling soil erosion, fertility restoration and crop yield in the Usambara mountains, Tanzania. *Land Degr. & Dev.*, 27, 1266e1275. <https://doi.org/10.1002/ldr.2332>.
- Mwendera, E.J. & J. Feyen. (1993). Predicting tillage effects on infiltration. *Soil Sci.* 155, 229-235.
- Myrold, D.D., Elliott, L.F., Papendick, R.I. & Campbell, G.S. (1981). Water potential-water content characteristics of wheat straw. *Soil Sci. Soc. Am. J.*, 45, 329–333.
- Nakaya, N. (1981). The moisture characteristics of soils in relation to organic matter with special reference to the condition of soil organic matter and water repellency. *Bull. Natl Inst.*
- Nakaya, N., Motomura, S., & Yokoi, H. (1977). Some aspects on water repellency of soils. *Soil Sci. Plant Nutr.*, 23, 409–415.
- Nash, J. E., & Sutcliffe, J. V. (1970). River flow forecasting through conceptual models. I. A discussion of principles. *J. Hydrol.*, 10, 282–290. [http://doi.org/10.1016/0022-1694\(70\)90255-6](http://doi.org/10.1016/0022-1694(70)90255-6)
- Nassif, S.H. & Wilson, E.M. (1975). The influence of slope and rain intensity on runoff and infiltration. *Hydrol. Sci. J.* 20(4), 539–553. DOI 10.1080/02626667509491586.
- Nawaz, M.F., Bourrié, G., & Trolard, F. (2013). Soil compaction impact and modelling. A review. *Agron. Sustain. Dev.*, 33, 291-309.
- Negi S.C., Raghaven G S., & Taylor F. (1981). Hydraulic characteristics of conventionally and zero-tilled field plots. *Soil Till. Res.*, 2, 281–292
- Neuman, S.P. (1976). Wetting front pressure head in the infiltration model of Green and Ampt. *Water Resour. Res.*, 12 (3), 564–566.

- Nimmo, J.R. (2004). Porosity and Pore Size Distribution, *in* Hillel, D., ed. Encyclopedia of Soils in the Environment: London, Elsevier, v. 3, p. 295-303.
- Nimmo, J.R. (2010a). A free-surface film differs hydraulically from a capillary bundle largely in having an air–water interface that is constrained by neither the solid material nor capillarity. *V. Z. J.*, 9, 295–306. doi:10.2136/vzj2009.0085.
- Nimmo, J. R. (2010b). Theory for source-responsive and free-surface film modeling of unsaturated flow. *V. Z. J.*, 9, 295–306.
- North, P.F. & Brown, N.J. (1982). The effect on some field-measured soil physical properties of restructuring a soil mechanically. Proceedings of the 9th Conference International on Soil Tillage Research, Socialist Federalist Republic of Yugoslavia, Osijek.
- Ohrstrom, P., Hamed, Y., Persson, M., & Berndtsson. R. (2004). Characterizing unsaturated solute transport by simultaneous use of dye and bromide. *J. Hydrol.*, 289:23Y35.
- Opara-Nadi, O.A. (1993). *Conservation tillage for increased crop production (Chapter 8)*. FAO Soils Bulletin (FAO). <http://www.fao.org/3/T1696E/t1696e09.htm>
- Osborne, G.J, Payne, D., Greenland, D.J., & Moseley, T. (1979). Pore size distribution of soils. Proceedings of the 8th Conference International on Soil Tillage Research, Germany.
- Pagliai, M., Vignozzi, N., & Pellegrini, S. (2004). Soil structure and the effect of management practices. *Soil Till. Res.*, 79, 131–143.
- Panagea, I.S., Berti, A., Čermak, P., Diels, J., Elsen, A., Kusá, H., Piccoli, I., Poesen, J., Stoate, C., Tits, M., Toth, Z., & Wyseure. (2021). Soil Water Retention as Affected by Management Induced Changes of Soil Organic Carbon: Analysis of Long-Term Experiments in Europe. *Land*, 10, 1362. <https://doi.org/10.3390/land10121362>
- Patle, G.T., Sikar, T.T., Rawat, K.S., & Singh, S.K. (2018). Estimation of infiltration rate from soil properties using regression model for cultivated land. *Geol. Ecol. Landsc.*, 3 (1), 1-13. <https://doi.org/10.1080/24749508.2018.1481633>.
- Pellichero, E., Glantz, R., Burns, M., Mallick, D., Hsu, S.Y., & Hilpert, M. (2012). Dynamic capillary pressure during water infiltration: Experiments and Green-Ampt modeling. *Water Resour. Res.*, 48, W06515, doi:10.1029/2011WR011541.
- Pérez, F. L. (2000). The influence of surface volcanoclastic layers from Haleakala (Maui, Hawaii) on soil water conservation. *Catena*, 38(4), 301–332. doi:10.1016/s0341-8162(99)00076-4
- Pervaiz, Z.H., Rabbani, M.A., Pearce, S.R., & Malik, S.A. (2009). Determination of genetic variability of Asian rice (*Oryza sativa* L.) varieties using microsatellite markers. *Afr. J. Biotechnol.*, 8: 5641-5651.

- Petersen, C. T., Jensen, H. E., Hansen, S., & Bender Koch, C. (2001). Susceptibility of a sandy loam soil to preferential flow as affected by tillage. *Soil Till. Res.*, 58, 81–89. doi: 10.1016/S0167-1987(00)00186-0
- Philip, J. R. (1957). The theory of infiltration: 4 sorptivity and algebraic infiltration equations. *Soil Sci.*, 84, 257–264.
- Pikul, J.L. & Aase, J.K. (1995). Infiltration and soil properties as affected by annual cropping in the Northern Great Plains. *J. Agron.*, 87 (4), 656–662. DOI 10.2134/agronj1995.00021962008700040009x
- Pikul, J.L., Zuzel, J.F., & Ramig, R.E. (1990). Effect of tillage induced soil macroporosity on water infiltration. *Soil Tillage Res.*, 17, 153-165. [https://doi.org/10.1016/0167-1987\(90\)90013-4](https://doi.org/10.1016/0167-1987(90)90013-4)
- Pimentel D., Harvey C., Resosudarmo, P., Sinclair K., Kurz D., McNair M., Crist S., Shpritz L., Fitton L., Saffouri R., & Blair R. (1995). Environmental and Economic Costs of Soil Erosion and Conservation Benefits. *Sci.*, 267, 1117-1123. DOI:10.1126/science.267.5201.1117.
- Pinheiro, E.F.M., Pereira, M.G., & Anjos, L.H.C. (2004). Aggregate distribution and soil organic matter under different tillage systems for vegetable crops in a Red Latosol from Brazil. *Soil & Till, Res.*, 77, 79–84.
- Prieksat, M.A., Kaspar, T.C. & Ankeny, M.D. (1994). Positional and temporal changes in ponded infiltration in a corn field. *Soil Sci. Soc. Am. J.*, 58, 181–184.
- Prosdocimi, M., Jordan, A., Tarolli, P., Keesstra, S., Novara, A., & Cerda, A. (2016). The immediate effectiveness of barley straw mulch in reducing soil erodibility and surface runoff generation in Mediterranean vineyards. *Sci. Total Environ.*, 547, 323e330.
- Pryor, S.C., Scavia, D., Downer, C., Gaden, M., Iverson, L., Nordstrom, R., Patz, J., & Robertson, G.P. (2014). Ch. 18: midwest. climate change impacts in the United States: the third national climate assessment. In: Melillo, J.M., Richmond, Terese (T.C.), Yohe, G.W. (Eds.), U.S. Global Change Research Program, pp. 418-440. doi:http://dx.doi.org/10.7930/J0J1012N.
- Puricelli, C., Barrios, C., & Masiero, Y.B. (1976). Determinaciones lisimétricas de evapotranspiración en maíz y evaporación durante el barbecho para Marcos Juárez. RIA, Serie 3, Vol. XIII.
- Qi, Z. & Helmers, M.J. (2010). Soil water dynamics under winter rye cover crop in central Iowa. *V. Z. J.*, 9, 53–60.
- Quemada, M. & Cabrera, M.L. (2002). Characteristic moisture curves and maximum water content of two crop residues. *Plant Soil*, 238, 295-299.
- Radcliffe, D.E., Tollner, E.W., Hargrave, W.L., Clark, R.L., & Galabi, M.H. (1988). Effect of tillage practices on infiltration and soil strength of a typic hapludult soil after ten years. *Soil Sci. Soc. Am. J.*, 52, 798-804. <https://doi.org/10.2136/sssaj1988.03615995005200030036x>

- Rahma, A.E., Lei, T.W., Shi, X.N., Dong, Y.Q., Zhou, S.M., & Zhao, J. (2013). Measuring flow velocity under straw mulch using the improved electrolyte tracer method. *J. Hydrol.*, 495, 121-125. <https://doi.org/10.1016/j.jhydrol.2013.04.049>.
- Rahma, A.E., Warrington, D.N., & Lei, T. (2019). Efficiency of wheat straw mulching in reducing soil and water losses from three typical soils of the Loess Plateau, China. *ISWCR*, 7, 335-345. <https://doi.org/10.1016/j.iswcr.2019.08.003>
- Ranjit Kumar, M., Meenambal, T., & Kumar, V. (2017). Macropore flow as a groundwater component in hydrologic simulation: modelling, applications and results. *Curr. Science*, 112 (6), 1197–1207.
- Reddy, K.N., Locke, M.A., Wagner, S.C., Zablutowicz, R.M., Gaston, L.A., & Smeda, R.J. (1995). Chlorimuron ethyl sorption and desorption kinetics in soils and herbicide-desiccated cover crop residues. *J. Agric. Food Chem.*, 43, 2752–2757.
- Reeves, M. J. (1980). Recharge of the English chalk, A possible mechanism. *Eng. Geol.*, 14 (4), 231-240.
- Reichert, J.M., Suzuki, L.E.A.S., Reinert, D.J., Horn, R., Håkansson, I. (2009). Reference bulk density and critical degree-of-compactness for no-till crop production in subtropical highly weathered soils. *Soil Till. Res.*, 102, 242–254.
- Ren, L., Nest, T.V., Ruyschaert, G., D'Hose, T., & Cornelis, W.M. (2019). Short-term effects of cover crops and tillage methods on soil physical properties and maize growth in a sandy loam soil. *Soil Till. Res.*, 192, 76–86. doi:10.1016/j.still.2019.04.026
- Reyes, J.I., Silva, P., Martínez, E., & Acevedo, E. (2002). Labranza y propiedades de un suelo aluvial de Chile Central. In: Proceedings del IX Congreso Nacional de la Ciencia del Suelo. Talca, Chile. Sociedad Nacional de la Ciencia del Suelo, Talca, Chile, pp. 78–81.
- Reynolds, W.D., Gregorich, E.G., & Curnoe, W.E. (1995). Characterization of water transmission properties in tilled and untilled soil using tension infiltrometers. *Soil Till. Res.*, 33, 117–131.
- Reynolds, W.D., Bowman, B.T., Drury, C.F., Tan, C.S., & Lu, X. (2002). Indicators of good soil physical quality: density and storage parameters. *Geoderma*, 110, 131-46.
- Reynolds, W.D., Drury, C.F., Yang, X.M., Fox, C.A., Tan, C.S., & Zhang, T.Q. (2007). Land management effects on the near-surface physical quality of a clay loam soil. *Soil Till. Res.*, 96, 316-30.
- Reynolds, W.D., Drury, C.F., Yang, X.M., & Tan, C.S. (2008). Optimal soil physical quality inferred through structural regression and parameter interactions. *Geoderma*, 146, 466-74.
- Reynolds, W.D., Drury, C.F., Tan, C.S., Fox, C.A., & Yang, X.M. (2009). Use of indicators and pore volume-function characteristics to quantify soil physical

- quality. *Geoderma*, 152 (3-4), 252–263. doi:10.1016/j.geoderma.2009.06.009 10.1016/j.geoderma.2009.06.009
- Richards, L. 1931. Capillary conduction of liquids through porous mediums. *J. Appl. Phys.*, 1, 318–333. <https://doi.org/10.1063/1.1745010>.
- Rodrigo-Comino, J., Giménez-Morera, A., Panagos, P., Pourghasemi, H.R., Pulido, M., & Cerdà, A. (2019). The potential of straw mulch as a nature-based solution for soil erosion in olive plantation treated with glyphosate: A biophysical and socioeconomic assessment. *Land Degrad Dev.*, 31, 1877–1889.
- Roldán, A., García-Orenes, F., & Lax, A. (1994). An incubation experiment to determine factors involving aggregation changes in an arid soil receiving urban refuse. *Soil Biol. Biochem.*, 26, 1699–1707.
- Roper, M.M., Ward, P.R., Keulen, A.F. & Hill, J.R. (2013). Under no-tillage and stubble retention, soil water content and crop growth are poorly related to soil water repellency. *Soil Till. Res.*, 126: 143–150. doi: 10.1016/j.still.2012.09.006
- Rosell, R. & Andriulo, A. (1989). Distribución de carbono y nitrógeno orgánicos, formas de fósforo y pH del suelo de un suelo bajo tres sistemas. *Agrochimica*, 33, 194-202.
- Ruan, H.X., Ahuja, L.R., Green, T.R., & Benjamin, J.G. (2001). Residue cover and surface sealing effects on infiltration: numerical simulations for field applications. *Soil Sci. Soc. Am. J.*, 65(3), 853–861.
- Saber, N. & Mrabet, R. (2002). Impact of no tillage and crop sequence on selected soil quality attributes of a vertic calcixeroll soil in Morocco. *Agron.*, 22, 451–459.
- Sahu, M., VM, V., Verma, A., & Agrawal, S. (2020). Study on physical and frictional properties of farmyard manure (FYM) to develop mechanized application and handling unit of FYM. *J. Pharm. Innov.*, 9 (1): 101-107.
- Salem, H.M., Valero, C., Munoz, M.A., Rodriguez, M.G., & Silva, L.L. (2014). Short-term effects of four tillage practices on soil physical properties, soil water potential, and maize yield. *Geoderma*, 237-238, 60-70. <https://doi.org/10.1016/j.geoderma.2014.08.014>
- Salem, H.M., Valero, C., Munoz, M.A., & Rodriguez, M.G. (2015). Effect of integrated reservoir tillage for in-situ rainwater harvesting and other tillage practices on soil physical properties. *Soil Tillage Res.*, 151, 50-60. <http://dx.doi.org/10.1016/j.still.2015.02.009>
- Sarauski, E., Buragiene, S., Romaneckas, K., Sakalauskas, A., Jasinskas, A., Vaiciukevicius, E., & Karayel, D. (2012). Working Time, Fuel Consumption and Economic Analysis of Different Tillage and Sowing Systems in Lithuania. Proceedings of 11th International Scientific Conference on Engineering for Rural Development. Jelgava, Latvia

- Sasal, M.C., Andriulo, A.E., & Taboada, M.A. (2006). Soil porosity characteristics and water movement under zero tillage in silty soils in Argentinian Pampas. *Soil Till. Res.*, 87 (1): 9–18. doi: 10.1016/j.still.2005.02.025
- Sauer, T.J., Clothier, B.E., & Daniel, T.C. (1990). Surface measurements of the hydraulic properties of a tilled and untilled soil. *Soil Till. Res.*, 15, 359–369.
- Sauer, T.J., Hatfield, J.L., & Prueger, J.H. (1996). Corn residue age and placement effects on evaporation and soil thermal regime. *Soil Sci. Soc. Am. J.*, 60, 1558–1564.
- Schippers, K.J., Nelson, W.S., & Wang, R. (1994). Effects of residue free band width on soil temperature and water content. *Trans. ASAE*, 37, 39–49.
- Schjønning, P. & Rasmussen, K.J. (2000). Soil strength and soil pore characteristics for direct drilled and ploughed soils. *Soil Till. Res.*, 57 (1), 69-82. DOI: 10.1016/S0167-1987(00)00149-5
- Schjønning, P., Munkholm, L.J., Moldrup, P. & Jacobsen, O.H. (2002). Modelling soil pore characteristics from measurements of air exchange: the long-term effects of fertilization and crop rotation. *Eur. J. Soil Sci.*, 53, 331–339.
- Schomberg, H.H., Ford, P.B., & Hargrove, W.L. (1994). *Influence of crop residues on nutrient cycling and soil chemical properties*. In: Unger, P.W. (Ed.), *Managing Agricultural Residues*. Lewis Publishers, Boca Raton, FL, USA pp. 99-121.
- Schneider, A., Hirsch, F., Raab, A., & Raab, T. (2018). Dye Tracer Visualization of Infiltration Patterns in Soils on Relict Charcoal Hearths. *Front. Environ. Sci.*, 6:143. doi: 10.3389/fenvs.2018.00143
- Schneider, C.A., Rasband, W.S., & Eliceiri, K.W. (2012). NIH Image to ImageJ: 25 years of image analysis. *Nature Methods*, 9 (7), 671–675. doi:10.1038/nmeth.2089
- Schwab, G.O., Frever, R.K., Edminster, T.W., & Barnes, K.K. (1993). *Soils and water conservation engineering*. New York: John Wiley and Sons, Inc.
- Selker, J.S., Duan, J., & Parlange, J-Y. (1999). Green and Ampt infiltration into soils of variable pore size with depth. *Water Resour. Res.*, 35 (5), 1685-1688.
- Shi, Z.H., Yue, B.J., Wang, L., Fang, N.F., Wang, D., & Wu, F.Z. (2013). Effects of mulch cover rate on interrill erosion processes and the size selectivity of eroded sediment on steep slopes. *Soil Sci. Soc. Am. J.*, 77 (1), 257e267. <https://doi.org/10.2136/sssaj2012.0273>.
- Shirani, H., Hajabbasi, M.A., Afyuni, M., & Hemmat, A. (2002). Effects of farmyard manure and tillage systems on soil physical properties and corn yield in central Iran. *Soil Till. Res.*, 68, 101-108. PII: S0167-1987(02)00110-1
- Shukla, M.K., Lal, R.B., Owens, L., & Unkefer, P. (2003). Land use management impacts on structure and infiltration characteristics of soils in the north Appalachian region of Ohio. *Soil Sci.*, 168, 167–177.

- Simunek, J., Jarvis, N.J., van Genuchten, M.T., & Gardenas, A. (2003). Review and comparison of models for describing non-equilibrium and preferential flow and transport in the vadose zone. *J. Hydrol.*, 272 (1), 14–35.
- Simunek, J. & van Genuchten, M.Th. (2008). Modeling nonequilibrium flow and transport processes using HYDRUS. *V. Z. J.*, 7, 782–797. doi:10.2136/vzj2007.0074
- Singh, B. & Malhi, S.S. (2006). Response of soil physical properties to tillage and residue management on two soils in a cool temperate environment. *Soil Till. Res.*, 85, 143-153. doi:10.1016/j.still.2004.12.005
- Singh, J., Heeren, D.M., Rudnick, D.R., Woldt, W.E., Bai, G., Ge, Y., & Luck, J.D. (2020). Soil structure and texture effects on the precision of soil water content measurements with a capacitance based electromagnetic sensor. *Transactions of the ASABE*, 63 (1), 141-152. <https://doi.org/10.13031/trans.13496>
- Singh, K., Mishra, A.K., Singh, B., Singh, R.P., & Patra, D.D. (2014). Tillage effects on crop yield and physicochemical properties of sodic soils. *Land Degrad. Dev.*, <http://dx.doi.org/10.1002/ldr.2266>.
- Singh, P., Wu, J.Q., McCool, D.K., Dun, S., Lin, C.-H., & Morse, J.R. (2009). Winter hydrologic and erosion processes in the U.S. Palouse Region: field experimentation and WEPP simulation. *V. Z. J.*, 8, 426–436.
- Six, J., Elliott, E.T., & Paustian, K. (2000). Soil structure and soil organic matter: II. A normalized stability index and the effect of mineralogy. *Soil Sci. Soc. Am. J.*, 64, 1042–1049.
- Smika, D.E. & Unger, P.W. (1986). Effect of surface residues on soil water storage. *Adv. Soil Sci.*, 5, 111-119.
- Standley, J., Hunter, H.M., Thomas, G.A., Blight, G.W., & Webb, A.A. (1990). Tillage and crop residue management affect Vertisol properties and grain sorghum growth over seven years in the semi-arid sub-tropics. II. Changes in soil properties. *Soil Till. Res.*, 18, 367-375.
- Startsev, A.D. & McNabb, D.H. (2001). Skidder traffic effects on water retention, pore-size distribution, and van Genuchten parameters of Boreal forest soils. *Soil Sci. Soc. Am. J.*, 65, 224-231. doi: 10.2136/sssaj2001.651224x
- Steenhuis, T.S., Staubitz, W., Andreini, M.S., Surface, J., Richard, T.L., Paulsen, R., Pickering, N.B., Hagerman, J.R., & Geohring, L.D. (1990). Preferential movement of pesticides and tracers in agricultural soils. *J. Irrig. Drain. Eng.*, 116, 50-66.
- Sternagel, A., Loritz, R., Wilcke, W., & Zehe, E. (2019). Simulating preferential soil water flow and tracer transport using the lagrangian soil water and solute transport model. *Hydrol. Earth Syst. Sci.*, 23, 4249–4267. <https://doi.org/10.5194/hess-23-4249-2019>.

- Stewart, R.D. (2018). A Dynamic Multidomain Green-Ampt Infiltration Model. *Water Resour. Res.*, 54, 6844-6859. <https://doi.org/10.1029/2018WR023297>
- Stewart, R.D. (2019). A generalized analytical solution for preferential infiltration and wetting. *V. Z. J.*, 18:180148. doi:10.2136/vzj2018.08.0148
- Stockdale, E. (2018). Measuring and managing soil organic matter. British Beet Research Organization. AHDB.
- Stone, L.R. & Schlegel, A.J. (2010). Tillage and crop rotation phase effects on soil physical properties in the west-central Great Plains. *Agron. J.*, 102, 483–491.
- Strudley, M.W., Green, T.R., & Ascough, J.C. (2008). Tillage effects on soil hydraulic properties in space and time: state of the science. *Soil Till. Res.*, 99, 4–48.
- Stumpp, C. & Maloszewski, P. (2010). Quantification of preferential flow and flow heterogeneities in an unsaturated soil planted with different crops using the environmental isotope delta O-18. *J. Hydrol.*, 394, 407–415.
- SSSA. (2008). Glossary of Soil Science Terms. SSSA, Madison, WI., www.soils.org/publications/soils-glossary.
- Su, Z., Li, Y., Zhang, J., Xiong, D., Dong, Y., & Zhang, S. (2017). Spatial variation in soil, SOC, and total N redistribution on affected and non-affected slope terraces due to the 8.0Wenchuan Earthquake in 2008 by using 137 Cs technique. *Catena*, 155, 191-199. <https://doi.org/10.1016/j.catena.2017.03.018>
- Tagar, A.A., Gujjar, M.A., Adamowski, J., Leghari, N., & Soomro, A. (2017). Assessment of implement efficiency and soil structure under different conventional tillage implements and soil moisture contents in a silty loam soil. *Catena*, 158, 413–420.
- Tanaka, D. & Anderson, R. (1997). Soil water storage and precipitation storage efficiency of conservation tillage systems. *J. Soil Water Conserv.*, 52, 363–367.
- Taser, O.F. & Metinoglu, F. (2005). Physical and mechanical properties of a clayey soil as affected by tillage systems for wheat growth. *Acta Agriculturae Scandinavica. Section B - Soil & Plant Sci.*, 55 (3), 186–191. doi:10.1080/09064710510008702
- Tebrugge, F. & During, R.A. (1999). Reducing tillage intensity – a review of results from a long-term study in Germany. *Soil Till. Res.*, 53 (1), 15–28.
- Thangarajan, R., Bolan, N.S., Tian, G., Naidu, R., & Kunhikrishnan, A. (2013). Role of organic amendment application on greenhouse gas emission from soil. *Sci. Total Environ.*, 465, 72–96. doi:10.1016/j.scitotenv.2013.01.031
- Thomas, G.W. (1985). Managing minimum-tillage fields, fertility and soil type. In: Wiese, A.F. (Ed.), *Weed Control in Limited-Tillage Systems*. Weed Science Society of America, Monograph 2, pp. 211-226.

- Tisdall, J.M. & Oades, J.M. (1982). Organic matter and water-stable aggregates in soils. *J. Soil Sci.*, 33, 141–163.
- Topp, G.C., Reynolds, W.D., Cook, F.J., Kirby, J.M., & Carter, M.R. (1997). Physical attributes of soil quality. In: E.G. Gregorich and M.R. Carter (ed.) *Soil quality for crop production and ecosystem health*. Dev. Soil Sci. 25. Elsevier, New York, NY, USA, pp 21-58.
- Tormena, C.A., da Silva, A.P., Imhoff, S.D.C., & Dexter, A.R. (2008). Quantification of the soil physical quality of a tropical oxisol using the S index. *Sci. Agric. (Piracicaba, Braz.)*, 65, 56–60.
- Triplett, Jr, G. B. & Dick, W.A. (2008). No-tillage crop production: A revolution in agriculture! *Agronomy J.*, 100, S-153.s
- Trojan, M.D. & Linden, D.R. (1998). Macroporosity and hydraulic properties of earthworm-affected soils as influenced by tillage and residue management. *Soil Sci. Soc. Am. J.*, 62 (6), 1687–1692.
- Troldborg, M., Aalders, I., Towers, W., Hallett, P.D., McKenzie, B.M., Bengough, A.G., Lilly, A., Ball, B.C., & Hough, R.L. (2013). Application of bayesian belief networks to quantify and map areas of risk to soil threats: using compaction as an example. *Soil Till. Res.*, 132, 56–68. <http://dx.doi.org/10.1016/j.still.2013.05.005>.
- Tuller, M. & Or, D. (2002). Unsaturated hydraulic conductivity of structured porous media. A review. *V. Z. J.*, 1, 14–37.
- Unger, P.W. (1971). Soil profile gravel layers: II. Effect on growth and water use by a hybrid forage sorghum. *Soil Sci. Soc. Am. Proc.*, 35, 980–983.
- Unger, P.W. (1991). Organic matter, nutrient, and pH distribution in no- and conventional-tillage semiarid soils. *Agron. J.*, 83, 186-191.
- Unger, P.W. (1992). Infiltration of simulated rainfall: tillage system and crop residue effects. *Soil Sci. Soc. Am. J.*, 56, 283–289.
- Unger, P.W. (1994). Impacts of tillage practices on water-use efficiency. White Paper—Farming for a Better Environment. Soil and Water Conservation Society, Ankeny, Iowa.
- Unger, P.W. & Vigil, M.F. (1998). Cover crop effects on soil water relationships. *J. Soil Water Conserv.*, 53, 200–207.
- U.S. Bureau of Reclamation. (1974). *Earth Manual*, 2nd Edition. U.S. Bureau of Reclamation. Denver, CO.
- van Bavel, C.H.M. (1950). Mean weight diameter of soil aggregates as a statistical index of aggregation. *Soil Sci. Soc. Am. Proc.*, 14, 20–23.
- van ES, H.M. (1993). Evaluation of temporal, spatial, and tillage induced variability for parameterization of soil infiltration. *Geoderma*, 60, 187-199.

- van Genuchten, M., Th. (1980). A closed-form equation for predicting the hydraulic conductivity of unsaturated soils. *Soil Sci. Soc. Am. J.*, 44, 892-898.
- van Genuchten, M. Th., Simunek, J., Leij, F.J., & Sejna, M. (1991). *The RETC code for quantifying the hydraulic functions of unsaturated soils*. Version 1.0. EPA Report 600/2-91/065, U.S. Salinity Laboratory, USDA, ARS, Riverside, California.
- VanWie, J.B., Adam, J.C., & Ullman, J.L. (2013). Conservation tillage in dryland agriculture impacts watershed hydrology. *J. Hydrol.*, 483, 26–38.
- Vereecken, H, Maes, J., Feyen, J., & Darius, P. (1989). Estimating the soil moisture retention characteristic from texture, bulk density, and carbon content. *Soil Sci.*, 148, 389-403.
- Villarreal, R., Soracco, C.G., Lozano, L.A., Melani, E.M., & Sarli, G.O. (2017). Temporal variation of soil sorptivity under conventional and no-till systems determined by a simple laboratory method. *Soil Till. Res.*, 168, 92–98.
- Vogel, H.J., Hoffmann, H., & Roth, K. (2005). Studies of crack dynamics in clay soil: I. Experimental methods, results, and morphological quantification. *Geoderma*, 125, 203–211. doi:10.1016/j.geoderma.2004.07.009
- Vogeler, I., Rogasik, J., Funder, U., Panten, K., & Schnug, E. (2009). Effect of tillage systems and P-fertilization on soil physical and chemical properties, crop yield and nutrient uptake. *Soil Till. Res.*, 103 (1), 137–143. doi:10.1016/j.still.2008.10.004
- Voorhees, W.B., Nelson, W.W., & Randall, G.W. (1986). Extent and persistence of subsoil compaction caused by heavy axle loads. *Soil Sci. Soc. Am. J.* 50, 428-433. <https://doi.org/10.2136/sssaj1986.03615995005000020035x>
- Wagger, M.G. & Mengel, D.B. (1988). The role of nonleguminous cover crops in the efficient use of water and nitrogen. p. 115–127. In W.L. Hargrove (ed.) *Cropping strategies for efficient use of water and nitrogen*. ASA, CSSA, and SSSA, Madison, WI
- Wahl, N.A, Bens, O., Buczko, U., Hangen, E., & Huttl, R.F. (2004). Effects of conventional and conservation tillage on soil hydraulic properties of a silty-loamy soil. *Phys. Chem. Earth, Parts A/B/C*, 29 (11–12): 821–829. doi: 10.1016/j.pce.2004.05.009
- Wall*, D.H., Nielsen*, U.N., Six*, J. (2015). Soil biodiversity and human health. *Nature*, 528, 69-76. doi:10.1038/nature15744.
- Wang, J., Hesketh, J.D., & Wooley, J.T. (1986). Preexisting channels and soyabean rooting patterns. *Soil Sci.*, 14(1),432–437.
- Wang, Q., Shao, M., & Horton, R. (1999). Modified Green and Ampt models for layered soil infiltration and muddy water infiltration. *Soil Sci.*, 164, 445–453.

- Wang, H., Garg, A., Huang, S., & Mei, G. (2020a). Mechanism of compacted biochar-amended expansive clay subjected to drying–wetting cycles: simultaneous investigation of hydraulic and mechanical properties. *Acta Geophysica*, 68, 737–749. <https://doi.org/10.1007/s11600-020-00423-2>
- Wang, Y., Dong, Y., Su, Z., Mudd, S.M., Zheng, Q., Hu, G., & Yan, D. (2020b). Spatial distribution of water and wind erosion and their influence on the soil quality at the agropastoral ecotone of North China. *Int. Soil Water Conserv. Res.*, 8, 253–265. <https://doi.org/10.1016/j.iswcr.2020.05.001>
- Weiler, M. & Naef, F. (2003). Simulating surface and subsurface initiation of macropore flow. *J. Hydrol.*, 273, 139Y154.
- Weiler, M. (2005). An infiltration model based on flow variability in macropores: development, sensitivity analysis and applications. *J. Hydrol.*, 310, 294–315. doi:10.1016/j.jhydrol.2005.01.010.
- Weitz, D. A., Stokes, J. P., Ball, R. C., & Kushnick, A. P. (1987). Dynamic capillary pressure in porous media: Origin of the viscous-fingering length scale. *Phys. Rev. Lett.*, 59(26), 2967–2970.
- Wilhelm, W.W., Bouzerzoar, H., & Power, J.F. (1989). Soil disturbance-residue management effect on winter wheat growth and yield. *Agron. J.*, 81, 581–588. <https://doi.org/10.2134/agronj1989.00021962008100040007x>
- Willaredt, M. & Nehls, T. (2021). Investigation of water retention functions of artificial soil-like substrates for a range of mixing ratios of two components. *JSS*, 21, 2118–2129. <https://doi.org/10.1007/s11368-020-02727-8>
- Wu, C.C., Chen, C., & Tsou, C. (1995). Effects of different mulching materials on soil moisture variation and erosion control for steep sloping lands. *J. Chinese Soil Water Conser.*, 26, 121e133. In Chinese.
- Wu, L., Swan, J. B., Paulson, W.H., & Randall, G.W. (1992). Tillage effects on measured soil hydraulic properties. *Soil Till. Res.*, 25, 17D33
- Yan, H., Wang, S., Wang, C., Zhang, G., & Patel, N. (2005). Losses of soil organic carbon under wind erosion in China. *Global Change Biology*, 11, 828–840. <https://doi.org/10.1111/j.1365-2486.2005.00950.x>
- Yan, Y., Xin, X., Xu, X., Wang, X., Yang, G., Yan, R., & Chen, B. (2013). Quantitative effects of wind erosion on the soil texture and soil nutrients under different vegetation coverage in a semiarid steppe of northern China. *Plant and Soil*, 369, 585–598. <https://doi.org/10.1007/s11104-013-1606-3>
- Yang, X. & Wander, M.M. (1998). Temporal changes in dry aggregate size and stability: tillage and crop effects on a silty loam Mollisol in Illinois. *Soil Till. Res.*, 49, 173–183.
- Yen, B.C. & Akan, A.O. (1983). Effects of soil properties on overland flow and infiltration. *J. Hydraul. Res.*, 21 (2), 153–173. DOI 10.1080/00221688309499442.

- Zehe, E. & Flühler, H. (2001). Preferential transport of isoproturon at a plot scale and a field scale tile-drained site. *J. Hydrol.*, 247, 100–115, [https://doi.org/10.1016/S0022-1694\(01\)00370-5](https://doi.org/10.1016/S0022-1694(01)00370-5).
- Zha, Y., Yang, J., Yin, L., Zhang, Y., Zeng, W., & Shi, L. (2017). A modified Picard iteration scheme for overcoming numerical difficulties of simulating infiltration into dry soil. *J. Hydrol.*, 551, 56–69. <https://doi.org/10.1016/j.jhydrol.2017.05.053>
- Zhao, Y., Wang, P., Li, J., Chen, Y., Ying, X., & Liu, S. (2009). The effects of two organic manures on soil properties and crop yields on a temperate calcareous soil under a wheat–maize cropping system. *Eur. J. Agron.*, 31 (1), 36–42. doi:10.1016/j.eja.2009.03.001
- Zhang, J., Yang, J., Yao, R., Yu, S., Li, F., & Hou, X. (2014). The Effects of Farmyard Manure and Mulch on Soil Physical Properties in a Reclaimed Coastal Tidal Flat Salt-Affected Soil. *J. Integr. Agric.*, 13(8), 1782–1790. doi:10.1016/s2095-3119(13)60530-4
- Zhang, Y., Cao, Z., Hou, F., & Cheng, J. (2021a). Characterizing Preferential Flow Paths in Texturally Similar Soils under Different Land Uses by Combining Drainage and Dye-Staining Methods. *Water*, 13, 219. <https://doi.org/10.3390/w13020219>
- Zhang, Y., Zhang, R., Zhang, B., & Xi, X. (2021b). Artificial Macropores with Sandy Fillings Enhance Desalinization and Increase Plant Biomass in Two Contrasting Salt-Affected Soils. *Appl. Sci.*, 11, 3037. <https://doi.org/10.3390/app11073037>
- Zonta, J.H., Martinez, M.A., Pruski, F.F., Silva, D.D., & Santos, M.R. (2012). Effect of successive rainfall with different patterns on soil water infiltration rate. *Braz. J. Soil Sci.*, 36 (2), 377e388. <https://doi.org/10.1590/S0100-06832012000200007>
- Zou, X., Li, J., Cheng, H., Wang, J., Zhang, C., Kang, L., Liu, W., & Zhang, F. (2018). Spatial variation of topsoil features in soil wind erosion areas of northern China. *Catena*, 167, 429-439. <https://doi.org/10.1016/j.catena.2018.05.022>

Appendix A

Soil Properties

Site 1: Loamy Sand

Appendix 1: Soil Size Distribution - Site 1

Sieve No.	Opening Size (mm)	Empty Mass (g)	Retained Mass + Sieve (g)	Retained Mass (g)	% Mass Retained	Cumulative % Retained	% Finer
4	4.75	754.30	832.44	78.14	5.27	5.27	94.73
8	2.36	708.14	757.22	49.08	3.31	8.59	91.41
16	1.18	641.44	697.75	56.31	3.80	12.39	87.61
30	0.60	606.30	876.97	270.67	18.27	30.66	69.34
40	0.43	574.15	733.76	159.61	10.77	41.43	58.57
50	0.36	334.53	420.23	85.70	5.78	47.22	52.78
60	0.25	541.19	623.12	81.93	5.53	52.75	47.25
100	0.15	519.86	780.45	260.59	17.59	70.34	29.66
200	0.08	301.06	521.12	220.06	14.85	85.19	14.81
Pan	0.00	430.87	650.27	219.40	14.81	100.00	0.00

Appendix 2: Soil Classification - Site 1

Properties			
D10	0.02	USCS	
D30	0.16	% Gravel	5.8
D60	0.45	% Sand	80.92
Cu	22.50	% Fines	13.28
Cc	2.84	Group Symbol	SW
LL	54.63	Group Name	Well-graded Sand
PL	44.06	USDA textural classification	
PI	10.57		SITE 1
OMC(%)	8.60	% Sand	86
% passing No. 200 sieve	14.81	% Silt	14
% retained on No. 200 sieve	85.19	% Clay	0
% passing No. 4 sieve	94.73	USDA textural class.	Loamy Sand
% retained on No. 4 sieve	5.27		

Appendix 3: BD and DD – Site 1

Treatment	Depth	Trial	L (cm)	V(m ³)	M(can1) (g)	M (moist soil+can1) (g)	M(can2) (g)	M (dry soil+can) (g)	Bulk Density	Dry Density
NT	0-10cm	1	8.6	0.000137	5.83	150.13	11.65	124.32	1055.00	823.75
		2	8.9	0.000142	5.83	176.33	11.65	144.14	1204.54	936.01
		3	8.9	0.000142	5.83	174.08	11.65	144.55	1188.64	938.90
RT	0-20cm	1	9.5	0.000151	5.83	146.01	11.65	121.17	927.79	724.86
		2	9.5	0.000151	5.83	142.92	11.65	114.34	907.33	679.66
		3	9.5	0.000151	5.83	161.36	11.65	129.96	1029.38	783.04
MTA	0-20cm	1	9.5	0.000151	5.83	112.03	11.65	95.44	702.89	554.57
		2	9.5	0.000151	5.83	135.69	11.65	115.55	859.48	687.67
		3	9.5	0.000151	5.83	156.02	11.65	131.96	994.04	796.28
MT	0-20cm	1	9.5	0.000151	5.83	109.26	11.65	91.69	684.55	529.75
		2	9.5	0.000151	5.83	131.87	11.65	110.15	834.20	651.93
		3	9.5	0.000151	5.83	143.08	11.65	118.36	908.39	706.26

Appendix 4: SD – Site 1

Treatment	Depth	L (cm)	V(m ³)	M (can) (g)	M (saturated+can) (g)	Saturated Density (kg/m ³)
NT	0-10cm	10	0.000159	55	267	1332.97177
RT	0-20cm	8	0.000127	50	216	1304.677558
MTA	0-20cm	8.5	0.000135	49	215	1227.931819
MT	0-20cm	9	0.000143	48	225	1236.561862

Appendix 5: Porosity – Site 1

Treatment	Dry Density	M (saturated+can) (g)	Porosity
NT	823.7491	1332.972	0.509223
	936.005	1332.972	0.396967
	938.9016	1332.972	0.39407
RT	724.8613	1304.678	0.579816
	679.6568	1304.678	0.625021
	783.0382	1304.678	0.521639
MTA	554.5666	1227.932	0.673365
	687.6652	1227.932	0.540267
	796.2752	1227.932	0.431657
MT	529.7471	1236.562	0.706815
	651.9251	1236.562	0.584637
	706.2632	1236.562	0.530299

Appendix 6: Residual Moisture Content – Site 1

Treatment	L (cm)	V(m3)	M (can) (g)	M (residual+can) (g)	M residual (g)	ρ (kg/m ³)	M dry (g)	Mw (g)	Vw (m3)	θ_r (m ³ /m ³)
NT	10	0.000159	55	208	153	962.0032	131.0116	21.98837	2.19884E-05	0.138254
	10	0.000159	55	208	153	962.0032	148.8652	4.134831	4.13483E-06	0.025998
	10	0.000159	55	208	153	962.0032	149.3258	3.674157	3.67416E-06	0.023102
RT	8	0.000127	50	148	98	770.2313	92.22737	5.772632	5.77263E-06	0.04537
	8	0.000127	50	148	98	770.2313	86.47579	11.52421	1.15242E-05	0.090575
	8	0.000127	50	148	98	770.2313	99.62947	-1.62947	1.62947E-06	0.01281
MTA	8.5	0.000135	49	155	106	784.101	74.97	31.03	0.00003103	0.229534
	8.5	0.000135	49	155	106	784.101	92.96316	13.03684	1.30368E-05	0.096436
	8.5	0.000135	49	155	106	784.101	107.6458	-1.64579	1.64579E-06	0.01217
MT	9	0.000143	48	152	104	726.5674	75.82737	28.17263	2.81726E-05	0.19682
	9	0.000143	48	152	104	726.5674	93.31579	10.68421	1.06842E-05	0.074642
	9	0.000143	48	152	104	726.5674	101.0937	2.906316	2.90632E-06	0.020304

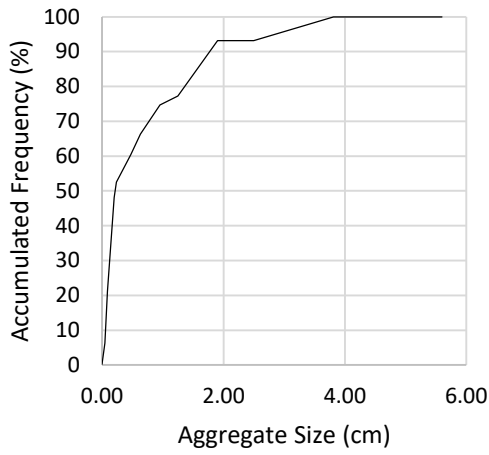
Appendix 7: Organic Matter Content – Site 1

Treatment	Depth	Trial	M(can) (g)	M (dry soil+can) (g)	M (burnt soil+can) (g)	%OMC
NT	0-10cm	1	2.37	35.06	32.21	8.72
		2	1.56	25.99	23.89	8.60
		3	1.53	38.75	35.59	8.49
RT	0-20cm	1	2.26	37.64	33.95	10.43
		2	1.54	38.05	34.41	9.97
		3	2.30	37.90	34.25	10.25
MTA	0-20cm	1	1.50	29.82	25.82	14.12
		2	2.54	35.25	30.53	14.43
		3	1.53	27.89	24.53	12.75
MT	0-20cm	1	2.31	22.71	20.13	12.65
		2	2.28	32.63	29.15	11.47
		3	2.28	37.81	33.76	11.40

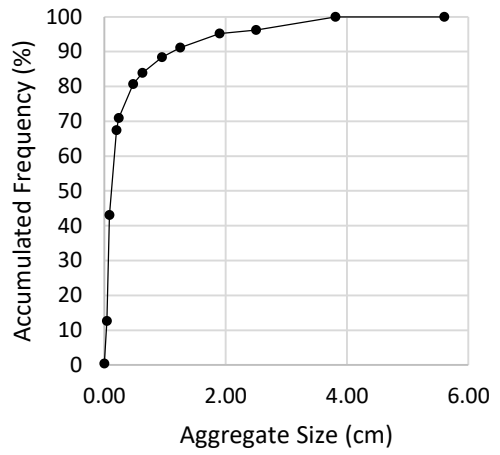
Appendix 8: Saturated Hydraulic Conductivity – Site 1

Treatment	Reading (Trial)	Length, L (cm)	Constant Head, h1 (cm)	Mass of Water Collected, M (g)	Volume of Water Collected, Q (m ³)	Duration of water collected, t (sec)	Hydraulic Conductivity, k (m/sec)
NT	1	13.6	547	123	1.30105E-05	600	1.66583E-07
	2	13.6	547	123	1.30105E-05	600	1.66583E-07
	3	13.6	547	122	1.20097E-05	600	1.53769E-07
	4	13.6	504	120.5	1.05085E-05	600	1.46343E-07
	5	13.6	504	120	1.00081E-05	600	1.39375E-07
	6	13.6	504	120	1.00081E-05	600	1.39375E-07
RT	1	13.5	267	132	2.20178E-05	60	5.88928E-06
	2	13.5	267	133	2.30186E-05	60	6.15698E-06
	3	13.5	267	133	2.30186E-05	60	6.15698E-06
	4	13.5	282	168	5.8047E-05	60	1.46589E-05
	5	13.5	282	140	3.00243E-05	60	7.58219E-06
	6	13.5	282	140	3.00243E-05	60	7.58219E-06
MT	1	14	157	127	1.70138E-05	60	8.33699E-06
	2	14	157	128	1.80146E-05	60	8.8274E-06
	3	14	157	127	1.70138E-05	60	8.33699E-06
	4	14	114	130.5	2.05166E-05	120	7.17745E-06
	5	14	114	131	2.1017E-05	120	7.35251E-06
	6	14	114	130	2.00162E-05	120	7.00239E-06
Treatment	Reading (Trial)	Length, L(cm)	h1 (cm)	h2 (cm)	t2 (sec)	Hydraulic Conductivity, k (m/sec)	
MTA	1	14	84	26.5	36.7	2.6041E-05	
	2	14	83	25	56.26	1.76689E-05	
	3	14	83.8	33	42.39	1.82121E-05	
	4	14	82.5	32.2	42.27	1.84383E-05	

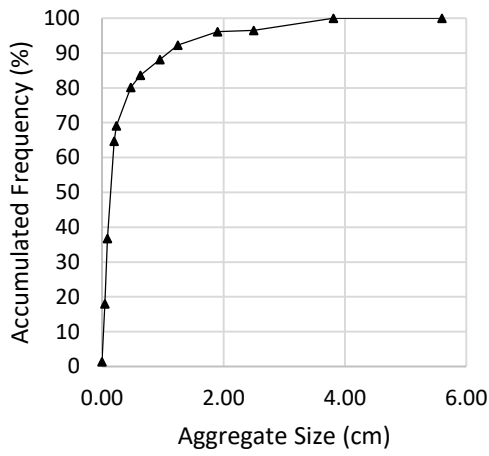
Appendix 9: Frequency density function (f) of the aggregate distribution – Site 1



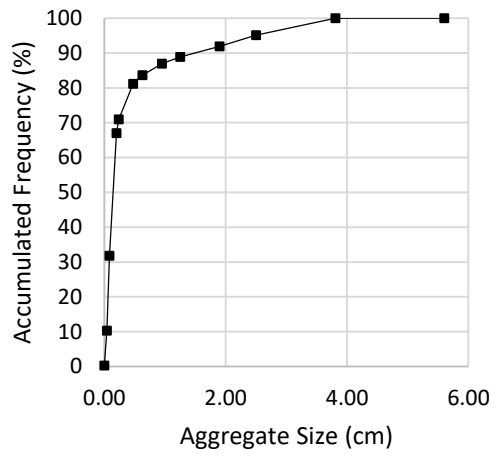
— NT



—● RT



—▲ MTA



—■ MT

Site 2: Clay Loam

Appendix 10: Soil Size Distribution - Site 2

Sieve No.	Opening Size (mm)	Empty Mass (g)	Retained Mass + Sieve (g)	Retained Mass (g)	% Mass Retained	Cumulative % Retained	% Finer
4	4.75	754.14	754.14	0.00	0.00	0.00	100.00
8	2.36	707.91	707.91	0.00	0.00	0.00	100.00
16	1.18	639.36	639.36	0.00	0.00	0.00	100.00
40	0.43	573.66	575.35	1.69	0.15	0.15	99.85
50	0.36	333.82	355.07	21.25	1.95	2.10	97.90
60	0.25	540.82	559.64	18.82	1.73	3.83	96.17
100	0.15	519.99	597.45	77.46	7.10	10.93	89.07
200	0.08	301.32	610.78	309.46	28.37	39.30	60.70
Pan	0.00	488.67	1150.85	662.18	60.70	100.00	0.00

Appendix 11: Soil Classification - Site 2

Properties		USCS	
D10	0.001		
D30	0.002	% Gravel	0
D60	0.73	% Sand	39.3
Cu	730.00	% Fines	60.7
Cc	0.003	Group Symbol	CH
LL	61.41	Group Name	Sandy Fat Clay
PL	26.02	USDA textural classification	
PI	35.39		SITE 1
OMC(%)	9.24	% Sand	45
% passing No. 200 sieve	60.70	% Silt	25
% retained on No. 200 sieve	39.30	% Clay	30
% passing No. 4 sieve	100.00	USDA textural class.	Clay Loam
% retained on No. 4 sieve	0.00		

Appendix 12: BD and DD – Site 2

Treatment	Depth	Trial	L (cm)	V(m ³)	M(can) (g)	M (moist soil+can) (g)	M (dry soil+can) (g)	Bulk Density	Dry Density
NT	0-10cm	1	7	0.000111	5.83	235.16	174.92	2059.91	1518.82
		2	7.5	0.000119	5.83	224.69	173.12	1834.84	1402.47
		3	8	0.000127	5.83	246.47	190.70	1891.30	1452.99
	10-20cm	1	6	9.54E-05	5.83	173.60	132.12	1758.08	1323.44
		2	6.5	0.000103	5.83	201.57	155.22	1893.41	1445.08
		3	5	7.95E-05	5.83	165.69	131.83	2010.27	1584.48

	20-30cm	1	9.5	0.000151	5.83	262.92	206.87	1701.54	1330.59
		2	9.5	0.000151	5.83	289.32	228.99	1876.29	1476.99
		3	8.5	0.000135	5.83	260.83	204.74	1886.30	1471.37
	30-40cm	1	6.5	0.000103	5.83	205.47	162.70	1931.16	1517.44
		2	8	0.000127	5.83	254.09	200.82	1951.20	1532.52
		3	9	0.000143	5.83	260.08	206.26	1776.27	1400.25
RT	0-20cm	1	10	0.000159	5.83	149.64	141.20	904.22	851.15
		2	10	0.000159	5.83	177.40	152.96	1078.76	925.09
		3	10	0.000159	5.83	144.14	133.85	869.64	804.94
MTA	0-20cm	1	10	0.000159	5.83	110.43	96.84	657.68	572.23
		2	10	0.000159	5.83	119.45	104.54	714.40	620.65
		3	10	0.000159	5.83	124.51	109.65	746.21	652.78
MT	0-20cm	1	10	0.000159	5.83	108.65	95.55	646.49	564.12
		2	10	0.000159	5.83	124.46	111.11	745.90	661.96
		3	10	0.000159	5.83	121.55	105.91	727.60	629.26

Appendix 13: SD – Site 2

Treatment	Depth	L (cm)	V(m3)	M (can) (g)	M (saturated+can) (g)	Saturated Density (kg/m3)
NT	0-10cm	10	0.000159	52	335	1779.391561
RT	0-20cm	6	9.54E-05	49	205	1634.776699
MTA	0-20cm	8	0.000127	48	220	1351.834578
MT	0-20cm	8.5	0.000135	49	235	1375.875412

Appendix 14: Porosity – Site 2

Treatment	Dry Density	Saturated Density (kg/m3)	Porosity
NT	1518.815	1779.392	0.260576
	1402.471	1779.392	0.376921
	1452.986	1779.392	0.326405
	1323.436	1779.392	0.455956
	1445.085	1779.392	0.334307
	1584.476	1779.392	0.194916
	1330.589	1779.392	0.448802
	1476.991	1779.392	0.302401
	1471.373	1779.392	0.308019
	1517.44	1779.392	0.261951
	1532.525	1779.392	0.246867
	1400.249	1779.392	0.379142
RT	851.1528	1634.777	0.783624
	925.095	1634.777	0.709682
	804.9389	1634.777	0.829838

MTA	572.2347	1351.835	0.7796
	620.6493	1351.835	0.731185
	652.7789	1351.835	0.699056
MT	564.1237	1375.875	0.811752
	661.9588	1375.875	0.713917
	629.2633	1375.875	0.746612

Appendix 15: Residual Moisture Content – Site 2

Treatment	L (cm)	V(m3)	M (can) (g)	M (residual+can) (g)	M residual (g)	ρ (kg/m ³)	M dry (g)	Mw (g)	Vw (m3)	θ_r (m ³ /m ³)
NT	10	0.000159	52	332	280	1760.529	241.5571	38.44286	3.84429E-05	0.241713
	10	0.000159	52	332	280	1760.529	223.0533	56.94667	5.69467E-05	0.358058
	10	0.000159	52	332	280	1760.529	231.0875	48.9125	4.89125E-05	0.307542
	10	0.000159	52	332	280	1760.529	210.4833	69.51667	6.95167E-05	0.437093
	10	0.000159	52	332	280	1760.529	229.8308	50.16923	5.01692E-05	0.315444
	10	0.000159	52	332	280	1760.529	252	28	0.000028	0.176053
	10	0.000159	52	332	280	1760.529	211.6211	68.37895	6.83789E-05	0.42994
	10	0.000159	52	332	280	1760.529	234.9053	45.09474	4.50947E-05	0.283538
	10	0.000159	52	332	280	1760.529	234.018	45.98824	4.59882E-05	0.289156
	10	0.000159	52	332	280	1760.529	241.3385	38.66154	3.86615E-05	0.243088
	10	0.000159	52	332	280	1760.529	243.7375	36.2625	3.62625E-05	0.228004
	10	0.000159	52	332	280	1760.529	222.7	57.3	0.0000573	0.36028
RT	6	9.54E-05	49	150	101	1058.413	81.222	19.778	0.000019778	0.20726
	6	9.54E-05	49	150	101	1058.413	88.278	12.722	0.000012722	0.133318
	6	9.54E-05	49	150	101	1058.413	76.812	24.188	0.000024188	0.253474
MTA	8	0.000127	48	166	118	927.4214	72.808	45.192	0.000045192	0.355187
	8	0.000127	48	166	118	927.4214	78.968	39.032	0.000039032	0.306772
	8	0.000127	48	166	118	927.4214	83.056	34.944	0.000034944	0.274642
MT	8.5	0.000135	49	165	116	858.0728	76.262	39.738	0.000039738	0.293949
	8.5	0.000135	49	165	116	858.0728	89.488	26.512	0.000026512	0.196114
	8.5	0.000135	49	165	116	858.0728	85.068	30.932	0.000030932	0.22881

Appendix 16: Organic Matter Content – Site 2

Treatment	Depth	Trial	M(can) (g)	M (dry soil+can) (g)	M (burnt soil+can) (g)	%OMC
NT	0-10cm	1	1.53	54.66	48.22	12.12
		2	1.52	59.94	46.25	23.43
		3	2.30	54.31	48.31	11.54
	10-20cm	1	2.35	59.47	54.20	9.23

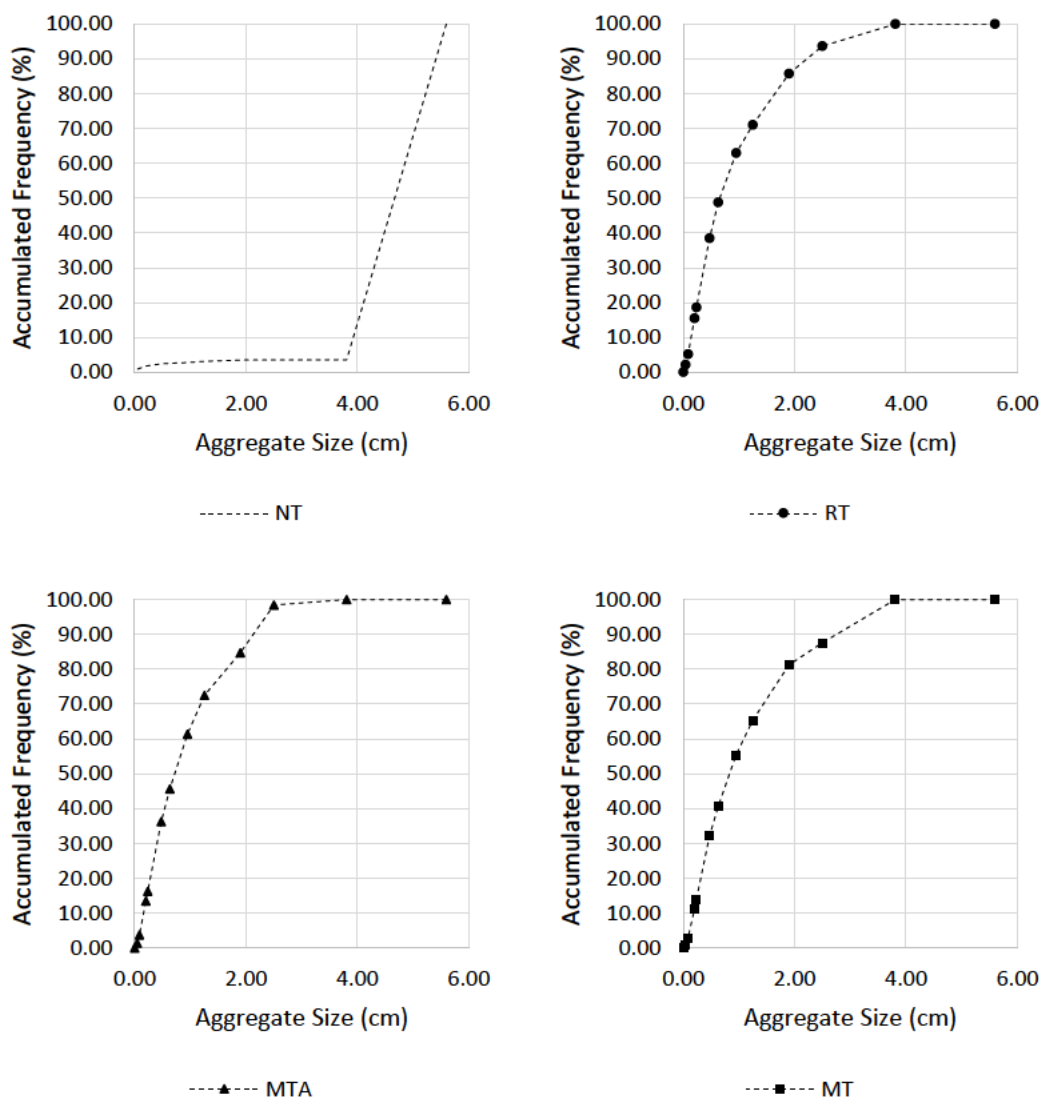
		2	1.51	35.57	32.33	9.51
		3	1.59	58.71	53.92	8.39
		1	1.53	52.45	47.54	9.64
	20-30cm	2	1.51	40.43	36.68	9.64
		3	1.52	46.87	42.46	9.72
		1	1.54	40.30	36.55	9.67
	30-40cm	2	2.30	52.62	48.60	7.99
		3	2.31	58.56	53.27	9.40
		1	1.52	47.02	42.55	9.82
RT	0-20cm	2	1.53	44.29	39.80	10.50
		3	1.53	49.47	44.58	10.20
		1	1.52	31.46	27.00	14.90
MTA	0-20cm	2	2.35	28.71	24.08	17.56
		3	2.29	36.26	31.50	14.01
		1	1.52	33.10	28.81	13.58
MT	0-20cm	2	2.26	46.27	41.60	10.61
		3	2.29	48.11	43.25	10.61

Appendix 17: Saturated Hydraulic Conductivity – Site 2

Treatment	Reading (Trial)	Length, L (cm)	Constant Head, h (cm)	Mass of Water Collected, M (g)	Volume of Water Collected, Q (m ³)	Duration of water collected, t (sec)	Hydraulic Conductivity, k (m/sec)
NT	1	13	413	111	1.00081E-06	3600	2.72621E-09
	2	13	413	111	1.00081E-06	3600	2.72621E-09
	3	13	413	112	2.00162E-06	3600	5.45242E-09
	4	13	413	111	1.00081E-06	3600	2.72621E-09
RT	1	12.7	547	169	5.90478E-05	60	7.06001E-06
	2	12.7	547	171	6.10495E-05	60	7.29933E-06
	3	12.7	547	170	6.00486E-05	60	7.17967E-06
	4	12.7	504	141	3.10251E-05	60	4.03469E-06
	5	12.7	504	140.5	3.05247E-05	60	3.96962E-06
	6	12.7	504	140	3.00243E-05	60	3.90454E-06
MT	1	13.3	547	142	3.20259E-05	60	4.01006E-06
	2	13.3	547	141	3.10251E-05	60	3.88475E-06
	3	13.3	547	141	3.10251E-05	60	3.88475E-06
	4	13.3	504	133	2.30186E-05	60	3.13491E-06
	5	13.3	504	132	2.20178E-05	60	2.99861E-06
	6	13.3	504	132	2.20178E-05	60	2.99861E-06
Treatment	Reading (Trial)	Length, L (cm)	h1 (cm)	h2 (cm)	delta_t (sec)	Hydraulic Conductivity, k (m/sec)	
MTA	1	13	91	42	12.75	4.6648E-05	
	2	13	86	42	11.25	4.90036E-05	
	3	13	84	45.5	11.45	4.11894E-05	

	4	13	87.5	43.5	12.37	4.34599E-05
--	---	----	------	------	-------	-------------

Appendix 18: Frequency density function (*f*) of the aggregate distribution – Site 2



Crop Residues & Chicken Manure

Appendix 19: BD and DD – CC & MC

Treat ment	Depth	Trial	L (cm)	V(m3)	M(can) (g)	M (moist soil+can) (g)	M (dry soil+can) (g)	Bulk Density	Dry Density
CC	0- - 5cm	1	10	0.000 159	5.83	19.05	19.05	83.12	83.12
		2	10	0.000 159	5.83	19.04	19.04	83.06	83.06
		3	10	0.000 159	5.83	19.33	19.33	84.88	84.88

MC	0- -5cm	1	9	0.000143	5.83	55.24	45.75	345.19	278.89
		2	9	0.000143	5.83	55.68	43.96	348.26	266.38
		3	9	0.000143	5.83	54.53	44.85	340.23	272.60

Appendix 20: SD – CC & MC

Treatment	Depth	L (cm)	V(m3)	M (can) (g)	M (saturated+can) (g)	Saturated Density (kg/m3)
CC	0- -5cm	8.3	0.000132	51	180	977.2298157
MC	0- -5cm	9.3	0.000148	50	200	1014.129466

Appendix 21: Porosity – CC & MC

Treatment	Dry Density	Saturated Density (kg/m3)	Porosity
CC	83.12211	977.2298	0.894108
	83.05923	977.2298	0.894171
	84.88264	977.2298	0.892347
MC	278.8901	1014.129	0.735239
	266.3848	1014.129	0.747745
	272.6025	1014.129	0.741527

Appendix 22: Residual Moisture Content – CC & MC

Treatment	L (cm)	V(m3)	M (can) (g)	M (residual+can) (g)	M residual (g)	ρ (kg/m3)	M dry (g)	Mw (g)	Vw (m3)	θ_r (m3/m3)
CC	8.3	0.000132	51	68	17	128.7822	10.9726	6.0274	6.0274E-06	0.04566
	8.3	0.000132	51	68	17	128.7822	10.9643	6.0357	6.0357E-06	0.045723
	8.3	0.000132	51	68	17	128.7822	11.205	5.795	0.000005795	0.0439
MC	9.3	0.000148	50	140	90	608.4777	41.25067	48.74933	4.87493E-05	0.329588
	9.3	0.000148	50	140	90	608.4777	39.401	50.599	0.000050599	0.342093
	9.3	0.000148	50	140	90	608.4777	40.32067	49.67933	4.96793E-05	0.335875

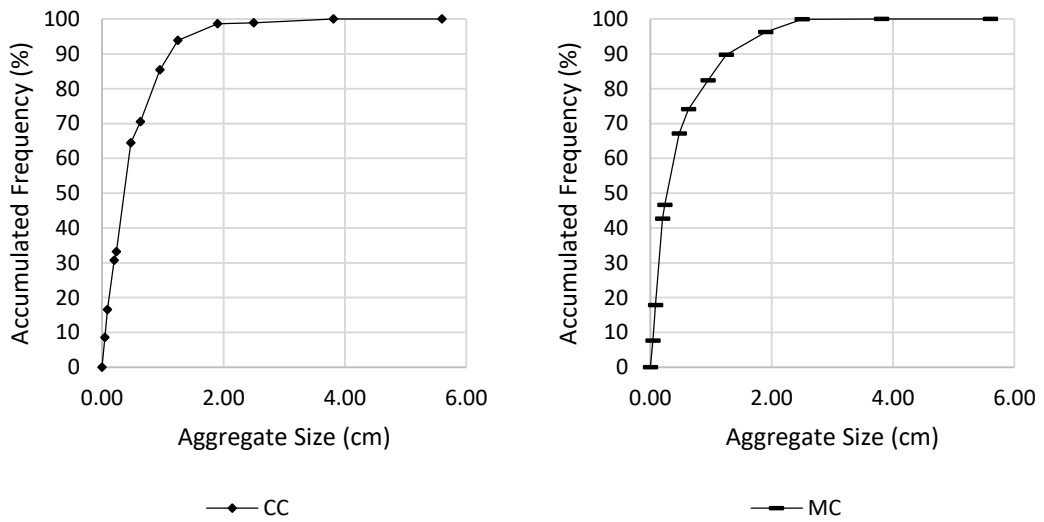
Appendix 23: Organic Matter Content – CC & MC

Treatment	Depth	Trial	M(can) (g)	M (dry soil+can) (g)	M (burnt soil+can) (g)	%OMC
CC	0- -5cm	1	1.52	4.76	1.77	92.28
		2	2.55	6.66	2.93	90.75
		3	2.24	5.68	2.56	90.70
MC	0- -5cm	1	2.28	17.50	10.83	43.82
		2	2.27	21.50	13.86	39.73
		3	2.33	17.23	11.14	40.87

Appendix 24: Saturated Hydraulic Conductivity – CC & MC

Treatment	Reading (Trial)	Length, L (cm)	Constant Head, h (cm)	Mass of Water Collected, M (g)	Volume of Water Collected, Q (m ³)	Duration of water collected, t (sec)	Hydraulic Conductivity, k (m/sec)
CC	1	12.5	132	205	9.5077E-05	10	0.000302239
	2	12.5	132	204	9.40762E-05	10	0.000299058
	3	12.5	132	208	9.80794E-05	10	0.000311783
	4	12.5	89	182	7.20584E-05	10	0.000359526
	5	12.5	89	175	6.50527E-05	10	0.000324573
	6	12.5	89	173	6.30511E-05	10	0.000314586
Treatment	Reading (Trial)	Length, L(cm)	h1 (cm)	h2 (cm)	delta_t (sec)	Hydraulic Conductivity, k (m/sec)	
MC	1	13	75	50	90	3.46551E-06	
	2	13	83	55	89	3.55668E-06	
	3	13	85	60	77	3.47959E-06	

Appendix 25: Frequency density function (*f*) of the aggregate distribution – CC & MC



Appendix B

Soil-Pore Structure

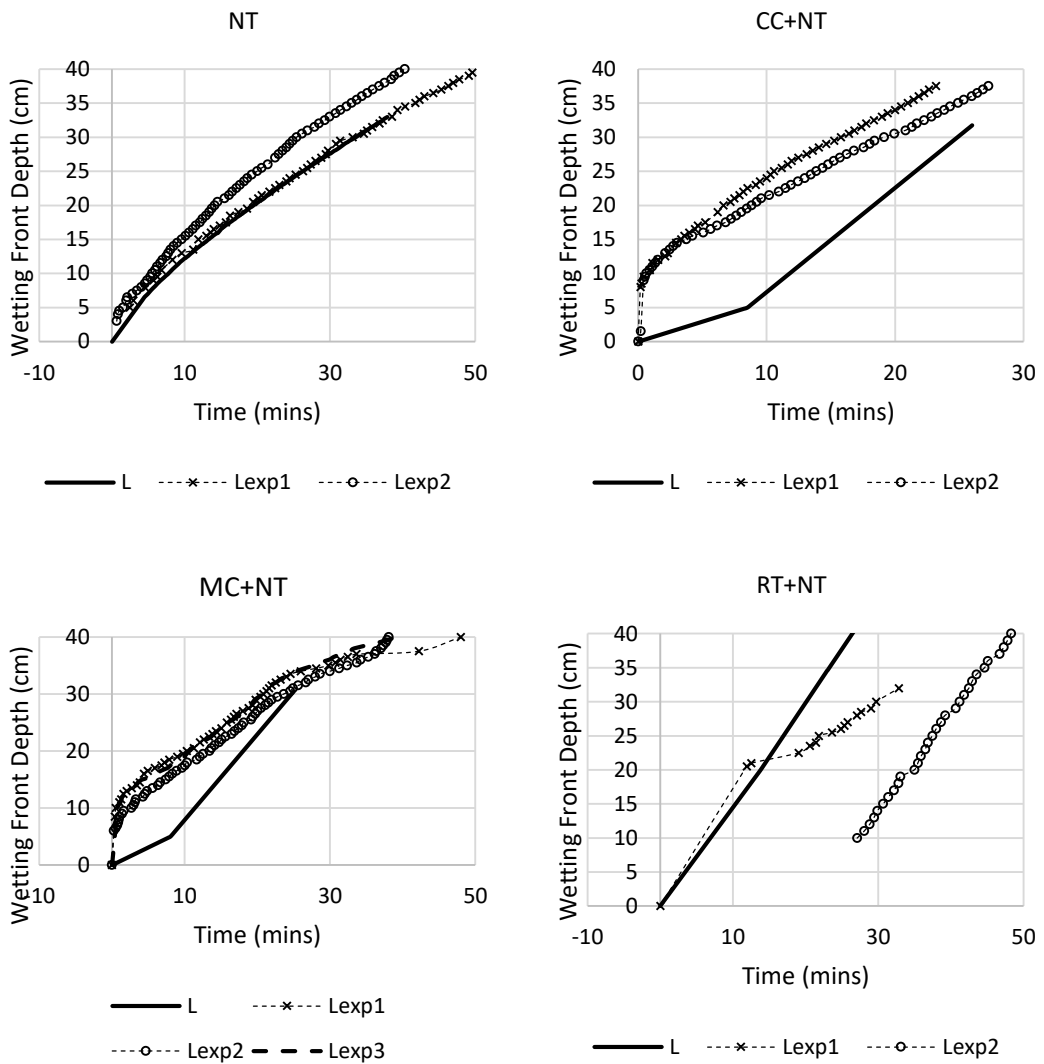
Appendix 26: Volumetric content of pores as calculated in ImageJ

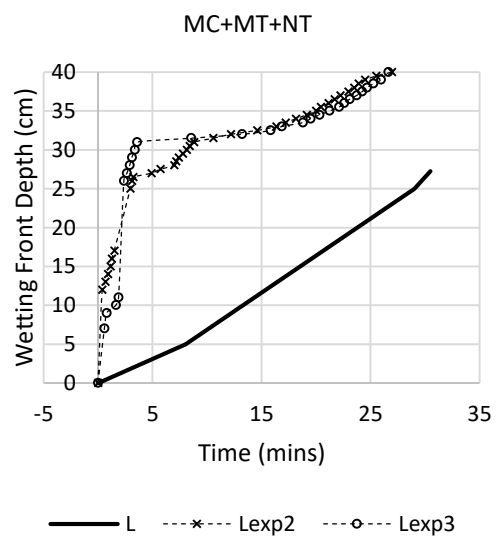
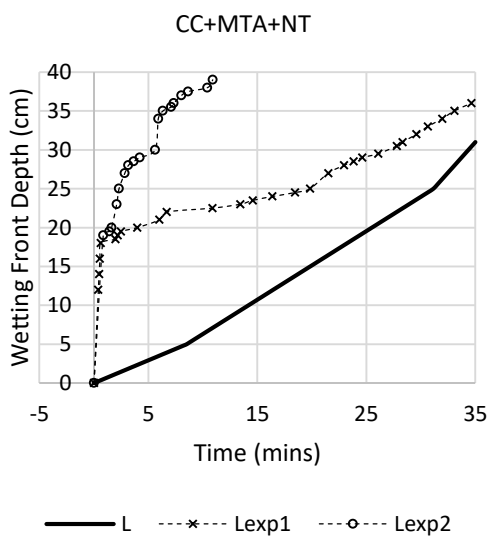
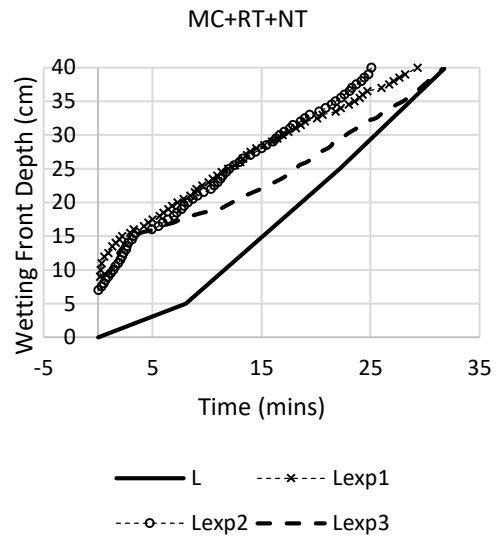
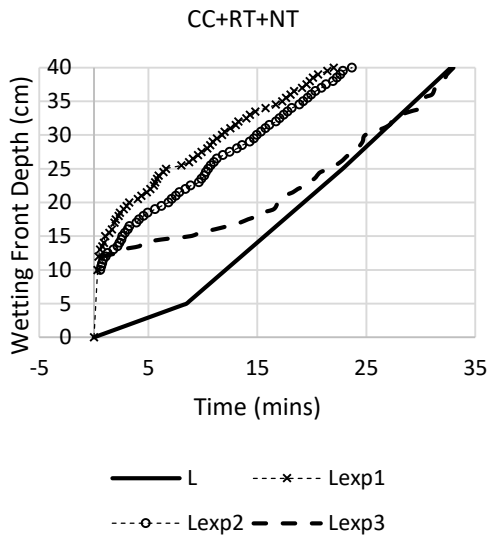
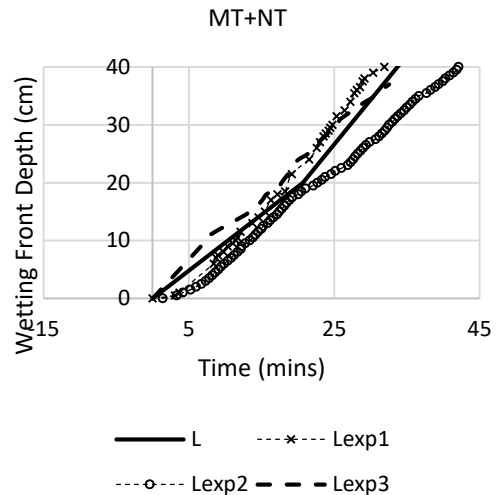
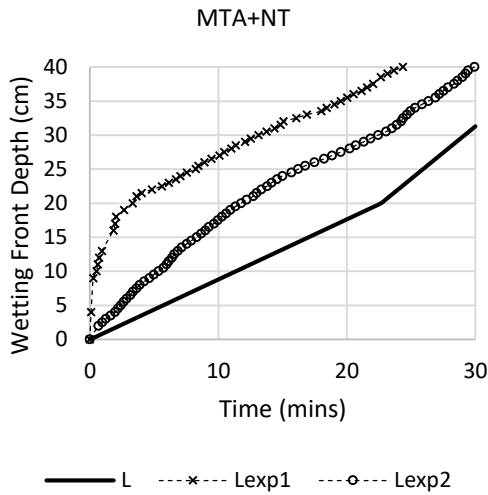
A(m m2)	r (mm)	h (mm)	Volumetric Content (%)									
			Crop Resid ues	Manur e	SITE 1				SITE 2			
					MT	MTA	NT	RT	MT	MTA	NT	RT
0.05	0.126 157	117.7 212	1.769 055	0 519 668	10.08 032	3.062 991	5.026 069	20.09 653	3.268 871	1.204 093	0.013 686	0.031 822
0.16	0.225 676	65.80 817	0.068 639	2 562 437	3.489 175	7.389 174	0.173 338	10.85 603	1.464 643	1.192 776	0.010 285	0.235 739
0.38	0.347 79	42.70 198	0.113 471	5.812 656	7.622 511	0.702 745	0.236 693	1.547 964	1.319 342	1.210 938	0	0.446 122
0.73	0.482 044	30.80 905	0.222 047	4 229 654	1.188 722	1.269 902	0.327 306	2.744 198	1.123 099	0.700 793	0	0.978 101
1.4	0.667 558	22.24 722	4.791 134	11.39 482	1.710 07	1.596 224	0.307 716	3.624 821	0.842 091	0.291 962	0	1.715 683
2.4	0.874 039	16.99 16	2.559 719	0.697 146	1.178 339	0.845 904	0.156 556	2.276 946	0.500 618	0.781 499	0	1.403 834
3.45	1.047 936	14.17 197	1.827 674	1.468 664	0.895 433	0.524 823	0.092 871	1.496 259	0.194 767	0.134 032	0	1.092 98
6	1.381 977	10.74 643	14.84 065	10.01 216	2.899 887	1.146 348	0.312 092	4.047 717	0.290 845	0.110 072	0	4.280 385
13.5	2.072 965	7.164 286	24.21 004	0 343 304	2.402 849	0.545 105	0.221 073	2.025 777	0.089 161	0.010 344	0	3.299 251
24	2.763 953	5.373 214	10.56 114	0.026 031	1.300 464	0.177 316	0.080 061	0.947 548	0.783 369	0.218 276	0	2.093 372
35	3.337 791	4.449 444	6.958 93	0	1.291 296	0.067 288	0.010 305	0.433 203	0.450 502	0.026 076	0	0.962 375
44	3.742 41	3.968 382	5.552 763	0	0.822 606	0.012 126	0.025 912	0.252 111	1.212 864	0	0	0.549 171
53	4.107 362	3.615 779	4.256 389	0	0.582 001	0.015 094	0.028 916	0.096 68	0.447 692	0	0	0.227 56
64	4.513 517	3.290 408	3.248 431	0	0.664 71	0.017 808	0.034 95	0.099 131	0.476 86	0	0	0.075 189
75	4.886 025	3.039 549	1.218 781	0	0.356 62	0	0.038 92	0	- 0.398 9	0	0	0.044 63
85	5.201 571	2.855 159	0.460 132	0	0.477 739	0	0.021 092	0	0.537 65	0	0	0.025 019
105	5.781 223	2.568 888	1.010 832	0	1.361 433	0	0.140 543	0	0.549 988	0	0	0.088 131
133	6.506 552	2.282 517	0	0	0.496 088	0	0.224 417	0	0.651 702	0	0	0
160	7.136 496	2.081 037	1.044 41	0	0.187 761	0	0.040 043	0	0.363 195	0	0	0
225	8.462 844	1.754 884	0	0	0.176 905	0	0	0	0.888 537	0	0	0
272	9.304 853	1.596 083	0	0	0	0	0	0	0.074 308	0	0	0
353	10.60 016	1.401 046	0	0	0	0	0	0	0.326 269	0	0	0
440	11.83 454	1.254 913	0	0	0	0	0	0	0.259 746	0	0	0
526	12.93 951	1.147 749	0	0 372 984	0	0	0	0	0	0	0	0
1265	20.06 644	0.740 107	0	0	0	0	0	0	0	0	0	0

Appendix C

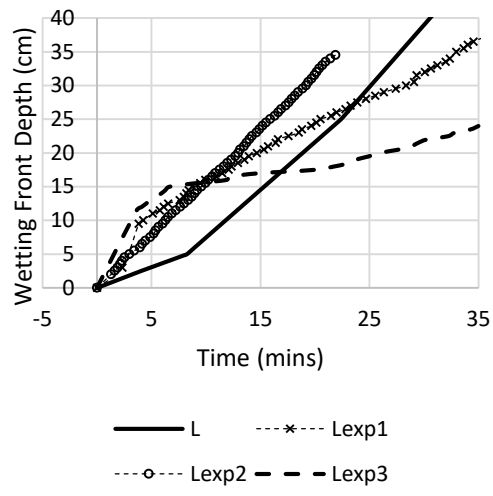
Experimental Data – Preferential Flow for Site 1

Appendix 27: Experimental vs Theoretical Wetting Front with respect to time





CC+MC+RT+NT



Appendix D

MATLAB Code for GARALS

2-Layers Soil Profile

```
%TWO LAYERS SOIL PROFILE
clc;
clear;

P=0.04; %water entry rate [cm/min]

%CC
Ksmo=1.91176478715198; %the saturated hydraulic conductivity of the modified layer
[cm/min]
MCI_mo=0.01; %the initial moisture content of the modified layer [m3/m3]
MCS_mo=0.893541823877931; %the saturated moisture content of the modified layer
[m3/m3]
dMCmo=MCS_mo-MCI_mo; %delta gamma of the modified layer which is the difference
between the saturated and the initial moisture contents [m3/m3]
H_mo=-17654.21; %matric potential of the modified layer [cm]
zmo=5; %depth of the modified layer [cm]

%MC
Ksmo=0.0210035543615512; %the saturated hydraulic conductivity of the modified layer
[cm/min]
MCI_mo=0.0357; %the initial moisture content of the modified layer [m3/m3]
MCS_mo=0.741503670980025; %the saturated moisture content of the modified layer
[m3/m3]
dMCmo=MCS_mo-MCI_mo; %delta gamma of the modified layer which is the difference
between the saturated and the initial moisture contents [m3/m3]
H_mo=-84076.2; %matric potential of the modified layer [cm]
zmo=5; %depth of the modified layer [cm]

%RT
Ksmo=0.0480265348303373; %the saturated hydraulic conductivity of the modified layer
[cm/min]
MCI_mo=0.05; %the initial moisture content of the modified layer [m3/m3]
MCS_mo=0.57549214025019; %the saturated moisture content of the modified layer
[m3/m3]
dMCmo=MCS_mo-MCI_mo; %delta gamma of the modified layer which is the difference
between the saturated and the initial moisture contents [m3/m3]
H_mo=-528.212623595688; %matric potential of the modified layer [cm]
zmo=20; %depth of the modified layer [cm]

%MTA
Ksmo=0.120540439180942; %the saturated hydraulic conductivity of the modified layer
[cm/min]
MCI_mo=0.078; %the initial moisture content of the modified layer [m3/m3]
MCS_mo=0.54842949366671; %the saturated moisture content of the modified layer
[m3/m3]
dMCmo=MCS_mo-MCI_mo; %delta gamma of the modified layer which is the difference
between the saturated and the initial moisture contents [m3/m3]
H_mo=-54879.88; %matric potential of the modified layer [cm]
zmo=20; %depth of the modified layer [cm]

%MT
Ksmo=0.0470337095427571; %the saturated hydraulic conductivity of the modified layer
[cm/min]
MCI_mo=0.0579; %the initial moisture content of the modified layer [m3/m3]
MCS_mo=0.6072500492759; %the saturated moisture content of the modified layer [m3/m3]
dMCmo=MCS_mo-MCI_mo; %delta gamma of the modified layer which is the difference
between the saturated and the initial moisture contents [m3/m3]
H_mo=-26534.97; %matric potential of the modified layer [cm]
zmo=20; %depth of the modified layer [cm]
```

```

%INPUT PROPERTIES

Ksumo=0.000912029168087834; %the saturated hydraulic conductivity of the unmodified
layer [cm/min]
MCI_umo=0.2; %the initial moisture content of the unmodified layer [m3/m3]
MCS_umo=0.433419880806727; %the saturated moisture content of the unmodified layer
[m3/m3]
dMCumo=MCS_umo-MCI_umo; %delta gamma of the unmodified layer which is the difference
between the saturated and the initial moisture contents [m3/m3]
H_umo=-1136.39; %matric potential of the unmodified layer [cm] measured using TEROS21
H0=0; %depth of ponded water [cm]
dHmo=abs(H0-H_umo);
dHumo=abs(H0-H_umo);
A_=(zmo*(dMCmo-dMCumo))/(Ksmo-Ksumo);
B_=(dMCumo/Ksumo);
tzmo=(zmo*dMCmo)/P;
tp1L=(Ksmo*dHmo*dMCmo)/(P*(P-Ksmo));
tp1L=abs(tp1L);
tp2L=tzmo+((Ksumo*dHumo*dMCumo)/(P*(P-Ksumo)));
tp2L=abs(tp2L);

zm=[0:1:100];
n=length(zm);
v=zeros(1,n);
t=zeros(1,n);
Zm=zeros(1,n);
Kc_=zeros(1,n);

if tp1L<=tzmo %1rst layer ponding
    tp=tp1L;
    Zp=P*tp;
    zp=Zp/dMCmo;
    a=find(zm<zp);
    i1=max(a);
    b=find(zm>=zp);
    i2=min(b);
    c=find(zm<zmo);
    i3=max(c);
    d=find(zm>=zmo);
    i4=min(d);

    for i=1:i1 %0<zm<=zp
        t(i)=(dMCmo*zmo(i))/P;
        Zm(i)=zmo(i)*dMCmo;
    end
    for i=i2:i3 %zp<zm<=zmo
        t(i)=tp+((1/Ksmo)*(((zmo(i)-
zp)*dMCmo)+(dHmo*dMCmo*(log((dHmo+zp)/(dHmo+zmo(i))))))); %Eq. (39b)
        Zm(i)=zmo(i)*dMCmo;
    end
    for i=i4:n %zm>zmo
        t_=(tp+((1/Ksmo)*(((zmo-zp)*dMCmo)+(dHmo*dMCmo*(log((dHmo+zp)/(dHmo+zmo)))))));
%Eq. (39b) replace zm with zmo
        Kc_(i)=(zmo(i)*dMCumo)/(((zmo*dMCmo)/Ksmo)+(((zmo(i)-zmo)*dMCumo)/Ksumo));
%Eq. (43)
        t(i)=t_+((A_-(B_*dHumo))*(log((zmo(i)+dHumo)/(zmo+dHumo)))+(B_*(zmo(i)-zmo)));
%Eq. (46)
        Zm(i)=(zmo*dMCmo)+((zmo(i)-zmo)*dMCumo); %Eq. (47)
    end

elseif tzmo<tp1L %2nd layer ponding
    tp=tp2L;
    Zp=P*tp;
    zp=(Zp-(zmo*(dMCmo-dMCumo)))/dMCumo;
    a=find(zm<zmo);
    i1=max(a);
    b=find(zm>=zmo);
    i2=min(b);
    c=find(zm<zp);
    i3=max(c);
    d=find(zm>=zp);
    i4=min(d);

    for i=1:i1 %0<zm<=zmo
        t(i)=(zmo(i)*dMCmo)/P;
        Zm(i)=zmo(i)*dMCmo;

```

```

end
for i=i2:i3 %zm<zm<=zp
t(i)=((zmo*dMCmo)+((zm(i)-zmo)*dMCumo))/P;
Zm(i)=(zmo*dMCmo)+((zm(i)-zmo)*dMCumo); %Eq.(47)
end
for i=i4:n %zm>zp
Kc_(i)=(zm(i)*dMCumo)/(((zmo*dMCmo)/Ksmo)+((zm(i)-zmo)*dMCumo)/Ksumo));
%Eq.(43)
t(i)=tp+((A_-(B_*dHumo))*(log((zm(i)+dHumo)/(zp+dHumo))))+(B_*(zm(i)-zp)));
%Eq.(53)
Zm(i)=(zmo*dMCmo)+((zp-zmo)*dMCumo)+((zm(i)-zp)*dMCumo);
end
end
zm=zm';
Zm=Zm';
t=t';
plot(t,zm)

```

3-Layers Soil Profile

```

%THREE LAYERS SOIL PROFILE
clc;
clear;

P=0.04; %water entry rate [cm/min]

%RT
Ksmo=0.0480265348303373; %the saturated hydraulic conductivity of the modified layer
[cm/min]
MCi_mo=0.05; %the initial moisture content of the modified layer [m3/m3]
MCs_mo=0.57549214025019; %the saturated moisture content of the modified layer
[m3/m3]
dMCmo=MCs_mo-MCi_mo; %delta gamma of the modified layer which is the difference
between the saturated and the initial moisture contents [m3/m3]
H_mo=-528.212623595688; %matric potential of the modified layer [cm]
zmo=20; %depth of the modified layer [cm]

%MTA
Ksmo=0.120540439180942; %the saturated hydraulic conductivity of the modified layer
[cm/min]
MCi_mo=0.078; %the initial moisture content of the modified layer [m3/m3]
MCs_mo=0.54842949366671; %the saturated moisture content of the modified layer
[m3/m3]
dMCmo=MCs_mo-MCi_mo; %delta gamma of the modified layer which is the difference
between the saturated and the initial moisture contents [m3/m3]
H_mo=-54879.88; %matric potential of the modified layer [cm]
zmo=20; %depth of the modified layer [cm]

%MT
Ksmo=0.0470337095427571; %the saturated hydraulic conductivity of the modified layer
[cm/min]
MCi_mo=0.0579; %the initial moisture content of the modified layer [m3/m3]
MCs_mo=0.6072500492759; %the saturated moisture content of the modified layer [m3/m3]
dMCmo=MCs_mo-MCi_mo; %delta gamma of the modified layer which is the difference
between the saturated and the initial moisture contents [m3/m3]
H_mo=-26534.97; %matric potential of the modified layer [cm]
zmo=20; %depth of the modified layer [cm]

%MC
Ksmo=0.0210035543615512; %the saturated hydraulic conductivity of the modified layer
[cm/min]
MCi_mo=0.0357; %the initial moisture content of the modified layer [m3/m3]
MCs_mo=0.741503670980025; %the saturated moisture content of the modified layer
[m3/m3]
dMCmo=MCs_mo-MCi_mo; %delta gamma of the modified layer which is the difference
between the saturated and the initial moisture contents [m3/m3]
H_mo=-84076.2; %matric potential of the modified layer [cm]
zmo=5; %depth of the modified layer [cm]

%INPUT PROPERTIES
Ksc=1.91176478715198; %the saturated hydraulic conductivity of the cover layer
[cm/min]

```

```

Ksumo=0.000912029168087834; %the saturated hydraulic conductivity of the unmodified
layer [cm/min]
MCi_c=0.01; %the initial moisture content of the cover layer [m3/m3]
MCs_c=0.893541823877931; %the saturated moisture content of the cover layer [m3/m3]
dMCC=MCs_c-MCi_c; %delta gamma of the cover layer which is the difference between the
saturated and the initial moisture contents [m3/m3]
MCi_umo=0.2; %the initial moisture content of the unmodified layer [m3/m3]
MCs_umo=0.433419880806727; %the saturated moisture content of the unmodified layer
[m3/m3]
dMCumo=MCs_umo-MCi_umo; %delta gamma of the unmodified layer which is the difference
between the saturated and the initial moisture contents [m3/m3]
H_c=-17654.21; %matric potential of the cover layer [cm]
H_umo=-1136.39; %matric potential of the unmodified layer [cm]
H0=0; %depth of ponded water [cm]
dHc=abs(H0-H_c);
dHmo=abs(H0-H_mo);
dHumo=abs(H0-H_umo);
zc=5; %depth of the cover layer [cm]
A_=(zc*(dMCC-dMCmo))/(Ksc-Ksmo);
B_ =dMCmo/Ksmo;
A__=((zc*(dMCC-dMCumo))/(Ksc-Ksumo))+((zmo*(dMCmo-dMCumo))/(Ksmo-Ksumo));
B__=dMCumo/Ksumo;
tzc=(zc*dMCC)/P; %Eq.(62)
tp1L=(Ksc*dHc*dMCC)/(P*(P-Ksc)); %Eq.(38)
tp1L=abs(tp1L);
tzmo=((zc*dMCC)/P)+((zmo*dMCmo)/P); %Eq.(64)
tp2L=tzc+((Ksmo*dHmo*dMCmo)/(P*(P-Ksmo))); %Eq.(65)
tp2L=abs(tp2L);
tp3L=tzmo+((Ksumo*dHumo*dMCumo)/(P*(P-Ksumo))); %Eq.(66)
tp3L=abs(tp3L);

zm=[0:1:100];
n=length(zm);
v=zeros(1,n);
t=zeros(1,n);
Zm=zeros(1,n);
Kc_=zeros(1,n);

if tp1L<=tzc %1rst layer ponding
    tp=tp1L;
    Zp=P*tp;
    zp=Zp/dMCC;
    a=find(zm<zp);
    i1=max(a);
    b=find(zm>=zp);
    i2=min(b);
    c=find(zm<zc);
    i3=max(c);
    d=find(zm>=zc);
    i4=min(d);
    e=find(zm<(zc+zmo));
    i5=max(e);
    f=find(zm>=(zc+zmo));
    i6=min(f);

    for i=1:i1 %0<zm<=zp
        t(i)=(dMCC*zm(i))/P;
        Zm(i)=zm(i)*dMCC; %Eq.(34)
    end
    for i=i2:i3 %zp<zm<=zc
        t(i)=tp+((1/Ksc)*(((zm(i)-zp)*dMCC)+(dHc*dMCC*(log((dHc+zp)/(dHc+zm(i)))))));
    %Eq.(39b)
        Zm(i)=zm(i)*dMCC; %Eq.(34)
    end
    for i=i4:i5 %zc<zm<=zmo
        t_ =tp+((1/Ksc)*(((zc-zp)*dMCC)+(dHc*dMCC*(log((dHc+zp)/(dHc+zc))))));
    %Eq.(39b) replace zm by zc
        t(i)=t_+(A_- (B_*dHmo))*(log((zm(i)+dHmo)/(zc+dHmo)))+(B_*(zm(i)-zc));
    %Eq.(46)
        Zm(i)=(zc*dMCC)+((zm(i)-zc)*dMCmo); %Eq.(47)
        Kc_(i)=(zm(i)*dMCmo)/(((zc*dMCC)/Ksc)+((zm(i)-zc)*dMCmo)/Ksmo)); %Eq.(43)
    end
    for i=i6:n %zm>zmo
        t__=t_+(A_- (B_*dHmo))*(log((zc+zmo+dHmo)/(zc+dHmo)))+(B_*(zmo)); %Eq.(46)
    replace zm by zmo+zc
        Kc__(i)=(zm(i)*dMCumo)/(((zc*dMCC)/Ksc)+((zmo*dMCmo)/Ksmo)+((zm(i)-zc-
zmo)*dMCumo)/Ksumo)); %Eq.(55)

```

```

t(i)=t_+(A_-(B_*dHmo))*(log((zm(i)+dHmo)/(zc+zmo+dHmo)))+(B_*(zm(i)-
zc-zmo)); %Eq. (58)
Zm(i)=(zc*dMCc)+(zmo*dMCmo)+((zm(i)-zc-zmo)*dMCumo); %Eq. (59)
end

elseif tzc<tp1L
if tp2L<=tzmo %2nd layer ponding
tp=tp2L;
Zp=P*tp;
zp=(Zp-(zc*(dMCc-dMCmo)))/dMCmo;
a=find(zm<zc);
i1=max(a);
b=find(zm>=zc);
i2=min(b);
c=find(zm<zp);
i3=max(c);
d=find(zm>=zp);
i4=min(d);
e=find(zm<(zc+zmo));
i5=max(e);
f=find(zm>=(zc+zmo));
i6=min(f);

for i=1:i1 %0<zm<=zc
t(i)=(dMCc*zm(i))/P;
Zm(i)=zm(i)*dMCc; %Eq. (34)
end
for i=i2:i3 %zc<zm<=zp
t(i)=((zc*dMCc)+((zm(i)-zc)*dMCmo))/P;
Zm(i)=(zc*dMCc)+((zm(i)-zc)*dMCmo); %Eq. (47)
end
for i=i4:i5 %zp<zm<=zmo
Kc_(i)=(zm(i)*dMCmo)/(((zc*dMCc)/Ksc)+(((zm(i)-zc)*dMCmo)/Ksmo)); %Eq. (43)
t(i)=tp+(A_-(B_*dHmo))*(log((zm(i)+dHmo)/(zp+dHmo)))+(B_*(zm(i)-zp));
%Eq. (53)
Zm(i)=(zc*dMCc)+((zm(i)-zc)*dMCmo); %Eq. (47)
end
for i=i6:n %zm>zmo
t_ =tp+(A_-(B_*dHmo))*(log((zc+zmo+dHmo)/(zp+dHmo)))+(B_*(zm(i)-zp));
%Eq. (53) replace zm by zc+zmo
Kc__(i)=(zm(i)*dMCumo)/(((zc*dMCc)/Ksc)+((zmo*dMCmo)/Ksmo)+((zm(i)-zc-
zmo)*dMCumo)/Ksumo)); %Eq. (55)
t(i)=t_+(A_-(
(B_*dHmo))*(log((zm(i)+dHmo)/(zc+zmo+dHmo)))+(B_*(zm(i)-zc-zmo)); %Eq. (58)
Zm(i)=(zc*dMCc)+(zmo*dMCmo)+((zm(i)-zc-zmo)*dMCumo); %Eq. (59)
end

elseif tp2L>tzmo %3rd layer ponding
tp=tp3L;
Zp=P*tp;
zp=(Zp-(zc*(dMCc-dMCumo))-(zmo*(dMCmo-dMCumo)))/dMCumo;
a=find(zm<zc);
i1=max(a);
b=find(zm>=zc);
i2=min(b);
c=find(zm<zmo);
i3=max(c);
d=find(zm>=zmo);
i4=min(d);
e=find(zm<zp);
i5=max(e);
f=find(zm>=zp);
i6=min(f);

for i=1:i1 %0<zm<=zc
t(i)=(dMCc*zm(i))/P;
Zm(i)=zm(i)*dMCc;
end
for i=i2:i3 %zc<zm<=zmo
t(i)=(((zc*dMCc)+((zm(i)-zc)*dMCmo))/P;
Zm(i)=(zc*dMCc)+((zm(i)-zc)*dMCmo); %Eq. (47)
end
for i=i4:i5 %zmo<zm<=zp
t(i)=(((zc*dMCc)+((zmo*dMCmo)+((zm(i)-zc-zmo)*dMCumo))/P;
Zm(i)=(zc*dMCc)+(zmo*dMCmo)+((zm(i)-zmo-zc)*dMCumo);
end
for i=i6:n %zmo<zm<=zp

```

```

        Kc__(i) = (zm(i) * dMCumo) / (((zc * dMCc) / Ksc) + ((zmo * dMCmo) / Ksmo) + (((zm(i) - zc -
zmo) * dMCumo) / Ksumo)); %Eq. (55)
        t(i) = tp + (A__ - (B__ * dHumo)) * (log((zm(i) + dHumo) / (zp + dHumo))) + (B__ * (zm(i) -
zp))); %Eq. (67)
        Zm(i) = (zc * dMCc) + (zmo * dMCmo) + ((zm(i) - zmo - zc) * dMCumo);
    end
end
zm = zm';
t = t';
Zm = Zm';
plot(t, zm)

```

Appendix E

Wetting Front at Field Irrigation Rate

Appendix 28: Time variation of wetting front arrivals at 1cm depth increment

time, t (mins)												
z_m (cm)	CC+MC +NT	z_m (cm)	CC+ NT	MC+ NT	CC+RT +NT	CC+MT A+NT	CC+MT +NT	z_m (cm)	NT	RT+ NT	MTA +NT	MT+ NT
-10.0	0.0	-5.0	0.0	0.0	0.0	0.0	0.0	0.0	66.2	0.0	0.0	0.0
-9.0	20.5	-4.0	20.5	16.4	20.5	20.5	20.5	1.0	66.3	12.2	10.9	12.8
-8.0	41.1	-3.0	41.1	32.8	41.1	41.1	41.1	2.0	66.7	24.4	21.9	25.5
-7.0	61.6	-2.0	61.6	49.2	61.6	61.6	61.6	3.0	67.2	36.6	32.8	38.3
-6.0	82.1	-1.0	82.1	65.6	82.1	82.1	82.1	4.0	68.0	48.8	43.7	51.1
-5.0	157.5	0.0	102.6	82.0	102.6	102.6	102.6	5.0	69.0	61.0	54.6	63.8
-4.0	162.9	1.0	108.1	87.4	114.8	113.6	115.4	6.0	70.3	73.3	65.6	76.6
-3.0	168.4	2.0	113.5	92.8	127.1	124.5	128.2	7.0	71.7	85.5	76.5	89.3
-2.0	173.8	3.0	118.9	98.3	139.3	135.4	140.9	8.0	73.4	97.7	87.4	102.1
-1.0	179.2	4.0	124.3	103.7	151.5	146.4	153.7	9.0	75.3	109.9	98.4	114.9
0.0	184.6	5.0	129.8	109.1	163.7	157.3	166.5	10.0	77.4	122.1	109.3	127.6
1.0	190.1	6.0	135.2	114.5	175.9	168.2	179.2	11.0	79.8	134.3	120.2	140.4
2.0	195.5	7.0	140.6	120.0	188.1	179.1	192.0	12.0	82.3	146.5	131.2	153.2
3.0	200.9	8.0	146.0	125.4	200.3	190.1	204.7	13.0	85.1	158.7	142.1	165.9
4.0	206.3	9.0	151.4	130.8	212.5	201.0	217.5	14.0	88.1	170.9	153.0	178.7
5.0	211.7	10.0	156.9	136.2	224.7	211.9	230.3	15.0	91.3	183.1	163.9	191.5
6.0	217.2	11.0	162.3	141.6	236.9	222.9	243.0	16.0	94.8	195.3	174.9	204.2
7.0	222.6	12.0	167.7	147.1	249.2	233.8	255.8	17.0	98.5	207.6	185.8	217.0
8.0	228.0	13.0	173.1	152.5	261.4	244.7	268.6	18.0	102.3	219.8	196.7	229.7
9.0	233.4	14.0	178.6	157.9	273.6	255.7	281.3	19.0	106.4	232.0	207.7	242.5
10.0	238.9	15.0	184.0	163.3	319.7	294.1	330.8	20.0	110.8	244.2	218.6	255.3
11.0	244.3	16.0	189.4	168.8	325.1	299.5	336.2	21.0	115.3	249.6	224.0	260.7
12.0	249.7	17.0	194.8	174.2	330.6	305.0	341.6	22.0	120.0	255.0	229.4	266.1
13.0	255.1	18.0	200.3	179.6	336.0	310.4	347.1	23.0	125.0	260.5	234.9	271.5
14.0	260.6	19.0	205.7	185.0	341.4	315.8	352.5	24.0	130.2	265.9	240.3	277.0
15.0	266.0	20.0	211.1	190.5	346.8	321.2	357.9	25.0	135.6	271.3	245.7	282.4
16.0	271.4	21.0	216.5	195.9	352.2	326.7	363.3	26.0	141.2	276.7	251.1	287.8

17.0	276.8	22.0	222.0	201.3	357.7	332.1	368.8	27.0	147.0	282.1	256.6	293.2
18.0	282.3	23.0	227.4	206.7	363.1	337.5	374.2	28.0	153.1	287.6	262.0	298.7
19.0	287.7	24.0	232.8	212.2	368.5	342.9	379.6	29.0	159.4	293.0	267.4	304.1
20.0	293.1	25.0	238.7	218.1	373.9	348.4	385.0	30.0	165.8	298.4	272.8	309.5
21.0	298.5	26.0	245.4	224.8	379.4	353.8	390.4	31.0	172.5	303.8	278.3	314.9
22.0	303.9	27.0	252.3	231.9	384.8	359.2	395.9	32.0	179.4	309.3	283.7	320.3
23.0	309.4	28.0	259.4	239.1	390.2	364.6	401.3	33.0	186.5	314.7	289.1	325.8
24.0	314.8	29.0	266.7	246.5	395.6	370.0	406.7	34.0	193.9	320.1	294.5	331.2
25.0	321.1	30.0	274.3	254.1	401.1	375.5	412.1	35.0	201.4	325.5	299.9	336.6
26.0	329.0	31.0	282.0	262.0	406.5	380.9	417.6	36.0	209.2	331.0	305.4	342.0
27.0	337.0	32.0	290.0	270.1	411.9	386.3	423.0	37.0	217.1	336.4	310.8	347.5
28.0	345.3	33.0	298.2	278.3	417.3	391.7	428.4	38.0	225.3	341.8	316.2	352.9
29.0	353.8	34.0	306.5	286.8	422.7	397.2	433.8	39.0	233.7	347.2	321.6	358.3
30.0	362.5	35.0	315.1	295.5	428.2	402.6	439.3	40.0	242.3	352.6	327.1	363.7
31.0	371.4	36.0	323.9	304.4	433.6	408.0	444.7	41.0	251.1	358.1	332.5	369.2
32.0	380.5	37.0	333.0	313.5	439.0	413.4	450.1	42.0	260.1	363.5	337.9	374.6
33.0	389.9	38.0	342.2	322.9	444.4	418.9	455.5	43.0	269.3	368.9	343.3	380.0
34.0	399.4	39.0	351.6	332.4	449.9	424.3	461.0	44.0	278.8	374.3	348.8	385.4
35.0	409.1	40.0	361.3	342.1	455.3	429.7	466.4	45.0	288.4	381.5	355.9	392.6
36.0	419.1	41.0	371.1	352.1	460.7	435.1	471.8	46.0	298.3	391.5	365.8	402.6
37.0	429.3	42.0	381.2	362.3	466.1	440.5	477.2	47.0	308.3	401.6	375.9	412.8
38.0	439.6	43.0	391.5	372.6	471.6	446.0	482.6	48.0	318.6	412.0	386.2	423.1
39.0	450.2	44.0	401.9	383.2	477.0	451.4	488.1	49.0	329.1	422.6	396.7	433.7
40.0	461.0	45.0	412.6	394.0	484.6	459.0	495.7	50.0	339.8	433.4	407.4	444.5

Appendix F

Field Data for Optimization

Appendix 29: Field moisture content variation with respect to time during and after the irrigation test application

Time (mins)	PLOTS					
	1a	1b	2a	2b	3a	3b
0	0.195	0.197	0.189	0.25	0.184	0.315
2	0.195	0.196	0.188	0.25	0.182	0.296
5	0.195	0.196	0.187	0.249	0.182	0.296
7.5	0.196	0.196	0.187	0.25	0.182	0.296
10	0.196	0.196	0.187	0.25	0.182	0.296
15	0.196	0.196	0.188	0.249	0.183	0.296
20	0.199	0.196	0.186	0.251	0.183	0.3
22	0.195	0.204	0.189	0.252	0.188	0.295
24	0.197	0.205	0.19	0.254	0.191	0.3
26	0.195	0.198	0.188	0.251	0.184	0.3
28.5	0.196	0.196	0.189	0.25	0.187	0.296
31	0.195	0.198	0.188	0.249	0.186	0.295
35	0.197	0.197	0.187	0.25	0.187	0.332
40	0.196	0.198	0.186	0.25	0.185	0.295
45	0.196	0.196	0.19	0.249	0.186	0.301
50	0.194	0.196	0.185	0.249	0.183	0.297
55	0.194	0.199	0.185	0.245	0.183	0.296
60	0.194	0.197	0.184	0.249	0.183	0.297
65	0.199	0.199	0.189	0.248	0.185	0.296
70	0.193	0.196	0.184	0.248	0.183	0.298
75	0.195	0.197	0.189	0.247	0.197	0.296
80	0.193	0.196	0.184	0.248	0.183	0.297
85	0.193	0.197	0.187	0.25	0.185	0.305
90	0.193	0.205	0.187	0.25	0.185	0.298
95	0.193	0.202	0.184	0.247	0.186	0.301
100	0.193	0.199	0.187	0.248	0.187	0.301
110	0.193	0.204	0.188	0.251	0.189	0.303
120	0.193	0.201	0.184	0.25	0.19	0.299
130	0.193	0.204	0.184	0.251	0.186	0.307
140	0.197	0.202	0.187	0.252	0.192	0.305
150	0.193	0.21	0.188	0.247	0.191	0.306
160	0.193	0.204	0.184	0.247	0.212	0.315

170	0.193	0.202	0.185	0.247	0.305	0.322
180	0.197	0.211	0.188	0.248	0.351	0.367
190	0.198	0.216	0.186	0.252	0.396	0.412
195	0.2	0.219	0.191	0.25	0.406	0.412
200	0.199	0.218	0.187	0.25	0.429	0.418
205	0.194	0.223	0.189	0.25	0.421	0.426
210	0.199	0.221	0.19	0.25	0.425	0.427
220	0.199	0.223	0.188	0.25	0.437	0.43
230	0.198	0.224	0.19	0.25	0.44	0.438
240	0.202	0.225	0.191	0.252	0.453	0.446
250	0.202	0.226	0.192	0.253	0.458	0.445
260	0.21	0.224	0.194	0.252	0.463	0.452
270	0.205	0.226	0.194	0.254	0.444	0.454
280	0.208	0.221	0.193	0.254	0.448	0.456
290	0.204	0.224	0.193	0.251	0.443	0.467
300	0.208	0.225	0.197	0.254	0.444	0.458
328	0.211	0.229	0.201	0.254	0.442	0.456
338	0.211	0.239	0.215	0.266	0.44	0.454
345	0.222	0.271	0.248	0.287	0.443	0.457
360	0.275	0.381	0.317	0.361	0.445	0.463
371	0.342	0.402	0.365	0.366	0.448	0.463
380	0.393	0.422	0.39	0.385	0.448	0.468
390	0.42	0.443	0.416	0.406	0.441	0.471
400	0.439	0.446	0.422	0.413	0.444	0.456
420	0.445	0.449	0.429	0.425	0.433	0.415
502	0.445	0.449	0.429	0.438	0.425	0.454
Time (day)	1a	1b	2a	2b	3a	3b
0.25	0.445	0.449	0.429	0.438	0.425	0.454
1	0.425	0.435	0.415	0.412	0.403	0.43
1.5	0.425	0.442	0.422	0.415	0.402	0.435
2	0.419	0.44	0.411	0.428	0.396	0.43
2.5	0.419	0.439	0.406	0.428	0.393	0.429
3	0.419	0.439	0.406	0.428	0.396	0.43
3.5	0.415	0.438	0.402	0.428	0.387	0.429
4	0.408	0.424	0.406	0.436	0.386	0.445
4.5	0.414	0.416	0.393	0.434	0.383	0.429
5	0.4	0.405	0.387	0.424	0.376	0.428
5.5	0.4	0.403	0.385	0.423	0.374	0.427
6	0.398	0.4	0.381	0.418	0.371	0.418